Tuning Reactivity in C(sp^3)–C(sp^2) Cross-Electrophile Coupling

by

Daniel C. Salgueiro

A dissertation submitted in partial fulfillment of

The requirements for the degree of

Doctor of Philosophy

(Chemistry)

at the

UNIVERSITY OF WISCONSIN-MADISON

2023

Date of final oral examination: 4/18/2023

The dissertation is approved by the following members of the Final Oral Committee

Daniel J. Weix, Wayland E. Noland Distinguished Professor, Chemistry

Jennifer M. Schomaker, Professor, Chemistry

Zachary K. Wickens, Assistant Professor, Chemistry

Jeffrey D. Martell, Professor, Chemistry

Dedication

To all those who have supported me and believed in me.

In loving memory of Pablo Larrea.

Biographical Sketch

The author was born on December 21st, 1996 in Miami, Florida. He attended Emory University for his undergraduate studies. While there he conducted research on rhodium catalyzed allylic C–H amination reactions under the supervision of Professor Simon B. Blakey from 2016 to 2018. During the summer of 2017 he participated in the Chemistry Summer Undergraduate Research Program through the Center for Selective C–H Functionalization at Emory University.

After graduating summa cum laude with a Bachelor's of Science in Chemistry in 2018, he joined the lab of Professor Daniel J. Weix at the University of Wisconsin-Madison. His researched focused on the use of redox active esters in cross-electrophile coupling, the coupling of aliphatic alcohols, and the coupling of aryl sulfonate esters. He was awarded the Pei Wang Fellowship in 2018, the National Science Foundation Graduate Research Fellowship in 2019, and was a finalist for the Gem Fellowship in 2022. In 2021 he participated in an internship in Discovery Chemistry at Janssen Pharmaceuticals under the supervision of Dr. Pablo García-Reynaga where he studied the cross-electrophile coupling of redox active esters derived from strained ring carboxylic acids. In 2023, he was awarded the Harlan L. and Margaret L. Goering Organic Chemistry Fellowship.

After graduation he will begin his career as a process chemist at Gilead Sciences.

The following publications were a result of work conducted during doctoral study:

1. Chi, B. K.; Widness, J. K.; Gilbert, M. M.; Salgueiro, D. C.; Garcia, K. J.; Weix, D. J. "In-Situ Bromination Enables Formal Cross-Electrophile Coupling of Alcohols with Aryl and Alkenyl Halides" *ACS Catal.* **2022**, *12*, 580-586.

2. Salgueiro, D. C.; Chi, B. K.; Guzei, I. A.; García-Reynaga, P.; Weix, D. J. "Control of Redox-Active Ester Reactivity Enables a General Cross-Electrophile Approach to Access Arylated Strained Rings" *Angew. Chem. Int. Ed*. **2022**, e202205673
3. Salgueiro, D. C.; Ehehalt, L. E.; Johnson, K. A.; Weix, D. J. "Discussion Addendum for: Nickel-Catalyzed Cross-Coupling of Aryl Halides with Alkyl Halides: Ethyl 4-(4-(4-methylphenylsulfonamido)-phenyl)butanoate" *Org. Synth.* **2022**, 99, 215-233

Acknowledgments

Science isn't done in a vacuum. My growth as a person and as a scientist has been the direct result of the love, support, and mentorship I've received throughout my life. I would be remiss if I did not take the time now to put my feelings of gratitude into writing.

First and foremost, I would like to thank my literal day one supporters, my family. Whether they bear the last name Salgueiro or Larrea, or one of the others that has made its way into El Pueblon, they have been responsible (for better or worse) for molding me into the passionate and independent person I am today. Though they may not know exactly what I've been working on, they have always been my cheerleaders and my support network.

Every teacher I have learned from helped put me on the path towards the PhD, but there are a few that have been the most impactful in framing the way that I think about science. I would like to thank Mrs. Hemisha Barkow, who spent three years teaching me chemistry at Coral Reef High School, for teaching me to love chemistry and for always pushing me to do my best. I would also like to thank Dr. Jose Soria, an outstanding teacher and mentor who put me on the path to graduate school by helping me get into research and guiding me through the decision of which graduate school to attend. I would like to thank Prof. Arri Eisen, whose truly interdisciplinary approach to science inspires me to seek out the connections between seemingly different schools of thought.

I would like to thank Prof. Simon Blakey at Emory University for being my mentor in my first foray into research and giving me a space to grow as a scientist. I would also like to thank Dr. Robert Harris, now a professor at Wofford College, for being a great mentor and for always telling me to "be better". I would like to thank former members of the Blakey lab, Caiti-Mac Farr, Amaan Kazerouni, Jacob Burman, Taylor Farmer Nelson, Christopher Poff, and Eric

Andreansky for making the Blakey lab a second home for a young chemist in the making (and for putting up with my shenanigans). My time in the Blakey lab certainly prepared me for graduate school.

I want to thank Prof Dan Weix for being a wonderful advisor, and for being both a great scientist and a great person. Whether they've been about possible directions for a project, the dangers of misleading graphics in the news, or the best place to find fresh vegetables while travelling, I've absolutely enjoyed our conversations over the years. Thank you for always pushing us, fighting for us, and being so supportive. It's been an honor and a pleasure to be part of the Weix lab. I'll try my best to live according to the advice you gave me while I was preparing to give supergroup, "You've got the goods, just make it entertaining".

Speaking of the Weix lab, I am so grateful for this quirky bunch of individuals. Your energy, enthusiasm, and chaos are what made coming into lab every day so fun. Whether you identify as a member of Cobalt lab, Zinc lab, Palladium lab, or our unnamed outpost with the Buller lab (maybe we should name that office after a biologically relevant metal) you have been such an important part of my time in Madison. To the original Merriment Committee: Sam Gavin, Nate Loud, and Jonas Widness. Grad school would not have been the same without our late-night lasagna and cake making, and I will forever be grateful for our friendships.

I would like to thank my committee members, Profs. Zach Wickens, Jen Schomaker, and Jeff Martell. To Zach, thank you for working on the NSF Graduate Research Fellowship with me, being an informal second advisor to me, and for teaching me the ways of the Aeropress. To Jen, thank you for always providing such helpful feedback during qualifying exams, and for taping a copy of my poorly photoshopped "Jen and Tonic" to your office door. To Jeff, thank

you for our weekly chats during the walk from the lecture hall in the new building to the 5th floor of Shain tower. And thank you all for your mentorship.

Abstract

In this thesis, efforts towards the improvement of cross-electrophile coupling reactions utilizing redox active esters will be described in detail.

Chapter 1 will provide a high-level overview of cross-electrophile coupling for a general audience.

Chapter 2 introduces redox-active esters and a summary of their applications. Their syntheses, reactivity, scope, and limitations will be discussed.

Chapter 3 describes the development of improved reaction conditions for nickel-catalyzed cross-electrophile coupling of redox-active esters with aryl iodides and bromides. The application of this system to various reaction modalities, substrate scope and limitations, and insights into tuning the reactivity of redox-active esters are also presented.

Chapter 4 discusses efforts towards further improvement of reaction conditions for nickel-catalyzed cross-electrophile coupling of redox-active esters with aryl halides. Details regarding catalyst screening and the effects of various reductant systems on the outcome of the reaction will be described.

Contributors and Funding Sources

This work was supervised by a dissertation committee consisting of Professors Daniel J. Weix (advisor), Zachary K. Wickens, Jennifer M. Schomaker, and Jeffrey D. Martell of the Department of Chemistry. The author performed all experimental procedures in this dissertation unless specified below:

Chapter 3:

Select entries in the substrate scope were performed by Benjamin K. Chi and Dr. Pablo García-Reynaga (Janssen). Flow experiments were performed by Dr. Pablo García-Reynaga. Synthesis and isolation of ($^{t\text{-bu}}$BpyCam^{CN})Ni(*o*-tol) was performed by Benjamin K. Chi, and characterization of this complex was performed by Ilia A. Guzei.

Chapter 4:

Catalyst screening plates were provided by Dr. Santiago Cañellas Román (Janssen) and Dr. José Enrique Gómez Pulido (Janssen).

All work presented in this dissertation was supported by the University of Wisconsin-Madison, the National Institutes of Health, the National Science Foundation Graduate Research Fellowship, and Janssen Pharmaceuticals.

Table of Contents

List of Figures

List of Tables

List of Symbols and Abbreviations

-	Minus, negative, or hyphen
%	Percent
[M]	Metal
+	Plus or positive
°C	Degrees Celsius
μ	Micro
μL	Microliter
μmol	Micromole
^{13}C	Carbon-13
^{19}F	Fluorine-19
^{1}H	Proton
α	alpha
ACN	Acetonitrile
aq	Aqueous
Ar	Aryl
B	Boron
$B(OH)_2$	Boronic acid
B_2pin_2	Bis(pinacolato)diboron
BCP	Bicyclo[1.1.1]pentane
Boc	*Tert*-butoxyllcarbonyl

Bpin	Pinacolato boron
Br	Bromide
C	Carbon
C(sp)	carbon with sp^3 hybridized orbitals
C(sp^2)	carbon with sp hybridized orbitals
C(sp^3)	carbon with sp^2 hybridized orbitals
Cbz	Benzyloxycarbonyl
CHO	Aldehyde
Cl	Chloride
cm	centimeter
CN	Nitrile
CO_2	Carbon dioxide
col	Column
COOH	Carboxylic Acid
Cs	Cesium
CsF	Cesium Fluoride
CV	Cyclic Voltammogram
d	Doublet
D	Deuterium
δ	delta
d.r.	Diastereomeric ratio
DABCO	1,4-diazabicyclooctane
DBU	1,8-Diazabicyclo[5.4.0]undec-7-ene

DCC	N,N′-Dicyclohexylcarbodiimide
DCM	Dichloromethane
DEL	DNA-encoded library
DIC	N,N′-Diisopropylcarbodiimide
DMA	N,N-dimethylacetamide
DMAP	4-(N,N-dimethylamino)pyridine
dme	1,2-Dimethoxyethane
EDC	1-Ethyl-3-(3-dimethylaminopropyl)carbodiimide
EDG	Electron-donating group
equiv	Equivalents
Et	Ethyl
Et_2O	Diethyl ether
EtOAc	Ethyl acetate
EtOH	Ethanol
eV	Electron volts
EWG	Electron-withdrawing group
FID	Flame Ionization Detector
FTIR	Fourier transform infrared
g	Gram
GC	Gas chromatography
GCMS	Gas chromatography mass spectrometry
H	Hydrogen
h	Hour(s)

Hex	Hexane
HRMS	High Resolution Mass Spectrometry
HTE	High-throughput experimentation
Hz	Hertz
I	Iodide
I-PrOH	Isopropanol
IR	Infrared
IS	Internal Standard
J	Coupling Constant
K	Potassium
K_2CO_3	Potassium Carbonate
KF	Potassium Fluoride
KNphth	Potassium Phthalimide
KOAc	Potassium Acetate
L	Liter
LC	Liquid Chromatography
m	Multiplet
m/z	Mass-to-charge ratio
Me	Methyl
MeOH	Methanol
mg	Milligram
Mg	Magnesium
$MgSO_4$	Magnesium Sulfate

MHz	Megahertz
min	Minute(s)
mL	Milliliter
mm	Millimeter
mmol	millimole
Mn	Manganese
mol	Mole
MP	Melting Point
MS	Mass Spectrometry
MW	Molecular Weight
N	Nitrogen atom
N_2	Nitrogen
Na	Sodium
Na_2SO_4	Sodium Sulfate
NaI	Sodium Iodide
NHNp	*N*-hydroxynapthaleneimide
NHP	*N*-hydroxyphthalimide
Ni	Nickel
NMR	Nuclear Magnetic Resonance
NO_2	Nitro
Nphth	Phthalimide
o	Ortho
OH	Alcohol

OMe	Methoxy
P	Product
π	pi
Pd	Palladium
PhMe	Toluene
PITU	*N*-hydroxyphthalimide tetramethyluronium hexaphosphate
ppm	Parts per milion
PROTAC	Proteolysis Targeting Chimera
psi	Pounds per square inch
PTFE	Polytetrafluoroethylene, teflon
q	Quartet
r.t	Room temperature
RAE	Redox-Active Ester
rpm	Revolutions per minute
s	Singlet or second
σ	sigma
SFC	Supercritical Fluid Chromatography
sp	linear hybridized orbitals with 50% s and 50% p character
sp^2	trigonal planar hybridized orbitals with 33% s and 67% p character
sp^3	tetrahedral hybridized orbitals with 25% s and 75% p character
t	Triplet
TBAF	Tetrabutylammonium fluoride

t-Bu	Tert-butyl
TCNHP	Tetrachloro-*N*-hydroxyphthalimide
TDAE	1,1,2,2-tetrakis(dimethylamino)ethylene
tert	Tertiary
THF	Tetrahydrofuran
TLC	Thin-layer chromatography
TMAF	Tetramethylammonium fluoride
TMS	Trimethhylsilyl, Tetramethylsilane
TMSBr	Bromotrimethylsilane
TMSCl	Chlorotrimethylsilane
UPLC	Ultra High Performance Liquid Chromatography
V	Volt
WISL	Wisconsin Institute for Scientific Literacy
wt	Weight
X	Halide
XC	Cross-Coupling
XEC	Cross-Electrophile Coupling
Zn	Zinc
$ZnBr_2$	Zinc bromide
ZnX_2	Zinc halide

Chapter 1: An Introduction to Cross-Electrophile Coupling

The sheer amount of jargon in chemistry can make chemistry research inaccessible to a general audience. I wrote this chapter to contextualize and share my doctoral research to my friends, family, and anyone else who wants to read it! I've had a lot of fun writing this, and I implore anyone in a specialized field to give this kind of writing a go. I would like to thank the Wisconsin Initiative for Science Literacy (WISL) at UW-Madison for providing this platform, and for sponsoring and supporting the creation of this chapter. I am especially grateful to Professor Bassam Shakhashiri, Elizabeth Reynolds, and Cayce Osborne for their help in making this chapter as clear as possible.

Organic chemistry is the study of carbon-based (organic) molecules. Some organic molecules are the building blocks that keep people alive. The sugars, fats, and proteins that we eat get broken down in our body into smaller building blocks that the body can use to create energy, make hormones that regulate bodily functions, and generally keep our bodies chugging along. Other organic molecules may not be used to keep us alive but still have important applications in everyday life. We can use dyes to make beautifully colored fabrics, plastics to make containers and toys, and drugs to treat diseases. Some of these organic molecules can be extracted from plants and other natural sources, but others need to be made in a lab using chemical reactions. Because organic molecules are primarily made of carbon atoms, reactions that form bonds between carbon atoms are especially powerful for building complex molecules that we can't find in nature.

Cross-coupling reactions are reactions that are commonly used to form carbon-carbon bonds in the synthesis of drugs and pesticides, allowing chemists to stitch two organic

fragments together to make a new, larger molecule. Cross-coupling reactions typically require a transition metal catalyst, a molecule that lowers the energetic barrier to a reaction by unlocking different mechanistic pathways, to form the desired carbon-carbon bond. Transition metals are any of the elements highlighted in the red box on the periodic table in **Figure 1.1**, with the most commonly used metal being Palladium (Pd). Transition metals make useful catalysts because they are stable at different oxidation states, meaning they can easily give up and take back electrons. These transition metal catalysts are made up of two distinct things: a transition metal and a ligand. Ligands are organic molecules that bind to transition metals and change how that metal reacts with other molecules. Palladium catalyzed cross-coupling reactions are so useful that Richard Heck, Ei-ichi Negishi, and Akira Suzuki were awarded the Nobel Prize in 2010 for their research in this area.

Figure 1.1: The Periodic Table of the Elements with transition metals highlighted by the red box, palladium is highlighted by the orange box, and nickel is highlighted by the blue box.

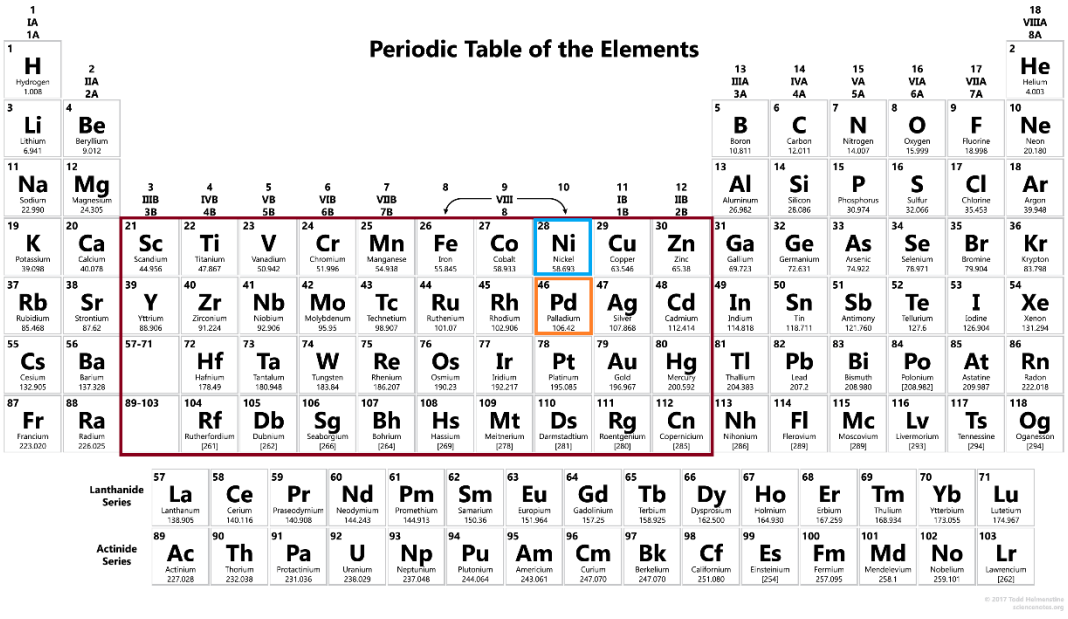

I like to think about a transition metal as a person, a ligand as a set of tools, and a chemical reaction as a task that needs to get done. You want to pick the right person with the right tools to get a job done. Some tasks can be done by most people and don't require specific tools: Most people can go pick up some milk, whether they walk, bike, take the bus, or drive to the store. Some tools can bridge a person's skill gap for some tasks. This thesis would be practically illegible if I wrote it all by hand, but a word processor lets me write this clearly. Certain tasks can only be done by masters of a craft and with specialized tools. You wouldn't want a chef to use a baseball bat to perform your open-heart surgery, just like a sports team would never pay a surgeon to hit baseballs with a chef's knife, and you would never ask a baseball star to prepare you a salad using a scalpel. Similarly, the task of forming the desired carbon-carbon bond can only be accomplished by using the right combination of transition metal and ligand.

A catalyzed reaction is like a frozen pizza factory, with reactants being the raw ingredients and the product being the pizza. Our jobs as people who develop new reactions is to make sure all the machines work together to make pizza and to make the manufacturing process more efficient. Every step needs to happen in the right order and at the right rate to make your pizza dreams come true. Some problems in the factory have simple solutions. If the pizzas aren't getting cold enough, you can just leave them in the freezer longer. Other problems in the factory have more flexible solutions. If cheese is being dispensed too quickly, you'll end up with some very cheesy pizzas and, once you run out of cheese, cheeseless pizzas. For this you could slow down the cheese machine, speed up every other machine, fill the cheese machine with more cheese at the start, or even market cheeseless pizzas as a great meal for lactose intolerant people.

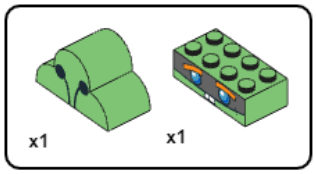

1

Conventional cross-coupling reactions use a palladium catalyst to form carbon-carbon bonds between nucleophiles (organic molecules that donate a pair of electrons) and electrophiles (organic molecules that accept pairs of electrons). The correct carbon-carbon bond is formed during the reaction because of how nucleophiles and electrophiles react together, like how two LEGO blocks just snap into place because of their complementary studs and anti-studs. Researchers have spent decades studying and improving palladium catalyzed cross-coupling reactions. However, there are still challenges, specifically centered around the use of palladium catalysts and the use of nucleophiles.

Palladium catalysts are highly efficient and useful, but palladium is expensive (~$1,400 per ounce) and not abundant (palladium makes up 0.0000015% of the earth's crust and is the 70th most abundant element) making it not ideal to use palladium for the synthesis of molecules

on large scale. The price and scarcity of palladium has sparked a lot of interest in finding alternative metals that can catalyze cross-coupling reactions. Nickel (Ni) is in the same group of the periodic table as palladium, so the two metals react similarly in some cases, but nickel is significantly cheaper (~$0.80 per ounce) and more abundant than palladium (nickel makes up 0.0084% of the earth's crust and is the 23rd most abundant element). 0.0084% may not seem like much, but that means there is 5600 times more nickel than palladium on earth.

The types of nucleophiles that are used in cross-coupling reactions are known as organometallic reagents, organic compounds that contain a carbon-metal bond. Organometallic reagents come with their own unique set of challenges. Organometallic reagents are highly sensitive to moisture; even humid air can be wet enough to decompose organometallic reagents, so researchers need to take extra precaution when storing or handling organometallic reagents. This means that, more often than not, if you want to use an organometallic reagent in a reaction you would have to make it and use it right away. These organometallic reagents are typically made by reacting an electrophile with a metal. You can buy thousands of times more electrophiles than nucleophiles because you don't have to take care to store electrophiles away from air and water. The abundance and stability of electrophiles has motivated researchers to spend the last several decades finding creative, useful reactions that rely on electrophiles.

You can avoid making organometallic reagents by cross-coupling two different electrophiles together: this is called cross-electrophile coupling. Reacting two electrophiles together is like trying to put two LEGO bricks together end to end. Normally this would be an impossible LEGO building technique, but with enough glue you can make the impossible possible. Nickel based catalysts are used a lot in cross-electrophile coupling reactions because

they are good at telling the difference between two different electrophiles. If nickel is like your hands that are putting the LEGO bricks together, ligands are like your eyes. If you have a pile of red and green LEGO bricks and pick two at random, you'll end up making a mixture of red-red, red-green, and green-green LEGO bricks stuck together. If you only want red and green LEGO bricks stuck together, you need to be able to see the difference between them.

Figure 1.2: LEGO analogy for Cross-Electrophile Coupling. Each tile only has anti-studs so putting the correct two pieces together requires you to be able to see color

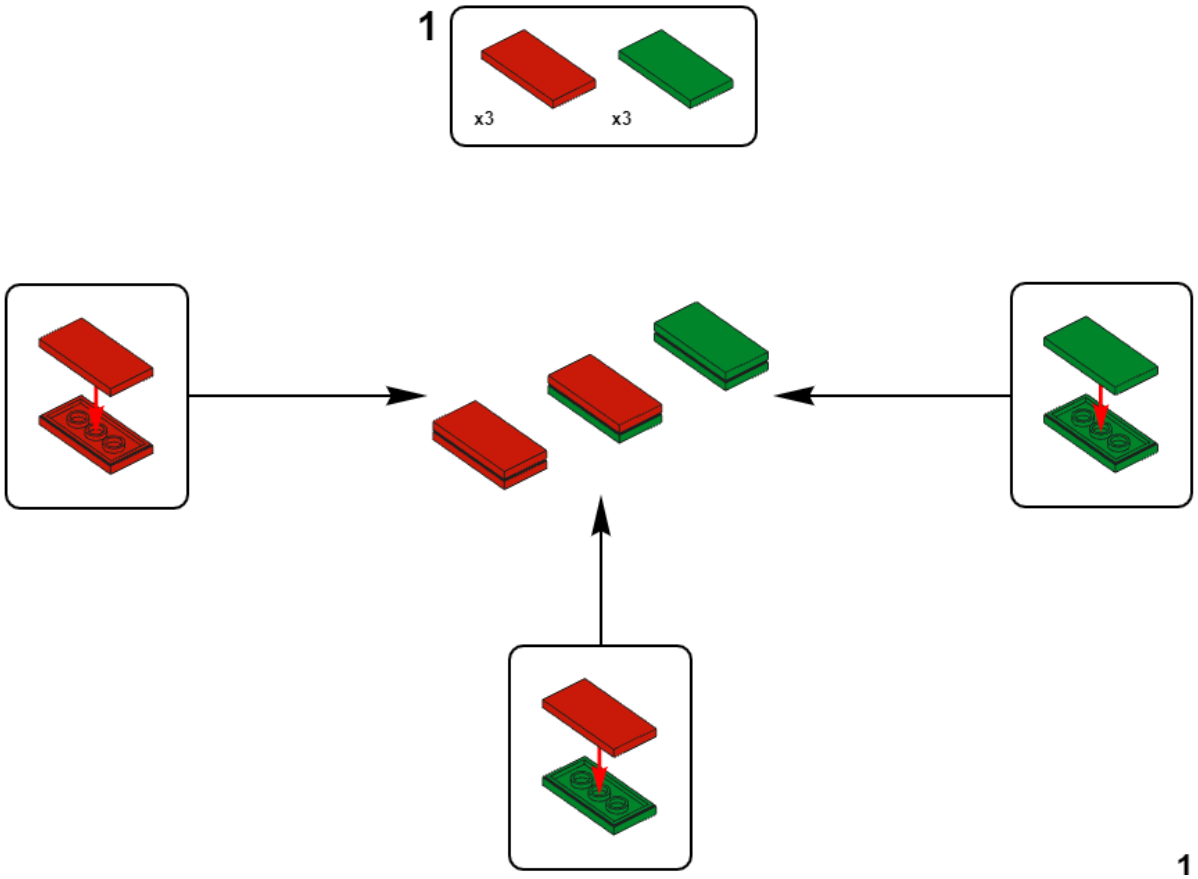

An important step of cross coupling involves the metal activating the electrophile, Nickel is capable of activating different types of electrophiles in different ways, functionally allowing it to tell the difference between electrophiles. Nickel based catalysts are really good at interacting with both polar molecules (molecules with a pair of reactive electrons) and

radicals (molecules with only one reactive electron). The cross-electrophile coupling reactions I have studied have been reactions between electrophiles that react through polar (two-electron) mechanisms and electrophiles that react through radical (one-electron) mechanisms.

In graduate school the molecules I was most interested in were ones that contained strained rings, cyclic molecules where the ring is only made up of three or four atoms. Strained rings can be made entirely of carbon atoms, or they could have either a nitrogen atom or an oxygen atom in the ring. These small rings can have big effects on how a drug behaves in your body: they can make it easier for your body to absorb a drug from your stomach, they can slow down how long it takes your body to metabolize so it can be effective in your body even longer, and they can even make a drug more potent so you don't need to take as large of a dose. Although strained rings can be a really useful part of drugs, we never know what type of ring is going to be a part of the best drug until we test each of them out, and to test each of them out you have to make every single variation. Usually, you would have to make each ring, building the molecule from the ground up. It would be nice if we could use our LEGO approach to trying each different strained ring. Cross-electrophile coupling reactions are really good at stitching together two organic molecules to make one larger molecule, so I thought it would be useful to have a cross-electrophile coupling reaction that could work with strained rings, making it easy to swap out one ring for another. I searched databases of molecules I could buy, and I found that you can buy most strained ring molecules with a carboxylic acid functional group attached to them. A functional group is a reactive part of a molecule. Normally carboxylic acids don't play nice with catalysts that are good at promoting cross-electrophile coupling reactions, but you can easily turn carboxylic acids into redox-active esters. Redox is a portmanteau of the words "**red**uction" and "**ox**idation", and the word redox is used to describe

a reaction that involves one molecule giving an electron to another molecule, so when a molecule is "redox-active" that means it can participate in a redox reaction. Once redox-active esters get reduced they form a radical, which is exactly what we need for a cross-electrophile coupling reaction.

Getting this reaction to work wasn't as simple as "throw in a redox-active ester and call it a day". The main problem I had to solve was that the two electrophiles were mismatched in how quickly they reacted. I used two different strategies to control the relative rates of different steps in the reactions. 1) The ligand on the catalyst has a big effect on how quickly the catalyst reacts with each electrophile, so I researched different ligands and even made a brand new one. 2) Electrophiles have their own innate reactivity, so I studied how changing things like the structure of the electrophile or the solvent the reaction is run in changes an electrophile's reactivity.

Let's start with the ligand. I mentioned before that ligands are like your eyes when you're trying to tell the difference between red and green LEGO bricks. Some people will have no problem distinguishing the two, but people that have certain colorblindness will struggle to tell the difference between red and green, and people who are completely blind won't be able to tell the difference at all. We might not be able to swap out our eyes very easily, but as chemists we can certainly change what ligand we put into a reaction. With so many different steps in a reaction, a ligand could be great for one step but terrible for the rest of them. When you're trying to find the right ligand for a new reaction you typically start by trying out ligands that have been used in similar reactions, bipyridine ligands are commonly used in cross-electrophile coupling reactions so they're a great place to start. Sometimes it's a great start and all you need to do is make minor changes to the structure of the ligand just to tweak its

reactivity. The reactivity of bipyridine ligands is easy to tweak by adding different substituents to them. These substituents can change things like how tightly the ligand binds to nickel or how much space it takes up around the nickel atom.

Figure 1.3: Illustration of the importance of finding the right ligand for a reaction. (Left) LEGO **Figure 1.3** image with a deuteranopia filter applied. (Right) Copy of **Figure 1.3**.

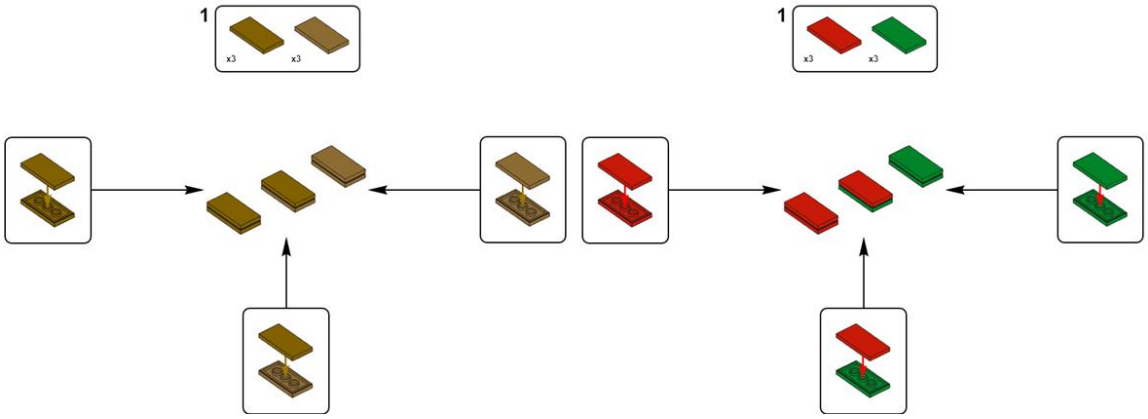

Sometimes making small tweaks to a ligand isn't enough and you need to explore different types of ligands. One way we categorize ligands is by their denticity. Denticity refers to how atoms on a ligand can stick to a metal, with monodentate meaning one sticky atom, bidentate meaning two sticky atoms, and so on. When I started studying this reaction, I tried out bipyridine ligands and other, similar, bidentate ligands to try and find the best one. These all worked pretty well, but the reactions were not totally selective for the desired product over side reactions. I then tried a bunch of other ligands, and eventually found one that made the desired product with the best selectivity and in the highest yield. And it had never been used before! Since this ligand was brand new, I wanted to study what made it different, so I made enough to use for two papers. Ben, a graduate student that was working with me, took some of the ligand and made one of the reaction intermediates. He grew a crystal of this intermediate and we got a molecular picture using X-rays.

Figure 1.4 Ligand structure can change how a catalyst reacts.

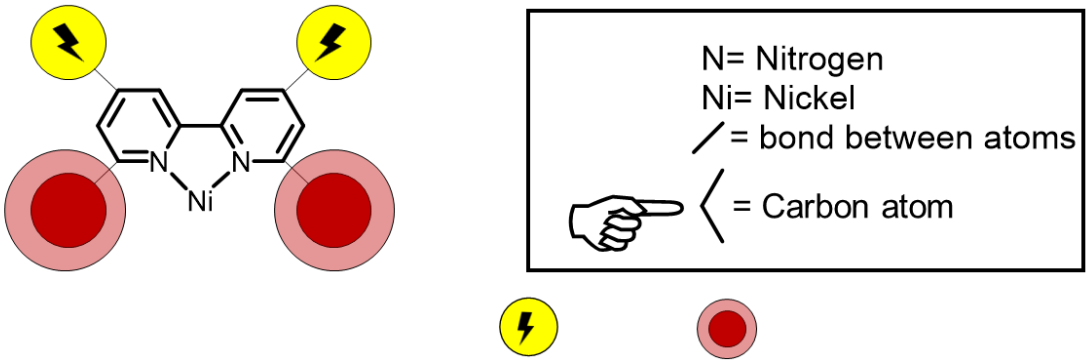

One of the challenges I faced in my research was that redox-active esters react too quickly. If a molecule is too reactive it's like when the cheese machine in a pizza factory is too fast: it uses up the cheese before we can make all of the cheese pizzas we want. In my reaction, the redox-active ester was being used up faster than the other electrophile could react so I had to figure out a way to slow down how quickly the redox-active ester was being consumed. You can figure out how reactive a redox-active molecule is by measuring the molecule's reduction potential. The reduction potential tells you how easy it is to give an electron to a molecule. I had the hypothesis that if a redox-active esters was harder to reduce it would react more slowly. First, I made several different redox-active esters and measured their reduction potentials. I made some that were easier to reduce and some that were harder to reduce. Then, I studied the reaction between these new redox-active esters and a reductant, taking samples from the reactions at different times to measure how quickly they reacted. I found that the redox-active ester that was the hardest to reduce was also the slowest to react. Lastly, I took each of the redox-active esters I had made and tried them out in a bunch of different cross-electrophile coupling reactions. I found a good correlation between the reduction potential of the redox-active esters and the yield of the reaction product, with the most reactive redox-active esters

giving the lowest yield of the product and the least reactive redox-active esters giving the highest yield of the product.

Figure 1.5 Redox-active esters which are harder to give an electron to are slower to react.

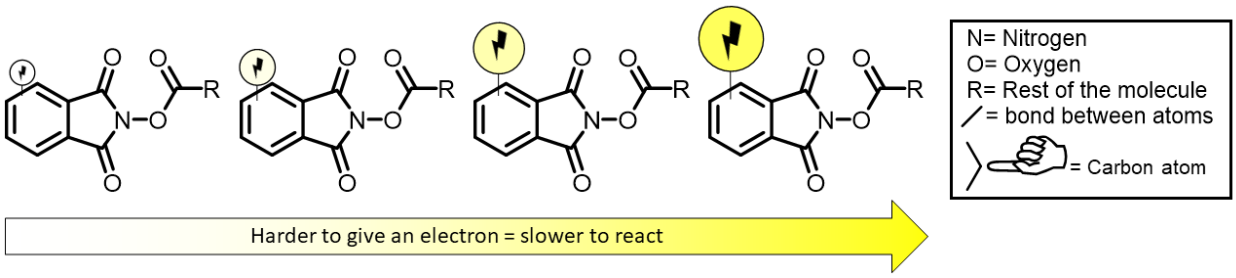

Once I had a grasp of what controls the selectivity of the reaction and what knobs I could turn to tweak reaction outcomes, I looked at what sorts of molecules I could make. I was able to make small, proof-of concept molecules, as well as larger complex molecules that have been studied for their medicinal properties. With the help of my collaborators, I showed that this reaction could be done in different types of reactors, which would be helpful for doing both large- and small-scale reactions. Since we published a paper on this work last year, a chemical supplier has already begun selling the new ligand I used for this work, and chemists at several different companies have started using this reaction to help with the discovery of potential drugs.

Chapter 2: Introduction to Decarboxylative Cross-Coupling

This chapter consists of a Concept Article that will be submitted to Chemistry: A European Journal, and is co-authored by Jonas K. Widness.

2.1 Introduction

Due to the structural diversity of carboxylic acids, reactions of carboxylic acids allow chemists to easily access unique chemical space. Historically, using a molecule from the carboxylic acid pool in a radical transformation required reduction of the carboxylic acid to an alcohol followed by an appel reaction to afford a primary alkyl halide, which could then participate in radical reactions. More modern approaches to generate radicals from carboxylic acids rely on decarboxylation of carboxylate radicals, opening chemical space to a shorter member of this homologous series and enabling the formation of secondary and tertiary radicals from this substrate pool. The approach for radical generation from the carboxylic acid pool that will be discussed in this review relies on the formation of redox-active esters (RAEs), molecules which furnish a stabilized anion, carbon dioxide, and an alkyl radical upon reduction by a single electron.

The use of alkanoic acids to generate alkyl radicals via decarboxylative mechanisms has, in part, been accelerated by the development of redox active esters. In the late 1980s work from Okada demonstrated that N-Hydroxyphthalimide esters (NHP esters), which were initially developed as activated esters for peptide synthesis, could be reduced by strong photogenerated reductants liberating anionic phthalimide, carbon dioxide, and the corresponding alkyl radical.[1] Overman showed the utility of this method of radical generation in the synthesis of (-)-Aplyviolene, where an NHP ester was to generate a radical for a conjugate addition.[2]

Figure 2.1 Initial disclosures for RAE reactivity.

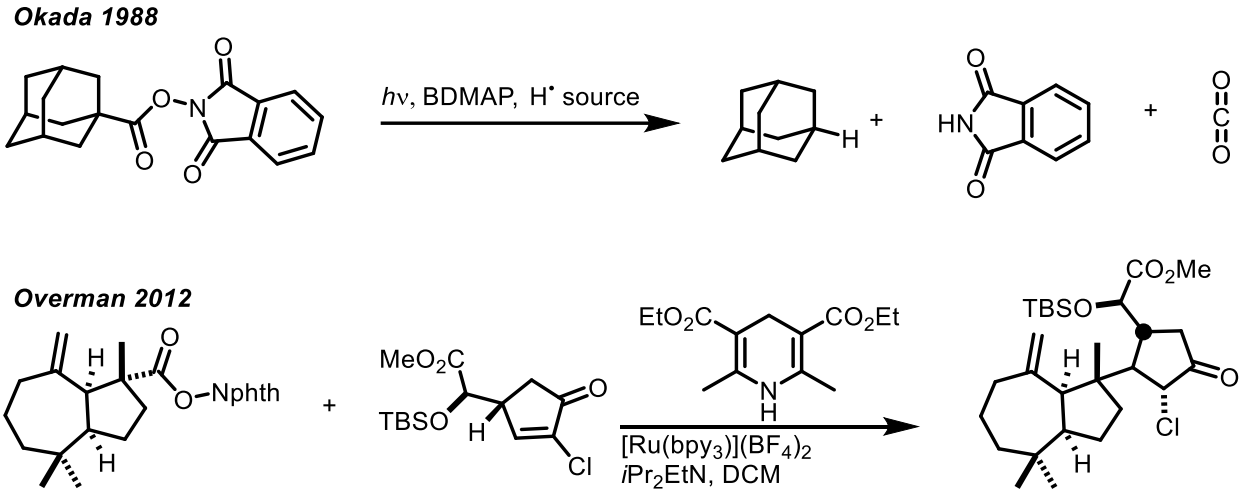

With radical-based cross-coupling methodologies emerging as powerful tools for the construction of C-C bonds, it was inevitable that conditions would be adapted to incorporate redox-active esters (RAEs) as radical precursors in these reactions. In 2016, Weix and Baran disclosed the first publications merging redox-active chemistry with transition-metal catalyzed cross-coupling reactions under thermal conditions.[3,4] In this Concept we will describe the recent advances in cross-couplings of redox-active esters. This Concept will focus on reactions in which C-C occurs via reductive elimination from a transition metal catalyst, not carbon-heteroatom bond forming reactions or those C-C bond forming reactions that are governed by free radical chemistry. Methods for decarboxylative cross-couplings which rely upon oxidation of carboxylates to generate the requisite alkyl radical are useful but will not be discussed in this review.

Figure 2.2 Top: General approaches for alkyl radical formation. Bottom: Structures of commonly used RAEs.

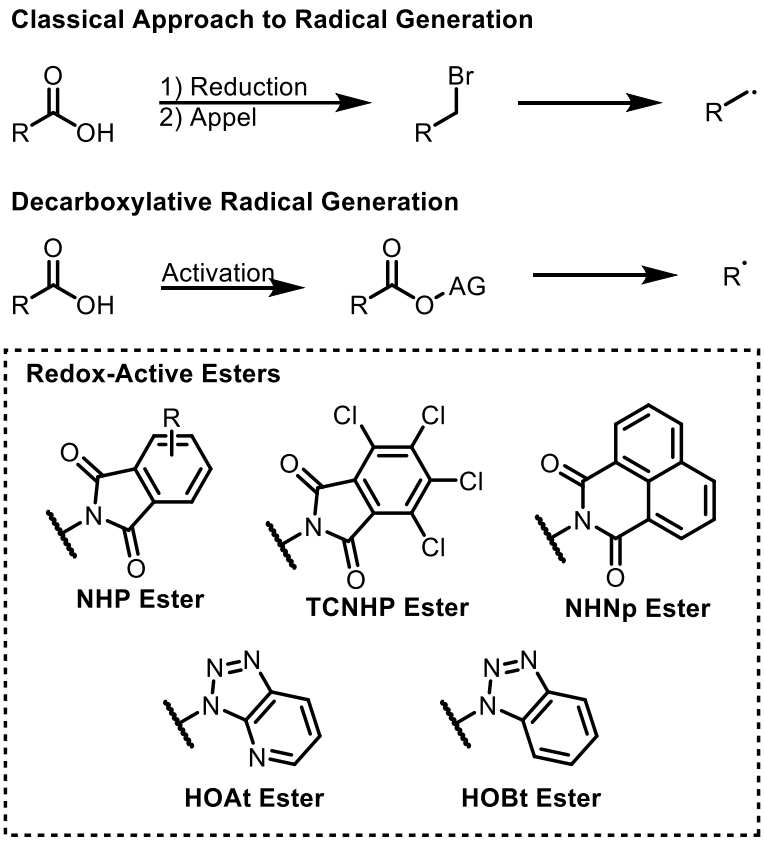

2.2 Synthesis

Redox-active esters can be synthesized in a multitude of ways from carboxylic acids and activating auxiliaries. The most common approach involves the pre-formation and purification of redox-active esters before cross-coupling. The use of common coupling reagents including N,N′-diisopropylcarbodiimide (DIC),[5] N,N′-dicyclohexylcarbodiimide (DCC),[6] and 1-Ethyl-3-(3-dimethylaminopropyl)carbodiimide (EDC)[7] enables the preparation of NHP esters and their derivatives from the carboxylic acid in high yields. Carboxylic acid chlorides can also be employed as acyl donors, however this approach is less commonly used due to the need for pre-synthesis of the acid chloride.[8] Some reports have observed variability in NHP ester reactivity based on the synthesis method, however the reasons for this are not currently

understood.[3] After synthesis, NHP esters can be purified by standard column chromatography or recrystallization .

Figure 2.3 Methods of synthesis of RAEs

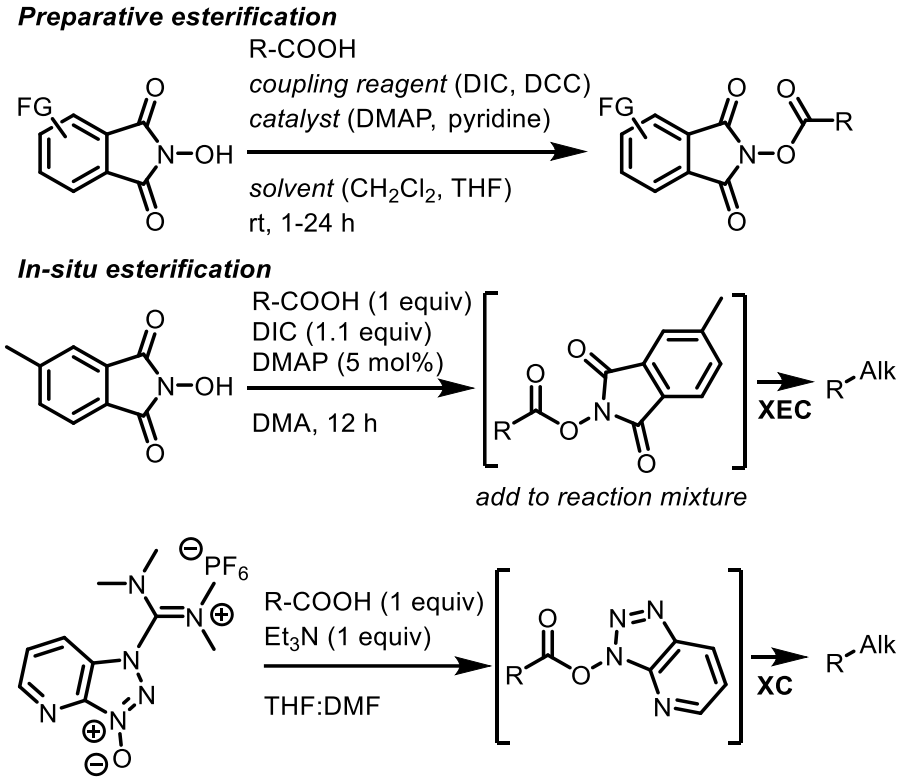

In order to save time and resources consumed by purifications, efforts have been made to develop telescopic or one-pot activation-cross coupling procedures. Specialized reagents have been developed for this purpose, such as O-(phthalimid-2-yl)-N,N,N′,N′-tetramethyluronium PF_6 (PITU), which Wang et al. used to form NHP esters for XEC, requiring only filtration through silica and removal of CH_2Cl_2 solvent before addition of other reaction components.[9] Analogous uronium reagents prepared from electronically varied NHP derivatives have also been reported.[10] More streamlined strategies bypass the need for any intermediate purification: Kang et al. found that NHP esters could be formed under DIC

conditions in DMA and be directly subjected to XEC conditions without purification or solvent exchange.[11] Further development of reagents and conditions is needed to synthesize NHP esters with short reaction times, high yields, and benign byproducts to better facilitate in-situ activation approaches.

2.3 Modes of Activation

So named, "redox active esters" can be activated by single-electron transfer, which promotes fragmentation to form radical intermediates (Figure X). NHP esters and their substituted derivatives constitute the most widely employed redox-active esters, which upon reduction undergo mesolytic fragmentation of the weak N-O bond. Decarboxylation of ensuing acyloxy radicals produces the desired carbon-centered radical for cross-coupling. The decarboxylation rate of acyloxy radicals depends significantly on the stability of the resulting radical, with more stabilized radicals faster to form (Figure X).[12] Many reducing systems have been described for the reduction of NHP esters, including metals,[3,4] photocatalysis,[1,2,13] electrochemistry,[7,14] and organic reductants with[15] or without[16] light.

Figure 2.4 Top: Fragmentation mechanism of NHP esters. Right: unimolecular rate constants for decarboxylation of acyloxy radicals, measured in MeOH at 20 °C. Bottom: Electron sources used to induce decarboxylative radical generation from NHP esters.

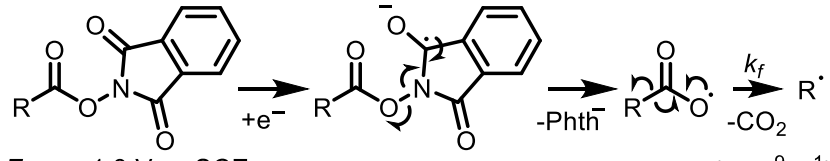

E_{red} ~ -1.3 V vs SCE

Electron sources	
Metals	Zn, L_nNi...
Photocatalysts	Ir(III)*, Ru(II)*...
Electrochemistry	cathode, mediators...
Organic reductants	TDAE, DHP + *hν*...

R	k_f ($\times 10^9$ s^{-1})
Me	<1.3 ± 0.2
Et	2.0 ± 0.3
*i*Pr	6.5 ± 0.8
*t*Bu	11 ± 2
Bn	5 ± 0.8
Ph	~0.001

2.4 Reaction Scopes and Applications

RAEs have seen widespread use as radical precursors in a variety of radical-based cross-coupling methods. The cross-coupling reactions of RAEs fall into two categories: 1) redox-neutral couplings and 2) net-reductive couplings. Redox-neutral couplings can be achieved using either iron- or nickel-based catalysts and work well with commonly used (hetero)aryl nucleophiles such as boronic acids, zinc reagents, and more nucleophilic Grignard reagants.[17] These couplings have been extended to work with alkynyl,[18] alkenyl,[19] and alkyl [20] zinc reagents. Couplings with alkyl zinc reagents can be rendered enantioselective with the use of a chiral nickel catalyst.[2122]

Figure 2.5 General scheme for cross-couplings of RAEs.

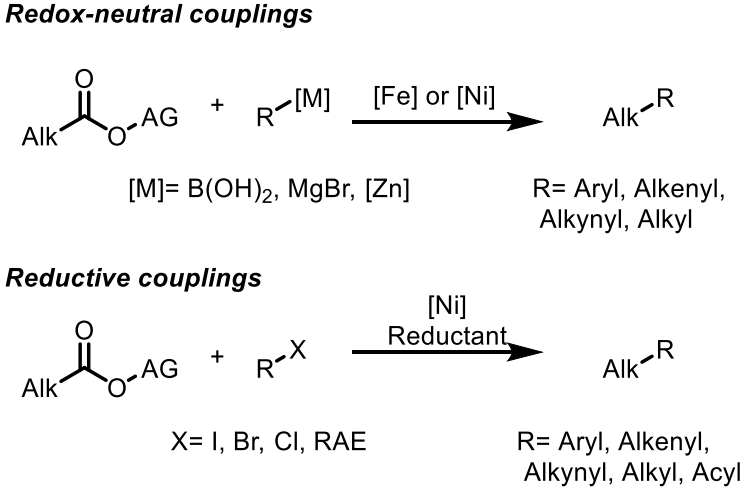

Reductive cross-couplings of RAEs, be they thermal, electrochemical, or photochemical have been used for arylation, alkenylation, and alkylation of RAEs and most commonly occur

in the presence of a nickel catalyst. Initial reports of reductive couplings of RAEs promoted by chemical reductants were limited to couplings of primary and secondary RAEs with aryl iodides.[3] The development of new catalysts as well as better understanding of the effects of additives, solvents, and RAE identity on RAE reactivity have expanded the scope to include (hetero)aryl iodides and electron deficient (hetero)aryl bromides, as well as tertiary RAEs.[15,23,24,] In 2017 Reisman reported the first enantioselective cross-coupling of RAEs, coupling secondary NHP esters with alkenyl bromides promoted by TDAE and a bromosilane additive.[16] Radicals generated from RAEs can be coupled to acyl electrophiles such as acyl chlorides, fluorides, and other activated esters to generate ketones.[9] Reductive alkylation of RAEs has been achieved through radical-radical cross-coupling of RAEs with alkyl bromides[1125] or other RAEs.[26] Selectivity in radical-radical couplings is generally achieved by employing an excess of one of the coupling partners or by sequestering one radical with an iron cocatalyst.

Improvements in the scope of what reactions are possible with RAEs has led researchers to explore ways in which decarboxylative cross-couplings can be adapted to suit the needs of both medicinal chemists and process chemists. Medicinal chemistry relies upon strategies that allow for rapid exploration of chemical space, with reactions typically being run at small enough scales to supply just enough product for biological testing. Adapting reactions to the smallest scale (nmol) platform for parallel synthesis, DNA-encoded library (DEL) synthesis, presents unique challenges as they typically require dilute aqueous reaction media with high concentrations of salts.[27] Salty aqueous conditions can be problematic for hydrolytically sensitive molecules like RAEs. One way to get around this is to remove the water altogether. Baran, in collaboration with Flood, developed a method for DEL synthesis which relies upon reversible adsorption of the DNA bound reactant onto polysterene beads, performing the

cross-coupling in an organic solvent, followed by desorption of the DNA bound product after the reaction is complete.[28] Molander also reported the use of RAEs to perform hydroalkylation of alkenes for the synthesis of DELs.[29]

Cross-couplings of RAEs can more easily adapted to larger (μmol) parallel synthesis platforms such as high-throughput experimentation (HTE) in a 96-well, or higher density, plate. The solution-phased dispensing of reagents required for HTE synthesis works well for RAEs as they are soluble in a variety of organic solvents. However, reductive cross-couplings of RAEs that rely upon a solid metal reductant such as zinc or manganese can be problematic to adapt to this format as these reductants cannot be dispensed as a solution. These reductants can be dispensed as a slurry, but the heterogeneous nature of this slurry can lead to inconsistent dosing of the reductant from well to well, so this strategy should only be employed if the reaction uses a large excess of the reductant.[30] A more consistent strategy is to coat the reductant onto small glass beads to make a 5-10 wt% solid solution of reductant. The relatively low loading of the reductant ensures that the physical properties of the solid solution are the same as the naked beads allowing the reductant to be accurately dispensed using calibrated scoops.[31] An added benefit of the glass beads is that they provide additional agitation to the reaction solution, enabling the use of shaker plates rather than tumble-stirrers for HTE. This strategy for reductant dosing has been successfully used to adapt the cross-coupling of RAEs with aryl halides to HTE.[23]

Scaling up reactions can provide additional challenges for reaction optimization, many of which can be attributed to issues associated with large scale batch reactions. Achieving efficient mixing, kinetics of surface chemistry at metal or electrode surfaces, and light penetration into a solution can be challenging as reactors grow larger. Flow reactors have

become a useful tool in the pharmaceutical industry as they enable continuous generation of the desired product, and the high surface area to volume ratio of these reactors circumvents some of the issues seen in batch chemistry. Reductive cross-couplings using RAEs have been adapted to work in flow reactors by either flowing the reaction mixture through a packed zinc bed column[32] or through an electrochemical flow cell.[7] Thus far, these reactions have been on millimolar scale and are largely proof-of-concept, but the findings in these reports will aid in the development of larger and larger scale flow reactions.

2.5 Tuning Reactivity

In cross-coupling reactions which rely upon the capture of radical intermediates, the rates of activation of both substrates must be matched in order for cross-coupling to predominate over dimerization or other possible reaction pathways. This makes strategies to control the rate of radical generation paramount to the successful development of new methodologies and expanding accessible chemical space.

In their initial series of disclosures, the Baran lab found that the identity and substitution pattern of the redox-active portion of a RAE had a profound effect on the reaction outcome. Some reactions would only provide synthetically tractable yields with one class of RAE, while others worked well with multiple RAEs.[17] The exact reason for this reaction-to-reaction variability was not well understood. In 2022, our group found a strong correlation between the reduction potential of a RAE, its rate of consumption, and product yield in the cross-electrophile coupling of RAEs with a variety of aryl bromides.[23]

Figure 2.6 Tuning NHP ester reactivity.

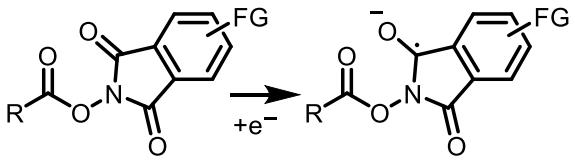

Faster Reactivity	Slower Reactivity
ZnX_2	*FG = EDG*
TMSX	*Ethereal solvent*
FG = EWG	
Amide solvent	

Additives and the reaction solvent have also been shown to have an effect on the reactivity of RAEs. Work from Rousseaux demonstrated that chlorosilane additives increased the rate of decarboxylation of NHP esters. Experimental evidence shows that the effect is not simply caused by activation of the zinc surface, rather stoichiometric to superstoichiometric amounts of TMSCl were needed to achieve the same effect even after pre-activation of the zinc surface. Increasing the stoichiometry of TMSCl from 1 equivalent to 3 equivalents led to improved reaction outcomes.[24] Other additives such as ZnX_2 salts have been shown to increase the rate of conversion of RAEs.[9] Presumably both halosilanes and zinc salts are acting as Lewis acids, coordinating to the RAE and making SET more facile. Cross-coupling reactions that employ RAEs as a coupling partner are typically run in mixtures of amide solvents and THF. Increased amount of THF in the solvent mixture has been shown to decrease the rate of conversion of NHP esters, while increased amide solvent increases the rate of conversion. The reason for this effect is not well understood, but this empirical finding should prove useful for further reaction development.

2.6 Summary and Outlook

The wealth of diverse, commercially available carboxylic acids makes them an ideal building block in the synthesis of complex molecules. Though carboxylic acids have canonically been

used as starting materials for amide bond formation and other functional group interconversions, efforts towards the development of general decarboxylative cross-coupling reactions have unlocked fundamentally different reactivity from this ubiquitous substrate pool. Redox-active esters, which have their roots as activated esters in the realm of peptide synthesis, are easily synthesized in one step and furnish a stabilized anion, carbon dioxide, and an alkyl radical upon reduction by a single electron. Initial applications of RAEs for organic synthesis were limited to radical additions to π-systems, but advancements in the field of cross-coupling led to the adoption of RAEs in radical-based cross-coupling methodologies.

RAEs can be used as isolated molecules, synthesized and telescoped into cross-coupling reactions, or generated in situ using commercially available or bespoke activating reagents. RAEs can be reduced photochemically, electrochemically, by a chemical reductant, or by a reduced form of the catalyst responsible for cross-coupling. These radical precursors, in the presence of either iron- or nickel-based catalysts, can be used to form a variety of C-C bonds under both redox-neutral and reductive conditions. Cross-coupling reactions of RAEs include arylation, alkenylation, alkynylation, alkylation, and ketone formation. In general, it would seem that the biggest hurdle to further expanding the scope is the high reactivity of RAEs. The reactivity of RAEs can be tuned through careful choice of solvent and additive. We have found that the rate of radical generation from a RAE is correlated with its reduction potential, with more negative reduction potentials correlating to slower rates of radical generation. RAEs have seen use in small-scale parallel synthesis applications such as DEL synthesis and HTE, as well as proof-of-concept flow reactions that could make scaling up reactions more facile.

2.7 References

[1] Okada, Keiji.; Okamoto, Kazushige.; Oda, Masaji. A New and Practical Method of Decarboxylation: Photosensitized Decarboxylation of N-Acyloxyphthalimides via Electron-Transfer Mechanism. *J. Am. Chem. Soc.* **1988**, *110* (26), 8736–8738. https://doi.org/10.1021/ja00234a047.

[2] Schnermann, M. J.; Overman, L. E. A Concise Synthesis of (−)-Aplyviolene Facilitated by a Strategic Tertiary Radical Conjugate Addition. *Angew. Chem. Int. Ed.* **2012**, *51* (38), 9576–9580. https://doi.org/10.1002/anie.201204977.

[3] Huihui, K. M. M.; Caputo, J. A.; Melchor, Z.; Olivares, A. M.; Spiewak, A. M.; Johnson, K. A.; DiBenedetto, T. A.; Kim, S.; Ackerman, L. K. G.; Weix, D. J. Decarboxylative Cross-Electrophile Coupling of *N* -Hydroxyphthalimide Esters with Aryl Iodides. *J. Am. Chem. Soc.* **2016**, *138* (15), 5016–5019. https://doi.org/10.1021/jacs.6b01533.

[4] Cornella, J.; Edwards, J. T.; Qin, T.; Kawamura, S.; Wang, J.; Pan, C.-M.; Gianatassio, R.; Schmidt, M.; Eastgate, M. D.; Baran, P. S. Practical Ni-Catalyzed Aryl–Alkyl Cross-Coupling of Secondary Redox-Active Esters. *J. Am. Chem. Soc.* **2016**, *138* (7), 2174–2177. https://doi.org/10.1021/jacs.6b00250.

[5] Pratsch, G.; Lackner, G. L.; Overman, L. E. Constructing Quaternary Carbons from *N* -(Acyloxy)Phthalimide Precursors of Tertiary Radicals Using Visible-Light Photocatalysis. *J. Org. Chem.* **2015**, *80* (12), 6025–6036. https://doi.org/10.1021/acs.joc.5b00795.

[6] Hu, C.; Chen, Y. Chemoselective and Fast Decarboxylative Allylation by Photoredox Catalysis under Mild Conditions. *Org. Chem. Front.* **2015**, *2* (10), 1352–1355. https://doi.org/10.1039/C5QO00187K.

[7] Li, H.; Breen, C. P.; Seo, H.; Jamison, T. F.; Fang, Y.-Q.; Bio, M. M. Ni-Catalyzed Electrochemical Decarboxylative C–C Couplings in Batch and Continuous Flow. *Org. Lett.* **2018**, *20* (5), 1338–1341. https://doi.org/10.1021/acs.orglett.8b00070.

[8] Syroeshkin, M. A.; Krylov, I. B.; Hughes, A. M.; Alabugin, I. V.; Nasybullina, D. V.; Sharipov, M. Yu.; Gultyai, V. P.; Terent'ev, A. O. Electrochemical Behavior of N-Oxyphthalimides: Cascades Initiating Self-Sustaining Catalytic Reductive N—O Bond Cleavage. *Journal of Physical Organic Chemistry* **2017**, *30* (9), e3744. https://doi.org/10.1002/poc.3744.

[9] Wang, J.; Cary, B. P.; Beyer, P. D.; Gellman, S. H.; Weix, D. J. Ketones from Nickel-Catalyzed Decarboxylative, Non-Symmetric Cross-Electrophile Coupling of Carboxylic Acid Esters. *Angew. Chem. Int. Ed.* **2019**, *58* (35), 12081–12085. https://doi.org/10.1002/anie.201906000.

[10] deGruyter, J. N.; Malins, L. R.; Wimmer, L.; Clay, K. J.; Lopez-Ogalla, J.; Qin, T.; Cornella, J.; Liu, Z.; Che, G.; Bao, D.; Stevens, J. M.; Qiao, J. X.; Allen, M. P.; Poss, M. A.; Baran, P. S. CITU: A Peptide and Decarboxylative Coupling Reagent. *Org. Lett.* **2017**, *19* (22), 6196–6199. https://doi.org/10.1021/acs.orglett.7b03121.

[11] Kang, K.; Weix, D. J. Nickel-Catalyzed C(Sp3)–C(Sp3) Cross-Electrophile Coupling of In Situ Generated NHP Esters with Unactivated Alkyl Bromides. *Org. Lett.* **2022**, *24* (15), 2853–2857. https://doi.org/10.1021/acs.orglett.2c00805.

[12] Hilborn, J. W.; Pincock, J. A. Rates of Decarboxylation of Acyloxy Radicals Formed in the Photocleavage of Substituted 1-Naphthylmethyl Alkanoates. *J. Am. Chem. Soc.* **1991**, *113* (7), 2683–2686. https://doi.org/10.1021/ja00007a049.

[13] Mao, R.; Balon, J.; Hu, X. Decarboxylative C(Sp3)−O Cross-Coupling. *Angew. Chem. Int. Ed.* **2018**, *57* (41), 13624–13628. https://doi.org/10.1002/anie.201808024.

[14] Koyanagi, T.; Herath, A.; Chong, A.; Ratnikov, M.; Valiere, A.; Chang, J.; Molteni, V.; Loren, J. One-Pot Electrochemical Nickel-Catalyzed Decarboxylative Sp2–Sp3 Cross-Coupling. *Org. Lett.* **2019**, *21* (3), 816–820. https://doi.org/10.1021/acs.orglett.8b04090.

[15] Kammer, L. M.; Badir, S. O.; Hu, R.-M.; Molander, G. A. Photoactive Electron Donor–Acceptor Complex Platform for Ni-Mediated $C(Sp^3)$–$C(Sp^2)$ Bond Formation. *Chem. Sci.* **2021**, *12* (15), 5450–5457. https://doi.org/10.1039/D1SC00943E.

[16] Suzuki, N.; Hofstra, J. L.; Poremba, K. E.; Reisman, S. E. Nickel-Catalyzed Enantioselective Cross-Coupling of *N* -Hydroxyphthalimide Esters with Vinyl Bromides. *Org. Lett.* **2017**, *19* (8), 2150–2153. https://doi.org/10.1021/acs.orglett.7b00793.

[17] Sandfort, F.; O'Neill, M. J.; Cornella, J.; Wimmer, L.; Baran, P. S. Alkyl−(Hetero)Aryl Bond Formation via Decarboxylative Cross-Coupling: A Systematic Analysis. *Angew. Chem. Int. Ed.* **2017**, *56* (12), 3319–3323. https://doi.org/10.1002/anie.201612314.

[18] Smith, J. M.; Qin, T.; Merchant, R. R.; Edwards, J. T.; Malins, L. R.; Liu, Z.; Che, G.; Shen, Z.; Shaw, S. A.; Eastgate, M. D.; Baran, P. S. Decarboxylative Alkynylation. *Angew. Chem. Int. Ed.* **2017**, *56* (39), 11906–11910. https://doi.org/10.1002/anie.201705107.

[19] Edwards, J. T.; Merchant, R. R.; McClymont, K. S.; Knouse, K. W.; Qin, T.; Malins, L. R.; Vokits, B.; Shaw, S. A.; Bao, D.-H.; Wei, F.-L.; Zhou, T.; Eastgate, M. D.; Baran, P. S. Decarboxylative Alkenylation. *Nature* **2017**, *545* (7653), 213–218. https://doi.org/10.1038/nature22307.

[20] Qin, T.; Cornella, J.; Li, C.; Malins, L. R.; Edwards, J. T.; Kawamura, S.; Maxwell, B. D.; Eastgate, M. D.; Baran, P. S. A General Alkyl-Alkyl Cross-Coupling Enabled by Redox-Active Esters and Alkylzinc Reagents. *Science* **2016**, *352* (6287), 801–805. https://doi.org/10.1126/science.aaf6123.

[21] Gao, Y.; Zhang, B.; Levy, L.; Zhang, H.-J.; He, C.; Baran, P. S. Ni-Catalyzed Enantioselective Dialkyl Carbinol Synthesis via Decarboxylative Cross-Coupling: Development, Scope, and Applications. *J. Am. Chem. Soc.* **2022**, *144* (24), 10992–11002. https://doi.org/10.1021/jacs.2c04358.

[22] Yang, Z.-P.; Freas, D. J.; Fu, G. C. The Asymmetric Synthesis of Amines via Nickel-Catalyzed Enantioconvergent Substitution Reactions. *J. Am. Chem. Soc.* **2021**, *143* (7), 2930–2937. https://doi.org/10.1021/jacs.0c13034.

[23] Salgueiro, D. C.; Chi, B. K.; Guzei, I. A.; García-Reynaga, P.; Weix, D. J. Control of Redox-Active Ester Reactivity Enables a General Cross-Electrophile Approach to Access Arylated Strained Rings**. *Angew. Chem. Int. Ed.* **2022**, *61* (33), e202205673. https://doi.org/10.1002/anie.202205673.

[24] Michel, N.; Edjoc, R.; Fagbola, E.; Hughes, J.; Campeau, L.-C.; Rousseaux, S. Nickel-Catalyzed Reductive Arylation of Redox Active Esters for the Synthesis of -Aryl Nitriles – Role of a Chlorosilane Additive; preprint; Chemistry, **2021**.

[25] Liu, W.; Lavagnino, M. N.; Gould, C. A.; Alcázar, J.; MacMillan, D. W. C. A Biomimetic S_H2 Cross-Coupling Mechanism for Quaternary Sp^3-Carbon Formation. *Science* **2021**, *374* (6572), 1258–1263. https://doi.org/10.1126/science.abl4322.

[26] Zhang, B.; Gao, Y.; Hioki, Y.; Oderinde, M. S.; Qiao, J. X.; Rodriguez, K. X.; Zhang, H.-J.; Kawamata, Y.; Baran, P. S. Ni-Electrocatalytic Csp3–Csp3 Doubly Decarboxylative Coupling. *Nature* **2022**, *606* (7913), 313–318. https://doi.org/10.1038/s41586-022-04691-4.

[27] Wang, J.; Lundberg, H.; Asai, S.; Martín-Acosta, P.; Chen, J. S.; Brown, S.; Farrell, W.; Dushin, R. G.; O'Donnell, C. J.; Ratnayake, A. S.; Richardson, P.; Liu, Z.; Qin, T.; Blackmond, D. G.; Baran, P. S. Kinetically Guided Radical-Based Synthesis of C(Sp3)−C(Sp3) Linkages on DNA. *PNAS* **2018**, *115* (28), E6404–E6410. https://doi.org/10.1073/pnas.1806900115.

[28] Flood, D. T.; Asai, S.; Zhang, X.; Wang, J.; Yoon, L.; Adams, Z. C.; Dillingham, B. C.; Sanchez, B. B.; Vantourout, J. C.; Flanagan, M. E.; Piotrowski, D. W.; Richardson, P.; Green, S. A.; Shenvi, R. A.; Chen, J. S.; Baran, P. S.; Dawson, P. E. Expanding Reactivity in DNA-Encoded Library Synthesis via Reversible Binding of DNA to an Inert Quaternary Ammonium Support. *J. Am. Chem. Soc.* **2019**, *141* (25), 9998–10006. https://doi.org/10.1021/jacs.9b03774.

[29] Badir, S. O.; Lipp, A.; Krumb, M.; Cabrera-Afonso, M. J.; Kammer, L. M.; Wu, V. E.; Huang, M.; Csakai, A.; Marcaurelle, L. A.; Molander, G. A. Photoredox-Mediated Hydroalkylation and

Hydroarylation of Functionalized Olefins for DNA-Encoded Library Synthesis. *Chem. Sci.* **2021**, *12* (36), 12036–12045. https://doi.org/10.1039/D1SC03191K.

[30] Aguirre, A. L.; Loud, N. L.; Johnson, K. A.; Weix, D. J.; Wang, Y. ChemBead Enabled High-Throughput Cross-Electrophile Coupling Reveals a New Complementary Ligand. *Chem. Eur. J.* **2021**, *27* (51), 12981–12986. https://doi.org/10.1002/chem.202102347.

[31] Tu, N. P.; Dombrowski, A. W.; Goshu, G. M.; Vasudevan, A.; Djuric, S. W.; Wang, Y. High-Throughput Reaction Screening with Nanomoles of Solid Reagents Coated on Glass Beads. *Ange. Chem. Int. Ed.* **2019**, *58* (24), 7987–7991. https://doi.org/10.1002/anie.201900536.

[32] Watanabe, E.; Chen, Y.; May, O.; Ley, S. V. A Practical Method for Continuous Production of Sp3-Rich Compounds from (Hetero)Aryl Halides and Redox-Active Esters. *Chem. Eur. J.* **2020**, *26* (1), 186–191. https://doi.org/10.1002/chem.201905048.

Chapter 3: Control of Redox-Active Ester Reactivity Enables a General Cross-Electrophile Approach to Access Arylated Strained Rings

3.1 Introduction

Molecules with strained rings, including 3- and 4-membered carbocycles, have gained prominence in medicinal chemistry due to the beneficial effects they impart on the pharmacokinetic and pharmacodynamic properties of drug candidates (**Figure 3.1**).[1,2,3,4,5,6,7] These include improved solubility, metabolic stability, and receptor/ligand binding interactions.[1,891011] Most often, incorporation of strained rings into molecules is accomplished by a ring-opening[12,13] or ring-closing reaction, typically involving a π-system.[14,15,16,17,18,19,20] These annulation reactions are well-studied and can be performed in a stereoselective and regioselective fashion.[14,21,22,23,24,25] However, each annulation reaction requires different conditions, and often require multiple steps, making parallel screening of different ring systems difficult.

An ideal strategy to enable the rapid access of these strained ring systems for medicinal chemistry would be a direct cross-coupling approach that would allow access to large pools of coupling partners and be general for a variety of strained rings.[26] Despite advances in strain-release methodologies utilizing "spring-loaded" reagents,[27,28,29,30,31,32,33,34,35] and cross-coupling of strained-ring units,[36,37,38,39,40,41,42,43,44] current approaches are limited by the availability of requisitely functionalized coupling partners and do not yet offer the substrate compatibility and scope needed to rapidly screen a variety of strained-rings.[36] In general, decarboxylative approaches, be they oxidative,[45,46] redox neutral,[47,48,49] or reductive,[50,51,52,53,54] would be the most attractive due to the widespread availability of strained-ring-containing carboxylic acids, owing to advancements in their syntheses, including strategies that directly furnish

cyclorpropyl redox-active esters.[21,36,55,56,57,58,59,60,61] Recent studies by Baran[47] and Molander[62] using *N*-hydroxyphthalimide (NHP) esters and Huestis[63] using carboxylates are attractive, but limited by the need for diarylzinc reagents (Baran) or were demonstrated for only bicyclo[1.1.1]pentane (Molander) and amino-oxetane units (Huestis). A general set of conditions that tolerate (hetero)aryl halides and is suited to the incorporation of a variety of strained rings would be ideal.

Figure 3.1: Arylation of strained rings using tuned redox-active esters.

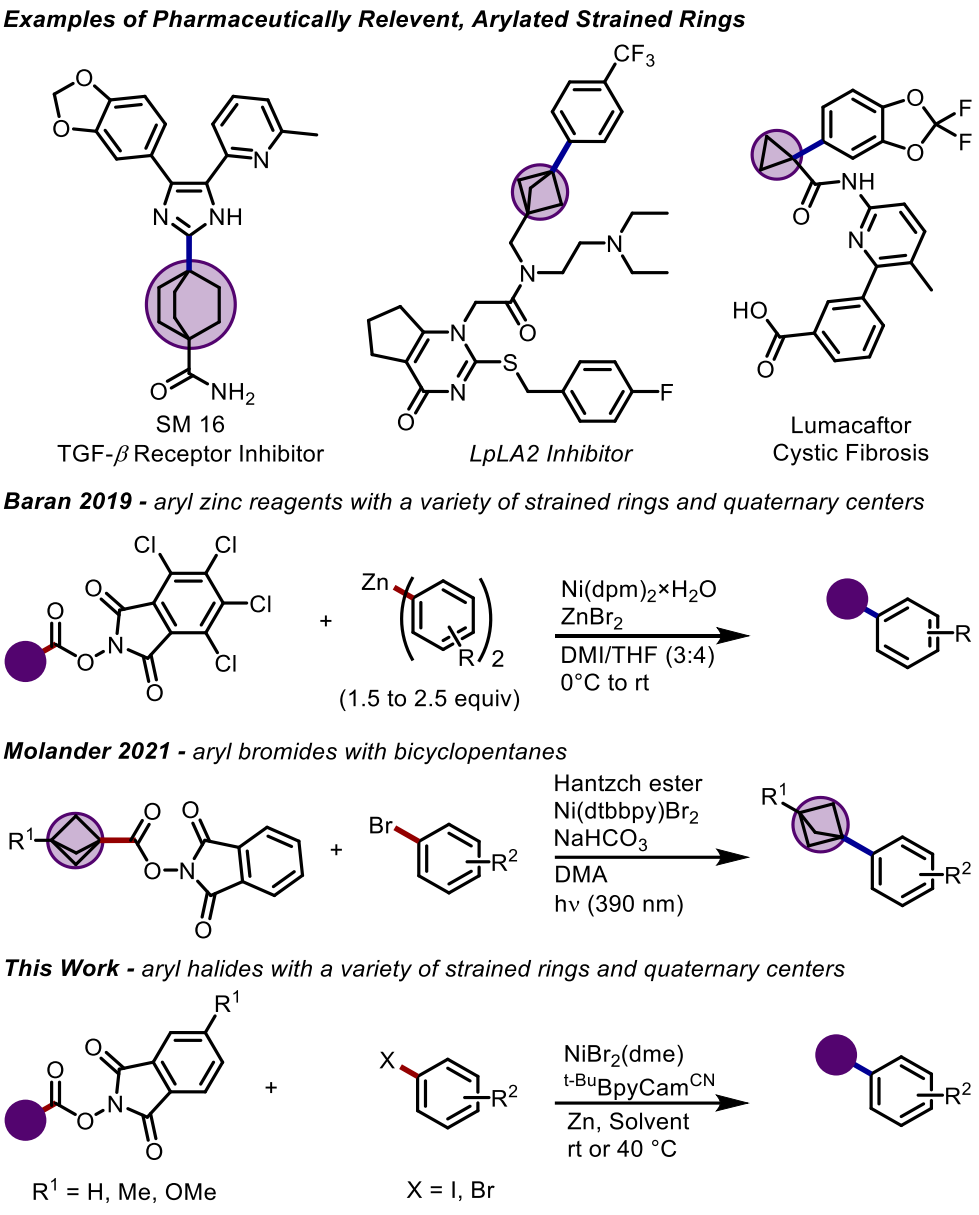

In order to develop a general cross-electrophile coupling of aryl halides with a variety of strained-ring NHP esters, we had to address two major challenges. First, formation of all-carbon quaternary centers by cross-electrophile coupling remains challenging [64,65,66,67,68,69,70,71,72] and a limited number of catalysts are reported to be effective. For tertiary radicals of strained rings, which have different catalyst requirements than unstrained tertiary

radicals,[73,74,75] 2,2′-bipyridine, dtbbpy (**L3.1**), 4,4′-dicarboxymethyl-2,2′-bipyridine (**L3.2**), bathophenanthroline (**L3.4**), as well as substituted pyridines and diketonate ligands have been reported to be effective for aryl[47,62,63,65-70] and acyl[76,77,78] coupling partners. We viewed the identification of additional catalysts as crucial to finding conditions suitable for a wide array of coupling partners. Second, cross-electrophile coupling can be challenging if the relative reactivity of the two substrates and intermediary steps are poorly matched.[79,80,81] While tuning the reactivity of alkyl halide radical donors by halide choice (iodide, bromide, chloride) or in-situ exchange is broadly useful, few analogous tools for NHP esters exist. Baran and co-workers found that tetrachloro-NHP esters are significantly more reactive and provided higher yields in cross-coupling using aryl metal reagents.[47] Because NHP esters are already more reactive than alkyl iodides,[50,51,52] methods to decrease the reactivity of NHP esters to the level of alkyl bromides would be helpful in allowing productive cross-electrophile coupling by better matching the rate of radical generation with oxidative addition. *In theory, NHP esters could allow a degree of fine-tuning not possible with alkyl halides*.

3.2 Results and Discussion

Initial screens began by investigating bidentate pyridine-type ligands (**L3.1**–**L3.4**) as these have been shown to support to nickel-catalyzed cross-electrophile coupling reactions and have been utilized in other reactions with NHP esters (

Table 3.1).[50,51,52,53,54,55,82] Informed by this precedent, we found that several of these ligands, as well as previously reported pyridinecarboxamidine ligands (**L3.5**–**L3.6**),[83,84] were effective at promoting the formation of **3.3** (entries **1,4** and **6**, ligands **L3.1**, **L3.4,** and **L3.6**). However, a new ligand recently reported by our lab,[85] 4,4′-di-*tert*-butyl-6-*N*-cyanocarboxamidine-2,2′-bipyridine ($^{t\text{-Bu}}$BpyCam^{CN}, **L3.7**) promoted the desired reaction with

higher yield due to increased selectivity for the cross-coupled product over alkyl and aryl dimerization reactions. Both a reductant and nickel catalyst are required, and performing the reaction in the absence of a ligand leads to poor selectivity and an overall diminished yield (entries **9**–**11**).

Table 3.1: Optimization of the reaction conditions for coupling with Ar-I.

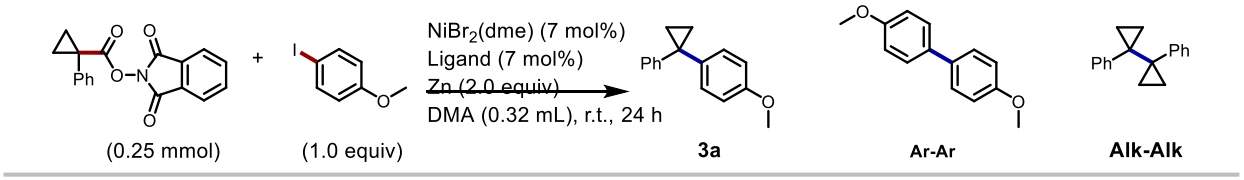

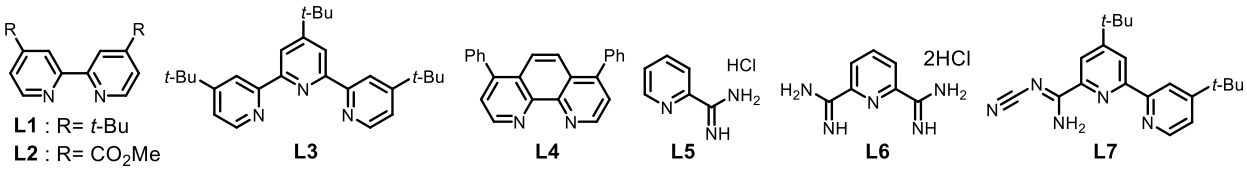

Entry[a]	Variation	**3.3** Yield (%)[b]	**Ar-Ar** Yield (%)[b]	**Alk-Alk** Yield (%)[b]
1[c]	**L3.1**	48	11	20
2[c]	**L3.2**	25	37	0
3[c]	**L3.3**	21	11	25
4[c]	**L3.4**	75	11	0
5[c]	**L3.5**	35	7	30
6[c]	**L3.6**	78	0	0
7[c]	**L3.7** ($^{t\text{-Bu}}$BpyCam^{CN})	92	0	0
8[d]	**L3.7**, Mn as reductant	4	0	1
9[d]	no ligand	21	2	3
10[d]	no nickel, no ligand	0	0	0
11[d]	**L3.7**, no Zn reductant	0	0	0
12[c]	**L3.7**, THF as solvent	72	0	0

[a] A mixture of NHP ester (0.25 mmol), aryl iodide (0.25 mmol), NiBr2(dme) (7 mol%), ligand (7 mol%), and Zn (0.5 mmol) was stirred at r.t. for 24 h. [b] Corrected GC yield.[c]Remaining mass balance corresponds to formation of cyclopropylbenzene and anisole. [d] Remaining mass balance corresponds to recovered starting material.

Applying the optimized conditions to a variety of different carboxylic acid and aryl halide pairs (**Figure 3.2**) demonstrated the utility of this method for the synthesis of diaryl cyclopropanes, a useful replacement for 1,1-diarylalkenes and diarylmethanes.[36,86,87,88] Optimized conditions employ a 1:1 stoichiometry of NHP ester and (hetero)aryl halide and a typical catalyst loading of 7 mol%, although increasing the catalyst loading to 20 mol% led to improved yields in some cases (**3.23, 3.24, 3.26**, **3.27**, **3.28**, **3.29**, **3.35**, **3.37**, **3.39**). A variety of arene-based functionalities that enable subsequent elaboration, such as nitriles (**3.6**), chlorides (**3.13**, **3.20**, **3.33**), esters (**3.17**, **3.18**, **3.22**), and pinacol boronate esters (**3.8**) were tolerated. Notably, an aryl iodide bearing a substituent in the *ortho* position (**3.9**) was coupled more efficiently when bidentate **L3.4** was employed, possibly stemming from increased steric hinderance around the reactive center. Less reactive aryl coupling partners such as aryl bromides (**3.3**, **3.4**, **3.5**, **3.6**) and heteroaryl bromides (**3.17**, **3.18**, **3.19**, **3.20**, **3.21**, **3.22**) can also engage in the cross-coupling reaction by changing the reaction solvent to THF and elevating the temperature. Coupling can be achieved at the 2-, 3-, and 4- position of pyridine and pyridine-like heterocycles (**3.17**, **3.18**, **3.19**, **3.20**, **3.21**, **3.22**). Aryl halides derived from pyrazole, azaindole, and indazole heterocycles can also be coupled in good yields (**3.10**, **3.26**, **3.27**, **3.28**, **3.39**). For rapid syntheses of analogues, carboxylic acids can be converted to the NHP ester and coupled in one pot to form **3.3**, albeit with decreased yield (From 75% with the isolated NHP ester to 56% with in situ generated NHP ester).

One potential advantage of this approach is that 1,1-diarylcyclopropanes can be synthesized in a modular fashion from two different aryl halides and cyclopropane carboxylic acid using α-arylation and decarboxylative cross-electrophile coupling. Using a-arylation conditions recently reported by Hartwig,[89] we were able to rapidly synthesize several

alternative NHP esters. Changing the arene of benzylic cyclopropyl NHP esters was well tolerated (**3.12**, **3.13**, **3.14**, **3.15**, **3.16**). We demonstrate the utility of this approach for the flexible construction of drug-like molecules through the preparation of the methyl ester of LG100268 **3.22**, a more potent and specific cyclopropyl analogue of the only FDA-approved RXR agonist Bexarotene.[90,91,92] The advantage of this new approach is that it allows for facile modification of the right-side arene, providing a route for the synthesis of a library of analogues from commercially available aryl halides.

Figure 3.2: Substrate scope for the decarboxylative coupling of strained-ring NHP esters with (hetero)aryl halides.[a]

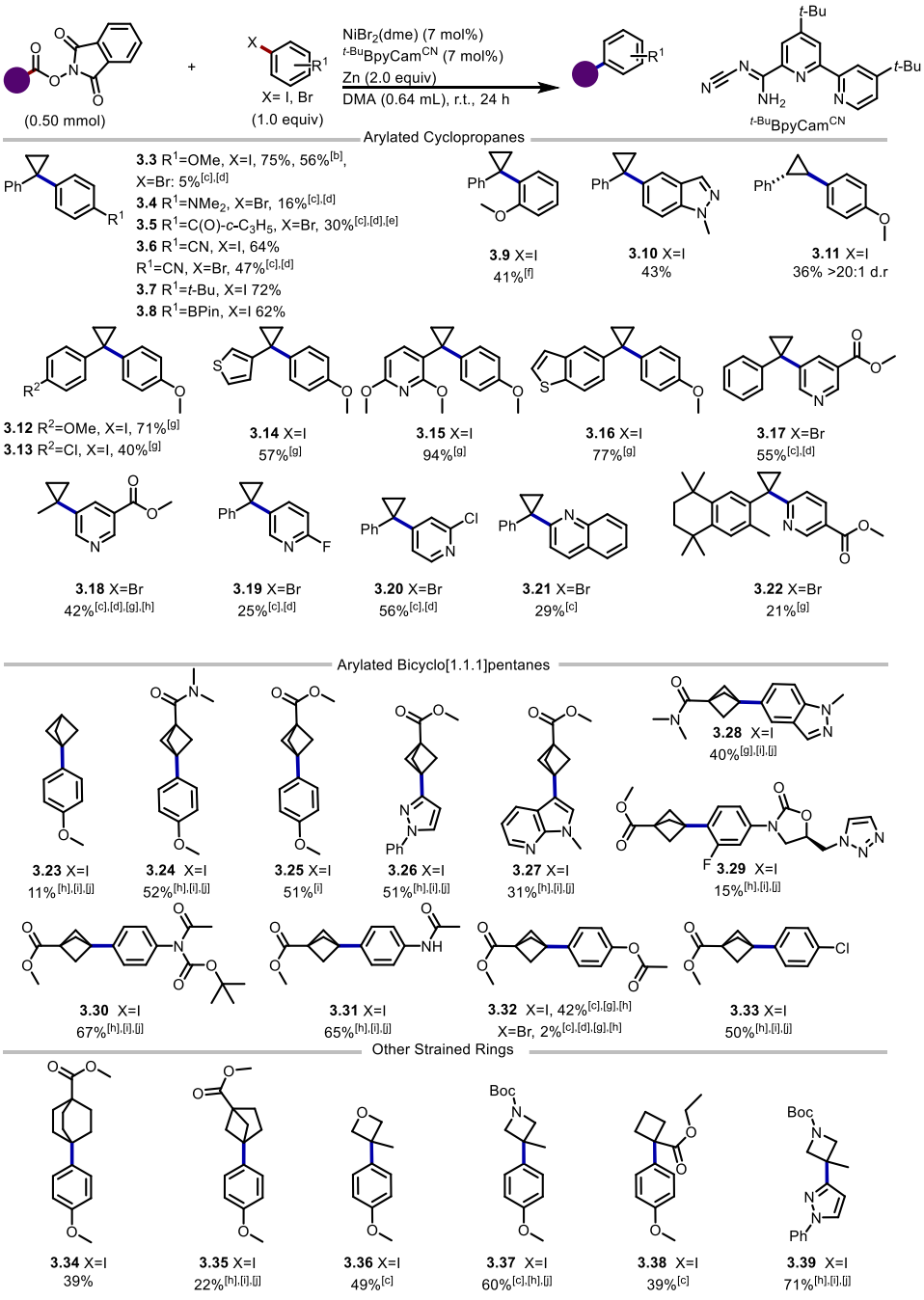

[a] Reactions were performed at a 0.5 mmol scale in 0.64 mL of DMA for 24 h. Yields are isolated yields after purification. [b] NHP ester was generated in situ. [c] Reaction was carried out in THF. [d] Reaction was carried out at 40 °C. [e] Bathophenanthroline (L4) was used as the ligand. [f] Reaction was carried out at 0.25 mmol scale. [g] Reaction was carried out with 20 mol% nickel and ligand. [h] Reaction was carried out in a 9:1 mixture of THF:DMA. [i] Reaction was carried out at 0.300 mmol scale.

A variety of other strained-ring carboxylic acid NHP esters are compatible with these conditions. Non-benzylic secondary and tertiary strained ring NHP esters (**Figure 3.2**, **3.11**, **3.18**) are tolerated under these conditions but are lower yielding, presumably due to the lower stability of the corresponding radicals. Notably, carboxylic acids bearing additional ester functionality can be successfully coupled, providing an easy entry for sequential arylation of bicyclo[1.1.1]pentane, bicyclo[2.2.2]octane, bicyclo[2.1.1]hexane, and cyclobutane ring systems (**3.25**, **3.34**, **3.35, 3.36)**. Other pharmaceutically relevant ring systems such as the NHP esters derived from bicyclo[1.1.1]pentane (**3.23-3.33**), bicyclo[2.2.2]octane (**3.34**), bicyclo[2.1.1]hexane (**3.35**), oxetane (**3.36**), azetidine (**3.37**, **3.39**), and, cyclobutane(**3.38**) ring systems were also coupled in good yield.[93]

This approach appears more general than and is complementary to other reported methods. Compared to reactions with arylzinc reagents, these conditions tolerate acidic N-H bonds (e.g., **3.31**) and avoid the use of super-stoichiometric amounts of coupling partners (3–5 equiv).[47] Moreover, in some cases our yields with bicyclo[1.1.1]pentane carboxylic acid NHP esters and aryl iodides were superior to the best yields reported under photochemical conditions with aryl bromides (**3.30**, 67% vs 24%; **3.32**, 42% vs 31%; **3.33**, 50% vs 33%; no aryl iodide couplings were reported in the previous study).[62] However, the coupling to form **3.32** from the corresponding aryl bromide was low-yielding (2%). The chemistry can be scaled in batch (3 mmol, 63% yield of **3.3**; See section **3.4.4.2.4**) or in flow using the zinc packed-bed strategy of Ley (tr = 45 min, 51% yield of **3.25**; Figure 1). [116]

Figure 3.3: Synthesis of **3.25** under continuous flow.

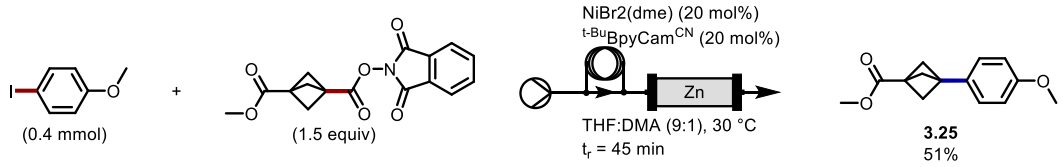

While exploring the scope with more challenging couplings we observed a mismatch in the reactivity of NHP esters and aryl bromides, often resulting in full conversion of the NHP ester and only partial conversion of the aryl bromide. We envisioned that altering the reduction potential of redox-active esters would enable us to tune their rate of consumption, thereby providing a new avenue to control the selectivity profile of this coupling. Our group has recently explored the use of modified NHP esters in couplings with alkyl halides, but the reason for their improved reactivity had not been determined.[94] We have found that a combination of solvent effects and NHP ester tuning can improve yields with aryl bromides by slowing the rate of radical generation (**Figure 3.4**). Methyl and methoxy-substituted NHP (^{Me}NHP and ^{MeO}NHP) esters are more difficult to reduce (shifts in E_p of 10-50 mV, **Figure 3.4** and **Figure 3.8**-**Figure 3.10**) and are consumed more slowly under reducing conditions (0.1 equiv $ZnBr_2$ with Zn reductant, **Table 3.2**).[95] In addition, we found that the time to complete consumption of the NHP ester by $ZnBr_2/Zn^0$ varied with the solvent (10 h in DMA, 17 h in 1:1 DMA/THF, >30 h in THF, **Table 3.2**).

Table 3.2: Effect of substitution and solvent on NHP ester consumption

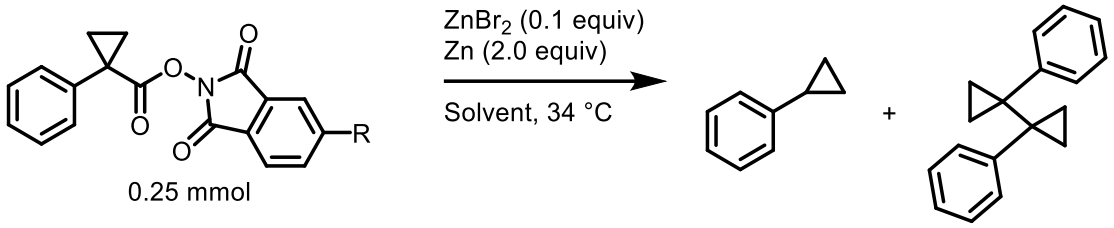

Entry	Substituent	Solvent	Time to full consumption of RAE[a]
1	R=H	DMA	10 h
2	R=Me	DMA	16 h
3	R=OMe	DMA	24 h
4	R=H	DMA	9 h
5	R=H	DMA/THF 1:1	18 h
6	R=H	THF	>30 h

[a] RAE consumption determined by SFC-MS analysis

These effects are complementary, *allowing fine-tuning of radical generation rates and significant improvements in yields* (up to 7× improvement in yield for **3.3**) for the coupling of both electron-rich and electron-deficient aryl bromides (**Figure 3.4**). Consistent with the hypothesis that better yields are obtained with esters that are more difficult to reduce, the use of redox active esters that are more easily reduced than NHP (TCNHP ester **Figure 3.12** and *N*-hydroxynaphthalimide ester **Figure 3.11**) led to a significant drop in yield (**Figure 3.4**). This ester-tuning strategy was also effective for improving reactions with challenging alkyl fragments that were more likely to participate in deleterious side reactions. Simply employing the ^{MeO}NHP ester in place of the NHP ester led to the formation of **3.24, 3.32,** and **3.36** in improved yields (31%, 9%, and 6% improvements respectively). Additionally, an aryl bromide derived from Loratadine could be coupled to form **3.40** using the ^{Me}NHP ester.

Figure 3.4: Electronic tuning of NHP esters enables improved yields with Ar-Br.

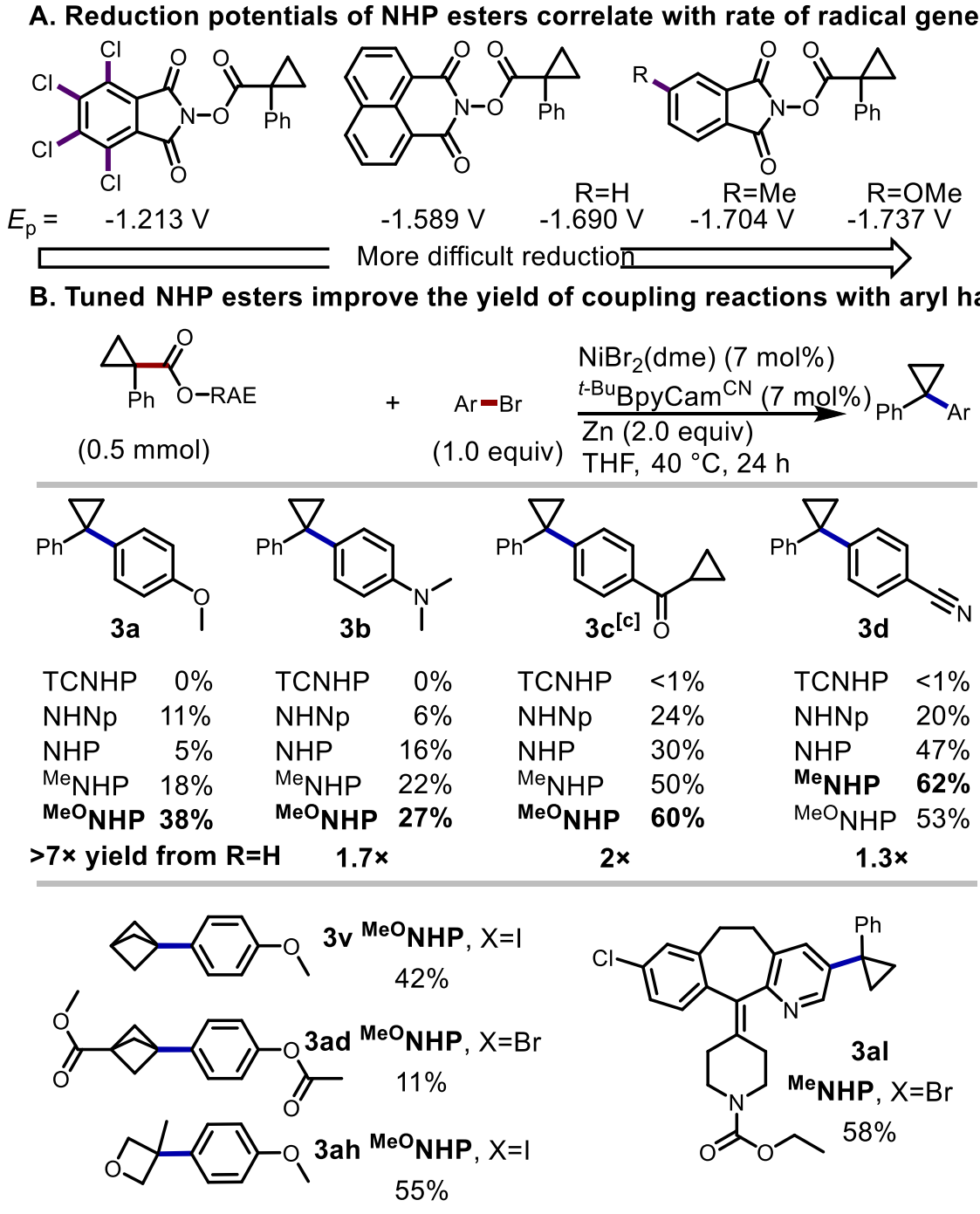

[a] Cathodic peak potentials vs Fc+/Fc. Radical generation from 0.1 equiv ZnBr2 with Zn reductant. See Supporting Information Figures S2-S5. [b] As in Scheme 2. Yields are isolated

yields after purification. TCNHP =N-hydroxytetrachlorophthalimide ester, NHNp= N-hydroxynapthalimide ester.

High throughput experimentation (HTE) methods are often used in medicinal chemistry to quickly synthesize small collections of molecules to explore structure activity relationships. We were able to adapt strained-ring cross-electrophile coupling to a 96-well plate format at 10 μmol scale using ChemBeads (**Figure 3.5**).[96,97] As a representative case, NHP esters of *N*-Boc-3-methylazetidine-3-carboxylic acid were coupled to each position of 1-methylindazole (**ArBr1**-**ArBr5**). To explore how ligand, solvent, and NHP ester can be used to tune reactivity, we examined three different ligands (dtbbpy **L1**, Bphen **L4**, $^{t\text{-}Bu}$BpyCam^{CN} **L7**), three different NHP esters (R = H, Me, OMe), and two different solvent regimes (1:1 THF/DMA and THF). These results make two important points. First, a single set of conditions is sufficient for initial screens: methyl NHP esters in THF with **L3.7** or **L3.4** provided usable results for all five products. Second, yields can be improved dramatically by adjusting the NHP ester, solvent, and ligand used. For example, while **L3.4** performed well in this series with methyl NHP esters in THF (best yields on the plate for **ArBr1**, **ArBr2**, **ArBr3**), the yield with **ArBr4** could be more than doubled by switching to **L3.7**, changing the solvent to THF/DMA, or by using an NHP ester. Finally, **L3.4** and **L3.7** performed about equally in this series and exhibited complementary reactivity to each other. **L3.1**, while common in cross-electrophile coupling, provided lower yields overall. In a similar small-scale optimization screen, we found that NHP ester substitution and choice of ligand were key to improving yields (**Table 3.3**).

Figure 3.5: HTE format coupling of NHP esters with bromoindazoles.[a]

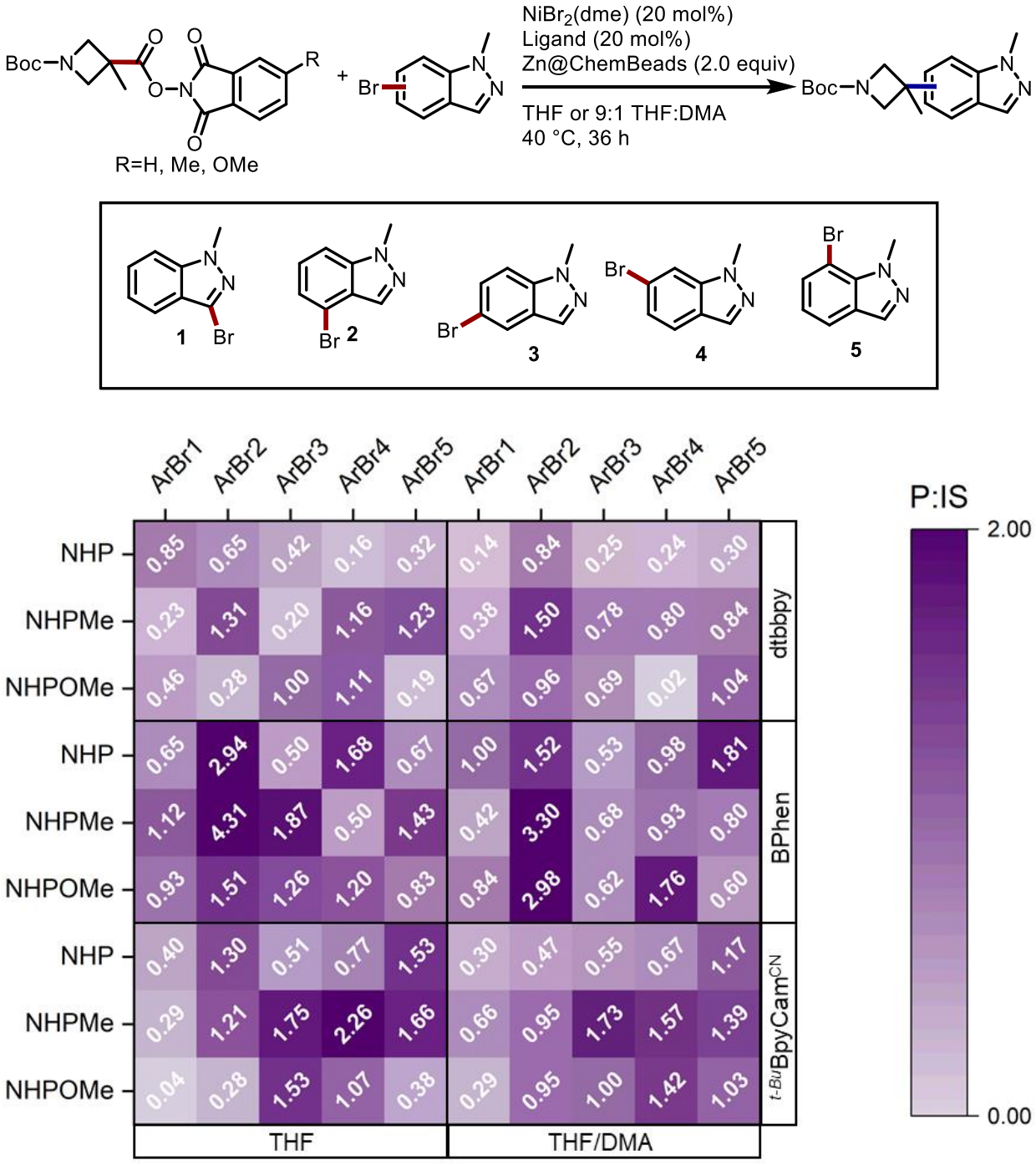

[a]Reactions run at 10 μmol scale. Assay yields are raw product/internal standard (UV) ratios vs 1,3,5-trimethoxybenzene. Note: comparisons of P/IS are only valid among the same aryl halide.

For small-scale screening campaigns, we recommend the following approach. Although ^{Me}NHP and ^{MeO}NHP esters often outperform NHP esters, NHP esters are sufficient for initial screens if they are more convenient (due to cost, availability for other reaction types). For couplings with aryl iodides, start with standard NHP esters, ligand **L3.7** (or **L3.4** if **L3.7** is unavailable), 20 mol% catalyst loading, and 9:1 THF:DMA mixture (additional DMA if needed for solubility considerations). For aryl bromides, if available, ^{Me}NHP esters are an optimal starting point (although NHP esters often still give product). THF (or a mixture of THF and DMA) should be used as the solvent, and these reactions may need to be run at elevated temperatures (40 °C). If the initial conditions do not provide sufficient yields, then an evaluation of the side products can point to optimization strategies: accelerate or slow radical formation using solvent and NHP ester tuning to balance reactivity with the aryl halide. Reactions that consume aryl halide before NHP ester need more polar solvents and more reactive NHP esters. Reactions that consume NHP ester before aryl halide need less polar solvents and less reactive NHP esters. Finally, **Figure 3.5** shows that a ligand screen could provide improved results. We note that a broader ligand screen that includes low-performing ligands from

Table 3.1 could be helpful.[96,97]

Table 3.3: HTE format coupling of NHP esters with informer library compound X5.[a]

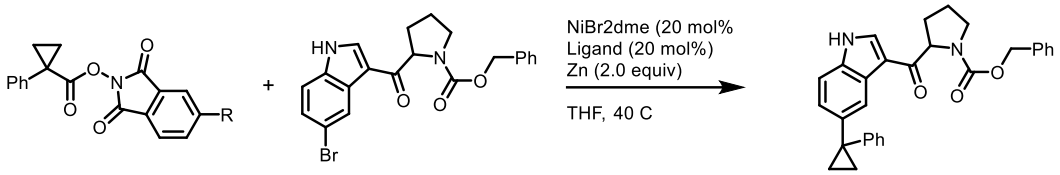

	$^{t\text{-bu}}$BpyCam^{CN} (L3.7)	Dtbbpy (L3.1)	PyBCam (L3.6)	Bphen (L3.4)	PyCam^{CN} (L3.8)
R=H	7.96	0.82	2.06	0.30	0.46
R=Me	10.27	0.14	2.05	0.61	0.85
R=OMe	0.63	0.36	0.42	0.39	0.40

[a]Reactions run at 10 μmol scale. Assay yields are raw product/internal standard (UV) ratios vs 1,3,5-trimethoxybenzene.

Whereas *N*-cyano carboxamidine ligands like **L3.7** have proven increasingly useful in cross-electrophile coupling,[83,84,85] no structural characterization of their nickel complexes has been reported. Ben Chi was able to synthesize Ni(**L3.7**)(*o*-tol) by reaction of the free ligand with *trans*-$(Ph_3P)_2$Ni(*o*-tol)Br. A single-crystal X-ray diffraction analysis revealed that Ni(**L3.7**)(*o*-tol) crystallizes as a solvate with two symmetry-independent Ni complexes in the asymmetric unit (**Figure 3.6**).[98] The complexes have similar geometries and both display positional disorder of the *o*-tolyl ligand. Disregarding the minor disorder components, the Ni coordination environment in this neutral metal complex is distorted square planar with the *cis* L–Ni–L angles ranging between 81.99(10)–95.3(7)°. The $^{t\text{-Bu}}$BpyCam^{CN} ligand binds in a tridentate fashion with the *o*-tolyl occupying the fourth coordination site. The Ni–N distances range between 1.857(2)–1.919(2) Å with the Ni1–N1 distance being ~0.052(10) Å longer than the other Ni–N distances. These bond lengths fall in the expected range and are not statistically

significantly different from 1.90(3) Å, the value obtained by averaging the Ni–N distances in five relevant nickel terpyridyl complexes reported to the Cambridge Structural Database.[99] The Ni–C distances in Ni(**L7**)(*o*-tol) measure av. 1.900(4) Å and are in excellent agreement with the averaged value of 1.89(3) Å calculated for the Ni–C distances in the same complexes.

Figure 3.6: Solid-state X-ray structure of (L7)Ni(o-tol) at 50% probability ellipsoids. Relevant bond lengths and bond angles are tabulated below. See Section **3.4.6** for more information.

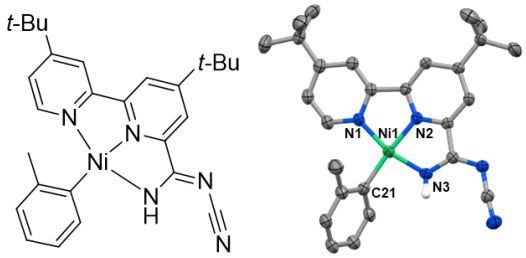

Atoms	Bond Length (Å)	Atoms	Bond Angle (°)
Ni1-N1	1.919(2)	*N1-Ni1-N2*	82.10(10)
Ni1-N2	1.857(2)	*N2-Ni1-N3*	81.99(10)
Ni1-N3	1.874(2)	*N3-Ni1-C21*	92.67(14)
Ni1-C21	1.901(4)	*C21-Ni1-N1*	94.8(4)

The most notable aspects of this structure are the finding that **L3.7** binds as a monoanionic ligand bound via the unsubstituted nitrogen of the amidinate, reminiscent of the ligand employed in recent work by Sevov.[100,101] Molander and Gutierrez have studied how LX and L2 ligands can result in different mechanisms and substrate scope in coupling reactions with tertiary radicals.[75] Further mechanistic studies will be needed to see if related changes in mechanism occur in cross-electrophile coupling reactions with L2X ligands like $^{t\text{-}Bu}$BpyCam^{CN}

(**L3.7**) and L2 ligands like Bphen (**L3.4**) and how ligands with such different coordination environments display such a large overlap in substrate scope. These findings are in agreement with recent work by Sevov and co-workers where both L2 and L2X ligands display similar efficiency in cross-electrophile coupling reactions.[100,101]

Although we have yet to study the mechanism of this reaction in detail, similarities to other cross-electrophile couplings with NHP esters and aryl halides suggest an analogous mechanism: (a) initial oxidative addition of the aryl halide to nickel(0) followed by oxidative radical capture by the resulting arylnickel(II) intermediate. Recent studies by the MacMillan group suggest that stoichiometric equivalents of phthalimide can stabilize arylnickel(II), however at this time we are unsure to what extent phthalimide derivatives have the same effect.[102] Reductive elimination from the resulting bisorgano-nickel(III) species gives the desired product with concomitant formation of a nickel(I) intermediate. The formation of radicals from NHP esters can be mediated by nickel or arise from direct reduction with zinc, assisted by Lewis acid coordination to the NHP ester. Under cross coupling conditions, the NHP ester is fully consumed more quickly than with $ZnBr_2/Zn^0$ alone (<1.5 h vs <10 h), suggesting that the nickel catalyst is also capable of reducing the redox-active esters.

3.3 Conclusions

In conclusion, we have expanded the scope of decarboxylative $C(sp^3)$–$C(sp^2)$ cross-electrophile coupling to include seven different classes of pharmaceutically-relevant strained rings and achieved coupling of NHP esters with (hetero)aryl bromides and iodides. *The generality of this approach with respect to strained-rings is the widest yet reported for decarboxylative coupling reactions with aryl reagents of any kind, including arylmetal reagents*. Two of these ring systems have never been coupled with aryl halides: arylated bicyclo[2.1.1]hexanes have only been synthesized via intramolecular photochemical

cyclizations[103,104] and bicyclo[2.2.2]octane rings have only been coupled to arylzinc reagents.47 Additionally, 1,1-diarylcyclopropanes have not been previously synthesized via a cross-electrophile coupling approach. This chemistry is enabled by a new ligand ($^{t\text{-Bu}}$BpyCam^{CN}) that promotes cross-selective coupling, and the tuning of NHP ester reactivity by altering the substituents on the phthalimide backbone and the reaction solvent. We envision that further ligand design and NHP ester tuning will enable the use of even less reactive coupling partners in the future, expanding the utility of redox active esters as a tool for C–C bond formation. We note that, while this manuscript was in review, the Baran group in collaboration with several pharmaceutical companies reported a complementary approach to tuning NHP ester reactivity under electrochemical conditions by doping the nickel cathode with silver;[105] we imagine that combining new ligands, tuned NHP esters, and electrochemistry could be particularly fruitful.

3.4 Experimental

3.4.1 General Information

Reagents

Metals

All metal catalysts and metal reductants, unless otherwise noted, were stored and handled in a nitrogen-filled glovebox. Nickel(II) bromide ethylene glycol dimethyl ether complex ($NiBr_2$(dme)) was purchased from Millipore Sigma and used as received. The reductant used was zinc flake, -325 mesh, 97% (Alfa Aesar). We observed no difference in reactivity between zinc flake and zinc dust.

Ligands

Pyridyl carboxamidine ligands were synthesized according to literature procedures. All other ligands were purchased from commercial suppliers and used without purification.

Substrates

Cyclopropyl carboxylic acids were synthesized from the corresponding *t*-Bu esters (**SI-1** – **SI-3**) prepared according to a literature procedure.[1] All other carboxylic acids were purchased from commercial suppliers.

Solvents

Tetrahydrofuran (THF) and dichloromethane (DCM) were purified by passage though activated alumina and molecular sieves in a solvent purification system (Inert Corporation) and stored in a nitrogen-filled glovebox. Anhydrous dimethylacetamide (DMA) was purchased from Millipore Sigma, stored in a glovebox, and used as received.

Other Reagents

All starting materials were purchased from commercial suppliers and used without purification unless otherwise indicated.

3.4.2 Methods

NMR Spectroscopy

UW-Madison:^{1}H and ^{13}C-NMR spectra were acquired on a 500 MHz Avance spectrometer equipped with a DCH cryoprobe (Bruker), at a sample temperature of 25 °C. NMR spectra were recorded with TopSpin 3.5.6 (Bruker).

Janssen: 500 MHz: ^{1}H NMR spectra were recorded on a Bruker Avance Neo NMR spectrometer operating at 500.13 MHz for ^{1}H with the following spectral parameters: acquisition time = 4 s, number of scans = 16, number of data points = 32 K and spectral width = 8197 Hz. ^{13}C NMR spectra were taken on the same instrument operating at 125.758 MHz for ^{13}C with the following spectral parameters: acquisition time = 1.1 s, number of scans = 2048, number of data points = 32K and spectral width = 30120 Hz. ^{19}F spectra were collected operating at 470.592 MHz for ^{19}F using acquisition time = 0.58 s, number of scans = 16, number of data points = 65K and spectral width = 113636 Hz. Measurements were made using 5 mm tubes in a BBFO probe.

600 MHz: ^{1}H NMR spectra were recorded on a Bruker Avance Neo NMR spectrometer operating at 500.13 MHz for ^{1}H with the following spectral parameters: acquisition time = 2.6 s, number of scans = 1, number of data points = 32 K and spectral width = 12500 Hz. ^{13}C NMR spectra were taken on the same instrument operating at 150.903 MHz for ^{13}C with the following spectral parameters: acquisition time = 0.92 s, number of scans = 512, number of data points = 32K and spectral width = 35713 Hz. ^{19}F spectra were collected operating at 564.686 MHz for

^{19}F using acquisition time = 0.5 s, number of scans = 4, number of data points = 65K and spectral width = 131579 Hz. Measurements were made using 5 mm tubes in a Prodigy Nitrogen cooled BBO cryoprobe.

Referencing and absolute referencing to TMS, apodization, Fourier transform, phase and baseline corrections, and spectral analyses were carried out with MestReNova 12.0.4 (Mestrelab Research). NMR chemical shifts are reported in ppm and are referenced to TMS (δ = 0.00 ppm). Coupling constants (J) are reported in Hz.

Gas Chromatography (GC)

GC analyses were performed on an Agilent 7890A GC equipped with dual DB-5 columns (20 m × 180 µm × 0.18 µm), dual FID detectors, and hydrogen as the carrier gas. A sample volume of 1 µL was injected at a temperature of 300 °C and a 100:1 split ratio. The initial inlet pressure was 20.3 psi but varied as the column flow was held constant at 1.8 mL/min for the duration of the run. The initial oven temperature of 50 °C was held for 0.46 min followed by a temperature ramp of 65 °C/min up to 300 °C. The total run time was 5.0 min and the FID temperature was 325 °C.

GC/MS Analysis

GC/MS analyses were performed on a Shimadzu GCMS-QP2010 equipped with an RTX-5MS column (30 m × 0.25 mm × 0.25 µm) with a quadrupole mass analyzer using helium as the carrier gas or with an Agilent 5977A GC/MSD using MassWorkds 4.0 from CERNO bioscience. The analysis method used in all cases was 1 µL injection of sample, an injection temp of 250 °C, and a 20:1 split ratio. The initial inlet pressure was 8.1 psi, but varied as the column flow was held constant at 1.0 mL/min for the duration of the run. The interface temperature was held

at 275 °C, and the ion source (EI^+, 30 eV) was held at 200 °C. The initial oven temperature was held at 60 °C for 1 min with the detector off, followed by a temperature ramp, with the detector on, to 300 °C at 20 °C/min. Total run time was 13.00 min.

Supercritical Fluid Chromatography Mass Spectrometry (SFC/MS)

SFC/MS analyses were performed on a Waters ACQUITY UPC^2 equipped with ACQUITY UPC^2 PDA and ACQUITY QDa Detector. A Daicel Dcpack SFC-A column (3 mm ID × 150 mm L, 3 µm PS) was used for separations. The eluent was a mixture (97:3 CO_2/MeOH) with a flow rate of 2 mL/min at 40 °C with a ABPR at 1500 psi. We are grateful to Joe Barendt and Chiral Technologies for the donation of the SFC-A column used in this work.

Liquid Chromatography Mass Spectrometry (LC/MS)

UW-Madison: UPLC-MS analyses were performed on a Waters Acquity UHPLC using a BEH-C18 column (1.7 µm, 2.1 x 50 mm) with an Acquity QDA MS detector. MPA: 0.05% TFA in H_2O; MPB: 100% ACN, starts from 1% B to 40% B for 0.5 minutes, then hold for 1.25 minutes, then increase to 65% B for 0.5 min, then hold for 1.1 minutes, then increase to 95% B over 0.15 minutes.

Janssen: Analytical LCMS was obtained on an Agilent 1200 Series using an ACE-C18 column (3µm, 3.0 x 50 mm, T=50°C). MPA: 0.05% TFA in H_2O; MPB: 100% ACN, Gradient method starts from 5% B to 100% B in 2.3 mins at a flow rate of 2.0 mL/min. MS detector is an Agilent G6125B API-ESI set in positive mode.

Infrared Spectroscopy

ATR-FTIR spectroscopy data was obtained using a Jasco FT/IR-4700 instrument.

Chromatography

Chromatography was performed on silica gel (EMD, silica gel 60, particle size 0.040-0.063 mm) using standard flash techniques, on a Teledyne Isco CombiFlash instrument using pre-packaged cartidges, on a Teledyne Isco Rf-200 (detection at 210 nm and 280 nm), or on a Biotage Isolera One (detection at 210 nm and 400 nm, on Sfar Duo columns). Products were visualized by UV, PMA stain, or fractions were analyzed by GC. Purifications using an HPLC were performed using a Teledyne ACCQ Prep HPLC system using an XBridge C18 column (5 μm, 100×50 mm), mobile phase of 5-100% ACN in 20 mM NH4OH over 17 min and then hold at 100% ACN for 3 min, at a flow rate of 80 mL/min.

Elemental Analysis

Elemental analyses were performed by CENTC Elemental Analysis Facility at University of Rochester, funded by NSF CHE-0650456.

High Resolution Mass Spectrometry

UW-Madison: High resolution mass spectra (HRMS) Mass spectrometry data was collected on a Thermo Q Exactive™ Plus (thermofisher.com) via flow injection with electrosprayionization or via ASAPMS™ (asap -ms.com) by the chemistry mass spectrometry facility at the University of Wisconsin – Madison. The purchase of the Thermo Q Exactive Plus in 2015 was funded by NIH Award 1S10 OD020022 to the Department of Chemistry

Janssen: High-resolution mass spectra (HRMS) were measured on an Agilent Technologies 6200 series mass spectrometer using electrospray ionization (ESI) time-of-flight (TOF) or on an Agilent 5975C GC/MSD (EI) using MassWorks 4.0 from CERNO bioscience.

Flow Chemistry Equipment

Flow chemistry was performed on a Vapourtec R2+R4 instrument.

3.4.3 Supplemental Data

Figure 3.7: Commercial Availability of Strained Ring-Containing Building Blocks.[a]

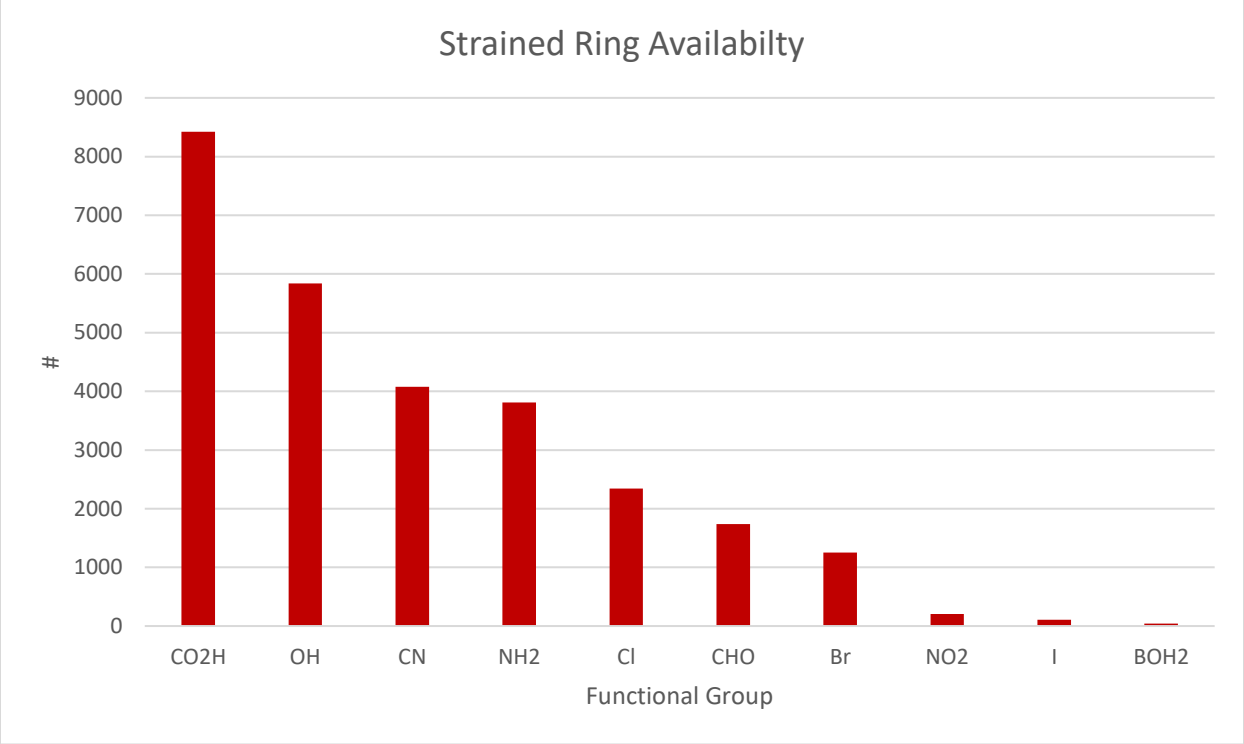

[a]3 and 4 membered carbocycle and heterocycle substrate commercial availability (Reaxys) as of November, 2021.

3.4.3.1 Cyclic Voltammograms of Substituted NHP Esters

[a]Cyclic voltammetry was performed using a NuVant EZStatPro Potentiostat at a sweep rate of 100 mV/s. Solutions were made to contain 5 mM of the analyte and 100 mM Bu_4NPF_6 in DMF. The sample was prepared in a vial equipped with a glassy carbon disk working electrode (3 mm diameter, purchased from BASi), Pt wire counter electrode (purchased from BASi) and a

Ag/AgCl reference electrode in 3 M NaCl (purchased from BASi). Before data collection, each solution was sparged vigorously with nitrogen for 10 minutes. The reversible peak following reduction of the NHP esters is consistent with the reduction of benzyl radicals to benzyl anions.[106]

Figure 3.8: Cyclic Voltammogram of 1,3-dioxoisoindolin-2-yl 1-phenylcyclopropane-1-carboxylate

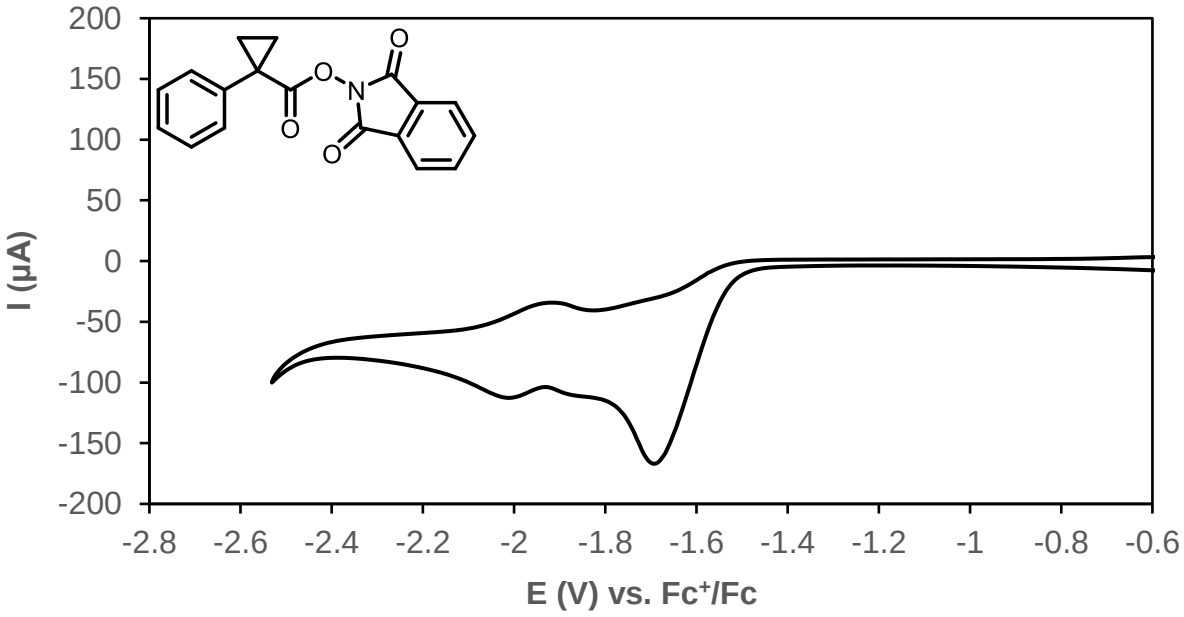

E_p=-1.690 vs Fc^+/Fc

Figure 3.9: Cyclic Voltammogram of 5-methyl-1,3-dioxoisoindolin-2-yl 1-phenylcyclopropane-1-carboxylate

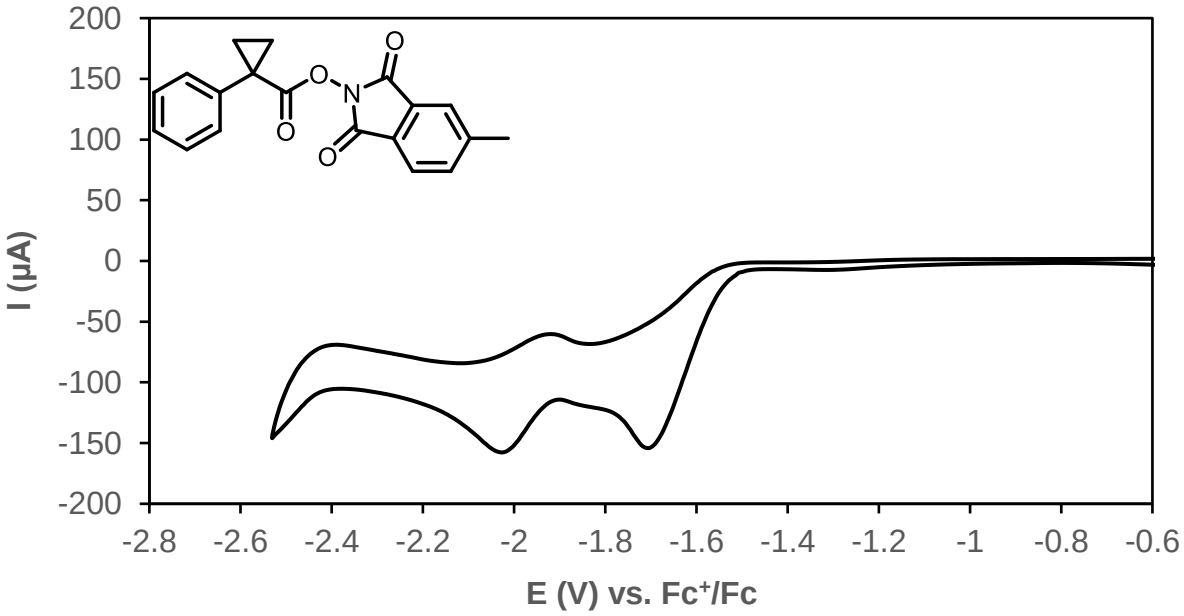

E_p=-1.704 vs Fc^+/Fc

Figure 3.10: Cyclic Voltammogram of 5-methoxy-1,3-dioxoisoindolin-2-yl 1-phenylcyclopropane-1-carboxylate

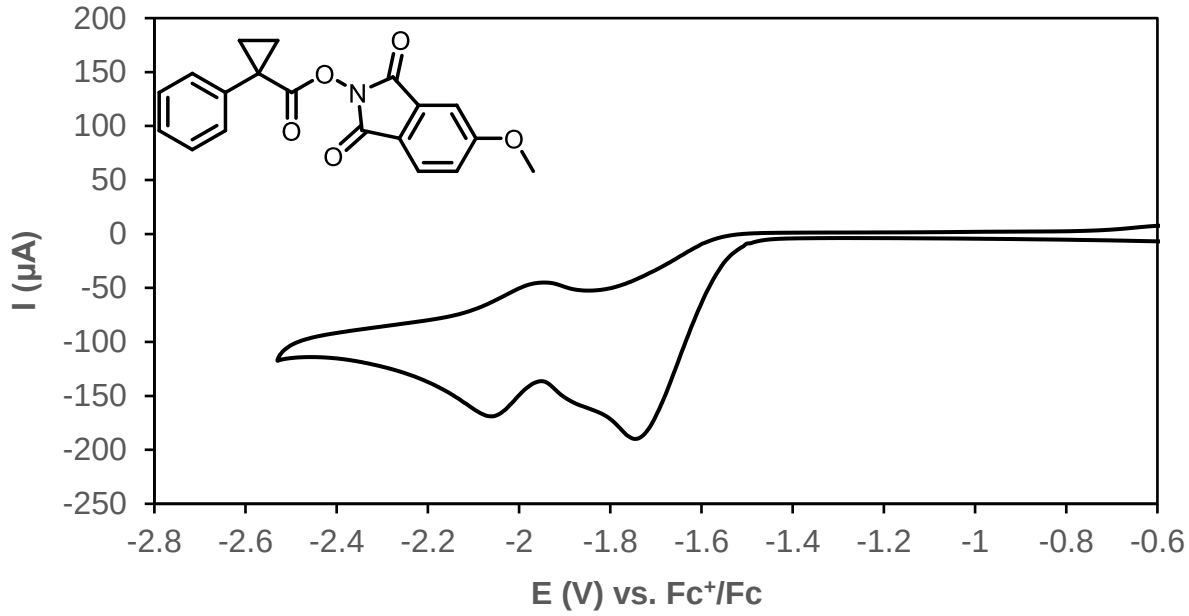

E_p= -1.737 vs Fc^+/Fc

Figure 3.11: Cyclic Voltammogram of 1,3-dioxo-1H-benzo[de]isoquinolin-2(3H)-yl 1-phenylcyclopropane-1-carboxylate

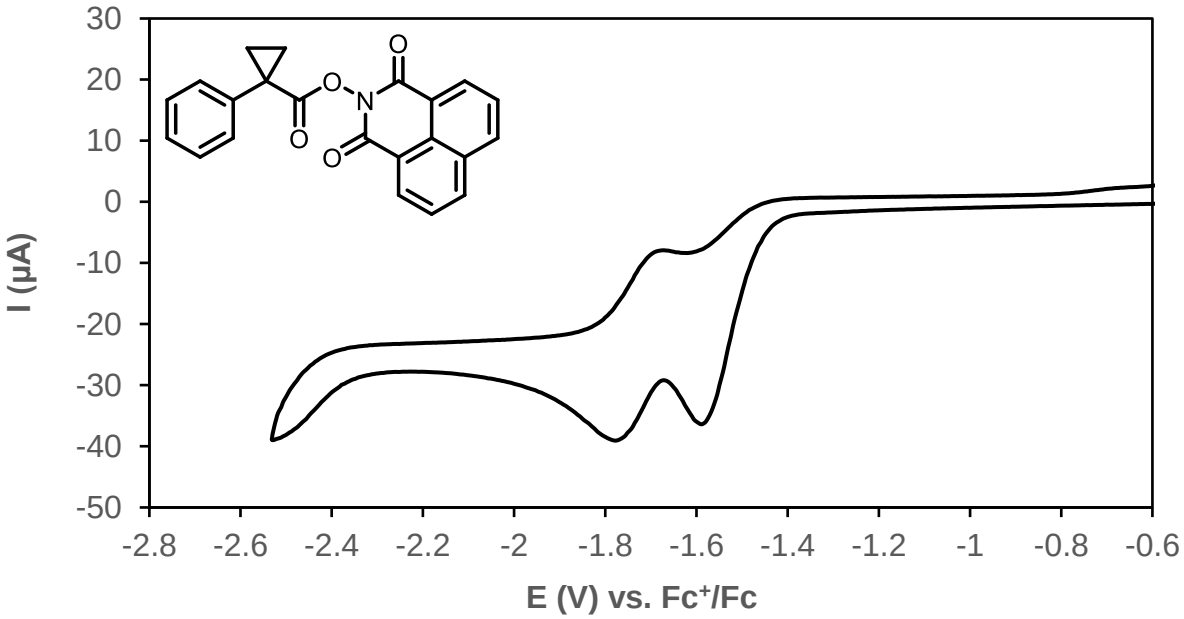

E_p= -1.589 vs Fc^+/Fc

Figure 3.12: Cyclic Voltammogram of 4,5,6,7-tetrachloro-1,3-dioxoisoindolin-2-yl 1-phenylcyclopropane-1-carboxylate

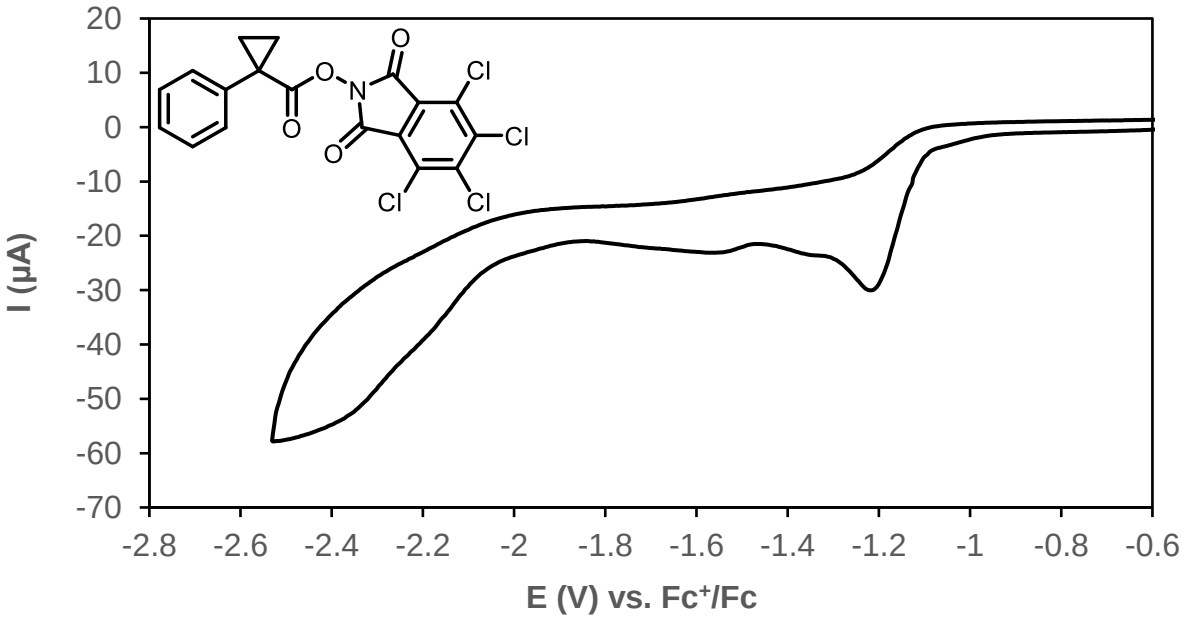

E_p= -1.213 vs Fc^+/Fc

3.4.3.2 Kinetics Studies

Figure 3.13: The effect of NHP ester substitution on the rate of decarboxylation.

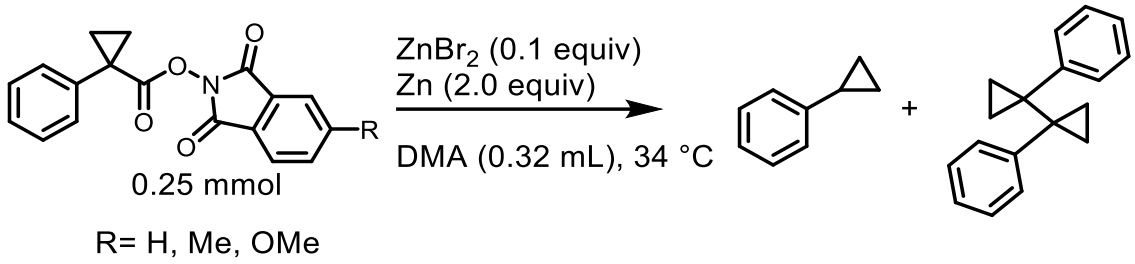

Reactions were setup in an N_2-filled glovebox for convenience. An oven-dried 1-dram vial with a PTFE-coated stirbar was charged with NHP ester (0.25 mmol, 1.0 equiv), zinc bromide (5.6 mg, 0.025 mmol, 0.10 equiv) and zinc (32.7 mg, 0.5 mmol, 2.0 equiv), and 1,3,5-trimethoxybenzene (21.1 mg, 0.125 mmol) internal standard, followed by the addition of DMA (0.32 mL). The reactions were sealed with a screw cap fitted with a PTFE-faced silicone septum and placed on a stir plate in the glovebox and were left to stir (1200 RPM) at 34 °C for 24 h. Aliquots of the reaction were taken, diluted with EtOAc, filtered through silica, and analyzed by SFC-MS.

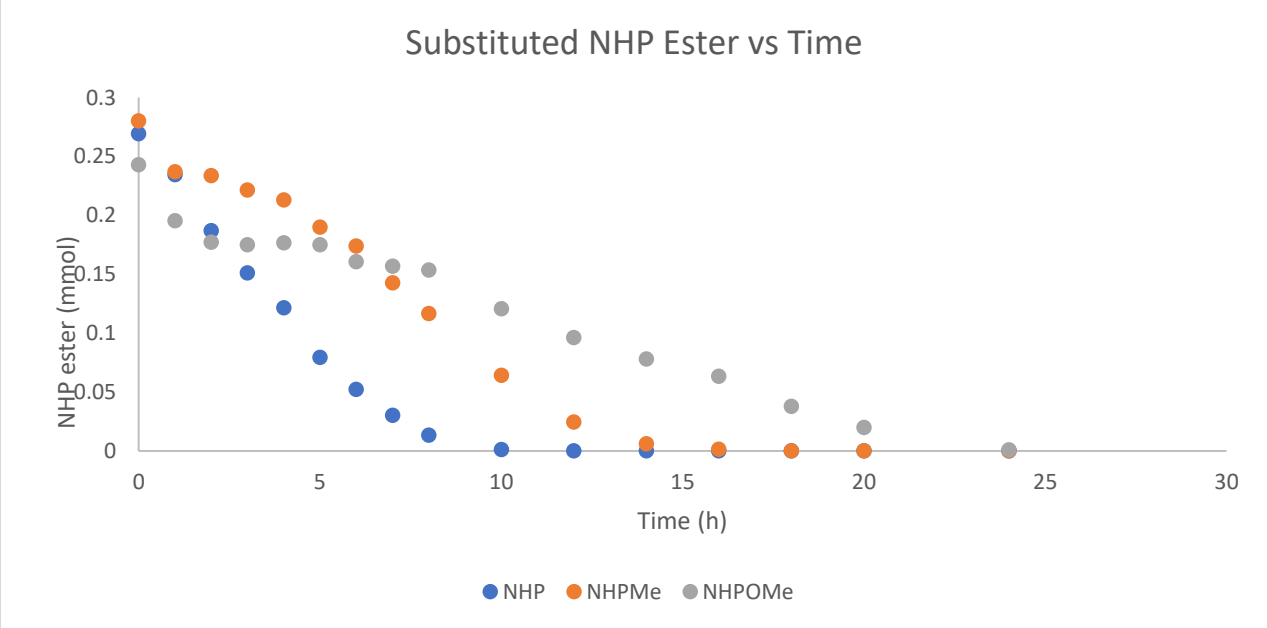

Figure 3.14: The effect of solvent on the rate of decarboxylation.

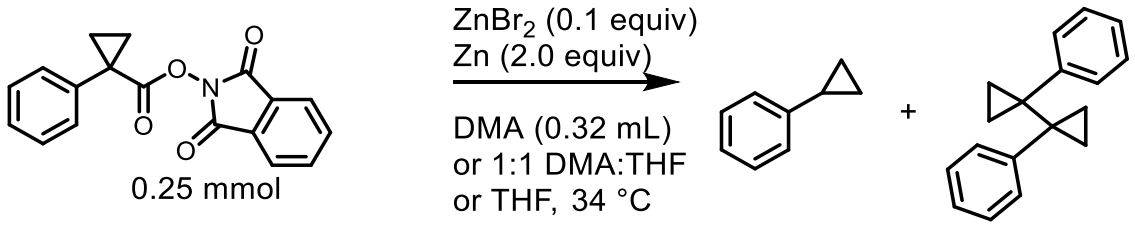

Reactions were setup in an N_2-filled glovebox for convenience. An oven-dried 1-dram vial with a PTFE-coated stirbar was charged with NHP ester (76.8 mg, 0.25 mmol, 1.0 equiv), zinc bromide (5.6 mg, 0.025 mmol, 0.10 equiv) and zinc (32.7 mg, 0.5 mmol, 2.0 equiv), and 1,3,5-trimethoxybenzene (21.1 mg, 0.125 mmol) internal standard, followed by the addition of solvent (0.32 mL). The reactions were sealed with a screw cap fitted with a PTFE-faced silicone septum and placed on a stir plate in the glovebox and were left to stir (1200 RPM) at 34 °C for 24 h. Aliquots of the reaction were taken, diluted with EtOAc, filtered through silica, and analyzed by SFC-MS.

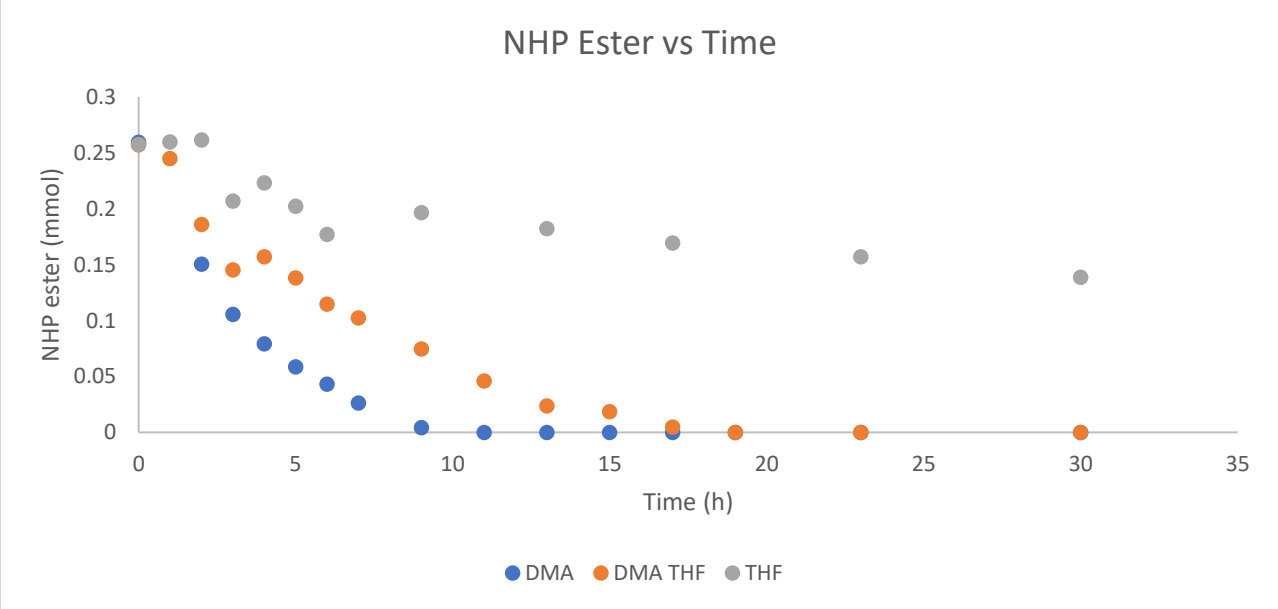

Figure 3.15: Time course for the model reaction.

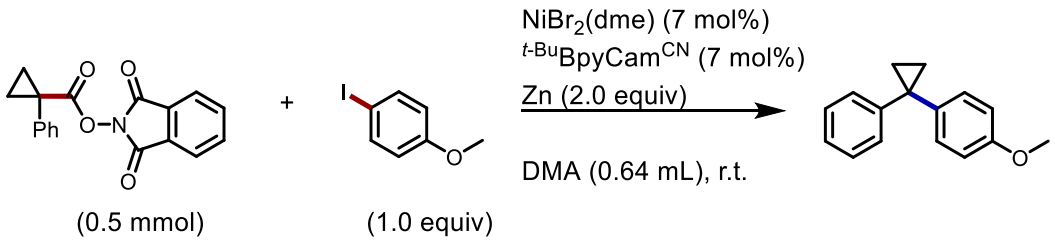

Reactions were setup in an N_2-filled glovebox for convenience. An oven-dried 1-dram vial with a PTFE-coated stirbar was charged with NHP ester (154 mg, 0.50 mmol, 1.0 equiv), aryl iodide (116 mg, 0.50 mmol, 1.0 equiv) and zinc (64.6 mg, 1.0 mmol, 2.0 equiv), and 1,3,5-trimethoxybenzene (7.4 mg, 0.044 mmol) internal standard, followed by the addition of solvent (0.32 mL). The reactions were sealed with a screw cap fitted with a PTFE-faced silicone septum , removed from the glovebox placed on a stir plate, and were left to stir (1200 RPM) at rt (20-22 °C) for 24 h. Aliquots of the reaction were taken, diluted with Et_2O, filtered through silica, and analyzed by GC.

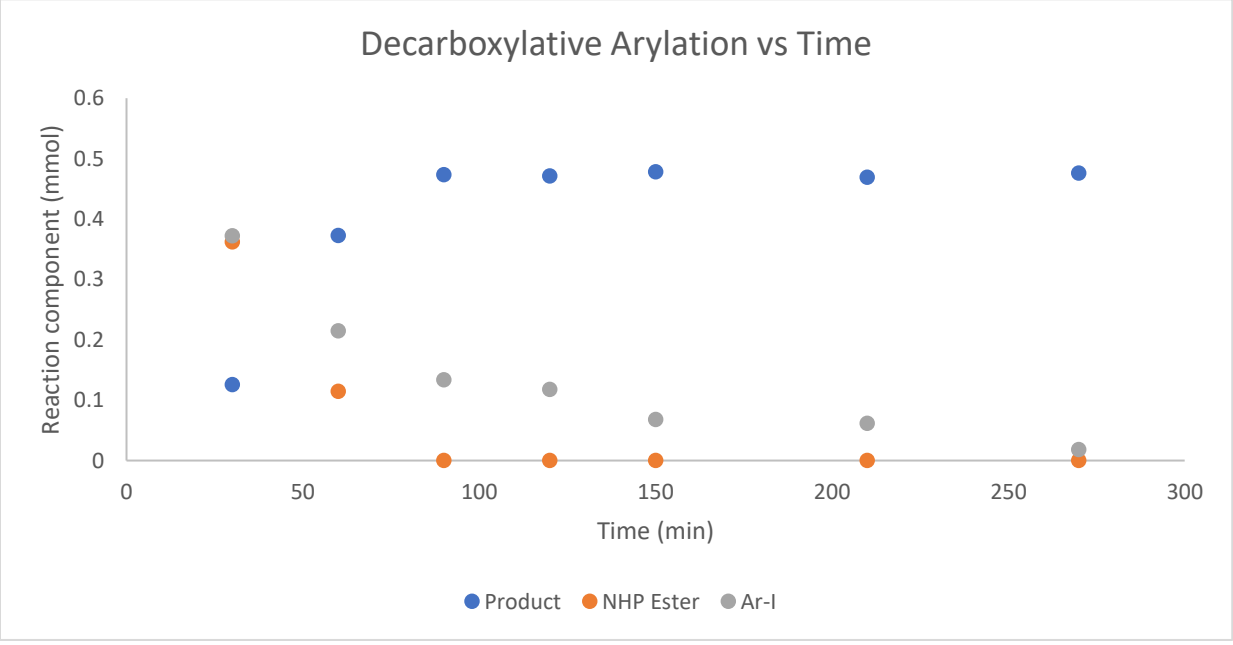

3.4.4 General Reaction Procedures

3.4.4.1 Synthesis of Tert-butyl Esters

Tert-butyl esters were prepared according to a previously reported procedure[107].

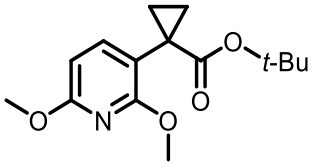

SI-1

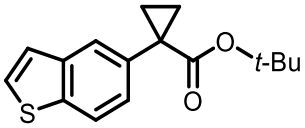

SI-2

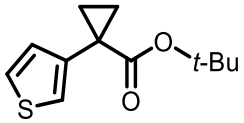

SI-3

To a 20 mL scintillation vial containing solid $LiNCy_2$ (2.1 equiv) was added dropwise a solution of tert-butyl cyclopropanecarboxylate (511.9 mg, 3.60 mmol, 2.0 equiv) in toluene (0.67 M) while stirring for 15 minutes. Meanwhile, to a separate 20 mL scintillation vial was charged $AgBF_4$ (0.05 equiv), Pd(1-tBu-Indenyl)($PtBu_3$)(Cl) (0.05 equiv), aryl bromide (1 equiv), and toluene (1 M). The resulting mixture was shaken by hand for 30 seconds before transferring the enolate solution into the vial. The vial was sealed with a screw cap fitted with a PTFE-faced silicone septum and removed from the glovebox. The reaction mixture was left stirring at 65 °C for 12 hours. After the specified time, the reaction mixture was concentrated *in vacuo* and directly loaded onto silica gel for column chromatography to afford the product.

3.4.4.2 Synthesis of NHP Esters

NHP esters were prepared according to previously reported procedures using DIC [108,109,110,111,112,113,114,115] **(General Procedure A)** or PITU[108] **(General Procedure B)** as the coupling agent.

3.4.4.2.1 General Procedure A: Synthesis of NHP Esters Using DIC.

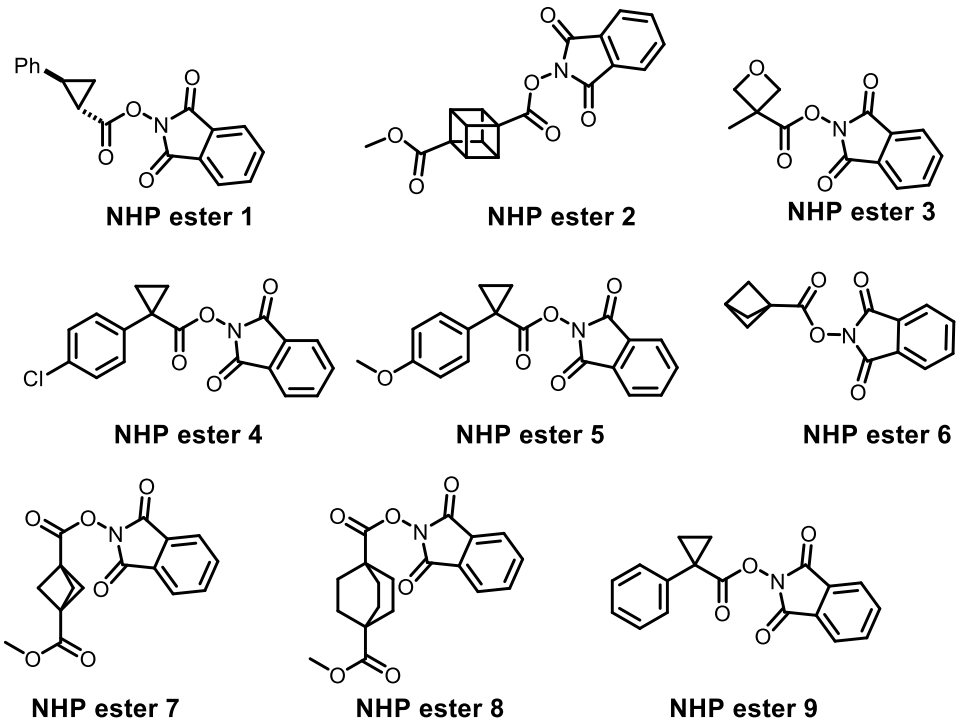

To a round-bottom flask charged with a magnetic stir bar was added carboxylic acid (1.0 equiv), *N*-hydroxyphthalimide (1.0 equiv), *N,N*-dimethylaminopyridine (DMAP) (0.1 equiv), and dichloromethane (resulting in a solution 0.1 M in carboxylic acid). To this solution was added *N,N*-diisopropylcarbodiimide (DIC) (1.1 equiv) and the flask was capped with a rubber septum affixed with a vent needle. The resulting mixture was allowed to stir for at rt (20-22 °C)18 h. After this time, the reaction mixture was then filtered through a short pad of silica gel into a round bottom flask. The silica gel was rinsed with additional dichloromethane (~50 mL) into

the flask. The solvent was removed under reduced pressure on a rotary evaporator. The crude material was recrystallized from hot methanol to afford the pure NHP ester. We and others have previously reported the synthesis of NHP esters shown below.

3.4.4.2.2 General Procedure B: Synthesis of NHP Esters Using PITU.

N-hydroxyphthalimide tetramethyluronium hexafluorophosphate[108] (PITU, 1.1 equiv) and N-methylmorpholine were added sequentially to a stirring 0.5 M solution of carboxylic acid (1.0 equiv) in N,N-dimethylformamide. The resulting mixture was stirred at room temperature (20-22 °C) for 16 h and then diluted with water (~0.2 M). Precipitated product, if formed, was collected by filtration, washed with water (2× 10 mL) and dried under high vacuum to yield analytically pure product. Alternatively, the crude aqueous mixture was extracted with 1:1 EtOAc/Hexanes (×× 20 mL). The combined organic extracts were dried over Na_2SO_4, concentrated in vacuo and purified by flash column chromatography (FCC) to yield pure NHP ester.

General Procedures for Decarboxylative Cross-Electrophile Coupling

3.4.4.2.3 General Procedure C.

Reactions were set up in a N_2 filled glove box. For a preparative-scale benchtop procedure, see **3.3. Preparative-Scale Benchtop Procedure**. A catalyst solution was prepared by sequentially charging an oven dried scintillation vial with a PTFE-coated stirbar, $NiBr_2$(dme) (10.1 mg, 0.035 mmol, 7 mol%) and $^{t\text{-}Bu}$BpyCam^{CN} (11.6 mg, 0.035 mmol, 7 mol%). The solids were dissolved in DMA (0.64 mL) and the contents were stirred for 30 min, resulting in a homogeneous solution. A separate oven-dried 1-dram vial with a PTFE-coated stirbar was charged with NHP ester (0.50 mmol, 1.0 equiv), aryl halide (0.50 mmol, 1.0 equiv), zinc (65.4 mg, 1.0 mmol, 2.0 equiv), and 1,3,5-trimethoxybenzene (4.2 mg, 0.025 mmol) internal standard. To the vial containing NHP ester, aryl halide, zinc, and internal standard was added 0.64 mL of the prepared catalyst solution. The reactions were sealed with a screw cap fitted with a PTFE-faced silicone septum before being removed from the glovebox. The contents of the reaction vessel were stirred (1200 RPM) at r.t. (20-22 °C) for 24 h.

<u>GC Analysis (modified below)</u>

The reactions were monitored by GC analysis. Samples were prepared by the removal of a 25 μL aliquot of the crude reaction mixture with a gas-tight syringe. The aliquot was diluted with EtOAc (1.00 mL), then the resulting solution was filtered through a 2-cm celite plug in a Pasteur pipette into a 2 mL GC vial. The resulting solution was analyzed by GC and yields were determined based on the peak area of the analyte compared to 1,3,5-trimethoxybenzene as an internal standard.

<u>Isolation and Purification (modified below)</u>

Purification A. Unless otherwise indicated, reactions assembled for isolation were performed on a 0.5 mmol scale of NHP ester and aryl halide without the addition of an internal standard to avoid difficulties in separating 1,3,5-trimethoxybenzene from the cross-coupled product. Upon the completion of the reaction, the crude reaction mixture was diluted with DCM (5 mL) and slurried with 1–3 g of silica gel before the volatile solvents were removed by rotary evaporation. The adsorbed crude residue was purified by column chromatography on silica to provide the cross-coupled products.

3.4.4.2.4 General Procedure D. Ni-catalyzed Decarboxylative Cross-Electrophile Coupling without the use of a Glovebox.

Reactions were set up under an N_2 atmosphere using standard Schlenk techniques. A catalyst solution was prepared by sequentially charging an oven-dried 1 dram vial with a PTFE-coated stirbar, $NiBr_2$(dme (18.5 mg, 0.060 mmol, 20 mol%) and $^{t\text{-}Bu}$BpyCam^{CN} (20 mg, 0.060 mmol, 20 mol%). The vial was purged with N_2 (3×). DMA (50 µL) was added to give a blue-green slurry, followed immediately by THF (450 µL). The headspace was evacuated and purged again quickly with N_2 (3×) before being stirred at r.t. (20-22 °C) for 15 min, resulting in a homogeneous dark amber-colored solution.

A separate oven-dried 1-dram vial with a PTFE-coated stirbar was charged with NHP ester (0.30 mmol, 1.0 equiv), aryl halide (0.30 mmol, 1.0 equiv), zinc dust (Sigma-Aldrich, ≥98%, <10 µm, 39.2 mg, 600 µmol, 2.0 equiv). The vial was sealed with a screw cap fitted with a PTFE-faced silicone septum and purged with N_2 (3×). Finally, 0.50 mL of the prepared catalyst solution was added via syringe. The vial was immediately sealed with parafilm and the reaction mixture was stirred (1200 RPM) at r.t. (20-22 °C) for 24 h. (Note: Reactions can be run at higher dilution without affecting yields significantly).

<u>GC/LCMS Analysis (combined with above)</u>

The reactions were monitored by GC or LCMS analysis. GC Samples were prepared by the removal of a 25 μL aliquot of the crude reaction mixture with a gas-tight syringe. The aliquot was diluted with EtOAc (1.00 mL), then the resulting solution was filtered through a 2-cm celite plug in a Pasteur pipette into a 2 mL GC vial. The resulting solution was analyzed by GC and yields were determined based on the peak area of the analyte compared to 1,3,5-trimethoxybenzene as an internal standard.

LCMS samples were prepared by the removal of a 5 μL aliquot of the crude reaction mixture with a gas-tight syringe. The aliquot was diluted with MeOH (200 µL) and the resulting solution analyzed by LCMS. When required, triphenylamine was used as an internal standard (0.33 equiv) an added to the bulk of the reaction mixture prior to analysis.

Isolation and Purification (combine with above)

Purification Method A. Unless otherwise indicated, reactions assembled for isolation were performed without the addition of an internal standard to avoid difficulties in separating the internal standard from the cross-coupled product. Upon the completion of the reaction, the crude reaction mixture was diluted with DCM (5 mL) and slurried with 1–3 g of silica gel before the volatile solvents were removed by rotary evaporation. The adsorbed crude residue was purified by column chromatography on silica to provide the cross-coupled products. (Note: For highly basic compounds, extraction from dilute aq. NH_4OH $NH_4Cl/NaHCO_3$ may be used to decomplex zinc salts)

Purification Method B. Unless otherwise indicated, reactions assembled for isolation were performed without the addition of an internal standard to avoid difficulties in separating the internal standard from the cross-coupled product. Upon the completion of the reaction, the crude reaction mixture was quenched by the addition of 5 N aq. NH_4OH (750 µL) (Note: For

sensitive substrates, sat'd. aq. NH_4Cl may be used, instead). The mixture was stirred at rt for 10 min, then diluted with DMA (2 mL), filtered through an Acrodisc® syringe filter (Note: Use of a centrifuge was employed as needed to avoid clogging), and purified by RP-HPLC (ACN/H_2O, 20 mM NH_4OH) to provide the cross-coupled products.

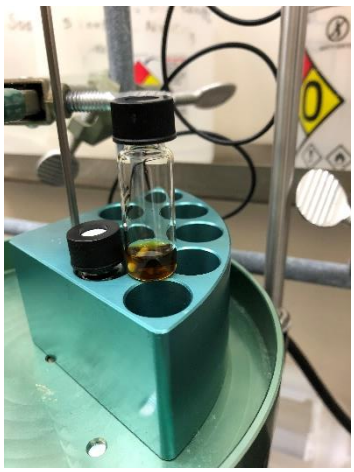

Formation of Ni catalyst solution in THF/DMA.

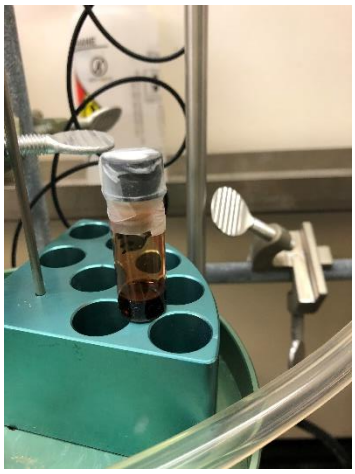

Final Reaction Mixture (t=24h).

Preparative-Scale Benchtop Procedure

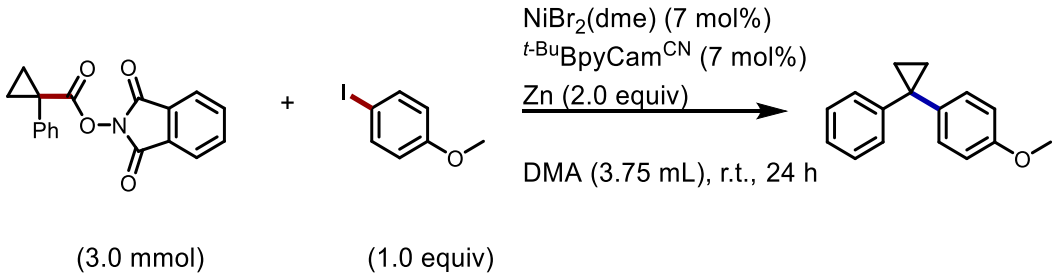

A catalyst solution was prepared on the benchtop by charging an oven-dried 20 mL scintillation vial with a PTFE-coated stirbar, $NiBr_2$•dme (65.1 mg, 0.21 mmol, 7 mol%), $^{t\text{-Bu}}$BpyCam^{CN} (70.4 mg, 0.21 mmol, 7 mol%). The scintillation vial sealed with a screw cap fitted with a PTFE-faced silicone septum. The scintillation vial was affixed with a N2 inlet line and a vent needle, and the headspace was purged with N2 for 10 min. Anhydrous DMA (3.75 mL) was added via syringe to the scintillation vial and the mixture was allowed to stir at rt for 30 min, resulting in a clear, homogeneous, dark orange solution. A separate oven dried 20 mL scintillation vial was charged with a PTFE-coated stirbar, 1,3-dioxoisoindolin-2-yl 1-phenylcyclopropane-1-carboxylate (922 mg, 3.0 mmol, 1.0 equiv), 4-iodoanisole (702 mg, 3.0 mmol, 1.0 equiv), and zinc (392 mg, 6.0 mmol, 2.0 equiv). The catalyst solution was transferred to the reaction vial via syringe, the vial containing the reaction mixture was affixed with a, N2 inlet line and a vent needle, the mixture was sparged with N_2 for 15 min, and the reaction mixture was allowed to stir at room temperature (20-22 °C) for 24 h.

Isolation and Purification

The reaction was diluted with DCM (60 mL) and the resulting solution was passed through a plug of silica gel and collected in a round bottom flask. The silica gel was washed twice with DCM (60 mL) and the resulting solution was slurried with silica gel (10 g). The slurry was concentrated under reduced pressure on a rotary evaporator. The resulting adsorbed crude residue was purified by column chromatography on silica to afford 1-methoxy-4-(1-phenylcyclopropyl)benzene as a clear, colorless oil (426 mg, 63% yield).

3.4.4.2.5 Decarboxylative Cross-Electrophile Coupling Under Continuous Flow Exemplified for the synthesis of 3-(4-methoxyphenyl)bicyclo[1.1.1]pentane-1-carboxylate (3.25).

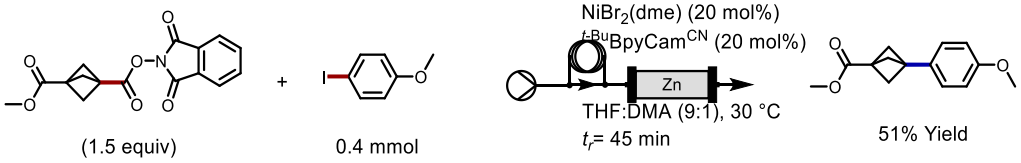

Note: This procedure was adapted from the literature[116] and modified for test-scale work using a syringe pump.

Step 1. Preparation of Zinc Column. Zinc ~30 mesh (Aldrich 565148) and Zinc ~325 mesh (Alfa-Aesar 13789) were throughly mixed in a 20 mL vial and then transferred to a 6 mm x 150 mm Omnifit column fitted with a fixed end piece at the bottom and a small amount of cotton wool at both ends. The column was capped with one fixed endpiece and one adjustable endpiece and attached to Vapourtec R2+R4 system. The column was flushed with THF (~2.5 mL column void volume) using a syringe pump. Note: A small amount of backpressure is observed.

Step 2. Activation of Zinc Column. An activating solution was prepared by adding chlorotrimethylsilane (800 µL) and 1-bromo-2-chloroethane (200 µL) to anhydrous THF (10 mL). The resulting solution was passed through the zinc column at 30 °C, at a flow rate of 1 mL/min. Once all of the activating solution had been passed through, anhydrous DMA (2 mL) was passed through the column to flush excess activating solution.

Step 3. Decarboxylative Cross-Electrophile Coupling in Flow. An oven-dried 2-dram vial was charged with a PTFE-coated stirbar, $NiBr_2$(dme) (24.7 mg, 0.080 mmol, 20 mol%), $^{t\text{-Bu}}$BpyCam^{CN} (29.5 mg, 0.088 mmol, 22 mol%). The vial was sealed with a screw cap fitted with a PTFE-faced silicone septum and purged with N2 (3×). DMA (50 µL) was added to give a blue-green slurry,

followed promptly by THF (450 μL). The headspace was purged again quickly with N_2 (3×) before being stirred at r.t. (20-22 °C) for 15 min, resulting in a homogeneous dark amber-colored solution. To this solution was quickly added 4-iodoanisole (93.6 mg, 0.40 mmol, 1.0 equiv) and 1-(1,3-dioxoisoindolin-2-yl) 3-methyl bicyclo[1.1.1]pentane-1,3-dicarboxylate (189 mg, 0.60 mmol, 1.5 equiv) in one portion. After the end of the addition, the vial was immediately sealed with a PTFE-faced silicone septum and the headspace quickly purged with N_2 (3×). The mixture was stirred at room temperature for 10 min to give a homogenous solution. The reactant solution thus formed was passed through the activated column from Step 2 at 30 °C, at a flow rate of 0.1 mL/min. Product was observed as a red-colored solution which was collected after the first ~2 mL of reaction solution had been flowed through. After the end of the addition, DMA (3 mL) was flowed through the column to complete the elution of product. Product was collected until the eluting solution became colorless (final product solution volume ~6 mL). This set-up gave a residence time through the zinc column, t_r, of approximately 45 min.

Step 4. Isolation of Cross-Coupled Product. The obtained product solution was diluted with sat'd aq. NH_4Cl (5 mL) and sat'd aq. $NaHCO_3$ (5 mL). The resulting aqueous mixture was extracted with 1:1 EtOAc/Hex (3×10 mL). The combined organic extracts were concentrated *in vacuo* and purified by flash chromatography (0-20% EtOAc/Hex) using 12 g silica to afford methyl 3-(4-methoxyphenyl)bicyclo[1.1.1]pentane-1-carboxylate (**3.25**, 47.3 mg, 204 μmol, 51%) as a semi-crystalline white solid. Analytical data was in accordance with that reported in entry **3.25**. Note: No further optimization of conditions was investigated at this time.

3.4.4.2.6 Decarboxylative Cross-Electrophile Coupling in a High-Throughput Experimentation (HTE) Mode

3.4.4.2.6.1 Coupling to X-Bromo *N*-methyl indazole

Catalyst Stock Solutions

Stock solutions of catalyst for HTE screening were prepared in a N_2-filled glovebox in separate dram vials. An oven dried dram vial equipped with a PTFE-coated stir bar was sequentially charged with $NiBr_2$dme, ligand, and THF (1.0 mL). The vial was capped with a Teflon-coated screw cap and the contents stirred at rt for 30 min to afford a (0.08 M) catalyst stock solution.

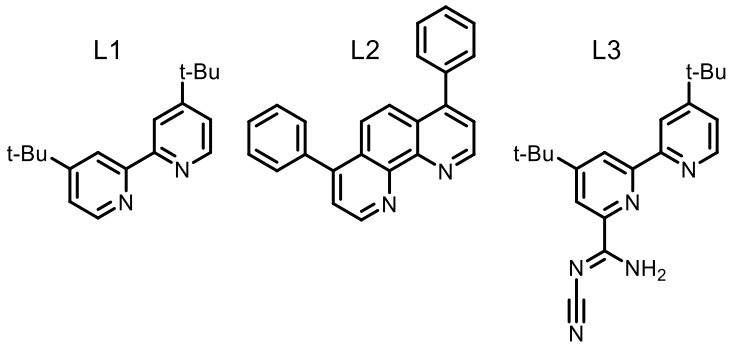

Solution 1: $NiBr_2$dme (23.4 mg, 0.08 mmol, 0.2 equiv) and dtbbpy (21.4 mg, 0.08 mmol, 0.2 equiv).

Solution 2: $NiBr_2$dme (23.4 mg, 0.08 mmol, 0.2 equiv) and bathophenanthroline (26.6 mg, 0.08 mmol, 0.2 equiv).

Solution 3: $NiBr_2$dme (23.4 mg, 0.08 mmol, 0.2 equiv), ^{tbu}bpyCAM^{CN} (26.8 mg, 0.08 mmol, 0.2 equiv)

Stock Solutions of NHP Esters

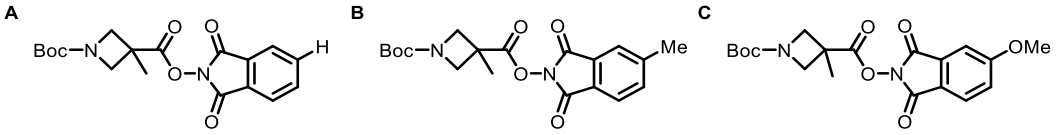

Note: Due to the poor solubility of these NHP esters in THF, the prepared stock solutions were made more dilute than the standard reaction conditions to afford homogeneous solutions. Eight NHP esters were chosen for high-throughput screening. Stock solutions of NHP esters **A-C**, sufficient for 40 reactions at a 0.01 mmol scale, were prepared in a N_2-filled glovebox by weighing each NHP ester (0.4 mmol) into a dram vial followed by addition of anhydrous THF (2.0 mL), before sealing the vial with a PTFE-lined cap and briefly shaking the mixture by hand for 30 seconds.

Stock Solutions of Bromo Indazoles

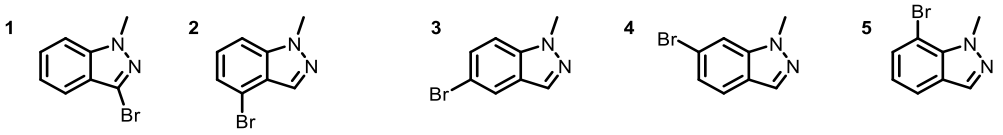

Note: Due to the poor solubility of these aryl bromides esters in THF, the prepared stock solutions were made more dilute than the standard reaction conditions to afford homogeneous solutions Five aryl bromide cores were chosen for high-throughput screening. In a N_2-filled glovebox, a stock solution of aryl bromides **1-3**, sufficient for 30 reactions at a 0.01 mmol scale, was prepared by weighing aryl bromide **1-3** (0.3 mmol) into a dram vial followed by the addition of anhydrous THF (1.5 mL) and briefly shaking the mixture by hand for 30 seconds until completely homogenous.

Preparation of Zinc-Coated ChemBeads

Zinc-coated ChemBeads (5% w/w) were prepared following a literature procedure. In a N_2-filled glovebox, to a 20-mL scintillation vial was charged 22.8 g of glass ChemBeads and 1.2 g (9.1 mmol) Zn. The vial was sealed, then removed from the glovebox. The vial was placed on a conical vortex mixer and agitated for 30 minutes to ensure even coating of the beads.

Preparation of Internal Standard Stock Solution

In a N_2-filled glovebox, an oven dried dram vial was sequentially charged with1,3,5-trimethoxybenzene (201.8 mg, 1.2 mmol) and THF (1.8 mL). The vial was capped with a Teflon-coated screw cap and the vial was shaken by hand for 30 seconds, resulting in a homogeneous solution

General Procedure for HTE Screening

All operations were performed in a N_2-filled glovebox. To each well of a 96-well (8 rows by 12 columns) aluminium block assembly equipped with 8 × 30 mm vials was dosed 30 mg of Zn-coated ChemBeads (5% loading wt/wt) using a calibrated scoop and a non-static funnel (Image 2). NHP Ester and aryl bromide substrates were dosed into each well by first transferring stock solutions of each NHP ester and aryl bromide into separate channels of eight-channel polypropylene deep-well reservoirs followed by transferring 50 µL of each NHP ester stock solution to their respective wells (Image 3) and 50 µL of each aryl bromide stock solutions to their respective wells (Image 3) using a multi-channel pipette. To each well was added 15 µL of a stock solution of trimethoxybenzene internal standard and 25 uL of a stock solution of catalyst (Image 3). 15 uL of DMA were added to the appropriate wells (see table below). The well-plate vials were sealed with an electric screwdriver at torque setting 6 in a diagonal pattern (Image 4), using an aluminum lid, and the block was placed onto a heater/shaker (Torrey Pines

Echotherm) set at 60 °C (actual temperature was found to be ~20 °C lower) and orbital speed at 8 to heat/shake for 36 h (Image 5).

	THF					THF:DMA					THF	THF:DMA	
	Col 1	Col 2	Col 3	Col 4	Col 5	Col 6	Col 7	Col 8	Col 9	Col 10	Col 11	Col 12	
Row 1	A, 1	A, 2	A, 3	A, 4	A, 5	A, 1	A, 2	A, 3	A, 4	A, 5	C, 1	C, 1	
Row 2	B, 1	B, 2	B, 3	B, 4	B, 5	B, 1	B, 2	B, 3	B, 4	B, 5	C, 2	C, 2	
Row 3	C, 1	C, 2	C, 3	C, 4	C, 5	C, 1	C, 2	C, 3	C, 4	C, 5	C, 3	C, 3	
Row 4	A, 1	A, 2	A, 3	A, 4	A, 5	A, 1	A, 2	A, 3	A, 4	A, 5	C, 4	C, 4	
Row 5	B, 1	B, 2	B, 3	B, 4	B, 5	B, 1	B, 2	B, 3	B, 4	B, 5	C, 5	C, 5	
Row 6	C, 1	C, 2	C, 3	C, 4	C, 5	C, 1	C, 2	C, 3	C, 4	C, 5			L1
Row 7	A, 1	A, 2	A, 3	A, 4	A, 5	A, 1	A, 2	A, 3	A, 4	A, 5			L2
Row 8	B, 1	B, 2	B, 3	B, 4	B, 5	B, 1	B, 2	B, 3	B, 4	B, 5			L3

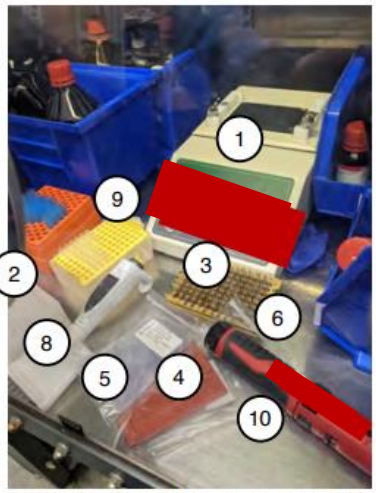

Image 1. HTE Equipment with prepared NHP ester and aryl bromide stock

Setup Parts (SKU#)

1. Torrey Pines Ectotherm Shaker/Heater
2. 8-Channel Deep Well Reservoir (32008)
3. Paradox 96-Well Photoredox Block Assembly (96973) loaded with 8×30mm shell vials (884001)
4. Rubber mat (96965)
5. Plastic film linings (96967)
6. Abbvie calibrated ChemBead scoops
7. Non-static funnel
8. Sartorius Picus electronic 8-channel pipette, 5 – 120 µL
9. Sartorius 0.5 – 200 µL pre-sterilized Optifit Tips (790200)
10. Milwaukee cordless screwdriver (2101-21)

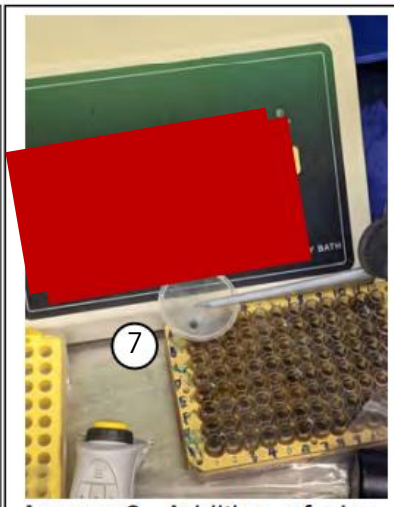

Image 2. Addition of zinc-coated ChemBeads

Image 3. Addition of stock solutions

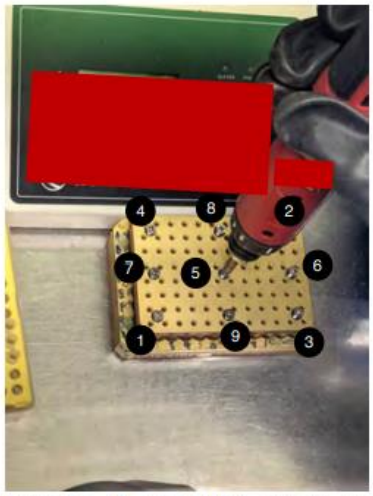

Image 4. Sealing plate in the pattern shown at torque setting of 6.

Image 5. Heating/shaking the block assembly in a glovebox for 36 hours.

Workup and Analysis

The reaction block was removed from the shaker apparatus and allowed to cool to rt. The aluminum block was then removed from the glovebox, the lid was removed, and 200 µL of MeOH was added to each well to dilute the reaction mixtures. 150 µL aliquots were taken from each well and were then filtered through a 0.2 µm filter plate into a 340 µL 96-well collection plate (Images 6 and 7). Each well of the filter plate was then washed with an additional 120 µL of MeOH The plate was then analyzed by UPLC-MS, product to internal standard ratios were determined by absorbance at 254 nm.

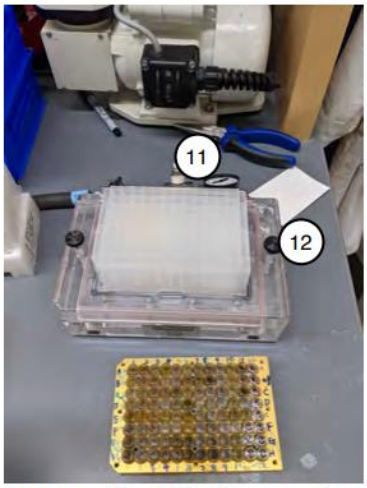

Image 6. Filtration setup into a 96-well collection plate.

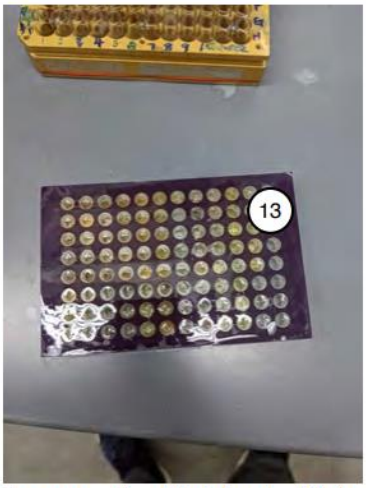

Image 7. Finished Plate sealed with a round well cap mat for SFC-MS analysis

Workup Parts (SKU#)

11. 2mL Hydrophilic filter plate, 0.2µm polypropylene membrane (96222-10)
12. Vacuum manifold filtration system (96844)
13. 340µL 96-well collection plate with V-shaped well bottoms and SiliGuard low binding coating (96340GC) with clear adhesive sealing film (Analytical Sales 961802)

3.4.4.2.6.2 HTE Aryl halide chemistry informer library compound X5

Catalyst Stock Solutions

Stock solutions of catalyst for HTE screening were prepared in a N_2-filled glovebox in separate dram vials. An oven dried dram vial equipped with a PTFE-coated stir bar was sequentially charged with $NiBr_2$dme, ligand, and THF (0.75 mL). The vial was capped with a Teflon-coated screw cap and the contents stirred at rt for 30 min to afford a (0.067 M) catalyst stock solution.

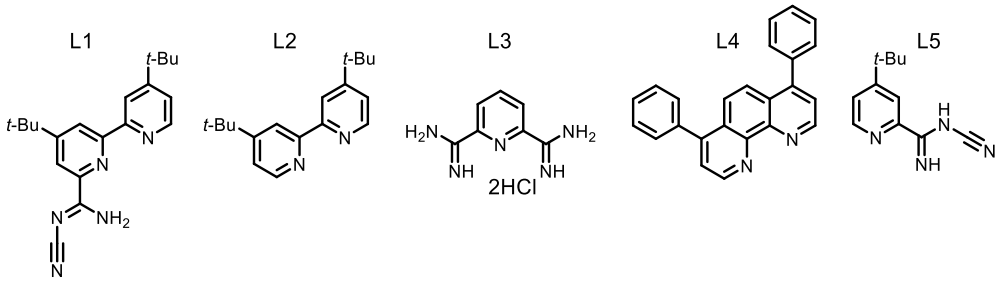

Solution 1: $NiBr_2$dme (14.6 mg, 0.05 mmol, 0.2 equiv), ^{tbu}bpyCAM^{CN} (16.8 mg, 0.05 mmol, 0.2 equiv)

Solution 2: $NiBr_2$dme (14.6 mg, 0.05 mmol, 0.2 equiv) and dtbbpy (13.4 mg, 0.05 mmol, 0.2 equiv).

Solution 3: $NiBr_2$dme (14.6 mg, 0.05 mmol, 0.2 equiv) and bathophenanthroline (16.6 mg, 0.05 mmol, 0.2 equiv).

Solution 4: $NiBr_2$dme (14.6 mg, 0.05 mmol, 0.2 equiv) and Pyridine-2,6-bis(carboximidamide) dihydrochloride (11.8 mg, 0.05 mmol, 0.2 equiv).

Solution 5: $NiBr_2$dme (14.6 mg, 0.05 mmol, 0.2 equiv) and 4-(tert-butyl)-N-cyanopicolinimidamide (10.1 mg, 0.05 mmol, 0.2 equiv).

Stock Solutions of NHP Esters

A 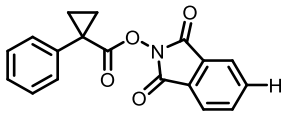 B 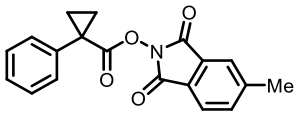 C 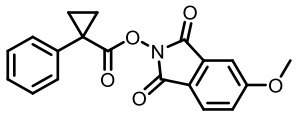

Stock solutions of NHP esters **A-C**, sufficient for 25 reactions at a 0.01 mmol scale, were prepared in a N_2-filled glovebox by weighing each NHP ester (0.25 mmol) into a dram vial followed by addition of anhydrous THF (2.25 mL), before sealing the vial with a PTFE-lined cap and briefly shaking the mixture by hand for 30 seconds. Stock solutions were prepared immediately prior to use in HTE screening studies.

Stock Solution of Aryl Bromide

1 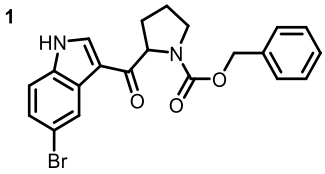

Note: Due to the poor solubility of this aryl bromide in THF, the prepared stock solutions were made more dilute than the standard reaction conditions to afford homogeneous solutions 5, sufficient for 20 reactions at a 0.01 mmol scale were prepared by weighing the aryl bromide (0.2 mmol) into a dram vial before addition of anhydrous THF (2.4 mL) and briefly shaking the mixture by hand for 30 seconds until completely homogenous.

Preparation of Zinc-Coated ChemBeads

Zinc-coated ChemBeads (5% w/w) were prepared following a literature procedure. In a N_2-filled glovebox, to a 20-mL scintillation vial was charged 22.8 g of glass ChemBeads and 1.2 g (9.1 mmol) Zn. The vial was sealed, then removed from the glovebox. The vial was placed on a conical vortex mixer and agitated for 30 minutes to ensure even coating of the beads.

Preparation of Internal Standard Stock Solution

In a N_2-filled glovebox, an oven dried dram vial was sequentially charged with1,3,5-trimethoxybenzene (201.8 mg, 1.2 mmol) and THF (1.8 mL). The vial was capped with a Teflon-coated screw cap and the vial was shaken by hand for 30 seconds, resulting in a homogeneous solution

General Procedure for HTE Screening

All operations were performed in a N_2-filled glovebox. To each well of a 96-well (8 rows by 12 columns) aluminium block assembly equipped with 8 × 30 mm vials was dosed 30 mg of Zn-coated ChemBeads (5% loading wt/wt) using a calibrated scoop and a non-static funnel (Image 2). The NHP esters and aryl bromide were dosed into each well by first transferring stock solutions of each NHP ester and aryl bromide into separate channels of eight-channel polypropylene deep-well reservoirs followed by transferring 90 μL of each NHP ester stock solution to their respective wells and 60 μL of the aryl bromide stock solutions to each well using a multi-channel pipette. To each well was added 15 μL of a stock solution of trimethoxybenzene internal standard (1.68 mg, 0.01 mmol, 1 equiv) in THF and 30 uL of a stock solution of catalyst. The well-plate vials were sealed with an electric screwdriver at torque setting 6 in a diagonal pattern (Image 4), using an aluminum lid, and the block was placed onto a heater/shaker (Torrey Pines Echotherm) set at 60 °C (actual temperature was found to be ~20 °C lower) and orbital speed at 8 to heat/shake overnight for 36 h.

<u>Workup and Analysis</u>

The reaction block was removed from the shaker apparatus and allowed to cool to rt. The aluminum block was then removed from the glovebox, the lid was removed, and 200 µL of MeOH was added to each well to dilute the reaction mixtures. 150 µL aliquots were taken from each well and were then filtered through a 0.2 µm filter plate into a 340 µL 96-well collection plate (Images 6 and 7). Each well of the filter plate was then washed with an additional 120 µL of MeOH The plate was then analyzed by UPLC-MS, product to internal standard ratios were determined by absorbance at 254 nm.

Figure S10. HTE coupling of Aryl halide chemistry informer library compound X5

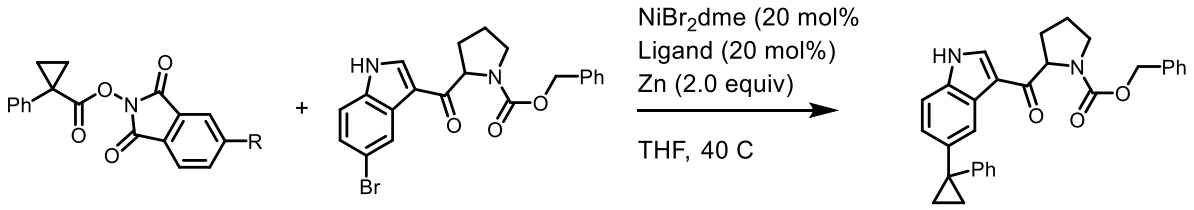

	$^{t\text{-bu}}$BpyCam^{CN}	dtbbpy	PyBCam	Bphen	PyCam^{CN}
R=H	7.96	0.82	2.06	0.30	0.46
R=Me	10.27	0.14	2.05	0.61	0.85
R=OMe	0.63	0.36	0.42	0.39	0.40

3.4.5 Specific Procedures and Product Characterization

3.4.5.1 Synthesis of 4,4'-di-*tert*-butyl-*N*-cyano-2,2'-bipyridine-6-carboximidamide (L7) 4,4'-di-*tert*-butyl-2,2'-bipyridine-1-oxide

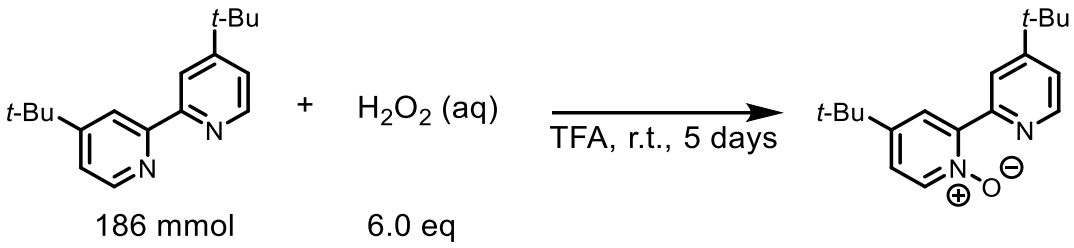

To a 1 L round-bottom flask equipped with a PTFE-coated stir bar was charged with 4,4′-di-tert-butyl-2,2′-bipyridine (50 g, 186 mmol, 1.0 equiv) and 125 mL of trifluoroacetic acid. The flask was placed in a water bath (to help control any potential exotherms) and the solution stirred. Aqueous H_2O_2 (30 mL of 30% solution, 279 mmol, 1.5 equiv) was added to the stirring solution in a steady stream and the resulting mixture was left to stir at r.t. (20-22 °C). Reaction progress was monitored via SFC-MS, and the presence of trifluoroperacetic acid was monitored using KI starch paper. Additional equivalents of H_2O_2 (30 mL of 30% solution, 279 mmol, 1.5 equiv) were added until the reaction was judged complete by SFC-MS as determined by the complete consumption of the 4,4′-di-tert-butyl-2,2′-bipyridine starting material. The reaction was quenched with the addition of $CHCl_3$ (400 mL). The resulting mixture was neutralized by the slow addition of aqueous 6 M NaOH (pH of 7). The resulting two layers were separated. The organic layer was washed with additional aqueous 6 M NaOH (2 × 200 mL). Finally, the organic layer was dried over Mg_2SO_4. After filtration to remove the drying agent, the filtrate was concentrated on a rotary evaporator under vacuum. A white powder was obtained which was further used in the next step without purification. Yield: 51 g (97%) of 95% pure material (95% *N*-oxide, 5% rsm).[117]

^{1}H NMR (500 MHz, $CDCl_3$) δ 8.91 (dd, *J* = 1.9, 0.8 Hz, 1H), 8.63 (dd, *J* = 5.3, 0.8 Hz, 1H), 8.23 (d, *J* = 6.9 Hz, 1H), 8.08 (d, *J* = 2.9 Hz, 1H), 7.33 (dd, *J* = 5.2, 2.0 Hz, 1H), 7.25 (dd, *J* = 6.9, 3.0 Hz, 1H), 1.37 (s, 9H), 1.37 (s, 9H).

^{13}C{^{1}H} NMR (126 MHz, $CDCl_3$) δ 160.2, 150.3, 150.1, 149.2, 146.7, 139.9, 124.7, 122.9, 122.5, 121.3, 35.0, 34.7, 30.6, 30.6.

4,4'-di-*tert*-butyl-2,2'-bipyridine-6-carbonitrile

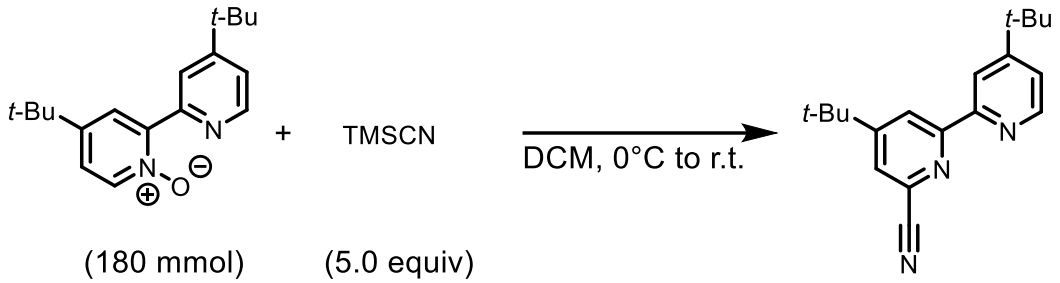

An oven-dried 500 mL 3-neck flask equipped with a PTFE-coated stirbar, an in situ thermometer, an addition funnel, was charged with 4,4′-di-tert-butyl2,2′-bipyridin-N-oxide (51 g, 180 mmol) and cooled under vacuum. The flask was placed under a N_2 atmosphere and dry, degassed CH_2Cl_2 (400 mL) was added via cannula, and the flask was lowered into an ice bath and cooled to 0 °C (determined by the in situ thermometer). Trimethylsilylcyanide (89 g, 900 mmol, 5.00 equiv) was added to the addition funnel via syringe and slowly added to this solution followed via the addition funnel. Benzoyl chloride (42 mL, 50.82 g, 361 mmol, 2.00 equiv) was added to the addition funnel, then added slowly to the reaction mixture to prevent any exotherms (as measured by the in situ thermometer. After complete addition, the mixture was warmed to rt (20-22 °C) and stirred for another 24 h. Then a 10% sodium hydrogencarbonate solution was added with caution until gas evolution has stopped. The resulting two-phase system was stirred for 24 h at rt. After this time, the mixture was transferred to a separatory funnel. Then, the two layers were separated and the aqueous layer was washed twice with CH_2Cl_2. Finally, the combined organic layers were dried over magnesium sulphate. After filtration, the solvent was removed in vacuum. The slightly brown residue was dried and recrystallized from hot *i*-PrOH. After drying under vacuum a white powder was obtained. Yield: 42 g (144 mmol, 80%).[117]

^{1}H NMR (500 MHz, CDCl3) δ 8.66 (d, J = 1.8 Hz, 1H), 8.59 (dd, J = 5.2, 0.8 Hz, 1H), 8.46 (d, J = 1.8 Hz, 1H), 7.69 (d, J = 1.8 Hz, 1H), 7.36 (dd, J = 5.2, 2.0 Hz, 1H), 1.41 (s, 9H), 1.40 (s, 9H). **^{13}C{^{1}H} NMR** (126 MHz, CDCl3) δ 162.5, 161.5, 158.0, 154.4, 149.2, 133.2, 125.6, 121.7, 121.5, 118.8, 118.0, 53.4, 35.4, 35.1, 30.6, 30.4.

4,4′-di-tert-butyl-6-N-cyanocarboxamidine-2,2-bipyridine ($^{t\text{-Bu}}$BpyCam^{CN})

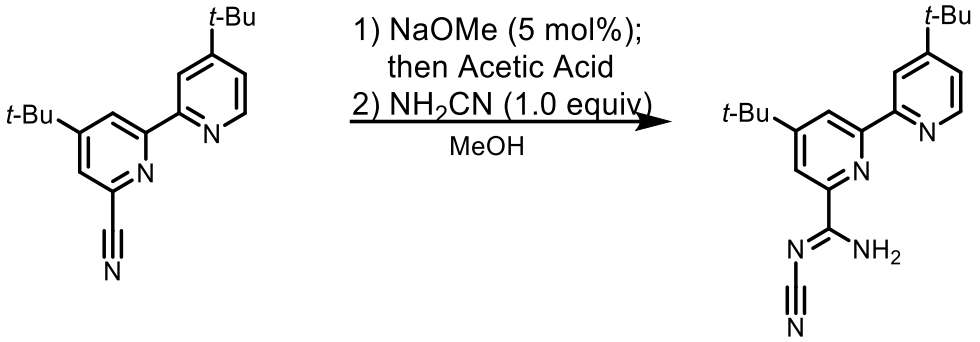

A flame-dried 1000 mL round-bottom flask equipped with a PTFE-coated stirbar was charged with 4,4'-di-tert-butyl-[2,2'-bipyridine]-6-carbonitrile (42.33 g, 144.3 mmol, 1.00 equiv) and sodium methoxide (42.33 g, 7.2 mmol, 0.05 equiv), and capped with a rubber suptem affixed with a N_2 inlet needle. The flask was evacuated and back-filled with N_2 three times, before addition of methanol (577 mL) via syringe. The reaction flask was lowered into an oil bath heated to 60 °C and left stirring for several hours until the formation of imidate was judged complete by SFC-MS. The oil bath was then set to 40 °C and the reaction mixture was stirred for an additional 2 hours, at which point a white precipitate formed. The mixture was quenched with acetic acid (0.41 mL, 7.2 mmol, 0.05 equiv) followed by addition of cyanamide (6.07 g, 144.3 mmol, 1.00 equiv) as a solution in 28.9 mL of methanol via syringe. The reaction mixture was then heated back to 60 °C and left stirring for several hours until the reaction was judged complete by SFC-MS. The reaction mixture was cooled to room temperature and filtered through a medium porosity fritted-glass funnel into a round bottom flask. The collected solids in the filter were analytically pure 4,4'-di-*tert*-butyl-*N*-cyano-2,2'-bipyridine-6-carboximidamide. The filtrate, containing additional product, was then concentrated in vacuo and the crude product recrystallized by completely dissolving the crude solid in THF followed

by careful layering of hexanes. Characterization data matched those reported in the literature.[118] Yield: 35 g (104 mmol, 72% yield).[119]

^{1}H NMR (500 MHz, $CDCl_3$) δ 8.64 (d, *J* = 1.8 Hz, 1H), 8.63 (dd, *J* = 5.3, 0.8 Hz, 1H), 8.42 (s, 1H), 8.31 (d, *J* = 1.8 Hz, 1H), 8.30 (dd, *J* = 2.0, 0.7 Hz, 1H), 7.37 (dd, *J* = 5.2, 1.9 Hz, 1H), 6.75 (s, 1H), 1.43 (s, 9H), 1.41 (s, 9H).

^{13}C{^{1}H} NMR (126 MHz, $CDCl_3$) δ 166.5, 163.4, 161.2, 156.1, 155.0, 149.4, 146.5, 122.4, 121.5, 119.7, 118.0, 116.2, 35.5, 35.0, 30.6, 30.6.

HRMS (ESI) m/z calculated for $C_{20}H_{26}N_5$ $[M+H]^+$ 336.21827, found 336.2179.

M.P. (°C) 272 – 275.

tert-butyl 1-(3,5,5,8,8-pentamethyl-5,6,7,8-tetrahydronaphthalen-2-yl)cyclopropane-1-carboxylate (3.41)

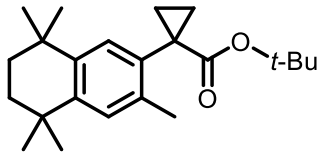

The following procedure was adapted from the method of Hartwig and coworkers. To a 20 mL scintillation vial containing solid $LiNCy_2$ (702 mg, 3.75 mmol, 2.1 equiv) was added dropwise a solution of tert-butyl cyclopropanecarboxylate (511.9 mg, 3.600 mmol, 2 equiv) in toluene (5.4 mL) while stirring for 15 minutes. Meanwhile, to a separate 20 mL scintillation vial was charged $AgBF_4$ (18 mg, 0.09 mmol, 0.05 equiv), Pd(1-tBu-Indenyl)($PtBu_3$)(Cl) (46.8 mg, 0.09 mmol, 0.05 equiv), 6-bromo-1,1,4,4,7-pentamethyl-1,2,3,4-tetrahydronaphthalene (506.4 mg, 1.800 mmol, 1 equiv), and toluene (1.8 mL). The resulting mixture was shaken by hand for 30 seconds before transferring the enolate solution into the vial. The vial was sealed with a screw cap fitted with a PTFE-faced silicone septum and removed from the glovebox. The reaction mixture was left stirring at 65 °C for 5 hours. After the specified time, the reaction mixture was concentrated *in vacuo* and directly loaded onto silica gel for column chromatography to afford the product as a white solid (0.45 g, 76% yield)

^{1}H NMR (500 MHz, $CDCl_3$) δ 7.10 (s, 1H), 7.03 (s, 1H), 2.26 (s, 3H), 1.64 (s, 4H), 1.57 – 151 (m, 2H), 1.35 (s, 9H), 1.25 (s, 6H), 1.24 (s, 6H), 1.11 – 1.08 (m, 2H).

^{13}C{^{1}H} NMR (126 MHz, $CDCl_3$) δ 173.6, 143.2, 141.6, 135.5, 135.4, 128.2, 127.7, 80.0, 35.3, 35.3, 33.9, 33.9, 31.9, 31.8, 28.5, 27.9, 19.0, 16.4.

HRMS (ESI) m/z calculated for $C_{23}H_{35}O_2$ $[M+H]^+$ 343.2632, found 343.2624.

MP = 117 – 119 °C.

1-(3,5,5,8,8-pentamethyl-5,6,7,8-tetrahydronaphthalen-2-yl)cyclopropane-1-carboxylic acid

(3.42)

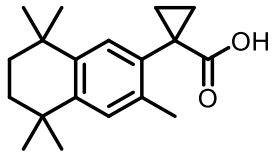

To a 20 mL scintillation vial under N_2 atmosphere was charged tert-butyl 1-(3,5,5,8,8-pentamethyl-5,6,7,8-tetrahydronaphthalen-2-yl)cyclopropane-1-carboxylate (814.1 mg, 2.47 mmol, 1.0 equiv) and anhydrous DCM (5.5 mL). To the vial was then added Et_3SiH (747 mg, 1.03 mL, 6.4 mmol, 2.6 equiv) followed by trifluoroacetic acid (3.67 g, 2.47 mL, 32.2 mmol, 13 equiv). The reaction mixture was left stirring at room temperature until complete conversion of the starting material was observed by TLC. The solvent was removed *in vacuo* to afford the product as a white solid (0.642 g, 91% yield).

^{1}H NMR (500 MHz, $CDCl_3$) δ 7.12 (s, 1H), 7.05 (s, 1H), 2.28 (s, 3H), 1.71 – 167 (m, 2H), 1.64 (s, 4H), 1.25 (s, 6H), 1.23 (s, 6H), 1.23 – 1.19 (m, 2H).

^{13}C{^{1}H} NMR (126 MHz, $CDCl_3$) δ 180.4, 144.0, 142.0, 135.7, 134.0, 128.4, 128.0, 35.2, 33.9, 31.9, 31.8, 27.3, 19.0, 18.2.

HRMS (ESI) m/z calculated for $C_{19}H_{25}O_2$ $[M-H]^-$ 285.1860, found 285.1861.

MP = 228 – 230 °C.

1-(thiophen-3-yl)cyclopropane-1-carboxylic acid (3.43)

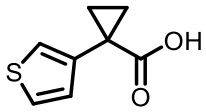

To a 20 mL scintillation vial under N_2 atmosphere was charged tert-butyl 1-(thiophen-3-yl)cyclopropane-1-carboxylate (164 mg, 0.73 mmol, 1.0 equiv) and anhydrous DCM (1.6 mL). To the vial was then added Et_3SiH (220.7 mg, 0.3 mL, 1.9 mmol, 2.6 equiv) followed by trifluoroacetic acid (1.08 g, 1.8 mL, 9.5 mmol, 13.0 equiv). The reaction mixture was left stirring at room temperature until complete conversion of the starting material was observed by TLC. The solvent was removed *in vacuo* to afford the product as a white solid (0.121 g, 99% yield). Characterization data matched those reported in the literature.[120]

1-(benzo[b]thiophen-5-yl)cyclopropane-1-carboxylic acid (3.44)

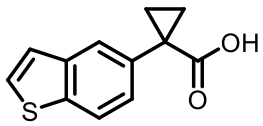

To a 20 mL scintillation vial under N_2 atmosphere was charged tert-butyl 1-(benzo[b]thiophen-5-yl)cyclopropane-1-carboxylate (419.6 mg, 1.9 mmol, 1.0 equiv) and anhydrous DCM (4.2 mL). To the vial was then added Et_3SiH (565.1 mg, 0.78 mL, 4.9 mmol, 2.6 equiv) followed by trifluoroacetic acid (2.77 g, 1.86 mL, 24.3 mmol, 13.0 equiv). The reaction mixture was left stirring at room temperature until complete conversion of the starting material was observed by TLC. The solvent was removed *in vacuo* to afford the product as a white solid (0.360 g, 88% yield).

^{1}H NMR (500 MHz, $CDCl_3$) δ 7.82 (dd, J = 8.3, 0.8 Hz, 2H), 7.79 (d, J = 1.6 Hz, 1H), 7.43 (d, J = 5.4 Hz, 1H), 7.36 (dd, J = 8.3, 1.7 Hz, 1H), 7.29 (dd, J = 5.5, 0.6 Hz, 1H), 1.75 – 1.69 (m, 2H), 1.36 – 1.30 (m, 2H).

^{13}C{^{1}H} NMR (126 MHz, $CDCl_3$) δ 179.9, 139.6, 139.0, 134.9, 127.1, 127.0, 125.2, 123.7, 122.3, 28.7, 17.6.

HRMS (ESI) m/z calculated for $C_{12}H_9O_2S$ $[M-H]^-$ 217.0329, found 217.0329.

MP = 206 – 208 °C.

1-(2,6-dimethoxypyridin-3-yl)cyclopropane-1-carboxylic acid (3.45)

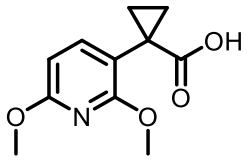

To a 20 mL scintillation vial under N_2 atmosphere was charged tert-butyl 1-(2,6-dimethoxypyridin-3-yl)cyclopropane-1-carboxylate (595.1 mg, 2.13 mmol, 1 equiv) and anhydrous DCM (4.73 mL). To the vial was then added Et_3SiH (644.0 mg, 0.884 mL, 5.5 mmol, 2.6 equiv) followed by trifluoroacetic acid (3.16 g, 2.12 mL, 27.7 mmol, 13.0 equiv). The reaction mixture was left stirring at room temperature until complete conversion of the starting material was observed by TLC. The solvent was removed *in vacuo* to afford the product as a white solid (0.470 g, 99% yield).

^{1}H NMR (500 MHz, $CDCl_3$) δ 7.37 (d, J = 8.0 Hz, 1H), 6.23 (d, J = 8.0 Hz, 1H), 3.94 (s, 3H), 3.89 (s, 3H), 1.67 – 1.61 (m, 2H), 1.14 – 1.08 (m, 2H).

^{13}C{^{1}H} NMR (126 MHz, $CDCl_3$) δ 180.3, 162.4, 161.8, 141.9, 112.4, 100.1, 53.5, 53.5, 23.5, 17.5.

HRMS (ESI) m/z calculated for $C_{11}H_{12}NO_4$ $[M-H]^-$ 222.0772, found 222.0771.

MP = 180 – 182 °C.

tert-butyl acetyl(4-iodophenyl)carbamate (3.46)

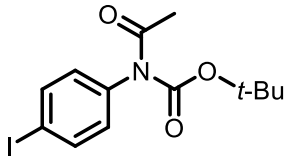

A solution of *N*-(4-iodophenyl)acetamide (500 mg, 1.192 mmol, 1.0 equiv), 4-dimethylaminopyridine (46.8 mg, 0.383 mmol, 0.2 equiv) and triethylamine (666 µL, 4.79 mmol, 2.5 equiv) was stirred at room temperature for 5 min. Di-*tert*-butyl dicarbonate (627 mg, 2.87 mmol, 1.5 equiv) was added subsequently and the resulting mixture was stirred at room temperature for 2.5 d. The reaction mixture was diluted with EtOAc (20 mL) and 1M aq. HCl (5 mL). The organic layer was separated and the aqueous layer was extracted with EtOAc (2×5 mL). The combined organic extracts were dried over Na_2SO_4, filtered, and concentrated *in vacuo* to give the crude product. Purification by silica gel flash chromatography afforded the target product (523 mg, 1.45 mmol) as a white solid. Analytical data was in accordance with that reported in the literature.[121]

^{1}H NMR (500 MHz, $CDCl_3$) δ 7.77 - 7.69 (m, 2H), 6.88 - 6.80 (m, 2H), 2.59 (s, 3H), 1.40 (s, 9H).

^{13}C{^{1}H} NMR (126 MHz, $CDCl_3$) δ 172.7, 152.3, 138.6, 138.1, 130.2, 93.2, 83.6, 27.8, 26.4.

HRMS (ESI) m/z calculated for $C_{13}H_{16}IO_2$ $[M+Na]^+$ 384.0067, found 384.0076.

MP = 115-118 °C.

FTIR (ATR, cm^{-1}) 1303, 1274, 1256, 1155, 1010, 710.

3.4.5.2 NHP Esters

5-methyl-1,3-dioxoisoindolin-2-yl 1-phenylcyclopropane-1-carboxylate (3.47)

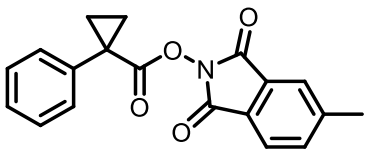

The title product was prepared according to General Procedure A using 1-phenylcyclopropane-1-carboxylic acid (0.81 g, 5.0 mmol, 1.0 equiv), 2-hydroxy-5-methylisoindoline-1,3-dione (0.89 g, 5.0 mmol, 1.0 equiv) *N,N*-dimethylaminopyridine (61 mg, 0.5 mmol, 0.1 equiv), and *N,N*-diisopropylcarbodiimide (0.69 g, 5.5 mmol. 1.1 equiv). Purification of the crude material by FCC (0-100% EtOAc/Hex) using 25 g silica afforded the title product (1.35 g, 4.20 mmol, 84%) as a pale yellow solid.

^{1}H NMR (500 MHz, $CDCl_3$) δ 7.72 (d, *J* = 7.6 Hz, 1H), 7.66 – 7.62 (m, 1H), 7.56 – 7.48 (m, 3H), 7.36 (tt, *J* = 7.3, 1.7 Hz, 2H), 7.31 (tt, *J* = 7.5, 1.4 Hz, 1H), 2.50 (s, 3H), 1.90 (m, 2H), 1.48 (m, 2H).

^{13}C{^{1}H} NMR (126 MHz, $CDCl_3$) δ 171.1, 162.1, 162.0, 146.1, 137.1, 135.1, 130.6, 129.2, 128.5, 127.9, 126.3, 124.4, 123.8, 77.0, 27.3, 22.1, 18.6.

HRMS (ESI) m/z calculated for $C_{19}H_{19}N_2O_4$ $[M+NH_4]+$ 339.1339, found 339.1335.

FTIR (ATR, cm^{-1})

MP = 185-191 °C.

5-methoxy-1,3-dioxoisoindolin-2-yl 1-phenylcyclopropane-1-carboxylate (3.48)

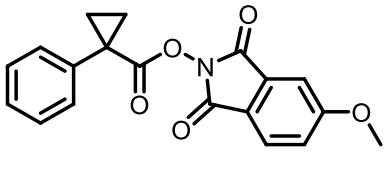

The title product was prepared according to General Procedure A using 1-phenylcyclopropane-1-carboxylic acid (0.81g, 5.0 mmol), 2-hydroxy-5-methoxyisoindoline-1,3-dione (0.97 g, 5.0 mmol) *N,N*-dimethylaminopyridine (61 mg, 0.50 mmol, 0.1 equiv), and *N,N*-diisopropylcarbodiimide (0.69 g, 5.5 mmol. 1.1 equiv). Purification of the crude material by FCC (0-100% EtOAc/Hex) using 25 g silica afforded the title product (1.39 g, 4.11 mmol, 82%) as a white solid.

^{1}H NMR (500 MHz, $CDCl_3$) δ 7.76 (d, *J* = 8.3 Hz, 1H), 7.54 – 7.48 (m, 2H), 7.38 – 7.28 (m, 4H), 7.18 (dd, *J* = 8.4, 2.4 Hz, 1H), 3.92 (s, 3H), 1.93 – 1.87 (m, 2H), 1.50 – 1.46 (m, 2H).

^{13}C{^{1}H} NMR (126 MHz, $CDCl_3$) δ 171.2, 165.1, 162.0, 161.9, 137.1, 131.5, 130.6, 128.5, 127.9, 125.8, 120.7, 120.2, 108.9, 77.0, 56.2, 27.3, 18.6.

HRMS (ESI) m/z calculated for $C_{19}H_{19}N_2O_5$ [M+NH_4]+ 355.1289, found 355.1285.

FTIR (ATR, cm^{-1})

MP = 154-157 °C.

4,5,6,7-tetrachloro-1,3-dioxoisoindolin-2-yl 1-phenylcyclopropane-1-carboxylate (3.49)

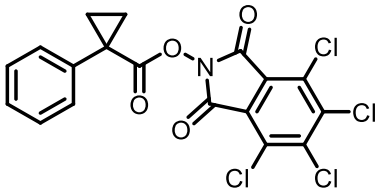

The title product was prepared according to General Procedure A using 1-phenylcyclopropane-1-carboxylic acid (0.81g, 5.0 mmol), *N*-hydroxytetrachlorophthalimide (1.50 g, 5.0 mmol) *N,N*-dimethylaminopyridine (61 mg, 0.50 mmol, 0.1 equiv), and *N,N*-diisopropylcarbodiimide (0.69 g, 5.5 mmol. 1.1 equiv). Purification of the crude material by FCC (0-100% EtOAc/Hex) using 25 g silica afforded the title product (1.78 g, 4.00 mmol, 80%) as an off-white solid, characterization data matched those reported in the literature.[122]

^{1}H NMR (500 MHz, $CDCl_3$) δ 7.51 – 7.48 (m, 2H), 7.37 (ddt, *J* = 8.1, 6.5, 1.1 Hz, 2H), 7.32 (dd, *J* = 7.2, 1.4 Hz, 1H), 1.90 (q, *J* = 4.3 Hz, 2H), 1.54 – 1.48 (m, 2H).

^{13}C{^{1}H} NMR (126 MHz, $CDCl_3$) δ 170.8, 157.6, 141.1, 136.7, 130.7, 130.5, 128.7, 128.3, 124.9, 27.4, 19.0.

1,3-dioxo-1H-benzo[de]isoquinolin-2(3H)-yl 1-phenylcyclopropane-1-carboxylate (3.50)

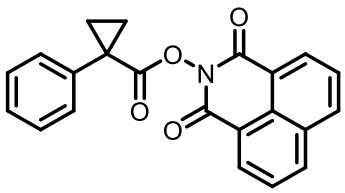

The title product was prepared according to General Procedure A using 1-phenylcyclopropane-1-carboxylic acid (0.81g, 5.0 mmol), *N*-hydroxynaphthalimide (1.06 g, 5.0 mmol) *N,N*-dimethylaminopyridine (61 mg, 0.50 mmol, 0.1 equiv), and *N,N*-diisopropylcarbodiimide (0.69 g, 5.5 mmol. 1.1 equiv). Purification of the crude material by FCC (0-100% EtOAc/Hex) using 25 g silica afforded the title product (1.78 g, 4.00 mmol, 80%) as an off-white solid.

^{1}H NMR (500 MHz, $CDCl_3$) δ 8.58 (dt, *J* = 7.5, 1.4 Hz, 2H), 8.26 – 8.20 (m, 2H), 7.80 – 7.72 (m, 2H), 7.64 – 7.57 (m, 2H), 7.38 (tt, *J* = 7.2, 1.8 Hz, 2H), 7.31 (dd, *J* = 7.2, 1.2 Hz, 1H), 1.98 (q, *J* = 4.3 Hz, 2H), 1.50 (q, *J* = 4.3 Hz, 2H).

^{13}C{^{1}H} NMR (126 MHz, $CDCl_3$) δ 171.1, 159.6, 137.7, 135.1, 132.0, 132.0, 130.8, 128.5, 127.9, 127.7, 127.2, 122.5, 27.8, 18.4.

HRMS (ESI) m/z calculated for $C_{22}H_{19}N2O_4$ [M+NH4]+ 375.1339, found 375.1337.

MP = 206-209 °C

1,3-dioxoisoindolin-2-yl 1-(thiophen-3-yl)cyclopropane-1-carboxylate (3.51)

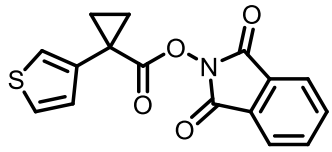

The title product was prepared according to General Procedure A using 1-(thiophen-3-yl)cyclopropane-1-carboxylic acid (0.260 g, 1.5 mmol, 1.0 equiv), *N*-hydroxyphthalimide (0.251 g, 1.5 mmol, 1.0 equiv), *N,N*-dimethylaminopyridine (0.019 g, 0.15 mmol, 0.1 equiv), and *N,N*-diisopropylcarbodiimide (0.214 g, 0.263 mL, 1.7 mmol, 1.1 equiv). Recrystallization from hot methanol afforded the product as a white solid (0.383 g, 79% yield).

^{1}H NMR (500 MHz, $CDCl_3$) δ 7.87 (m, 2H), 7.81 – 7.73 (m, 2H), 7.32 – 7.28 (m, 2H), 7.27 – 7.23 (m, 1H), 1.90 (m, 2H), 1.51 – 1.46 (m, 2H).

^{13}C{^{1}H} NMR (126 MHz, $CDCl_3$) δ 170.5, 161.9, 137.7, 134.7, 129.1, 129.0, 125.7, 124.1, 123.9, 22.4, 19.4.

HRMS (ESI) m/z calculated for $C_{16}H_{11}NNaO_4S$ [M+Na]+ 336.0301, found 336.0297.

MP = 169–171 °C.

1,3-dioxoisoindolin-2-yl1-(2,6-dimethoxypyridin-3-yl)cyclopropane-1-carboxylate (3.52)

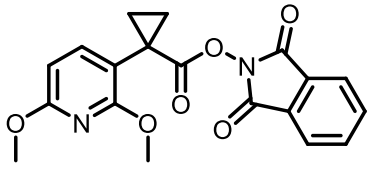

The title product was prepared according to General Procedure A using 1-(2,6-dimethoxypyridin-3-yl)cyclopropane-1-carboxylic acid (0.218 g, 1.0 mmol, 1.0 equiv), *N*-hydroxyphthalimide (0.159 g, 1.0 mmol, 1.0 equiv), *N,N*-dimethylaminopyridine (0.012 g, 0.1 mmol, 0.1 equiv), and *N,N*-diisopropylcarbodiimide (0.136 g, 0.167 mL, 1.1 mmol, 1.1 equiv). Recrystallization from hot methanol afforded the product as a white solid (0.206 g, 57% yield).

^{1}H NMR (500 MHz, $CDCl_3$) δ 7.84 (m, 2H), 7.75 (m, 2H), 7.49 (d, J = 8.0 Hz, 1H), 6.27 (d, J = 8.0 Hz, 1H), 4.07 (s, 3H), 3.92 (s, 3H), 1.85 (m, 2H), 1.33 (m, 2H).

^{13}C{^{1}H} NMR (126 MHz, $CDCl_3$) δ 171.0, 162.9, 162.2, 161.9, 141.5, 134.6, 129.1, 123.8, 110.7, 100.2, 53.7, 53.6, 22.1, 18.5.

HRMS (ESI) m/z calculated for $C_{19}H_{17}N_2O_6$ [M+H]+ 369.1081, found 369.1075.

MP = 130–131 °C.

1,3-dioxoisoindolin-2-yl 1-(benzo[b]thiophen-5-yl)cyclopropane-1-carboxylate (3.53)

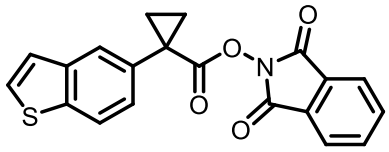

The title product was prepared according to General Procedure A using 1-(benzo[b]thiophen-5-yl)cyclopropane-1-carboxylic acid (0.600 g, 2.75 mmol, 1.0 equiv), *N*-hydroxyphthalimide (0.450 g, 2.75 mmol, 1.0 equiv), *N,N*-dimethylaminopyridine (0.0346 g, 0.28 mmol, 0.1 equiv), and *N,N*-diisopropylcarbodiimide (0.382 g, 0.470 mL, 3.03 mmol, 1.1 equiv). Recrystallization from hot methanol afforded the product as a white solid (0.768 g, 77% yield).

^{1}H NMR (500 MHz, $CDCl_3$) δ 7.96 (d, J = 1.7 Hz, 1H), 7.88 (s, 1H), 7.87 – 7.82 (m, 2H), 7.75 (m, 2H), 7.54 (dd, J = 8.4, 1.8 Hz, 1H), 7.46 (d, J = 5.5 Hz, 1H), 7.34 (dd, J = 5.5, 0.8 Hz, 1H), 1.96 (m, 2H), 1.55 (m, 2H).

^{13}C{^{1}H} NMR (126 MHz, $CDCl_3$) δ 171.2, 161.9, 139.7, 139.4, 134.6, 133.2, 129.0, 127.2, 127.1, 125.4, 123.9, 123.8, 122.5, 27.3, 19.0.

HRMS (ESI) m/z calculated for $C_{20}H_{13}NNaO_4S$ [M+Na]+ 386.0458, found 386.0452.

MP = 146–148 °C.

1,3-dioxoisoindolin-2-yl 1-methylcyclopropane-1-carboxylate (3.54)

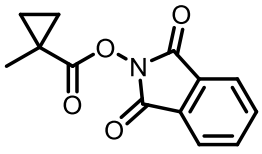

The title product was prepared according to General Procedure A using 1-phenylcyclopropane-1-carboxylic acid (0.50 g, 5.0 mmol, 1.0 equiv), *N*-hydroxyphthalimide (0.89 g, 5.0 mmol, 1.0 equiv) *N,N*-dimethylaminopyridine (61 mg, 0.5 mmol, 0.1 equiv), and *N,N*-diisopropylcarbodiimide (0.69 g, 5.5 mmol. 1.1 equiv). Purification of the crude material by FCC (0-100% EtOAc/Hex) using 12 g silica afforded the title product (0.97 g, 3.95 mmol, 79%) as a white powder.

^{1}H NMR (500 MHz, $CDCl_3$) δ 7.93 – 7.84 (m, 2H), 7.81 – 7.74 (m, 2H), 1.60 – 1.54 (m, 2H), 1.48 (s, 3H), 1.00 – 0.94 (m, 2H).

^{13}C{^{1}H} NMR (126 MHz, $CDCl_3$) δ 172.2, 162.2, 134.8, 129.1, 124.0, 77.2, 19.0, 18.7, 17.5.

HRMS (ESI) m/z calculated for $C_{13}H_{12}NO_4$[M+H]+ 246.0761, found 246.0758.

MP = 125-126 °C.

1,3-dioxoisoindolin-2-yl 1-(3,5,5,8,8-pentamethyl-5,6,7,8-tetrahydronaphthalen-2-yl)cyclopropane-1-carboxylate (3.55)

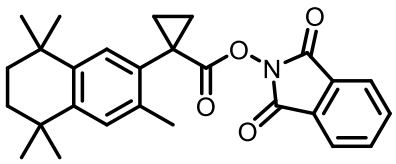

The title product was prepared according to General Procedure A using 1-(3,5,5,8,8-pentamethyl-5,6,7,8-tetrahydronaphthalen-2-yl)cyclopropane-1-carboxylic acid (0.411 g, 1.5 mmol, 1.0 equiv), *N*-hydroxyphthalimide (0.250 g, 1.5 mmol, 1.0 equiv), *N,N*-dimethylaminopyridine (0.019 g, 0.1 mmol, 0.1 equiv), and *N,N*-diisopropylcarbodiimide (0.212 g, 0.260 mL, 1.7 mmol, 1.1 equiv). Recrystallization from hot methanol afforded the product as a white solid (0.382 g, 58% yield).

^{1}H NMR (500 MHz, $CDCl_3$) δ 7.84 (m, 2H), 7.75 (m, 2H), 7.26 (s, 1H), 7.10 (s, 1H), 2.47 (s, 1H), 1.93 (m, 2H), 1.66 (s, 4H), 1.43 (m, 2H), 1.28 (s, 6H), 1.26 (s, 6H.

^{13}C{^{1}H} NMR (126 MHz, $CDCl_3$) δ 171.3, 162.0, 144.5, 142.2, 136.3, 134.6, 132.4, 129.1, 128.6, 128.2, 123.8, 35.2, 35.1, 34.0, 34.0, 31.9, 31.8, 25.8, 19.6, 19.1.

HRMS (ESI) m/z calculated for $C_{27}H_{33}N_2O_4$ $[M+NH_4]+$ 449.2435, found 449.2433.

MP = 201–203 °C.

5-methoxy-1,3-dioxoisoindolin-2-yl bicyclo[1.1.1]pentane-1-carboxylate (3.56)

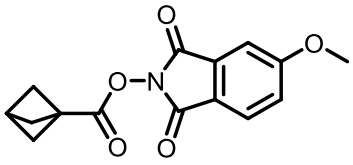

The title product was prepared according to General Procedure A using bicyclo[1.1.1]pentane-1-carboxylic acid (4.46 mmol), 2-hydroxy-5-methoxyisoindoline-1,3-dione (4.46 mmol) *N,N*-dimethylaminopyridine (55 mg, 0.446 mmol, 0.1 equiv), and *N,N*-diisopropylcarbodiimide (0.768 µL, 4.91 mmol, 1.1 equiv). Purification of the crude material by FCC (0-100% EtOAc/Hex) using 12 g silica afforded the title product (1.15 g, 4.00 mmol, 90%) as a white solid.

^{1}H NMR (600 MHz, $CDCl_3$) δ 7.80 (d, J = 8.3 Hz, 1H), 7.37 (d, J = 2.3 Hz, 1H), 7.22 (dd, J = 2.4, 8.4 Hz, 1H), 3.95 (s, 3H), 2.56 (s, 1H), 2.33 (s, 6H).

^{13}C{^{1}H} NMR (151 MHz, $CDCl_3$) δ 165.1, 164.7, 162.0, 161.8, 131.5, 125.9, 120.7, 120.3, 108.9, 56.2, 52.4, 39.9, 29.1.

HRMS (ESI) m/z calculated for $C_{15}H_{14}NO_5$ [M+H]+ 288.0867, found 288.0864.

FTIR (ATR, cm^{-1}) 2995, 1781, 1740, 1490, 1360, 1289, 1040.

MP = 116-124 °C.

1,3-dioxoisoindolin-2-yl 3-(dimethylcarbamoyl)bicyclo[1.1.1]pentane-1-carboxylate (3.57)

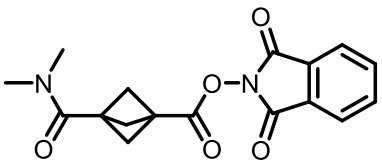

The title product was prepared according to General Procedure B using 3-(dimethylcarbamoyl)bicyclo[1.1.1]pentane-1-carboxylic acid (4.09 mmol). Collection of the precipitate resulting from dilution of the crude reaction mixture with water (~20 mL) afforded the title compound as a white solid (1.02 g, 3.11 mmol, 76% yield).

^{1}H NMR (600 MHz, $CDCl_3$) δ 7.94 - 7.86 (m, 2H), 7.83 - 7.77 (m, 2H), 3.12 (s, 3H), 2.96 (s, 3H), 2.64 (s, 6H).

^{13}C{^{1}H} NMR (151 MHz, $CDCl_3$) δ 167.7, 164.9, 161.7, 134.8, 128.9, 124.0, 54.5, 40.9, 37.2, 36.2, 36.1.

HRMS (ESI) m/z calculated for $C_{17}H_{18}N_2O_5$ [M+H]+ 329.1132, found 329.1134.

FTIR (ATR, cm^{-1}) 2925, 1778, 1739, 1628, 1181, 995, 913, 745.

MP =130-133 °C.

1-methyl 3-(5-methyl-1,3-dioxoisoindolin-2-yl) bicyclo[1.1.1]pentane-1,3-dicarboxylate (3.58)

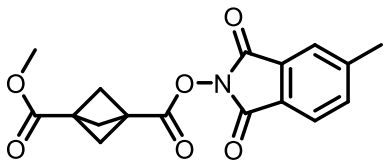

The title product was prepared according to General Procedure A using 3-(methoxycarbonyl)bicyclo[1.1.1]pentane-1-carboxylic acid (0.17 g, 1.0 mmol, 1.0 equiv), 2-hydroxy-5-methylisoindoline-1,3-dione (0.18 g, 1.0 mmol, 1.0 equiv) *N,N*-dimethylaminopyridine (12 mg, 0.1 mmol, 0.1 equiv), and *N,N*-diisopropylcarbodiimide (0.14 g, 1.1 mmol. 1.1 equiv). Purification of the crude material by FCC (0-100% EtOAc/Hex) using 12 g silica afforded the title product (286 mg, 0.87 mmol, 87%) as a white solid.

^{1}H NMR (500 MHz, $CDCl_3$) δ 7.77 (d, *J* = 7.7 Hz, 1H), 7.69 (dt, *J* = 1.5, 0.7 Hz, 1H), 7.58 (ddd, *J* = 7.7, 1.5, 0.8 Hz, 1H), 3.72 (s, 3H), 2.55 (s, 6H), 2.53 (s, 3H).

^{13}C{^{1}H} NMR δ 168.9, 164.8, 162.0, 161.9, 146.4, 135.3, 129.2, 126.2, 124.6, 124.0, 77.0, 53.6, 52.0, 38.6, 35.4, 22.2.

HRMS (ESI) m/z calculated for $C_{17}H_{15}NNaO_6$ [M+Na]+ 352.07916, found 352.0791.

MP =165-168 °C.

1-(5-methoxy-1,3-dioxoisoindolin-2-yl) 3-methyl bicyclo[1.1.1]pentane-1,3-dicarboxylate (3.59)

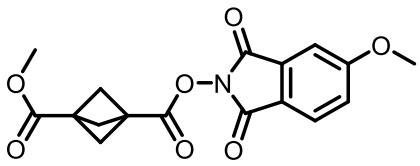

The title product was prepared according to General Procedure A using 3-(methoxycarbonyl)bicyclo[1.1.1]pentane-1-carboxylic acid (0.17 g, 1.0 mmol, 1.0 equiv), 2-hydroxy-5-methoxyisoindoline-1,3-dione (0.19 g, 1.0 mmol, 1.0 equiv) *N,N*-dimethylaminopyridine (12 mg, 0.1 mmol, 0.1 equiv), and *N,N*-diisopropylcarbodiimide (0.14 g, 1.1 mmol. 1.1 equiv). Purification of the crude material by FCC (0-100% EtOAc/Hex) using 12 g silica afforded the title (310 mg, 0.90 mmol, 90%) as a white solid.

^{1}H NMR (600 MHz, $CDCl_3$) δ 7.81 (d, J = 8.4 Hz, 1H), 7.37 (d, J = 2.3 Hz, 1H), 7.23 (dd, J = 2.3, 8.4 Hz, 1H), 3.95 (s, 3H), 3.73 (s, 3H), 2.56 (s, 6H).

^{13}C{^{1}H} NMR (151 MHz, $CDCl_3$) δ 168.9, 165.2, 164.8, 161.8, 161.6, 131.4, 126.0, 120.5, 120.4, 109.0, 56.2, 53.6, 52.0, 38.5, 35.4.

HRMS (ESI) m/z calculated for $C_{17}H_{16}NO_7$ [M+H]+ 346.0922, found 346.0916.

FTIR (ATR, cm^{-1}) 1778, 1738, 1488, 1354, 1238, 1213, 999, 913, 745.

MP = 191-193 °C.

1,3-dioxoisoindolin-2-yl bicyclo[1.1.1]pentane-1-carboxylate (3.60)

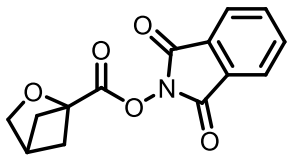

The title product was prepared according to General Procedure B using 2-oxabicyclo[2.1.1]hexane-1-carboxylic acid (2.03 mmol). After dilution of the crude reaction mixture with water (~20 mL), the resulting aqueous mixture was extracted with EtOAc/Hex (1:1, 3× 20 mL). The combined organic extracts were dried over Na_2SO_4, and concentrated in vacuo to give the crude NHP ester which was purified by FCC (0-50% EtOAc/Hex) using 12 g silica to yield the title product (301 mg, 1.10 mmol, 54%) as a white solid.

^{1}H NMR (600 MHz, $CDCl_3$) δ 7.93 - 7.88 (m, 2H), 7.82 - 7.78 (m, 2H), 4.00 - 3.97 (m, 2H), 3.10 (t, J = 3.2 Hz, 1H), 2.43 (ddd, J = 1.9, 3.1, 4.7 Hz, 2H), 2.02 - 1.98 (m, 2H).

^{13}C{^{1}H} NMR (151 MHz, $CDCl_3$) δ 164.3, 161.5, 134.8, 128.9, 124.1, 83.2, 70.0, 43.6, 38.6.

HRMS (ESI) m/z calculated for $C_{14}H_{13}NO_5$ [M+H]+ 274.0710, found 274.0716.

FTIR (ATR, cm^{-1}) 2963, 2894, 1816, 1784, 1738, 1031, 913, 745, 696.

MP = 125-128 °C.

1-(1,3-dioxoisoindolin-2-yl) 4-methyl bicyclo[2.1.1]hexane-1,4-dicarboxylate (3.61)

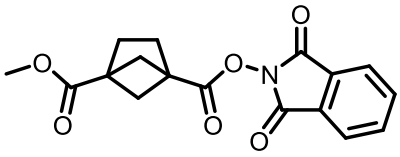

The title product was prepared according to General Procedure B using 4-(methoxycarbonyl)bicyclo[2.1.1]hexane-1-carboxylic acid (2.72 mmol). After dilution of the crude reaction mixture with water (~20 mL), the resulting aqueous mixture was extracted with EtOAc/Hex (1:1, 3× 20 mL). The combined organic extracts were dried over Na_2SO_4, and concentrated in vacuo to give the crude NHP ester which was purified by FCC (0-50% EtOAc/Hex) using 12 g silica to yield the title product (717 mg, 2.18 mmol, 80%) as a white solid.

^{1}H NMR (600 MHz, $CDCl_3$) δ 7.93 - 7.85 (m, 2H), 7.84 - 7.74 (m, 2H), 3.73 (s, 3H), 2.45 - 2.39 (m, 2H), 2.28 - 2.21 (m, 2H), 2.13 - 2.09 (m, 2H), 1.94 - 1.90 (m, 2H).

^{13}C{^{1}H} NMR (151 MHz, $CDCl_3$) δ 172.2, 168.2, 161.8, 134.7, 128.9, 124.0, 51.8, 49.7, 46.5, 44.9, 30.0, 29.5.

HRMS (ESI) m/z calculated for $C_{17}H_{16}NO_6$ [M+H]+ 330.0973, found 330.0972.

FTIR (ATR, cm^{-1}) 2950, 1779, 1732, 1263, 1141, 987, 693.

MP = 104-106 °C.

1-(tert-butyl) 3-(1,3-dioxoisoindolin-2-yl) 3-methylazetidine-1,3-dicarboxylate (3.62)

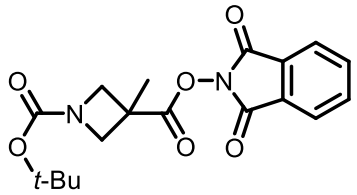

The title product was prepared according to General Procedure A using 1-(tert-butoxycarbonyl)-3-methylazetidine-3-carboxylic acid (0.500 g , 2.32 mmol), *N*-hydroxyphthalimide (0.379 g, 2.32 mmol, 1.0 equiv), *N,N*-dimethylaminopyridine (28 mg, 0.232 mmol, 0.1 equiv), and *N,N*-diisopropylcarbodiimide (0.363 mL, 5.5 mmol. 1.0 equiv). Purification of the crude material by FCC (0-50% EtOAc/Hex) using 12 g silica afforded the title product (708 mg, 1.97 mmol, 85%) as a white solid.

^{1}H NMR (500 MHz, $CDCl_3$) δ 7.93 - 7.88 (m, 2H), 7.85 - 7.78 (m, 2H), 4.48 (m, 2H), 3.85 (m, 2H), 1.77 (s, 3H), 1.47 (s, 9H).

^{13}C{^{1}H} NMR (151 MHz, $CDCl_3$) δ 170.7, 161.7, 155.9, 134.8, 128.8, 124.0, 80.1, 58.1, 37.4, 28.3, 22.2.

HRMS (ESI) m/z calculated for $C_{18}H_{20}N_2O_6Na$ [M+Na]+ 383.1214, found 383.1216.

FTIR (ATR, cm^{-1}) 1746, 1698, 1684, 1052, 912, 743.

MP = 126-128 °C.

1-(tert-butyl) 3-(5-methyl-1,3-dioxoisoindolin-2-yl) 3-methylazetidine-1,3-dicarboxylate (3.63)

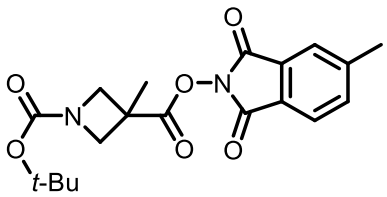

The title product was prepared according to General Procedure A using 1-(tert-butoxycarbonyl)-3-methylazetidine-3-carboxylic acid (1.08 g, 5.0 mmol), 2-hydroxy-5-methylisoindoline-1,3-dione (0.815 g, 5.0 mmol, 1.0 equiv), *N,N*-dimethylaminopyridine (60 mg, 0.50 mmol, 0.1 equiv), and *N,N*-diisopropylcarbodiimide (0.861 mL, 5.5 mmol. 1.0 equiv). Purification of the crude material by FCC (0-50% EtOAc/Hex) using 25 g silica afforded the title product (1.49 g, 4.0 mmol, 80%%) as a white solid.

^{1}H NMR (500 MHz, $CDCl_3$) δ 7.78 (d, *J* = 7.6 Hz, 1H), 7.72 – 7.68 (m, 1H), 7.62 – 7.56 (m, 1H), 4.47 (d, *J* = 8.7 Hz, 2H), 3.84 (d, *J* = 8.7 Hz, 2H), 2.54 (s, 3H), 1.76 (s, 3H), 1.46 (s, 9H).

^{13}C{^{1}H} NMR (126 MHz, $CDCl_3$) δ 170.8, 162.0, 161.9, 156.0, 146.4, 135.4, 129.2, 126.2, 124.6, 124.0, 80.2, 37.5, 28.3, 22.3, 22.2.

HRMS (ESI) m/z calculated for $C_{19}H_{22}N_2O_6Na$ [M+Na]+ 397.130, found 397.1361

MP = 97-99 °C.

1-(tert-butyl) 3-(5-methoxy-1,3-dioxoisoindolin-2-yl) 3-methylazetidine-1,3-dicarboxylate (3.64)

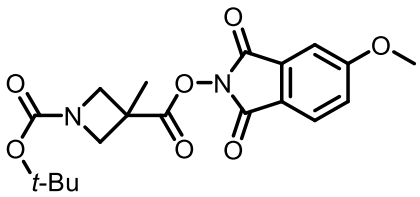

The title product was prepared according to General Procedure A using 1-(tert-butoxycarbonyl)-3-methylazetidine-3-carboxylic acid (1.08 g, 5.0 mmol), 2-hydroxy-5-methoxyisoindoline-1,3-dione (0.965 g, 5.0 mmol, 1.0 equiv), *N,N*-dimethylaminopyridine (60 mg, 0.5 mmol, 0.1 equiv), and *N,N*-diisopropylcarbodiimide (0.861 mL, 5.5 mmol. 1.0 equiv). Purification of the crude material by FCC (0-50% EtOAc/Hex) using 25 g silica afforded the title product (1.65 g, 4.25 mmol, 85%) as a white solid.

^{1}H NMR (500 MHz, $CDCl_3$) δ 7.81 (d, *J* = 8.4 Hz, 1H), 7.37 (d, *J* = 2.3 Hz, 1H), 7.23 (dd, *J* = 8.4, 2.3 Hz, 1H), 4.47 (d, *J* = 8.7 Hz, 2H), 3.95 (s, 3H), 3.83 (d, *J* = 8.8 Hz, 2H), 1.76 (s, 3H), 1.46 (s, 9H).

^{13}C{^{1}H} NMR (126 MHz, $CDCl_3$) δ 170.9, 165.3, 161.9, 161.7, 156.0, 131.5, 126.0, 120.6, 120.5, 109.1, 80.2, 56.2, 37.5, 28.4, 22.3.

HRMS (ESI) m/z calculated for $C_{19}H_{22}N_2O_7Na$ [M+Na]+ 413.1319, found 413.1307

MP = 90-92 °C.

1-(1,3-dioxoisoindolin-2-yl) 1-ethyl cyclobutane-1,1-dicarboxylate (3.65)

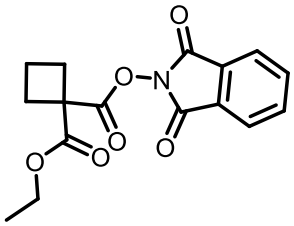

The title product was prepared according to General Procedure A using 1-(ethoxycarbonyl)cyclobutane-1-carboxylic acid (0.86 g, 5 mmol, 1.0 equiv), *N*-hydroxyphthalimide (0.82 g, 5.0 mmol, 1.0 equiv), *N,N*-dimethylaminopyridine (61 mg, 0.5 mmol, 0.1 equiv), and *N,N*-diisopropylcarbodiimide (0.69 g, 5.5 mmol. 1.1 equiv). Recrystallization from hot methanol afforded the product as a white solid (1.12g, 71% yield)

^{1}H NMR (500 MHz, $CDCl_3$) δ 7.89 (m, 2H), 7.80 (m, 2H), 4.32 (q, *J* = 7.2 Hz, 2H), 2.86 – 2.76 (m, 2H), 2.76 – 2.67 (m, 2H), 2.13 (ddqd, *J* = 13.6, 9.0, 4.4, 2.0 Hz, 2H), 1.37 (t, *J* = 7.1 Hz, 3H).

^{13}C{^{1}H} NMR (126 MHz, $CDCl_3$) δ 169.9, 168.4, 161.7, 134.8, 129.0, 124.0, 62.3, 53.5, 51.0, 29.1, 16.5, 13.9.

HRMS (ESI) m/z calculated for $C_{16}H_{15}NO_6Na$ [M+Na]+ 340.07916, found 340.0784

MP =165-168 °C.

5-methyl-1,3-dioxoisoindolin-2-yl 3-methyloxetane-3-carboxylate (3.66)

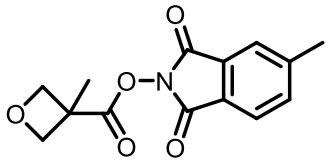

The title product was prepared according to General Procedure A using 3-methyloxetane-3-carboxylic acid (0.58 g, 5.0 mmol), 2-hydroxy-5-methylisoindoline-1,3-dione (0.815 g, 5.0 mmol, 1.0 equiv), *N,N*-dimethylaminopyridine (60 mg, 0.50 mmol, 0.1 equiv), and *N,N*-diisopropylcarbodiimide (0.861 mL, 5.5 mmol. 1.0 equiv). Purification of the crude material by FCC (0-50% EtOAc/Hex) using 25 g silica afforded the title product (1.49 g, 4.0 mmol, 80%%) as a white solid.

^{1}H NMR (500 MHz, $CDCl_3$) δ 7.71 (d, *J* = 7.6 Hz, 1H), 7.64 (s, 1H), 7.52 (d, *J* = 7.7 Hz, 1H), 5.10 (d, *J* = 6.2 Hz, 2H), 4.47 (d, *J* = 6.2 Hz, 2H), 2.47 (s, 3H), 1.77 (s, 3H).

^{13}C{^{1}H} NMR (126 MHz, $CDCl_3$) δ 170.5, 162.1, 162.0, 146.5, 135.4, 129.2, 126.2, 124.6, 124.0, 79.1, 43.3, 22.2, 21.4.

HRMS (ESI) m/z calculated for $C_{14}H_{14}NO_5$[M+H]+ 276.0867, found 276.0863

MP = 94-96 °C.

5-methoxy-1,3-dioxoisoindolin-2-yl 3-methyloxetane-3-carboxylate (3.67)

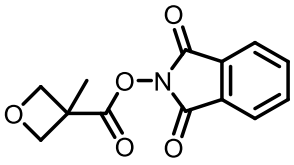

The title product was prepared according to General Procedure A using 3-methyloxetane-3-carboxylic acid (0.58 g, 5.0 mmol), 2-hydroxy-5-methoxyisoindoline-1,3-dione (0.965 g, 5.0 mmol, 1.0 equiv), *N,N*-dimethylaminopyridine (60 mg, 0.50 mmol, 0.1 equiv), and *N,N*-diisopropylcarbodiimide (0.861 mL, 5.5 mmol. 1.0 equiv). Purification of the crude material by FCC (0-50% EtOAc/Hex) using 25 g silica afforded the title product (1.49 g, 4.0 mmol, 80%%) as a white solid.

^{1}H NMR (500 MHz, $CDCl_3$) δ 7.81 (d, *J* = 8.3 Hz, 1H), 7.38 (d, *J* = 2.3 Hz, 1H), 7.23 (dd, *J* = 8.4, 2.3 Hz, 1H), 5.17 (d, *J* = 6.2 Hz, 2H), 4.54 (d, *J* = 6.3 Hz, 2H), 3.95 (s, 3H), 1.84 (s, 3H).

^{13}C{^{1}H} NMR (126 MHz, $CDCl_3$) δ 170.6, 165.3, 161.9, 161.8, 131.5, 126.0, 120.6, 120.5, 109.1, 79.1, 56.2, 43.3, 21.5.

HRMS (ESI) m/z calculated for $C_{14}H_{14}NO_6$ [M+H]+ 292.0816, found 292.0811

MP = 89-92 °C.

3.4.5.3 Products

1-methoxy-4-(1-phenylcyclopropyl)benzene (3.3)

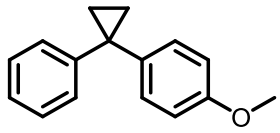

The title product was prepared according to General Procedure C at a 0.50 mmol scale using $NiBr_2$(dme) (10.8 mg, 0.035 mmol, 0.07 equiv), $^{t\text{-}Bu}$BpyCam^{CN} (11.8 mg, 0.035 mmol, 0.07 equiv), zinc flake (64.6 mg, 1.0 mmol, 2.0 equiv), and DMA (0.64 mL) employing 1,3-dioxoisoindolin-2-yl 1-phenylcyclopropane-1-carboxylate (154 mg, 0.50 mmol, 1.00 equiv) and 4-iodoanisole (116 mg, 0.50 mmol, 1.00 equiv) at r.t. (20-22 °C). Purification of the crude reaction mixture using Purification Method A afforded the title product as a colorless oil, 86 mg (77% yield). Characterization data matched those reported in the literature.[118]

The title product was prepared according to General Procedure C at a 0.50 mmol scale using $NiBr_2$(dme) (10.8 mg, 0.035 mmol, 0.07 equiv), $^{t\text{-}Bu}$BpyCam^{CN} (11.8 mg, 0.035 mmol, 0.07 equiv), zinc flake (64.6 mg, 1.0 mmol, 2.0 equiv), and THF (0.64 mL) employing 1,3-dioxoisoindolin-2-yl 1-phenylcyclopropane-1-carboxylate (154 mg, 0.5 mmol, 1.0 equiv) and 4-bromoanisole (91 mg, 0.5 mmol, 1.0 equiv) at 40 °C. Purification of the crude reaction mixture using Purification Method A afforded the title product as a colorless oil, 5 mg (5% yield). Modification of this procedure using 5-methyl-1,3-dioxoisoindolin-2-yl 1-phenylcyclopropane-1-carboxylate (161 mg, 0.5 mmol, 1.0 equiv) or 5-methoxy-1,3-dioxoisoindolin-2-yl 1-phenylcyclopropane-1-carboxylate (169 mg, 0.5 mmol, 1.0 equiv), 4,5,6,7-tetrachloro-1,3-dioxoisoindolin-2-yl 1-phenylcyclopropane-1-carboxylate (222 mg, 0.5 mmol, 1.0 equiv), or 1,3-dioxo-1H-benzo[de]isoquinolin-2(3H)-yl 1-phenylcyclopropane-1-carboxylate (178 mg,

0.5 mmol, 1.0 equiv) afforded the title product, 20 mg (18% yield), 43 mg (38% yield), 12 mg (11% yield), and 0 mg (0%) respectively.

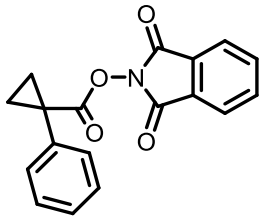

(154 mg, 0.50 mmol)

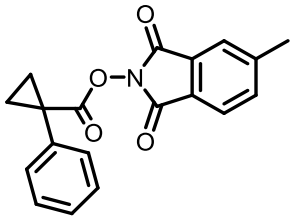

(161 mg, 0.50 mmol)

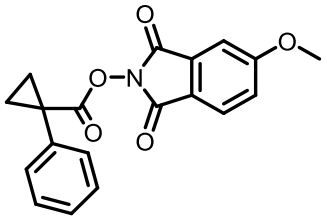

(169 mg, 0.50 mmol)

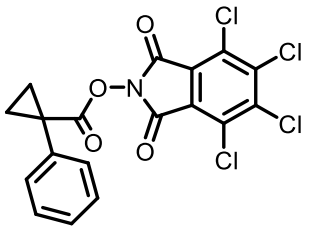

(222 mg, 0.50 mmol)

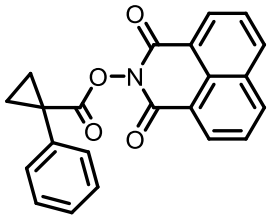

(178 mg, 0.50 mmol)

^{1}H NMR (500 MHz, $CDCl_3$) δ 7.27 – 7.10 (m, 7H), 6.84 – 6.78 (m, 2H), 3.75 (s, 3H), 1.25 (m, 4H).

^{13}C{^{1}H} NMR (126 MHz, $CDCl_3$) δ 157.9, 146.3, 137.8, 129.8, 128.2, 127.9, 125.7, 113.7, 55.2, 29.2, 16.3.

HRMS (ESI) m/z calculated for $C_{16}H_{17}O$ [M+H]+ 225.1274, found 225.1273

N,N-dimethyl-4-(1-phenylcyclopropyl)aniline (3.4)

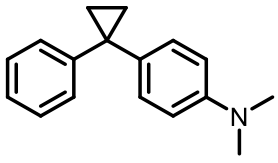

The title product was prepared according to General Procedure C at a 0.50 mmol scale using $NiBr_2$(dme) (10.8 mg, 0.035 mmol, 0.07 equiv), $^{t\text{-}Bu}BpyCam^{CN}$ (11.8 mg, 0.035 mmol, 0.07 equiv), zinc flake (64.6 mg, 1.0 mmol, 2.0 equiv), and THF (0.64 mL) employing 1,3-dioxoisoindolin-2-yl 1-phenylcyclopropane-1-carboxylate (154 mg, 0.5 mmol, 1.0 equiv) and 4-bromo-N,N-dimethylaniline (100 mg, 0.5 mmol, 1.0 equiv) at 40 °C. Purification of the crude reaction mixture using Purification Method A afforded the title product as a colorless oil, 20 mg (16% yield). Modification of this procedure using 5-methyl-1,3-dioxoisoindolin-2-yl 1-phenylcyclopropane-1-carboxylate (161 mg, 0.5 mmol, 1.0 equiv) or 5-methoxy-1,3-dioxoisoindolin-2-yl 1-phenylcyclopropane-1-carboxylate (169 mg, 0.5 mmol, 1.0 equiv), 4,5,6,7-tetrachloro-1,3-dioxoisoindolin-2-yl 1-phenylcyclopropane-1-carboxylate (222 mg, 0.5 mmol, 1.0 equiv), or 1,3-dioxo-1H-benzo[de]isoquinolin-2(3H)-yl 1-phenylcyclopropane-1-carboxylate (178 mg, 0.5 mmol, 1.0 equiv) afforded the title product, 26 mg (22% yield), 32 mg (27% yield), 0 mg (0% yield), and 7 mg (6% yield) respectively.

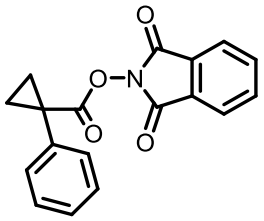

(154 mg, 0.50 mmol)

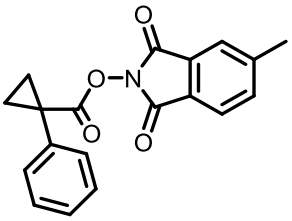

(161 mg, 0.50 mmol)

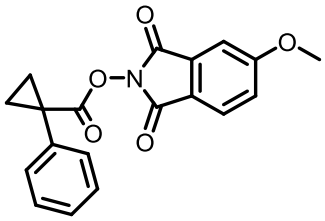

(169 mg, 0.50 mmol)

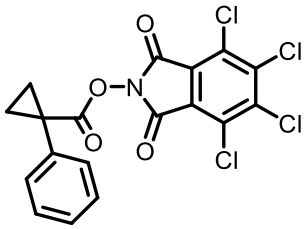

(222 mg, 0.50 mmol)

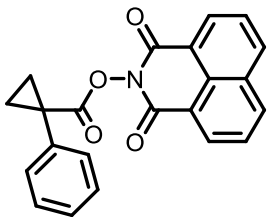

(178 mg, 0.50 mmol)

^{1}H NMR (500 MHz, $CDCl_3$) δ 7.26 – 7.08 (m, 6H), 6.72 – 6.64 (m, 2H), 2.90 (s, 6H), 1.23 (m, 4H).

^{13}C{^{1}H} NMR (126 MHz, $CDCl_3$) δ 149.1, 146.8, 133.6, 129.6, 128.1, 127.8, 125.5, 112.7, 40.8, 29.0, 16.3.

HRMS (ESI)) m/z calculated for $C_{17}H_{20}N$ [M+H]+ 238.15903, found 238.1588.

cyclopropyl(4-(1-phenylcyclopropyl)phenyl)methanone (3.5)

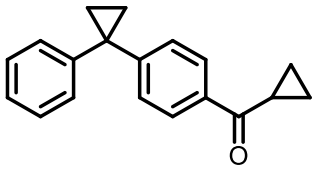

The title product was prepared according to General Procedure C at a 0.50 mmol scale using $NiBr_2$(dme) (10.8 mg, 0.035 mmol, 0.07 equiv), $^{t\text{-Bu}}$BpyCam^{CN} (11.8 mg, 0.035 mmol, 0.07 equiv), zinc flake (64.6 mg, 1.0 mmol, 2.0 equiv), and THF (0.64 mL) employing 1,3-dioxoisoindolin-2-yl 1-phenylcyclopropane-1-carboxylate (154 mg, 0.5 mmol, 1.0 equiv) and (4-bromophenyl)(cyclopropyl)methanone (112 mg, 0.5 mmol, 1.0 equiv) at 40 °C. Purification of the crude reaction mixture using Purification Method A afforded the title product as a colorless oil, 42 mg (isolated with 5% aryl dimer) (30% yield). Modification of this procedure using 5-methyl-1,3-dioxoisoindolin-2-yl 1-phenylcyclopropane-1-carboxylate (161 mg, 0.5 mmol, 1.0 equiv) or 5-methoxy-1,3-dioxoisoindolin-2-yl 1-phenylcyclopropane-1-carboxylate (169 mg, 0.5 mmol, 1.0 equiv), 4,5,6,7-tetrachloro-1,3-dioxoisoindolin-2-yl 1-phenylcyclopropane-1-carboxylate (222 mg, 0.5 mmol, 1.0 equiv), or 1,3-dioxo-1H-benzo[de]isoquinolin-2(3H)-yl 1-phenylcyclopropane-1-carboxylate (178 mg, 0.5 mmol, 1.0 equiv) afforded the title product, 65 mg (50% yield) and 78 mg (60% yield), 0 mg (0% yield), and 32 mg (24% yield) respectively.

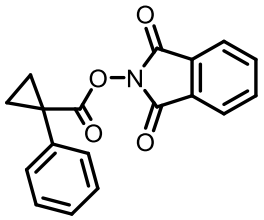

(154 mg, 0.50 mmol)

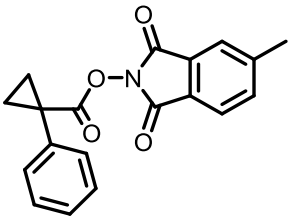

(161 mg, 0.50 mmol)

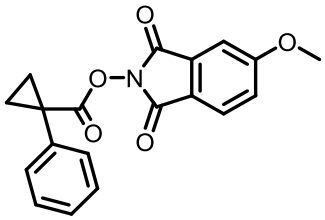

(169 mg, 0.50 mmol)

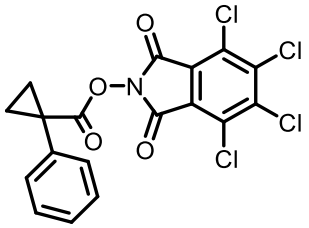

(222 mg, 0.50 mmol)

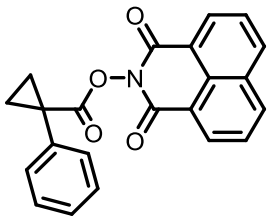

(178 mg, 0.50 mmol)

^{1}H NMR (400 MHz, $CDCl_3$) δ 7.95 – 7.87 (m, 2H), 7.34 – 7.17 (m, 7H), 2.63 (tt, *J* = 7.8, 4.6 Hz, 1H), 1.41 – 1.36 (m, 2H), 1.37 – 1.31 (m, 2H), 1.20 (dt, *J* = 4.6, 3.3 Hz, 2H), 1.00 (dq, *J* = 7.2, 3.6 Hz, 2H).

^{13}C{^{1}H} NMR (101 MHz, $CDCl_3$) δ 200.1, 151.3, 144.6, 135.7, 128.9, 128.5, 128.1, 127.9, 126.4, 77.1, 30.0, 17.1, 17.0, 11.5.

HRMS (ESI)) m/z calculated for $C_{19}H_{19}O$ [M+H]+ 263.1430, found 263.1428.

4-(1-phenylcyclopropyl)benzonitrile (3.6)

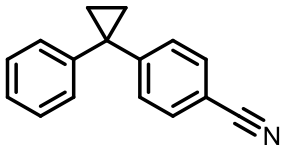

The title product was prepared according to General Procedure C at a 0.50 mmol scale using $NiBr_2$(dme) (10.8 mg, 0.035 mmol, 0.07 equiv), $^{t\text{-Bu}}$BpyCam^{CN} (11.8 mg, 0.035 mmol, 0.07 equiv), zinc flake (64.6 mg, 1.0 mmol, 2.0 equiv), and DMA (0.64 mL) employing 1,3-dioxoisoindolin-2-yl 1-phenylcyclopropane-1-carboxylate (154 mg, 0.5 mmol, 1.0 equiv) and 4-iodobenzonitrile (115 mg, 0.5 mmol, 1.0 equiv) at r.t. (20-22 °C). Purification of the crude reaction mixture using Purification Method A afforded the title product as a colorless oil, 69 mg (64% yield).

The title product was prepared according to General Procedure C at a 0.50 mmol scale using $NiBr_2$(dme) (10.8 mg, 0.035 mmol, 0.07 equiv), $^{t\text{-Bu}}$BpyCam^{CN} (11.8 mg, 0.035 mmol, 0.07 equiv), zinc flake (64.6 mg, 1.0 mmol, 2.0 equiv), and THF (0.64 mL) employing 1,3-dioxoisoindolin-2-yl 1-phenylcyclopropane-1-carboxylate (154 mg, 0.5 mmol, 1.0 equiv) and 4-bromobenzonitrile (91 mg, 0.5 mmol, 1.0 equiv) at 40 °C. Purification of the crude reaction mixture using Purification Method A afforded the title product as a colorless oil, 51 mg (47% yield). Modification of this procedure using 5-methyl-1,3-dioxoisoindolin-2-yl 1-phenylcyclopropane-1-carboxylate (161 mg, 0.5 mmol, 1.0 equiv) or 5-methoxy-1,3-dioxoisoindolin-2-yl 1-phenylcyclopropane-1-carboxylate (169 mg, 0.5 mmol, 1.0 equiv), 4,5,6,7-tetrachloro-1,3-dioxoisoindolin-2-yl 1-phenylcyclopropane-1-carboxylate (222 mg, 0.5 mmol, 1.0 equiv), or 1,3-dioxo-1H-benzo[de]isoquinolin-2(3H)-yl 1-phenylcyclopropane-1-carboxylate (178 mg, 0.5 mmol, 1.0 equiv) afforded the title product, 68 mg (62% yield) 58 mg (53% yield), 0 mg (0% yield), and 21 mg (20% yield) respectively.

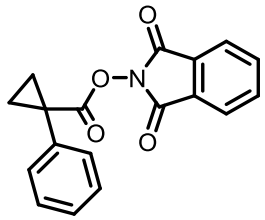

(154 mg, 0.50 mmol)

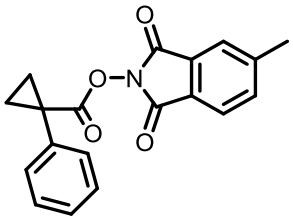

(161 mg, 0.50 mmol)

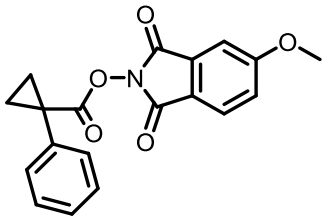

(169 mg, 0.50 mmol)

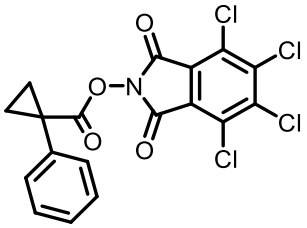

(222 mg, 0.50 mmol)

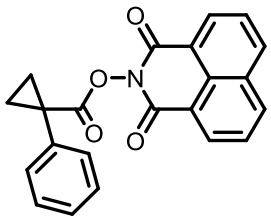

(178 mg, 0.50 mmol)

^{1}H NMR (400 MHz, $CDCl_3$) δ 7.56 – 7.50 (m, 2H), 7.38 – 7.28 (m, 2H), 7.26 – 7.18 (m, 5H), 1.44 – 1.38 (m, 2H), 1.37 – 1.28 (m, 2H).

^{13}C{^{1}H} NMR (101 MHz, $CDCl_3$) δ 151.7, 143.8, 132.2, 132.1, 129.1, 128.6, 128.2, 126.8, 119.1, 109.4, 30.1, 17.3.

HRMS (ESI)) m/z calculated for $C_{16}H_{14}N$ [M+H]+ 220.1121, found 220.1118.

1-(tert-butyl)-4-(1-phenylcyclopropyl)benzene (3.7)

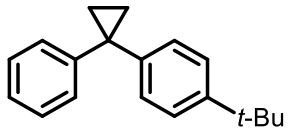

The title product was prepared according to General Procedure C at a 0.50 mmol scale using $NiBr_2$(dme) (10.8 mg, 0.035 mmol, 0.07 equiv), $^{t\text{-Bu}}$BpyCam^{CN} (11.8 mg, 0.035 mmol, 0.07 equiv), zinc flake (64.6 mg, 1.0 mmol, 2.0 equiv), and DMA (0.64 mL) employing 1,3-dioxoisoindolin-2-yl 1-phenylcyclopropane-1-carboxylate (154 mg, 0.5 mmol, 1.0 equiv) and 2-(4-iodophenyl)-4,4,5,5-tetramethyl-1,3,2-dioxaborolane (165 mg, 0.5 mmol, 1.0 equiv) at r.t. (20-22 °C). Purification of the crude reaction mixture using Purification Method A afforded the title product as a colorless oil, 90 mg (72% yield)

^{1}H NMR (500 MHz, $CDCl_3$) δ 7.29 – 7.28 (m, 1H), 7.27 – 7.23 (m, 5H), 7.17 (ddd, *J* = 6.0, 5.0, 2.7 Hz, 1H), 7.15 – 7.13 (m, 1H), 7.13 – 7.11 (m, 1H), 1.29 (s, 9H), 1.28 – 1.27 (m, 4H).

^{13}C{^{1}H} NMR (126 MHz, $CDCl_3$) δ 148.6, 145.9, 142.7, 128.6, 128.2, 127.8, 125.9, 125.1, 34.3, 31.4, 29.4, 16.4.

HRMS (ESI) m/z calculated for $C_{19}H_{23}$ [M+H]+ 251.1794, found 251.1792.

4,4,5,5-tetramethyl-2-(4-(1-phenylcyclopropyl)phenyl)-1,3,2-dioxaborolane[123] (3.8)

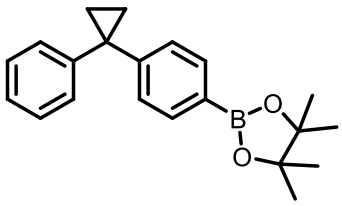

The title product was prepared according to General Procedure C at a 0.50 mmol scale using $NiBr_2$(dme) (10.8 mg, 0.035 mmol, 0.07 equiv), $^{t\text{-Bu}}$BpyCam^{CN} (11.8 mg, 0.035 mmol, 0.07 equiv), zinc flake (64.6 mg, 1.0 mmol, 2.0 equiv), and DMA (0.64 mL) employing 1,3-dioxoisoindolin-2-yl 1-phenylcyclopropane-1-carboxylate(154 mg, 0.5 mmol, 1.0 equiv) and 2-(4-iodophenyl)-4,4,5,5-tetramethyl-1,3,2-dioxaborolane (165 mg, 0.5 mmol, 1.0 equiv) at r.t. (20-22 °C). Purification of the crude reaction mixture using Purification Method A afforded the title product as a white powder, 99 mg (62% yield)

^{1}H NMR (500 MHz, $CDCl_3$) δ 7.71 (d, *J* = 8.2 Hz, 2H), 7.28 – 7.20 (m, 6H), 7.17 (tt, *J* = 7.1, 7.0, 1.3, 1.3 Hz, 1H), 1.32 (s, 12H), 1.31 (s, 4H).

^{13}C{^{1}H} NMR (126 MHz, $CDCl_3$) δ 149.1, 145.4, 134.8, 128.5, 128.3, 127.7, 126.0, 83.7, 30.0, 24.9, 24.8, 16.6.

HRMS (ESI) m/z calculated for $C_{21}H_{26}BO_2$ [M+H]+ 320.2057, found 320.2054.

MP = 98-100 °C.

1-methoxy-2-(1-phenylcyclopropyl)benzene (3.9)

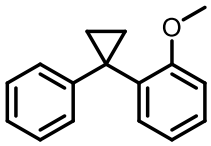

The title product was prepared according to General Procedure C at a 0.50 mmol scale using $NiBr_2$(dme) (10.8 mg, 0.035 mmol, 0.07 equiv), Bathophenanthroline (11.6 mg, 0.035 mmol, 0.07 equiv), zinc flake (64.6 mg, 1.0 mmol, 2.0 equiv), and DMA (0.64 mL) employing 1,3-dioxoisoindolin-2-yl 1-phenylcyclopropane-1-carboxylate (154 mg, 0.50 mmol, 1.0 equiv) and 2-iodoanisole (116 mg, 0.50 mmol, 1.0 equiv) at r.t. (20-22 °C). Purification of the crude reaction mixture using Purification Method A afforded the title product as a yellow oil, 46 mg (41% yield)

^{1}H NMR (400 MHz, $CDCl_3$) δ 7.41 (dd, *J* = 7.5, 1.8 Hz, 1H), 7.33 – 7.02 (m, 7H), 6.93 (td, *J* = 7.4, 1.2 Hz, 1H), 6.85 (dd, *J* = 8.3, 1.2 Hz, 1H), 3.76 (s, 3H), 1.28 (m, 2H), 1.22 (m, 2H).

^{13}C{^{1}H} NMR (101 MHz, $CDCl_3$) δ 159.1, 146.1, 133.1, 131.5, 128.0, 127.9, 126.8, 125.2, 120.4, 110.9, 55.4, 26.1, 16.3.

HRMS (ESI) m/z calculated for $C_{16}H_{17}O$ [M+H]+ 225.1274, found 225.1273

1-methyl-5-(1-phenylcyclopropyl)-1H-indazole (3.10)

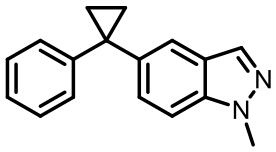

The title product was prepared according to General Procedure C at a 0.50 mmol scale using $NiBr_2$(dme) (5.4 mg, 0.0175 mmol, 0.07 equiv), $^{t\text{-}Bu}$BpyCam^{CN} (5.9 mg, 0.0175 mmol, 0.07 equiv), zinc flake (32.3 mg, 0.5 mmol, 2.0 equiv), and DMA (0.32 mL) employing 1,3-dioxoisoindolin-2-yl 1-phenylcyclopropane-1-carboxylate (77 mg, 0.25 mmol, 1.0 equiv) and 5-iodo-1-methyl-indazole (32.7 mg, 0.25 mmol, 1.0 equiv) at r.t. (20-22 °C). Purification of the crude reaction mixture using Purification Method A afforded the title product as a colorless oil, 27 mg (43% yield)

^{1}H NMR (500 MHz, $CDCl_3$) δ 7.90 (d, *J* = 1.0 Hz, 1H), 7.64 (dd, *J* = 1.6, 0.9 Hz, 1H), 7.36 (dd, *J* = 8.7, 1.6 Hz, 1H), 7.30 (dt, *J* = 8.7, 1.0 Hz, 1H), 7.27 – 7.22 (m, 2H), 7.21 – 7.18 (m, 2H), 7.15 (tt, *J* = 6.8, 1.3 Hz, 1H), 4.04 (s, 3H), 1.33 (m, 4H).

^{13}C{^{1}H} NMR (126 MHz, $CDCl_3$) δ 146.3, 138.8, 137.9, 132.6, 128.5, 128.2, 127.7, 125.8, 124.1, 120.6, 108.8, 35.6, 29.9, 16.3.

HRMS (ESI) m/z calculated for $C_{17}H_{17}N_2$ [M+H]+ 249.13863, found 249.1383

MP = 63-66 °C.

1-methoxy-4-(2-phenylcyclopropyl)benzene (3.11)

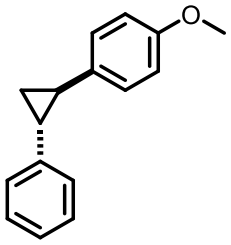

The title product was prepared according to General Procedure C at a 0.50 mmol scale using $NiBr_2$(dme) (10.8 mg, 0.035 mmol, 0.07 equiv), $^{t\text{-}Bu}$BpyCam^{CN} (11.8 mg, 0.035 mmol, 0.07 equiv), zinc flake (64.6 mg, 1.0 mmol, 2.0 equiv), and DMA (0.64 mL) employing 1,3-dioxoisoindolin-2-yl trans-2-phenylcyclopropane-1-carboxylate (154 mg, 0.5 mmol, 1.0 equiv) and 4-iodoanisole (116 mg, 0.50 mmol, 1.0 equiv) at r.t. (20-22 °C). Purification of the crude reaction mixture using Purification Method A afforded the title product as a colorless oil, 40 mg (36% yield). Characterization data matched those reported in the literature.[124]

^{1}H NMR (400 MHz, $CDCl_3$) δ 7.41 (dd, *J* = 7.5, 1.8 Hz, 1H), 7.33 – 7.02 (m, 7H), 6.93 (td, *J* = 7.4, 1.2 Hz, 1H), 6.85 (dd, *J* = 8.3, 1.2 Hz, 1H), 3.76 (s, 3H), 1.28 (m, 2H), 1.22 (m, 2H).

^{13}C{^{1}H} NMR (101 MHz, $CDCl_3$) δ 159.1, 146.1, 133.1, 131.5, 128.0, 127.9, 126.8, 125.2, 120.4, 110.9, 55.4, 26.1, 16.3.

HRMS (ESI) m/z calculated for $C_{16}H_{17}O$ [M+H]+ 225.1274, found 225.1272

4,4'-(cyclopropane-1,1-diyl)bis(methoxybenzene) (3.12)

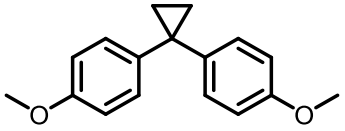

The title product was prepared according to General Procedure C at a 0.25 mmol scale using $NiBr_2$(dme) (5.4 mg, 0.0175 mmol, 0.07 equiv), $^{t\text{-Bu}}$BpyCam^{CN} (5.9 mg, 0.0175 mmol, 0.07 equiv), zinc flake (32.3 mg, 0.5 mmol, 2.0 equiv), and DMA (0.32 mL) employing 1,3-dioxoisoindolin-2-yl 1-(4-methoxyphenyl)cyclopropane-1-carboxylate (84.3 mg, 0.25 mmol, 1.0 equiv) and 1-iodo-4-methoxybenzene (58.5 mg, 0.25 mmol, 1.0 equiv). Purification Method A afforded the title product as a white solid, 45 mg (71% yield).

^{1}H NMR (500 MHz, $CDCl_3$) δ 7.18 – 7.10 (m, 4H), 6.83 – 6.76 (m, 4H), 3.76 (s, 6H), 1.20 (s, 4H).

^{13}C{^{1}H} NMR (126 MHz, $CDCl_3$) δ 157.7, 138.3, 129.3, 113.6, 55.2, 28.5, 16.0.

HRMS (ESI-MS) $[M+H]^+$ *m/z* calculated for $C_{17}H_{19}O_2^+$ 255.1380, found 255.1375.

MP = 56 – 58 °C.

1-chloro-4-(1-(4-methoxyphenyl)cyclopropyl)benzene (3.13)

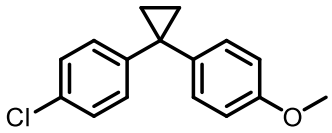

The title product was prepared according to General Procedure C at a 0.25 mmol scale using $NiBr_2$(dme) (5.4 mg, 0.0175 mmol, 0.07 equiv), $^{t\text{-Bu}}$BpyCam^{CN} (5.9 mg, 0.0175 mmol, 0.07 equiv), zinc flake (32.3 mg, 0.5 mmol, 2.0 equiv), and DMA (0.32 mL) employing 1,3-dioxoisoindolin-2-yl 1-(4-chlorophenyl)cyclopropane-1-carboxylate (85.4 mg, 0.25 mmol, 1.0 equiv) and 1-iodo-4-methoxybenzene (58.5 mg, 0.25 mmol, 1.0 equiv). Purification Method A afforded the title product as a colorless oil, 25.9 mg (40% yield).

^{1}H NMR (500 MHz, $CDCl_3$) δ 7.22 – 7.18 (m, 2H), 7.18 – 7.14 (m, 2H), 7.12 – 7.08 (m, 2H), 6.85 – 6.78 (m, 2H), 3.77 (s, 3H), 1.27 – 1.24 (m, 2H), 1.23 – 1.20 (m, 2H).

^{13}C{^{1}H} NMR (126 MHz, $CDCl_3$) δ 158.0, 144.8, 137.2, 131.4, 129.7, 129.3, 128.3, 113.7, 55.3, 28.7, 16.3.

HRMS (ESI-MS) $[M+H]^+$ *m/z* calculated for $C_{16}H_{16}ClO^+$ 259.0884, found 259.0879.

3-(1-(4-methoxyphenyl)cyclopropyl)thiophene (3.14)

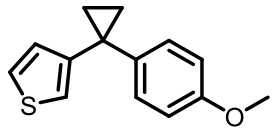

The title product was prepared according to General Procedure C at a 0.25 mmol scale using $NiBr_2$(dme) (5.4 mg, 0.0175 mmol, 0.07 equiv), $^{t\text{-}Bu}$BpyCam^{CN} (5.9 mg, 0.0175 mmol, 0.07 equiv), zinc flake (32.3 mg, 0.5 mmol, 2.0 equiv), and DMA (0.32 mL) employing 1,3-dioxoisoindolin-2-yl 1-(thiophen-3-yl)cyclopropane-1-carboxylate (78.3 mg, 0.25 mmol, 1.0 equiv) and 1-iodo-4-methoxybenzene (58.5 mg, 0.25 mmol, 1.0 equiv). Purification Method A afforded the title product as a colorless oil, 32.8 mg (57% yield).

^{1}H NMR (500 MHz, $CDCl_3$) δ 7.28 – 7.21 (m, 2H), 7.18 (dd, J = 5.0, 3.0 Hz, 1H), 6.87 – 6.80 (m, 2H), 6.78 (dd, J = 5.0, 1.4 Hz, 1H), 6.69 (dd, J = 3.0, 1.4 Hz, 1H), 3.79 (s, 3H), 1.26 – 1.18 (m, 4H).

^{13}C{^{1}H} NMR (126 MHz, $CDCl_3$) δ 158.1, 148.3, 137.1, 130.2, 126.6, 125.3, 119.9, 113.7, 55.3, 25.8, 16.6.

HRMS (ESI-MS) $[M+H]^+$ *m/z* calculated for $C_{14}H_{15}OS^+$ 231.0838, found 231.0834.

2,6-dimethoxy-3-(1-(4-methoxyphenyl)cyclopropyl)pyridine (3.15)

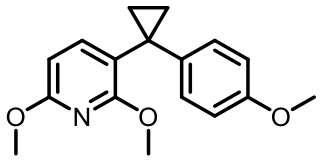

The title product was prepared according to General Procedure C at a 0.25 mmol scale using $NiBr_2$(dme) (5.4 mg, 0.0175 mmol, 0.07 equiv), $^{t\text{-Bu}}$BpyCam^{CN} (5.9 mg, 0.0175 mmol, 0.07 equiv), zinc flake (32.3 mg, 0.5 mmol, 2.0 equiv), and DMA (0.32 mL) employing 1,3-dioxoisoindolin-2-yl 1-(2,6-dimethoxypyridin-3-yl)cyclopropane-1-carboxylate (92.1 mg, 0.25 mmol, 1.0 equiv) and 1-iodo-4-methoxybenzene (58.5 mg, 0.25 mmol, 1.0 equiv). Purification Method A afforded the title product as a white solid, 67.1 mg (94% yield).

^{1}H NMR (500 MHz, $CDCl_3$) δ 7.56 (d, J = 7.9 Hz, 1H), 7.18 – 7.09 (m, 2H), 6.78 – 6.72 (m, 2H), 6.24 (d, J = 8.0 Hz, 1H), 3.91, (s, 3H), 3.88 (s, 3H), 3.74 (s, 3H), 1.22 – 1.14 (m, 2H), 1.14 – 1.06 (m, 2H).

^{13}C{^{1}H} NMR (126 MHz, $CDCl_3$) δ 161.6, 161.4, 157.5, 142.2, 137.9, 128.2, 118.7, 113.4, 100.0, 55.2, 53.4, 53.2, 24.2, 15.4.

HRMS (ESI-MS) $[M+H]^+$ *m/z* calculated for $C_{17}H_{20}NO_3^+$ 286.1438, found 286.1433.

MP = 79 – 81 °C.

5-(1-(4-methoxyphenyl)cyclopropyl)benzo[b]thiophene (3.16)

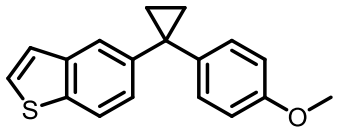

The title product was prepared according to General Procedure C at a 0.25 mmol scale using $NiBr_2$(dme) (5.4 mg, 0.0175 mmol, 0.07 equiv), $^{t\text{-Bu}}$BpyCam^{CN} (5.9 mg, 0.0175 mmol, 0.07 equiv), zinc flake (32.3 mg, 0.5 mmol, 2.0 equiv), and DMA (0.32 mL) employing 1,3-dioxoisoindolin-2-yl 1-(benzo[b]thiophen-5-yl)cyclopropane-1-carboxylate (90.8 mg, 0.25 mmol, 1.0 equiv) and 1-iodo-4-methoxybenzene (58.5 mg, 0.25 mmol, 1.0 equiv). Purification Method A afforded the title product as a colorless oil, 54 mg (77% yield).

^{1}H NMR (500 MHz, $CDCl_3$) δ 7.74 (d, J = 8.4 Hz, 1H), 7.67 (d, J = 1.7 Hz, 1H), 7.38 (d, J = 5.4 Hz, 1H), 7.26 – 7.21 (m, 2H), 7.21 – 7.16 (m, 2H), 6.84 – 6.77 (m, 2H), 3.76 (s, 3H), 1.33 – 1.26 (m, 4H).

^{13}C{^{1}H} NMR (126 MHz, $CDCl_3$) δ 157.8, 142.4, 139.7, 138.1, 137.4, 129.5, 126.6, 125.2, 123.8, 123.1, 122.2, 113.7, 55.2, 29.3, 16.2.

HRMS (ESI-MS) $[M+H]^+$ *m/z* calculated for $C_{18}H_{17}OS^+$ 281.0995, found 291.0988.

methyl 5-(1-phenylcyclopropyl)nicotinate (3.17)

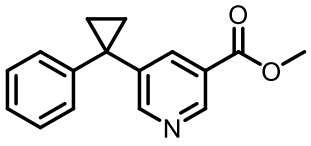

The title product was prepared according to General Procedure C at a 0.50 mmol scale using $NiBr_2$(dme) (10.8 mg, 0.035 mmol, 0.07 equiv), $^{t\text{-Bu}}$BpyCam^{CN} (11.8 mg, 0.035 mmol, 0.07 equiv), zinc flake (64.6 mg, 1.0 mmol, 2.0 equiv), and THF (0.64 mL) employing 1,3-dioxoisoindolin-2-yl 1-phenylcyclopropane-1-carboxylate (154 mg, 0.5 mmol, 1.0 equiv) and methyl 5-bromonicotinate (108 mg, 0.5 mmol, 1.0 equiv) at 40 °C. Purification of the crude reaction mixture using Purification Method A afforded the title product as a colorless oil, 69 mg (with 10% phthalimide) (50% yield)

^{1}H NMR (600 MHz, $CDCl_3$) δ 9.03 (d, *J* = 2.0 Hz, 1H), 8.65 (d, *J* = 2.3 Hz, 1H), 8.13 (t, *J* = 2.1 Hz, 1H), 7.35 – 7.27 (m, 2H), 7.26 – 7.18 (m, 3H), 3.93 (s, 3H), 1.42 – 1.39 (m, 2H), 1.35 – 1.32 (m, 2H).

^{13}C{^{1}H} NMR (151 MHz, $CDCl_3$) δ 165.9, 153.9, 148.3, 143.7, 141.3, 136.4, 128.7, 128.6, 126.7, 125.6, 52.4, 27.8, 16.0.

HRMS (ESI) m/z calculated for $C_{16}H_{16}NO_2$ [M+H]+ 254.11756, found 254.1171

methyl 5-(1-methylcyclopropyl)nicotinate (3.18)

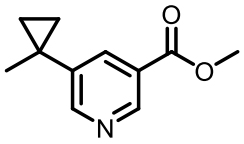

The title product was prepared according to General Procedure C at a 0.25 mmol scale using $NiBr_2$(dme) (15.4 mg, 0.05 mmol, 0.20 equiv), ^{tbu}bpyCam^{CN} (16.8 mg, 0.05 mmol, 0.2 equiv), zinc flake (33 mg, 0.50 mmol, 2.0 equiv), and THF (0.32 mL) employing 1,3-dioxoisoindolin-2-yl 1-methylcyclopropane-1-carboxylate (61.3 mg, 0.25 mmol, 1.0 equiv) and and methyl 5-bromonicotinate (54 mg, 0.25 mmol, 1.0 equiv) at 40 °C. Purification of the crude reaction mixture using Purification Method A afforded the title product as a colorless oil, 20 mg (42% yield).

^{1}H NMR (500 MHz, $CDCl_3$) δ 9.02 (d, *J* = 2.0 Hz, 1H), 8.68 (d, *J* = 2.3 Hz, 1H), 8.12 (t, *J* = 2.2 Hz, 1H), 3.95 (s, 3H), 1.46 (s, 3H), 0.95 – 0.91 (m, 2H), 0.87 – 0.83 (m, 2H).

^{13}C{^{1}H} NMR (126 MHz, $CDCl_3$) δ 166.2, 152.6, 148.1, 142.5, 135.3, 125.6, 77.2, 52.5, 25.2, 17.9, 15.7.

HRMS (ESI) m/z calculated for $C_{11}H_{14}NO_2$[M+H]+ 192.1019, found 192.1016

2-fluoro-5-(1-phenylcyclopropyl)pyridine (3.19)

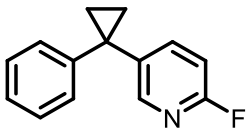

The title product was prepared according to General Procedure C at a 0.50 mmol scale using $NiBr_2$(dme) (10.8 mg, 0.035 mmol, 0.07 equiv), $^{t\text{-}Bu}$BpyCam^{CN} (11.8 mg, 0.035 mmol, 0.07 equiv), zinc flake (64.6 mg, 1.00 mmol, 2.00 equiv), and THF (0.64 mL) employing 1,3-dioxoisoindolin-2-yl 1-phenylcyclopropane-1-carboxylate (154 mg, 0.50 mmol, 1.00 equiv) and 5-bromo-2-fluoropyridine (88 mg, 0.5 mmol, 1.0 equiv) at 40 °C. Purification of the crude reaction mixture using Purification Method A afforded the title product as a pale yellow oil, 26 mg (25% yield)

^{1}H NMR (600 MHz, $CDCl_3$) δ 8.10 (dt, *J* = 1.8, 0.9 Hz, 1H), 7.64 (ddd, *J* = 8.4, 7.7, 2.6 Hz, 1H), 7.32 – 7.26 (m, 2H), 7.24 – 7.17 (m, 3H), 6.82 (ddd, *J* = 8.5, 3.1, 0.7 Hz, 1H), 1.37 – 1.35 (m, 2H), 1.29 – 1.26 (m, 2H).

^{13}C{^{1}H} NMR (151 MHz, $CDCl_3$) δ 162.13 (d, *J* = 237.7 Hz), 147.47 (d, *J* = 14.7 Hz), 144.27, 141.55 (d, *J* = 7.9 Hz), 138.90 (d, *J* = 4.6 Hz), 128.59, 128.16, 126.51, 108.95 (d, *J* = 34.5 Hz), 27.16 (d, *J* = 1.7 Hz), 15.91.

^{19}F{^{1}H} NMR (377 MHz, $CDCl_3$) δ -71.6.

HRMS (ESI) m/z calculated for $C_{14}H_{13}NF$ [M+H]+ 214.1027, found 214.1027

2-chloro-4-(1-phenylcyclopropyl)pyridine (3.20)

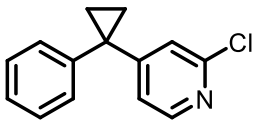

The title product was prepared according to General Procedure C at a 0.50 mmol scale using $NiBr_2$(dme) (10.8 mg, 0.035 mmol, 0.07 equiv), $^{t\text{-}Bu}$BpyCam^{CN} (11.8 mg, 0.035 mmol, 0.07 equiv), zinc flake (64.6 mg, 1.0 mmol, 2.0 equiv), and THF (0.64 mL) employing 1,3-dioxoisoindolin-2-yl 1-phenylcyclopropane-1-carboxylate (154 mg, 0.5 mmol, 1.0 equiv) and 4-bromo-2-chloropyridine (95 mg, 0.50 mmol, 1.0 equiv) at 40 °C. Purification of the crude reaction mixture using Purification Method A afforded the title product as a colorless oil, 64 mg (56% yield)

^{1}H NMR (500 MHz, $CDCl_3$) δ 8.18 (d, *J* = 5.3 Hz, 1H), 7.39 – 7.32 (m, 2H), 7.29 (dt, *J* = 5.8, 1.5 Hz, 3H), 6.93 (d, *J* = 1.7 Hz, 1H), 6.83 (dd, *J* = 5.3, 1.7 Hz, 1H), 1.48 – 1.42 (m, 2H), 1.38 – 1.32 (m, 2H).

^{13}C{^{1}H} NMR (126 MHz, $CDCl_3$) δ 159.1, 151.7, 149.2, 142.2, 129.9, 128.8, 127.3, 122.1, 120.5, 29.2, 18.0.

HRMS (ESI) m/z calculated for $C_{15}H_{13}ClN$ [M+H]+ 230.0730, found 230.0731

2-(1-phenylcyclopropyl)quinoline (3.21)

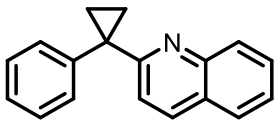

The title product was prepared according to General Procedure C at a 0.50 mmol scale using $NiBr_2$(dme) (10.8 mg, 0.035 mmol, 0.07 equiv), $^{t\text{-}Bu}$BpyCam^{CN} (11.8 mg, 0.035 mmol, 0.07 equiv), zinc flake (64.6 mg, 1.0 mmol, 2.0 equiv), and THF (0.64 mL) employing 1,3-dioxoisoindolin-2-yl 1-phenylcyclopropane-1-carboxylate (154 mg, 0.5 mmol, 1.0 equiv) and 5-bromo-2-fluoropyridine (88 mg, 0.5 mmol, 1.0 equiv) at r.t. (20-22 °C). Purification of the crude reaction mixture using Purification Method A afforded the title product as a pale yellow oil, 36 mg (29% yield)

^{1}H NMR (500 MHz, $CDCl_3$) δ 8.01 (d, *J* = 8.5 Hz, 1H), 7.89 (d, *J* = 8.5 Hz, 1H), 7.72 (dd, *J* = 8.2, 1.4 Hz, 1H), 7.66 (ddd, *J* = 8.4, 6.8, 1.5 Hz, 1H), 7.52 – 7.40 (m, 3H), 7.39 – 7.33 (m, 2H), 7.29 (1, 1H), 7.08 (1, *J* = 8.6 Hz, 1H), 1.85 (m, 2H), 1.38 (m, 2H).

^{13}C{^{1}H} NMR (126 MHz, $CDCl_3$) δ 164.3, 147.8, 143.7, 135.4, 130.4, 129.2, 129.1, 128.6, 127.4, 126.8, 126.4, 125.5, 121.2, 32.3, 17.7, 0.0.

HRMS (ESI) m/z calculated for $C_{18}H_{16}N$ [M+H]+ 246.12773, found 246.1277

Methyl 6-(1-(3,5,5,8,8-pentamethyl-5,6,7,8-tetrahydronaphthalen-2-yl)cyclopropyl)nicotinate (3.22)

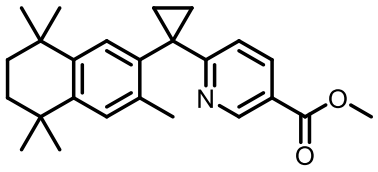

The title product was prepared according to General Procedure C at a 0.25 mmol scale using $NiBr_2$(dme) (5.4 mg, 0.0175 mmol, 0.07 equiv), $^{t\text{-Bu}}$BpyCam^{CN} (5.9 mg, 0.0175 mmol, 0.07 equiv), zinc flake (32.3 mg, 0.5 mmol, 2.0 equiv), and DMA (0.32 mL) employing 1,3-dioxoisoindolin-2-yl 1-(3,5,5,8,8-pentamethyl-5,6,7,8-tetrahydronaphthalen-2-yl)cyclopropane-1-carboxylate (92.1 mg, 0.25 mmol, 1.0 equiv) and methyl 6-bromonicotinate (54 mg, 0.25 mmol, 1.0 equiv). Purification Method A afforded the title product as a white solid, 20.1 mg (21% yield).

^{1}H NMR (500 MHz, $CDCl_3$) δ 9.08 (dd, J = 2.2, 0.8 Hz, 1H), 7.97 (dd, J = 8.3, 2.2 Hz, 1H), 7.27 (s, 1H), 7.11 (s, 1H), 6.74 (dd, J = 8.3, 0.8 Hz, 1H), 3.90 (s, 3H), 2.11 (s, 3H), 1.83 (m, 2H), 1.69 (s, 4H), 1.35 (m, 2H), 1.30 (s, 6H), 1.27 (s, 6H).

^{13}C{^{1}H} NMR (126 MHz, $CDCl_3$) δ 169.3, 166.1, 150.5, 143.8, 142.7, 137.2, 136.6, 135.8, 129.2, 128.3, 122.2, 120.7, 52.1, 35.2, 35.2, 34.0, 33.9, 32.0, 31.9, 30.3, 20.2, 19.3.

HRMS (ESI-MS) $[M+H]^+$ *m/z* calculated for $C_{25}H_{32}NO_2^+$ 378.2428, found 378.2421.

MP = 182 – 183 °C.

1-(4-methoxyphenyl)bicyclo[1.1.1]pentane (3.23)

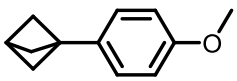

The title product was prepared according to General Procedure D at a 0.300 mmol scale using $NiBr_2$(dme) (18.5 mg, 0.060 mmol, 0.20 equiv), $^{t\text{-}Bu}$BpyCam^{CN} (20.1 mg, 0.060 mmol, 0.20 equiv), zinc dust (39.2 mg, 0.6 mmol, 2.0 equiv), and THF (0.450 mL)/DMA (0.050 mL), employing 1,3-dioxoisoindolin-2-yl bicyclo[1.1.1]pentane-1-carboxylate (77.1 mg, 0.300 mmol, 1.0 equiv) and 4-iodoanisole (70.2 mg, 0.30 mmol, 1.0 equiv). Purification of the crude reaction mixture using Purification Method A afforded the title product (5.8 mg, 11% yield) as a white solid. Modification of this procedure using 5-methoxy-1,3-dioxoisoindolin-2-yl bicyclo[1.1.1]pentane-1-carboxylate (86.2 mg, 0.300 mmol, 1.0 equiv) afforded the title product (22 mg, 42% yield)

^{1}H NMR (500 MHz, $CDCl_3$) δ 7.14 (d, *J* = 8.7 Hz, 2H), 6.83 (d, *J* = 8.7 Hz, 2H), 3.79 (s, 3H), 2.53 (s, 1H), 2.05 (s, 6H).

^{13}C{^{1}H} NMR (151 MHz, $CDCl_3$) δ 158.2, 134.2, 127.0, 113.5, 55.3, 52.2, 46.7, 26.5.

HRMS (ESI) m/z calculated for $C_{12}H_{15}O$ [M]+ 175.1117, found 175.1117

FTIR (ATR, cm^{-1}) 2966, 2906, 2869, 1737, 1519, 1501, 1246, 1207, 1174, 1032, 833.

MP = 48-50 °C.

3-(4-methoxyphenyl)-N,N-dimethylbicyclo[1.1.1]pentane-1-carboxamide (3.24)

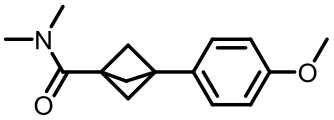

The title product was prepared according to General Procedure D at a 0.300 mmol scale using $NiBr_2$(dme) (18.5 mg, 0.060 mmol, 0.20 equiv), $^{t\text{-Bu}}$BpyCam^{CN} (20.1 mg, 0.060 mmol, 0.20 equiv), zinc dust (39.2 mg, 0.6 mmol, 2.0 equiv), and THF (0.450 mL)/DMA (0.050 mL), employing 1,3-dioxoisoindolin-2-yl 3-(dimethylcarbamoyl)bicyclo[1.1.1]pentane-1-carboxylate (98.5 mg, 0.30 mmol, 1.0 equiv) and 4-iodoanisole (70.2 mg, 0.30 mmol, 1.0 equiv). Purification of the crude reaction mixture using Purification Method B afforded the title product (38.4 mg, 157 μmol, 52%) as a white solid.

^{1}H NMR (600 MHz, $CDCl_3$) δ 7.17 - 7.12 (m, 2H), 6.88 - 6.81 (m, 2H), 3.80 (s, 3H), 3.15 (s, 3H), 2.96 (s, 3H), 2.37 (s, 6H).

^{13}C{^{1}H} NMR (151 MHz, $CDCl_3$) δ 169.7, 158.5, 132.2, 127.1, 113.6, 55.3, 54.4, 42.1, 39.0, 37.3, 36.0.

HRMS (ESI) m/z calculated for $C_{15}H_{20}NO_2$ [M+H]+ 246.1489, found 246.1486.

FTIR (ATR, cm^{-1}) 1615, 1506, 1247, 1034, 912, 743, 646.

MP = 122-127 °C.

methyl 3-(4-methoxyphenyl)bicyclo[1.1.1]pentane-1-carboxylate (3.25)

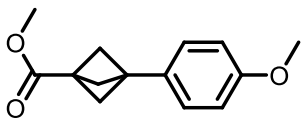

The title product was prepared according to General Procedure C at a 0.50 mmol scale using $NiBr_2$(dme) (10.8 mg, 0.035 mmol, 0.07 equiv), $^{t\text{-Bu}}$BpyCam^{CN} (11.8 mg, 0.035 mmol, 0.07 equiv), zinc flake (64.6 mg, 1.0 mmol, 2.0 equiv), DMA (0.064 mL) and THF (0.58 mL) employing 1-(1,3-dioxoisoindolin-2-yl) 3-methyl bicyclo[1.1.1]pentane-1,3-dicarboxylate (157 mg, 0.50 mmol, 1.0 equiv) and 4-iodoanisole (116 mg, 0.50 mmol, 1.0 equiv) at r.t. (20-22 °C). Purification of the crude reaction mixture using Purification Method A afforded the title product as a white powder, 58 mg (51% yield). Characterization data matched those reported in the literature.[125]

^{1}H NMR (500 MHz, CDCl3) δ 7.17 – 7.10 (m, 2H), 6.88 – 6.81 (m, 2H), 3.79 (s, 3H), 3.71 (s, 3H), 2.29 (s, 6H).

^{13}C{^{1}H} NMR (126 MHz, $CDCl_3$) δ 170.8, 158.7, 132.0, 127.2, 113.7, 55.3, 53.4, 51.7, 41.4, 36.9.

HRMS (ESI) m/z calculated for $C_{14}H_{17}O_3$ [M+H]+ 233.1172, found 233.1169.

MP = 113-116 °C.

methyl 3-(1-phenyl-1H-pyrazol-3-yl)bicyclo[1.1.1]pentane-1-carboxylate (3.26)

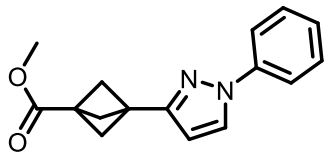

The title product was prepared according to General Procedure D at a 0.300 mmol scale using $NiBr_2$(dme) (18.5 mg, 0.060 mmol, 0.20 equiv), $^{t\text{-Bu}}$BpyCam^{CN} (20.1 mg, 0.060 mmol, 0.20 equiv), zinc dust (39.2 mg, 0.6 mmol, 2.0 equiv), and THF (0.450 mL)/DMA (0.050 mL),employing 1-(1,3-dioxoisoindolin-2-yl) 3-methyl bicyclo[1.1.1]pentane-1,3-dicarboxylate (94.6 mg, 0.30 mmol, 1.0 equiv) and 3-iodo-1-phenyl-1H-pyrazole (81.0 mg, 0.30 mmol, 1.0 equiv, 95% purity). Purification of the crude reaction mixture using Purification Method B afforded the title product (40.9 mg, 0.152 mmol, 51%) as a colorless oil.

^{1}H NMR (600 MHz, $CDCl_3$) δ 7.86 - 7.81 (m, 1H), 7.71 - 7.65 (m, 2H), 7.48 - 7.42 (m, 2H), 7.32 - 7.26 (m, 1H), 6.34 - 6.30 (m, 1H), 3.74 (s, 3H), 2.45 (s, 6H).

^{13}C{^{1}H} NMR (151 MHz, $CDCl_3$) δ 170.5, 152.5, 140.0, 129.3, 127.6, 126.4, 119.4, 105.8, 53.8, 51.6, 38.2, 36.4.

HRMS (ESI) m/z calculated for $C_{16}H_{16}N_2O_2$ [M+H]+ 269.1285, found 269.1287.

FTIR (ATR, cm^{-1}) 2992, 1727, 1600, 1510, 1330, 1211, 1034, 760.

methyl 3-(1-methyl-1H-pyrrolo[2,3-b]pyridin-3-yl)bicyclo[1.1.1]pentane-1-carboxylate (3.27)

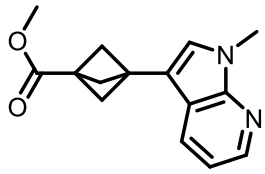

The title product was prepared according to General Procedure D at a 0.30 mmol scale using $NiBr_2$(dme) (18.5 mg, 0.060 mmol, 0.20 equiv), $^{t\text{-}Bu}$BpyCam^{CN} (20.1 mg, 0.060 mmol, 0.20 equiv), zinc dust (39.2 mg, 0.6 mmol, 2.0 equiv), and THF (0.450 mL)/DMA (0.050 mL),employing 1-(1,3-dioxoisoindolin-2-yl) 3-methyl bicyclo[1.1.1]pentane-1,3-dicarboxylate (94.6 mg, 0.30 mmol) and 3-iodo-1-methyl-1H-pyrrolo[2,3-b]pyridine (77.4 mg, 0.30 mmol, 1.0 equiv). Purification of the crude reaction mixture using Purification Method B afforded the title product (23.9 mg, 93.2 μmol, 31%) as a pale yellow solid.

^{1}H NMR (600 MHz, $CDCl_3$) δ 8.37 - 8.30 (m, 1H), 7.94 (dd, J = 1.5, 7.9 Hz, 1H), 7.11 - 7.04 (m, 1H), 6.99 (s, 1H), 3.86 (s, 3H), 3.72 (s, 3H), 2.44 (s, 6H).

^{13}C{^{1}H} NMR (151 MHz, $CDCl_3$) δ 170.5, 147.7, 142.8, 127.8, 126.4, 119.6, 115.2, 112.4, 54.2, 51.7, 38.9, 36.4, 31.1.

HRMS (ESI) m/z calculated for $C_{15}H_{17}N_2O_2$ [M+H]+ 257.1285, found 257.1291.

FTIR (ATR, cm^{-1}) 2976, 2875, 1725, 1466, 1325, 1296, 1206, 1166, 772.

MP = 82-84 °C.

methyl 3-(1-methyl-1H-indazol-5-yl)bicyclo[1.1.1]pentane-1-carboxylate (3.28)

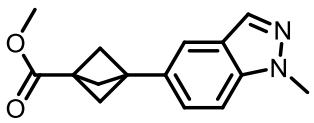

The title product was prepared according to General Procedure D at a 0.300 mmol scale using $NiBr_2$(dme) (18.5 mg, 0.060 mmol, 0.20 equiv), $^{t\text{-Bu}}$BpyCam^{CN} (20.1 mg, 0.060 mmol, 0.20 equiv), zinc dust (39.2 mg, 0.6 mmol, 2.0 equiv), and THF (0.450 mL)/DMA (0.050 mL),employing 1-(1,3-dioxoisoindolin-2-yl) 3-methyl bicyclo[1.1.1]pentane-1,3-dicarboxylate (94.6 mg, 0.30 mmol, 1.0 equiv) and 5-iodo-1-methyl-1H-indazole (77.4 mg, 0.30 mmol, 1.0 equiv). Purification of the crude reaction mixture using Purification Method B afforded the title product (30.8 mg, 0.120 mmol, 40%) as a semi-crystalline white solid.

^{1}H NMR (600 MHz, $CDCl_3$) δ 7.95 (s, 1H), 7.55 (dd, J = 0.9, 1.4 Hz, 1H), 7.37 - 7.34 (m, 1H), 7.32 - 7.27 (m, 1H), 4.08 (s, 3H), 3.75 (s, 3H), 2.39 (s, 6H).

^{13}C{^{1}H} NMR (151 MHz, $CDCl_3$) δ 170.7, 139.1, 132.5, 132.1, 124.8, 123.9, 118.0, 108.8, 53.5, 51.7, 41.9, 36.9, 35.5.

HRMS (ESI) m/z calculated for $C_{15}H_{17}N_2O_2$ [M+H]+ 257.1285, found 257.1288.

FTIR (ATR, cm^{-1}) 2984, 2950, 2912, 2875, 1730, 1449, 1435, 1344, 1305, 1206, 1094, 986, 798.

MP = 137-139 °C.

methyl (R)-3-(4-(5-((1H-1,2,3-triazol-1-yl)methyl)-2-oxooxazolidin-3-yl)-2-fluorophenyl)bicyclo[1.1.1]pentane-1-carboxylate (3.29)

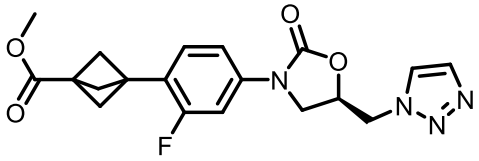

The title product was prepared according to General Procedure D at a 0.300 mmol scale using $NiBr_2$(dme) (18.5 mg, 0.060 mmol, 0.20 equiv), $^{t\text{-Bu}}$BpyCam^{CN} (20.1 mg, 0.060 mmol, 0.20 equiv), zinc dust (39.2 mg, 0.6 mmol, 2.0 equiv), and THF (0.810 mL)/DMA (0.090 mL),employing 1-(1,3-dioxoisoindolin-2-yl) 3-methyl bicyclo[1.1.1]pentane-1,3-dicarboxylate (94.6 mg, 0.30 mmol, 1.0 equiv), (R)-5-((1H-1,2,3-triazol-1-yl)methyl)-3-(3-fluoro-4-iodophenyl)oxazolidin-2-one (116.4 mg, 0.30 mmol, 1.0 equiv). Purification of the crude reaction mixture using Purification Method B afforded the title product (11.7 mg, 30.3 mol, 15%) as a white solid.

^{1}H NMR (600 MHz, $CDCl_3$) δ 7.92 - 7.66 (m, 2H), 7.25 (m, 1H), 7.10 - 7.04 (m, 1H), 7.03 - 6.98 (m, 1H), 5.14 - 5.01 (m, 1H), 4.86 - 4.71 (m, 2H), 4.22 - 4.09 (m, 1H), 3.98 - 3.87 (m, 1H), 3.75 - 3.67 (m, 3H), 2.40 - 2.34 (m, 6H).

^{13}C{^{1}H} NMR (151 MHz, $CDCl_3$) δ 170.4, 161.9 (d, *J* = 247.8 Hz), 153.2, 137.8 (d, *J* = 10.3 Hz), 134.7, 129.3 (d, *J* = 6.2 Hz), 125.3, 122.9 (d, *J* = 15.7 Hz), 113.4 (d, *J* = 3.3 Hz), 106.4 (d, *J* = 27.0 Hz), 70.5, 53.8, 52.2, 51.8, 47.4, 38.7, 38.3.

^{19}F{^{1}H} NMR (471 MHz, $CDCl_3$) δ -113.9.

HRMS (ESI) m/z calculated for $C_{19}H_{20}N_4O_4$ [M+H]+ 387.1463, found 387.1461.

FTIR (ATR, cm^{-1}) 1749, 1723, 1409, 1435, 1409, 1207, 1125.

MP = 162-166 °C.

methyl 3-(4-(N-(tert-butoxycarbonyl)acetamido)phenyl)bicyclo[1.1.1]pentane-1-carboxylate (3.30)

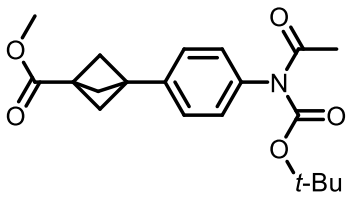

The title product was prepared according to General Procedure D at a 0.300 mmol scale using $NiBr_2$(dme) (18.5 mg, 0.060 mmol, 0.20 equiv), $^{t\text{-Bu}}$BpyCam^{CN} (20.1 mg, 0.060 mmol, 0.20 equiv), zinc dust (39.2 mg, 0.6 mmol, 2.0 equiv), and THF (0.450 mL)/DMA (0.050 mL),employing 1-(1,3-dioxoisoindolin-2-yl) 3-methyl bicyclo[1.1.1]pentane-1,3-dicarboxylate (94.6 mg, 0.30 mmol, 1.0 equiv), tert-butyl acetyl(4-iodophenyl)carbamate (108 mg, 0.30 mmol, 1.0 equiv). Purification of the crude reaction mixture using Purification Method A afforded the title product (71.8 mg, 0.20 mmol, 67%) as a white solid. Analytical data was in accordance with that reported in the literature.[108]

^{1}H NMR (600 MHz, $CDCl_3$) δ 7.24 - 7.20 (m, 2H), 7.05 - 6.99 (m, 2H), 3.71 (s, 3H), 2.56 (s, 3H), 2.33 (s, 6H), 1.40 (s, 9H).

^{13}C{^{1}H} NMR (151 MHz, $CDCl_3$) δ 172.9, 170.6, 152.8, 139.2, 137.6, 128.0, 126.8, 83.3, 53.4, 51.7, 41.6, 37.0, 27.9, 26.5.

HRMS (ESI) m/z calculated for $C_{20}H_{25}NO_5Na$ [M+Na]+ 382.1625, found 382.1630.

methyl 3-(4-acetamidophenyl)bicyclo[1.1.1]pentane-1-carboxylate (3.31)

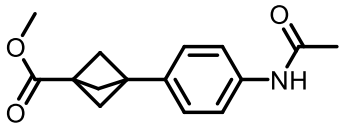

The title product was prepared according to General Procedure D at a 0.300 mmol scale using $NiBr_2$(dme) (18.5 mg, 0.060 mmol, 0.20 equiv), $^{t\text{-Bu}}$BpyCam^{CN} (20.1 mg, 0.060 mmol, 0.20 equiv), zinc dust (39.2 mg, 0.6 mmol, 2.0 equiv), and THF (0.450 mL)/DMA (0.050 mL),employing 1-(1,3-dioxoisoindolin-2-yl) 3-methyl bicyclo[1.1.1]pentane-1,3-dicarboxylate (94.6 mg, 0.30 mmol, 1.0 equiv), *N*-(4-iodophenyl)acetamide (78.3 mg, 0.30 mmol, 1.0 equiv). Purification of the crude reaction mixture using Purification Method B afforded the title product (50.4 mg, 0.194 mmol, 65%) as a white solid.

^{1}H NMR (600 MHz, $CDCl_3$) δ 7.80 (br s, 1H), 7.45 (d, *J* = 8.4 Hz, 1H), 7.14 (d, *J* = 8.2 Hz, 2H), 3.71 (s, 3H), 2.29 (s, 6H), 2.15 (s, 3H).

^{13}C{^{1}H} NMR (151 MHz, $CDCl_3$) δ 170.7, 168.6, 136.8, 135.6, 126.6, 119.9, 53.3, 51.6, 41.4, 36.8, 24.4.

HRMS (ESI) m/z calculated for $C_{15}H_{18}NO_3$ [M+H]+ 260.1281, found 260.1279.

MP = 172-175 °C.

FTIR (ATR, cm^{-1}) 2984, 1720, 1667, 1600, 1530, 1507, 1405, 1298, 1210, 911, 740.

methyl 3-(4-acetoxyphenyl)bicyclo[1.1.1]pentane-1-carboxylate (3.32)

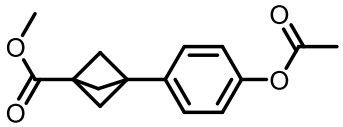

The title product was prepared according to General Procedure C at a 0.25 mmol scale using $NiBr_2$(dme) (14.6 mg, 0.05 mmol, 0.20 equiv), $^{t\text{-Bu}}$BpyCam^{CN} (16.7 mg, 0.05 mmol, 0.20 equiv), zinc flake (32.3 mg, 0.5 mmol, 2.0 equiv), and THF (0.32 mL) employing 1-(1,3-dioxoisoindolin-2-yl) 3-methyl bicyclo[1.1.1]pentane-1,3-dicarboxylate (79 mg, 0.25 mmol, 1.0 equiv) and 4-iodophenyl acetate (65 mg, 0.25 mmol, 1.0 equiv) at r.t. (20-22 °C). Purification of the crude reaction mixture using Purification Method A afforded the title product as a colorless oil, 27 mg (42% yield). Characterization data matched those reported in the literature.[108]

The title product was prepared according to General Procedure C at a 0.25 mmol scale using $NiBr_2$(dme) (14.6 mg, 0.05 mmol, 0.20 equiv), $^{t\text{-Bu}}$BpyCam^{CN} (16.7 mg, 0.05 mmol, 0.20 equiv), zinc flake (32.3 mg, 0.5 mmol, 2.0 equiv), and THF (0.32 mL) employing 1-(1,3-dioxoisoindolin-2-yl) 3-methyl bicyclo[1.1.1]pentane-1,3-dicarboxylate (79 mg, 0.25 mmol, 1.0 equiv) and 4-bromophenyl acetate (54 mg, 0.25 mmol, 1.0 equiv) at r.t. (20-22 °C). Purification of the crude reaction mixture using Purification Method A afforded the title product as a colorless oil, 1.3 mg (2% yield). Modification of this procedure using 5-methoxy-1,3-dioxoisoindolin-2-yl 3-methyl bicyclo[1.1.1]pentane-1,3-dicarboxylate (86.2 mg, 0.250 mmol, 1.0 equiv) afforded the title product (7 mg, 11% yield)

^{1}H NMR (500 MHz, $CDCl_3$) δ 7.24 – 7.18 (m, 2H), 7.04 – 6.99 (m, 2H), 3.71 (s, 3H), 2.31 (s, 6H), 2.29 (s, 3H).

^{13}C{^{1}H} NMR (126 MHz, $CDCl_3$) δ 170.6, 169.6, 149.6, 137.3, 127.2, 126.7, 121.4, 121.3, 53.5, 51.7, 41.4, 36.9, 21.1.

HRMS (ESI) m/z calculated for $C_{15}H_{17}O_4$ [M+H]+ 261.1121, found 261.1120.

methyl 3-(4-chlorophenyl)bicyclo[1.1.1]pentane-1-carboxylate (3.33)

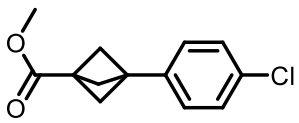

The title product was prepared according to General Procedure D at a 0.300 mmol scale using $NiBr_2$(dme) (18.5 mg, 0.060 mmol, 0.20 equiv), $^{t\text{-Bu}}$BpyCam^{CN} (20.1 mg, 0.060 mmol, 0.20 equiv), zinc dust (39.2 mg, 0.6 mmol, 2.0 equiv), and THF (0.450 mL)/DMA (0.050 mL),employing 1-(1,3-dioxoisoindolin-2-yl) 3-methyl bicyclo[1.1.1]pentane-1,3-dicarboxylate (94.6 mg, 0.30 mmol, 1.0 equiv), 1-chloro-4-iodobenzene (71.5 mg, 0.30 mmol, 1.0 equiv). Purification of the crude reaction mixture using Purification Method A afforded the title product (35.8 mg, 0.151 mmol, 50%) as a white solid. Analytical data was in accordance with that reported in the literature.[108]

^{1}H NMR (600 MHz, $CDCl_3$) δ 7.21 - 7.18 (m, 1H), 7.08 - 7.04 (m, 2H), 3.64 (s, 3H), 2.23 (s, 6H).

^{13}C{^{1}H} NMR (151 MHz, $CDCl_3$) δ 170.4, 138.1, 132.8, 128.4, 127.5, 53.4, 51.7, 41.3, 36.9.

Methyl 4-(4-methoxyphenyl)bicyclo[2.2.2]octane-1-carboxylate (3.34)

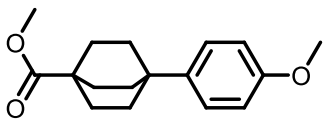

The title product was prepared according to General Procedure C at a 0.50 mmol scale using $NiBr_2$(dme) (10.8 mg, 0.035 mmol, 0.07 equiv), $^{t\text{-Bu}}$BpyCam^{CN} (11.8 mg, 0.035 mmol, 0.07 equiv), zinc flake (64.6 mg, 1.0 mmol, 2.0 equiv), and DMA (0.64 mL) employing 1-(1,3-dioxoisoindolin-2-yl) 4-methyl bicyclo[2.2.2]octane-1,4-dicarboxylate (179 mg, 0.50 mmol, 1.0 equiv) and 4-iodoanisole (116 mg, 0.50 mmol, 1.0 equiv) at r.t. (20-22 °C). Purification of the crude reaction mixture using Purification Method A afforded the title product as a white powder, 54 mg (39% yield). Characterization data matched those reported in the literature.[122]

^{1}H NMR (500 MHz, CDCl3) δ 7.25 – 7.19 (m, 2H), 6.87 – 6.80 (m, 2H), 3.78 (s, 3H), 3.66 (s, 3H), 1.91 (dd, J = 10.3, 4.9 Hz, 6H), 1.83 (dd, J = 10.4, 4.9 Hz, 6H).

^{13}C{^{1}H} NMR (126 MHz, $CDCl_3$) δ 178.47, 157.56, 141.33, 126.41, 113.49, 55.22, 51.68, 39.06, 33.96, 31.89, 28.84.

HRMS (ESI) m/z calculated for $C_{17}H_{23}O_3$ [M+H]+ 275.16417, found 275.1638.

MP = 115-116 °C.

methyl 4-(4-methoxyphenyl)bicyclo[2.1.1]hexane-1-carboxylate (3.35)

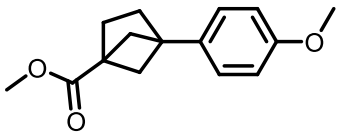

The title product was prepared according to General Procedure D at a 0.30 mmol scale using $NiBr_2$(dme) (18.5 mg, 0.060 mmol, 0.20 equiv), $^{t\text{-Bu}}$BpyCam^{CN} (20.1 mg, 0.060 mmol, 0.20 equiv), zinc dust (39.2 mg, 0.6 mmol, 2.0 equiv), and THF (0.450 mL)/DMA (0.050 mL), employing 1-(1,3-dioxoisoindolin-2-yl) 4-methyl bicyclo[2.1.1]hexane-1,4-dicarboxylate (98.8 mg, 0.30 mmol, 1.0 equiv) and 4-iodoanisole (70.2 mg, 0.30 mmol, 1.0 equiv). Purification of the crude reaction mixture using Purification Method B afforded the title product (16.1 mg, 65.4 µmol, 22%) as a colorless oil.

^{1}H NMR (600 MHz, $CDCl_3$) δ 7.21 - 7.15 (m, 2H), 6.91 - 6.84 (m, 2H), 3.79 (s, 3H), 3.72 (s, 3H), 2.11 - 2.04 (m, 4H), 2.02 - 1.96 (m, 2H), 1.84 - 1.77 (m, 2H).

^{13}C{^{1}H} NMR (151 MHz, $CDCl_3$) δ 174.0, 158.2, 135.0, 127.0, 113.7, 55.3, 51.5, 50.6, 48.9, 46.3, 33.5, 30.8.

HRMS (ESI) m/z calculated for $C_{15}H_{19}NO_3$ [M+H]+ 247.1329, found 247.1335.

FTIR (ATR, cm^{-1}) 2951, 1731, 1518, 1352, 1261, 1248, 1179, 1095.

3-(4-methoxyphenyl)-3-methyloxetane (3.36)

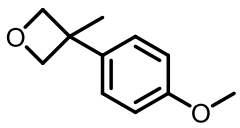

The title product was prepared according to General Procedure C at a 0.50 mmol scale using $NiBr_2$(dme) (10.8 mg, 0.035 mmol, 0.07 equiv), $^{t\text{-}Bu}$BpyCam^{CN} (11.8 mg, 0.035 mmol, 0.07 equiv), zinc flake (64.6 mg, 1.0 mmol, 2.0 equiv), and THF (0.64 mL) employing 1,3-dioxoisoindolin-2-yl 3-methyloxetane-3-carboxylate (130 mg, 0.5 mmol, 1.0 equiv) and 4-iodoanisole (116 mg, 0.5 mmol, 1.0 equiv) at r.t. (20-22 °C). Purification of the crude reaction mixture using Purification Method A afforded the title product as a colorless oil, 44 mg (49% yield). Characterization data matched those reported in the literature.[122]

Modification of this procedure using 5-methoxy-1,3-dioxoisoindolin-2-yl 3-methyloxetane-3-carboxylate (145 mg, 0.5 mmol, 1.0 equiv) afforded the title product as a colorless oil, 49 mg (55% yield)

^{1}H NMR (500 MHz, $CDCl_3$) δ 7.19 – 7.12 (m, 2H), 6.93 – 6.86 (m, 2H), 4.93 (d, *J* = 5.5 Hz, 2H), 4.61 (d, *J* = 5.5 Hz, 2H), 3.81 (s, 3H), 1.71 (s, 3H).

^{13}C{^{1}H} NMR (126 MHz, $CDCl_3$) δ 158.0, 138.6, 126.2, 113.9, 84.0, 65.9, 55.3, 42.8, 27.7, 15.3.

HRMS (ESI) m/z calculated for $C_{11}H_{15}O_2$ [M+H]+ 179.10666, found 179.1065

tert-butyl 3-(4-methoxyphenyl)-3-methylazetidine-1-carboxylate (3.37)

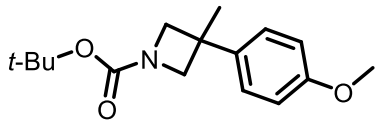

The title product was prepared according to General Procedure D at a 0.300 mmol scale using $NiBr_2$(dme) (18.5 mg, 0.060 mmol, 0.20 equiv), $^{t\text{-Bu}}$BpyCam^{CN} (20.1 mg, 0.060 mmol, 0.20 equiv), zinc dust (39.2 mg, 0.6 mmol, 2.0 equiv), and THF (0.750 mL,employing 1-(tert-butyl) 3-(1,3-dioxoisoindolin-2-yl) 3-methylazetidine-1,3-dicarboxylate (108.1 mg, 0.30 mmol, 1.0 equiv) and 4-iodoanisole (70.2 mg, 0.30 mmol, 1.0 equiv). Purification of the crude reaction mixture using Purification Method A afforded the title product (50.1 mg, 0.181 mmol, 60%) as a colorless oil, which solidified on standing.

^{1}H NMR (600 MHz, $CDCl_3$) δ 7.17 - 7.11 (m, 2H), 6.90 - 6.86 (m, 2H), 4.16 (m, 2H), 3.90 (m, 2H), 3.80 (s, 3H), 1.60 (s, 3H), 1.46 (s, 9H).

^{13}C{^{1}H} NMR (151 MHz, $CDCl_3$) δ 157.9, 156.5, 138.9, 126.2, 113.8, 79.3, 61.8, 55.2, 37.1, 29.0, 28.3.

HRMS (ESI) m/z calculated for $C_{16}H_{23}NO_3Na$ [M+Na]+ 300.1570, found 300.1580.

FTIR (ATR, cm^{-1}) 1699, 1517, 1396, 1249, 1153, 913, 746.

ethyl 1-(4-methoxyphenyl)cyclobutane-1-carboxylate (3.38)

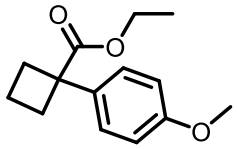

The title product was prepared according to General Procedure C at a 0.50 mmol scale using $NiBr_2$(dme) (10.8 mg, 0.035 mmol, 0.07 equiv), $^{t\text{-}Bu}$BpyCam^{CN} (11.8 mg, 0.035 mmol, 0.07 equiv), zinc flake (64.6 mg, 1.0 mmol, 2.0 equiv), and THF (0.64 mL) employing 1-(1,3-dioxoisoindolin-2-yl) 1-ethyl cyclobutane-1,1-dicarboxylate (159 mg, 0.5 mmol, 1.0 equiv)and 4-iodoanisole (116 mg, 0.5 mmol, 1.0 equiv) at r.t. (20-22 °C). Purification of the crude reaction mixture using Purification Method A afforded the title product as a colorless oil 45 mg (with 5% aryl dimer) (37% yield).

^{1}H NMR (400 MHz, $CDCl_3$) δ 7.27 – 7.20 (m, 2H), 6.89 – 6.82 (m, 2H), 4.09 (q, *J* = 7.1 Hz, 2H), 3.79 (s, 3H), 2.85 – 2.75 (m, 1H), 2.51 – 2.41 (m, 2H), 2.06 – 1.92 (m, 1H), 1.85 (dtt, *J* = 10.9, 9.1, 5.3 Hz, 1H), 1.17 (t, *J* = 7.1 Hz, 3H).

^{13}C{^{1}H} NMR (101 MHz, $CDCl_3$) δ 176.2, 158.2, 135.9, 127.4, 113.6, 60.8, 55.2, 51.7, 32.3, 16.5, 14.1.

HRMS (ESI) m/z calculated for $C_{14}H_{19}O_3$ [M+H]+ 235.1329, found 235.1325

tert-butyl 3-methyl-3-(1-phenyl-1H-pyrazol-3-yl)azetidine-1-carboxylate (3.39)

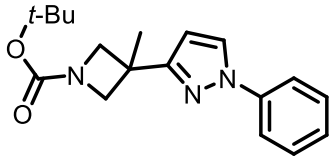

The title product was prepared according to General Procedure D at a 0.300 mmol scale using $NiBr_2$(dme) (18.5 mg, 0.060 mmol, 0.20 equiv), $^{t\text{-Bu}}$BpyCam^{CN} (20.1 mg, 0.060 mmol, 0.20 equiv), zinc dust (39.2 mg, 0.6 mmol, 2.0 equiv), and THF (0.810 mL)/DMA (0.090 mL),employing 1-(tert-butyl) 3-(1,3-dioxoisoindolin-2-yl) 3-methylazetidine-1,3-dicarboxylate (108.1 mg, 0.30 mmol, 1.0 equiv), 3-iodo-1-phenyl-1H-pyrazole (81.2 mg, 0.30 mmol, 1.0 equiv, 95% purity). Purification of the crude reaction mixture using Purification Method A afforded the title product (66.5 mg, 0.212 mmol, 71%) as a colorless oil.

^{1}H NMR (600 MHz, $CDCl_3$) δ 7.90 - 7.86 (m, 1H), 7.73 - 7.67 (m, 2H), 7.49 - 7.43 (m, 2H), 7.31 - 7.26 (m, 1H), 6.38 (d, J = 2.4 Hz, 1H), 4.35 - 4.29 (m, 2H), 3.94 - 3.87 (m, 2H), 1.72 (s, 3H), 1.46 (s, 9H).

^{13}C{^{1}H} NMR (151 MHz, $CDCl_3$) δ 158.5, 156.7, 140.1, 129.4, 127.7, 126.2, 119.0, 104.5, 79.3, 61.4, 33.7, 28.4, 25.7.

HRMS (ESI) m/z calculated for $C_{18}H_{24}N_3O_2$ [M+H]+ 314.1863, found 314.1875.

FTIR (ATR, cm^{-1}) 2965, 1696, 1403, 1391, 1366, 1164, 1106, 913, 746.

Ethyl 4-(8-chloro-3-(1-phenylcyclopropyl)-5,6-dihydro-11H-benzo[5,6]cyclohepta[1,2-b]pyridin-11-ylidene)piperidine-1-carboxylate (3.40)

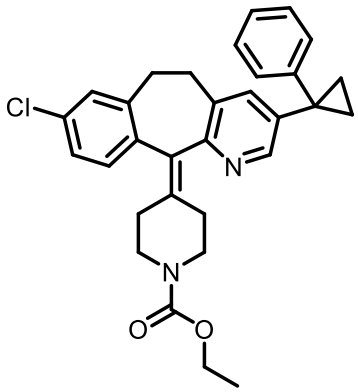

The title product was prepared according to General Procedure C at a 0.10 mmol scale using NiBr2(dme) (5.2 mg, 0.05 mmol, 0.20 equiv), ^{tbu}bpyCam^{CN} (5.8 mg, 0.0175 mmol, 0.2 equiv), zinc flake (13 mg, 0.2 mmol, 2.0 equiv), and THF (0.20 mL) employing 5-methyl-1,3-dioxoisoindolin-2-yl 1-phenylcyclopropane-1-carboxylate (32.1 mg, 0.10 mmol, 1.0 equiv) and and ethyl 4-(3 bromo-8-chloro-5,6-dihydro-11H-benzo[5,6]cyclohepta[1,2-b]pyridin-11-ylidene)piperidine-1-carboxylate (43 mg, 0.10 mmol, 1.0 equiv) at 40 °C. Purification of the crude reaction mixture using Purification Method A afforded the title product as a colorless oil, 29 mg (58% yield).

^{1}H NMR (500 MHz, $CDCl_3$) δ 8.26 (d, J = 2.2 Hz, 1H), 7.31 – 7.07 (m, 9H), 4.13 (q, J = 7.1 Hz, 2H), 3.79 (s, 2H), 3.41 – 3.21 (m, 2H), 3.13 (dddd, J = 13.1, 9.0, 4.1, 2.1 Hz, 2H), 2.83 – 2.71 (m, 2H), 2.54 – 2.44 (m, 1H), 2.32 (dt, J = 14.4, 5.0 Hz, 3H), 1.31 (s, 2H), 1.28 – 1.22 (m, 5H).

^{13}C{^{1}H} NMR (126 MHz, $CDCl_3$) δ 155.7, 146.6, 144.5, 139.9, 139.8, 137.8, 137.7, 134.1, 133.0, 132.7, 130.5, 129.0, 128.7, 128.6, 126.6, 126.3, 61.5, 45.0, 45.0, 31.8, 31.7, 30.7, 27.8, 15.9, 14.8.

HRMS (ESI) m/z calculated for $C_{31}H_{32}ClN_2O_2$ [M+H]+ 499.2147, found 499.2143

3.4.5.4 Preparation of ($^{t\text{-Bu}}$BpyCam^{CN})Ni(*o*-tol)

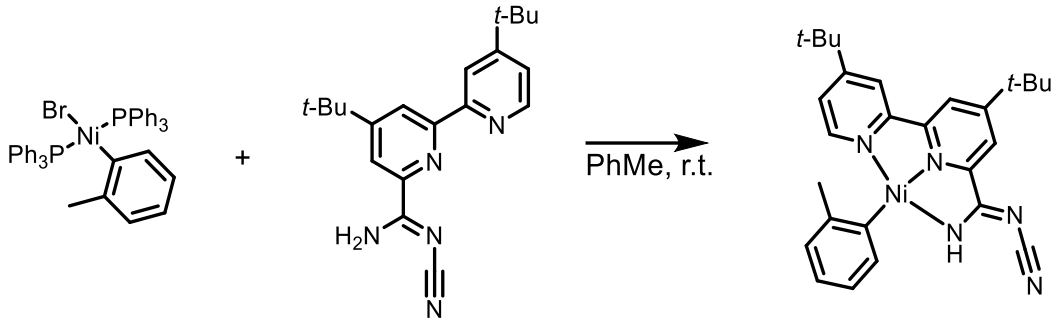

To a flame-dried 200 mL Schlenk flask equipped with a stir bar was charged 4,4′-di-tert-butyl-6-*N*-cyanocarboxamidine-2,2-bipyridine (120.8 mg, 0.36 mmol, 1.03 equiv) and dry toluene (100 mL). The mixture was heated gently, while stirring, using a heatgun until the solution was completely homogenous. The flask was then brought into a N_2-filled glovebox and *trans*-[$(PPh_3)_2$Ni(*o*-tol)]Br (264 mg, 0.35 mmol, 1.0 equiv) was added (*trans*-[$(PPh_3)_2$Ni(*o*-tol)]Br can also be added outside of a glovebox while maintaining positive nitrogen pressure in the reaction vessel). The flask was sealed, removed from the glovebox, and left to stir at room temperature (20-22 °C) for 26 h. After this time, the mixture was concentrated on a Schlenk line using an external solvent trap to approximately half its original volume. The flask then brought into a N_2-filled glovebox, and the mixture was filtered to afford an orange solid, which was subsequently washed multiple times with dry toluene. Pentane was added to the filtrate solution to afford the product as an orange solid. The product was washed several times with pentane to afford 162 mg of an impure orange solid, which was subsequently purified by layered recrystallization, carefully layering pentane onto a solution of the complex in DCM.

^{1}H NMR (500 MHz, CD_2Cl_2) δ 7.90 (d, *J* = 1.5 Hz, 1H), 7.88 (d, *J* = 1.5 Hz, 1H), 7.85 (d, *J* = 2.1 Hz, 1H), 7.62 – 7.56 (m, 1H), 7.51 (d, *J* = 6.0 Hz, 1H), 7.24 (dd, *J* = 6.0, 2.1 Hz, 1H), 6.97 – 6.92 (m, 1H), 6.91 – 6.86 (m, 2H), 2.87 (s, 3H), 1.46 (s, 9H), 1.37 (s, 9H).

$^{13}C\{^{1}H\}$ NMR (126 MHz CD_2Cl_2) δ 166.3, 164.6, 156.0, 154.8, 153.1, 151.2, 144.5, 136.6, 127.8, 124.7, 123.9, 123.8, 120.3, 118.9, 118.1, 53.8, 36.8, 36.0, 30.7, 30.3, 25.6.

3.4.6 Crystallographic Data
Data Collection

A red crystal with approximate dimensions 0.129 × 0.028 × 0.028 mm^3 was selected under oil under ambient conditions and attached to the tip of a MiTeGen MicroMount©. The crystal was mounted in a stream of cold nitrogen at 100(1) K and centered in the X-ray beam by using a video camera.

The crystal evaluation and data collection were performed on a Bruker D8 VENTURE PhotonIII four-circle diffractometer with Cu Kα (λ = 1.54178 Å) radiation and the detector to crystal distance of 5.0 cm.[12622]

The initial cell constants were obtained from a 180° ϕ scan conducted at a 2θ = 50° angle with the exposure time of 1 second per frame. The reflections were successfully indexed by an automated indexing routine built in the APEX3 program. The final cell constants were calculated from a set of 9840 strong reflections from the actual data collection.

The data were collected by using the data collection routine to survey the necessary portion of the reciprocal space to a resolution of 0.81 Å. A total of 126026 data were harvested by collecting 17 sets of frames with 0.9-1.0° scans in ω and ϕ with an exposure time 1–30 sec per frame. These highly redundant datasets were corrected for Lorentz and polarization effects. The absorption correction was based on fitting a function to the empirical transmission surface as sampled by multiple equivalent measurements.[12723]

Structure Solution and Refinement

The systematic absences in the diffraction data were uniquely consistent for the space group $P2_1/c$ that yielded chemically reasonable and computationally stable results of refinement.[128129130131132133]

A successful solution by intrinsic phasing provided most non-hydrogen atoms from the *E*-map. The remaining non-hydrogen atoms were located in an alternating series of least-squares cycles and difference Fourier maps. All non-hydrogen atoms were refined with anisotropic displacement coefficients. All hydrogen atoms were included in the structure factor calculation at idealized positions and were allowed to ride on the neighboring atoms with relative isotropic displacement coefficients.

The asymmetric unit contains two symmetry-independent Ni complexes and several unidentified solvent molecules.

The two Ni complexes have identical composition but minor geometrical differences (Figure 3). In each complex the tolyl ligand is disordered over two positions. The major disorder component has occupancy of 0.747(7) in the Ni1 complex and 0.766(6) in the Ni1A complex. The minor disorder components were refined with restraints.

There are several solvent-accessible voids (total volume ~ 1102 $Å^3$) in the unit cell. They contained two or more types of partially occupied solvent molecules. A significant amount of time was invested in identifying and refining the disordered molecules. Bond length restraints were applied to model the molecules but the resulting isotropic displacement coefficients suggested the molecules were mobile. In addition, the refinement was computationally unstable. Option Solvent Mask of program OLEX2[28] was used to correct the diffraction data for

diffuse scattering effects and to identify the solvent molecules. Solvent Mask calculated 250 electrons in the unit cell for the diffuse species. The compound was crystallized from DCM, heptane, pentane and toluene, thus it is difficult to determine the composition of the solvent mixture is in the voids. Please note that all derived results in the following tables are based on the known contents. No data are given for the diffusely scattering species.

The final least-squares refinement of 739 parameters against 11647 data resulted in residuals *R* (based on F^2 for $I \geq 2\sigma$) and *wR* (based on F^2 for all data) of 0.0624 and 0.1735, respectively. The final difference Fourier map was featureless.

Summary

Crystal Data for $C_{27}H_{31}N_5Ni$ (*M* =484.28 g/mol): monoclinic, space group $P2_1/c$ (no. 14), *a* = 24.446(3) Å, *b* = 11.886(2) Å, *c* = 21.571(3) Å, β = 114.747(7)°, *V* = 5692.3(15) $Å^3$, *Z* = 8, *T* = 100.00 K, μ(Cu Kα) = 1.135 mm^{-1}, *Dcalc* = 1.130 g/cm^3, 126026 reflections measured (3.98° ≤ 2Θ ≤ 149.478°), 11647 unique (R_{int} = 0.0879, R_{sigma} = 0.0377) which were used in all calculations. The final R_1 was 0.0624 (I > 2σ(I)) and wR_2 was 0.1735 (all data).

Acknowledgement

The purchase of the Bruker D8 VENTURE Photon III X-ray diffractometer was partially funded by NSF Award #CHE-1919350 to the UW–Madison Department of Chemistry.

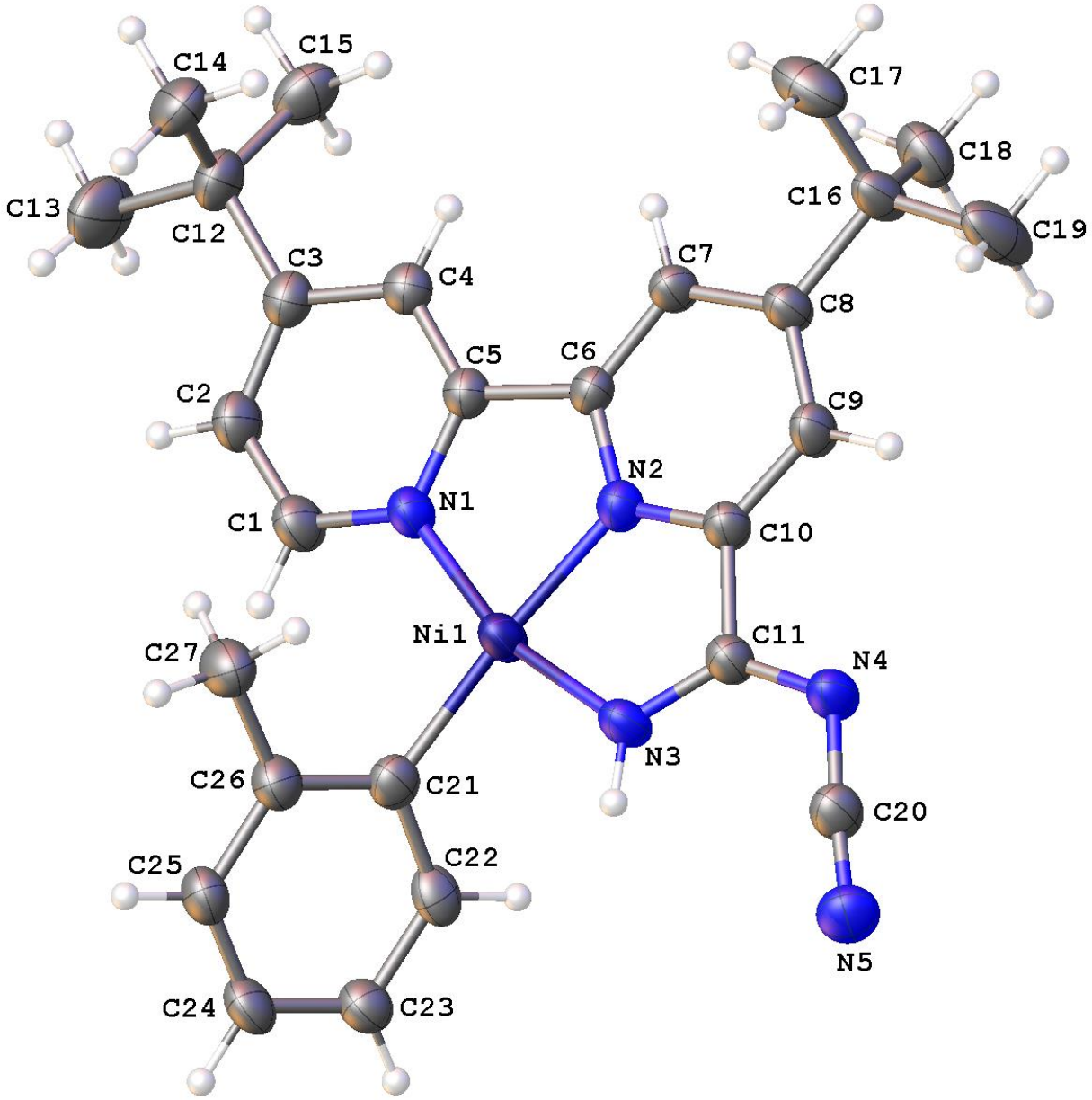

Figure S8. A molecular drawing of the first symmetry-independent complex in Weix10 shown with 50% probability ellipsoids. All H atoms are shown but the minor disorder components are omitted.

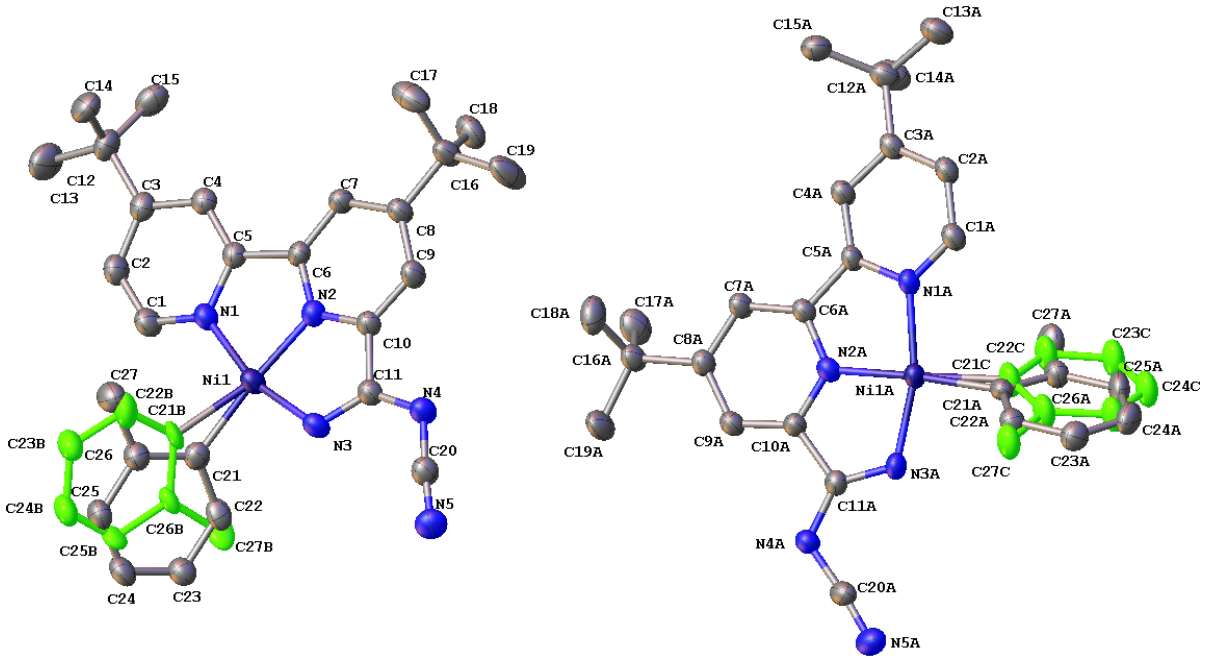

Figure S9. A molecular drawing of Weix10 shown with 50% probability ellipsoids. All H atoms are omitted but the minor disorder components are shown in green.

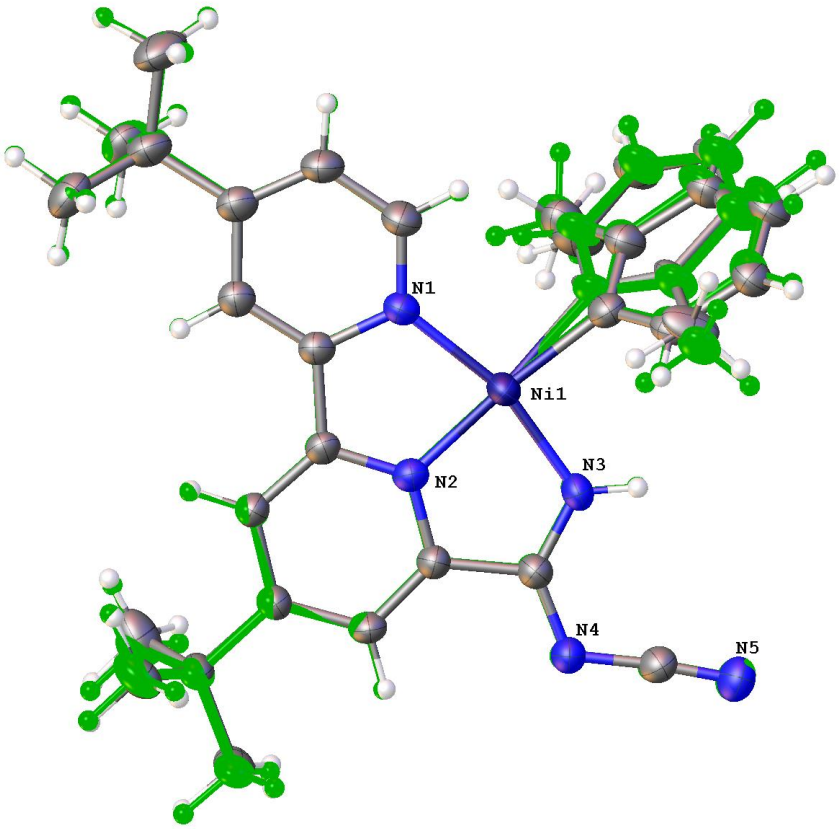

Figure S10. A superposition of the two Ni complexes shown with 50% probability ellipsoids. The Ni1A complex is shown in green.

Table 1 Crystal data and structure refinement for weix10.

Identification code	weix10
Empirical formula	$C_{27}H_{31}N_5Ni$·solvent
Formula weight	484.28
Temperature/K	100.00
Crystal system	monoclinic
Space group	$P2_1/c$
a/Å	24.446(3)
b/Å	11.886(2)
c/Å	21.571(3)
α/°	90
β/°	114.747(7)
γ/°	90
Volume/Å^3	5692.3(15)
Z	8
ρ_{calc}g/cm^3	1.130
μ/mm^{-1}	1.135
F(000)	2048.0
Crystal size/mm^3	0.129 × 0.028 × 0.028
Radiation	Cu Kα (λ = 1.54178)
2Θ range for data collection/°	3.98 to 149.478
Index ranges	-30 ≤ h ≤ 30, -13 ≤ k ≤ 14, -26 ≤ l ≤ 26
Reflections collected	126026
Independent reflections	11647 [R_{int} = 0.0879, R_{sigma} = 0.0377]
Data/restraints/parameters	11647/243/739
Goodness-of-fit on F^2	1.059
Final R indexes [I>=2σ (I)]	R_1 = 0.0624, wR_2 = 0.1654

Final R indexes [all data] $R_1 = 0.0744$, $wR_2 = 0.1735$

Largest diff. peak/hole / e Å^{-3} 0.41/-0.67

Table 2 Fractional Atomic Coordinates (×10^4) and Equivalent Isotropic Displacement Parameters (Å^2×10^3) for weix10. U_{eq} is defined as 1/3 of the trace of the orthogonalised U_{IJ} tensor.

Atom	*x*	*y*	*z*	U(eq)
Ni1	10429.7(2)	1461.5(5)	4457.9(2)	36.50(14)
N1	10660.0(10)	1140(2)	5406.0(12)	36.1(5)
N2	9698.0(10)	1790(2)	4487.2(12)	34.1(5)
N3	9999.3(11)	1859(2)	3539.3(12)	38.3(6)
N4	9009.7(11)	2451(3)	2729.5(12)	41.3(6)
N5	9269.0(13)	2504(3)	1736.8(14)	47.5(7)
C1	11189.8(14)	757(3)	5876.0(16)	42.9(7)
C2	11316.8(14)	662(3)	6563.4(16)	44.2(7)
C3	10899.1(13)	997(3)	6809.9(15)	39.6(7)
C4	10337.6(13)	1345(3)	6317.1(14)	35.3(6)
C5	10227.6(12)	1402(3)	5638.9(14)	33.5(6)
C6	9652.4(12)	1777(3)	5084.0(13)	32.5(6)
C7	9124.5(13)	2102(3)	5125.9(14)	35.5(6)
C8	8631.6(13)	2463(3)	4527.3(14)	36.7(6)
C9	8700.1(13)	2473(3)	3912.0(14)	38.5(7)
C10	9239.8(12)	2142(3)	3913.2(14)	33.9(6)
C11	9426.6(12)	2152(3)	3339.7(14)	35.7(6)
C12	11029.3(15)	1067(3)	7561.6(16)	47.4(8)
C13	11622(2)	476(5)	8010.9(19)	71.3(13)
C14	11075.6(17)	2327(4)	7748.6(18)	54.1(9)
C15	10520.1(17)	534(3)	7704.8(16)	52.1(8)
C16	8045.6(13)	2808(3)	4571.2(15)	43.4(7)
C17	8176.6(18)	3744(4)	5093(2)	61.2(10)
C18	7799.8(15)	1766(4)	4795(2)	53.3(9)
C19	7566.5(18)	3188(5)	3879(2)	71.5(14)
C20	9168.3(14)	2474(3)	2218.1(15)	40.2(7)
C21	11141.9(18)	1147(4)	4338(2)	37.1(10)
C22	11139(3)	328(7)	3878(4)	37.5(15)
C23	11628.1(18)	128(4)	3730(2)	41.6(10)

Table 2 Fractional Atomic Coordinates (×10^4) and Equivalent Isotropic Displacement Parameters (Å^2×10^3) for weix10. U_{eq} is defined as 1/3 of the trace of the orthogonalised U_{IJ} tensor.

Atom	*x*	*y*	*z*	U(eq)
C24	12133.6(18)	795(5)	4031(3)	44.1(11)
C25	12152(2)	1621(6)	4483(3)	43.8(14)
C26	11655(2)	1812(4)	4641(2)	41.6(11)
C27	11685(3)	2772(8)	5102(5)	51.5(19)
C21B	11268(4)	1697(9)	4557(6)	38(3)
C22B	11601(8)	2610(20)	4923(17)	63(8)
C23B	12181(4)	2826(10)	5003(7)	48(3)
C24B	12422(4)	2176(10)	4649(6)	46(3)
C25B	12098(4)	1288(12)	4258(8)	34(4)
C26B	11515(4)	1048(8)	4200(5)	30(3)
C27B	11184(9)	57(19)	3787(17)	48(7)
Ni1A	4599.7(2)	3398.4(4)	-868.2(2)	32.27(14)
N1A	4365.3(10)	3869(2)	-163.5(11)	31.5(5)
N2A	5335.3(10)	3166(2)	-123.3(12)	33.4(5)
N3A	5034.8(10)	2890(2)	-1351.3(12)	36.5(5)
N4A	6038.2(10)	2322(2)	-1183.2(12)	38.9(6)
N5A	5781.0(13)	2065(3)	-2414.6(15)	53.9(8)
C1A	3836.4(12)	4283(3)	-220.8(15)	35.6(6)
C2A	3699.5(12)	4474(3)	331.2(14)	36.5(6)
C3A	4113.6(12)	4221(3)	992.4(14)	34.9(6)
C4A	4684.0(12)	3843(3)	1060.4(14)	35.1(6)
C5A	4796.8(11)	3697(3)	491.9(13)	30.8(6)
C6A	5377.7(12)	3307(3)	509.2(14)	31.8(6)
C7A	5918.5(12)	3093(3)	1071.7(14)	34.6(6)
C8A	6418.2(12)	2720(3)	963.5(14)	34.5(6)
C9A	6348.6(12)	2564(3)	291.7(14)	35.8(6)
C10A	5798.9(12)	2795(3)	-240.6(13)	32.7(6)
C11A	5610.3(12)	2656(3)	-989.0(14)	34.7(6)
C12A	3970.0(14)	4261(3)	1615.6(16)	42.5(7)
C13A	3373.9(16)	4850(4)	1460.8(18)	54.2(9)
C14A	3935.2(18)	3049(4)	1829(2)	57.4(9)
C15A	4474.3(15)	4876(4)	2214.3(16)	51.2(9)
C16A	7020.5(13)	2506(3)	1577.0(14)	40.1(7)
C17A	6933.3(16)	1570(4)	2020.8(19)	54.6(9)
C18A	7224.5(16)	3589(4)	1988.0(19)	56.8(9)
C19A	7512.8(15)	2139(4)	1355.3(17)	59.5(11)
C20A	5880.7(13)	2189(3)	-1842.6(16)	41.7(7)
C21A	3875.2(18)	3579(4)	-1668(2)	34.3(10)

Table 2 Fractional Atomic Coordinates (×10^4) and Equivalent Isotropic Displacement Parameters (Å^2×10^3) for weix10. U_{eq} is defined as 1/3 of the trace of the orthogonalised U_{IJ} tensor.

Atom	*x*	*y*	*z*	U(eq)
C22A	3858.5(19)	4332(4)	-2170(2)	38.3(10)
C23A	3354.2(19)	4462(4)	-2785(2)	46.5(11)
C24A	2843(2)	3834(5)	-2910(3)	53.1(14)
C25A	2857(2)	3073(5)	-2424(2)	50.8(13)
C26A	3365.2(17)	2917(4)	-1809(2)	39.3(10)
C27A	3349(2)	2026(5)	-1317(3)	54.8(13)
C21C	3781(6)	3299(18)	-1588(7)	48(3)
C22C	3406(5)	2525(14)	-1477(6)	50(2)
C23C	2838(5)	2269(13)	-1963(6)	52(2)
C24C	2624(5)	2822(14)	-2582(6)	51(2)
C25C	2977(5)	3609(16)	-2708(7)	49(2)
C26C	3564(4)	3836(12)	-2219(5)	48(2)
C27C	3943(6)	4664(14)	-2385(7)	49(3)

Table 3 Anisotropic Displacement Parameters (Å^2×10^3) for weix10. The Anisotropic displacement factor exponent takes the form: $-2\pi^2[h^2a^{*2}U_{11}+2hka^*b^*U_{12}+\ldots]$.

Atom	U_{11}	U_{22}	U_{33}	U_{23}	U_{13}	U_{12}
Ni1	25.2(2)	55.4(3)	30.0(3)	5.1(2)	12.59(19)	7.1(2)
N1	24.8(11)	51.1(15)	31.0(12)	1.3(10)	10.4(9)	4.9(10)
N2	26.9(11)	46.2(14)	26.9(11)	1.2(10)	9.1(9)	1.0(10)
N3	29.1(12)	57.7(16)	32.7(12)	4.3(11)	17.6(10)	5.3(11)
N4	30.9(12)	64.7(17)	29.8(12)	4.5(11)	14.1(10)	5.0(11)
N5	47.6(15)	62.4(18)	36.4(13)	5.6(12)	21.2(12)	-0.4(13)
C1	30.1(14)	59(2)	37.5(15)	4.7(14)	12.3(12)	11.4(13)
C2	29.9(14)	61(2)	35.0(15)	2.7(14)	6.6(12)	8.1(13)
C3	32.4(14)	49.0(18)	32.0(14)	-2.8(12)	8.2(12)	0.9(12)
C4	30.3(14)	43.3(16)	31.1(14)	-2.0(11)	11.7(11)	-0.3(11)
C5	26.8(13)	42.8(16)	28.6(13)	-1.1(11)	9.2(11)	1.7(11)
C6	26.0(13)	45.2(16)	23.9(12)	-3.4(11)	8.0(10)	-2.3(11)

Table 3 Anisotropic Displacement Parameters ($Å^2×10^3$) for weix10. The Anisotropic displacement factor exponent takes the form: $-2π^2[h^2a^{*2}U_{11}+2hka^*b^*U_{12}+...]$.

Atom	U_{11}	U_{22}	U_{33}	U_{23}	U_{13}	U_{12}
C7	29.3(13)	53.1(18)	24.5(12)	2.3(12)	11.7(11)	4.2(12)
C8	27.1(13)	55.0(18)	29.9(13)	3.8(12)	14.0(11)	5.6(12)
C9	26.6(13)	58.1(19)	27.3(13)	6.7(12)	7.9(11)	7.1(12)
C10	26.8(13)	48.9(17)	26.4(13)	2.3(11)	11.5(10)	1.7(11)
C11	27.3(13)	50.7(17)	29.5(13)	1.5(12)	12.2(11)	2.5(12)
C12	36.7(16)	67(2)	29.0(14)	-2.0(14)	4.3(12)	3.1(15)
C13	60(2)	104(4)	34.5(18)	8(2)	4.2(16)	25(2)
C14	46.9(19)	74(3)	37.4(16)	-17.0(16)	13.7(14)	-8.6(17)
C15	59(2)	65(2)	29.6(15)	2.1(14)	15.9(14)	-0.2(17)
C16	30.5(14)	72(2)	31.4(14)	12.8(14)	16.5(12)	13.7(14)
C17	52(2)	66(2)	80(3)	-4(2)	42(2)	6.5(18)
C18	32.4(16)	73(3)	57(2)	2.6(18)	21.2(15)	-1.1(15)
C19	42.6(19)	126(4)	51(2)	32(2)	25.4(17)	39(2)
C20	33.5(14)	54.6(19)	31.5(14)	7.1(13)	12.4(12)	3.9(13)
C21	32(2)	50(3)	27(2)	5.1(17)	9.7(17)	2.8(19)
C22	27(3)	40(4)	41(3)	9(3)	10(2)	7(3)
C23	33(2)	54(3)	39(2)	0.2(18)	15.1(17)	6.4(17)
C24	26(2)	61(3)	45(3)	2(2)	14.1(18)	9(2)
C25	26(2)	62(5)	40(4)	-4(3)	12(2)	-2(2)
C26	30(2)	54(3)	38(2)	-3.2(19)	11.2(17)	4.6(18)
C27	39(3)	67(4)	50(5)	-14(3)	19(4)	-7(3)
C21B	11(6)	62(9)	38(7)	-1(6)	9(5)	2(5)
C22B	27(8)	100(16)	50(16)	-11(10)	5(8)	-4(8)
C23B	27(6)	64(8)	51(7)	-13(6)	13(5)	-1(5)
C24B	22(6)	63(9)	51(7)	-8(6)	11(5)	0(6)

Table 3 Anisotropic Displacement Parameters ($Å^2×10^3$) for weix10. The Anisotropic displacement factor exponent takes the form: $-2π^2[h^2a^{*2}U_{11}+2hka^*b^*U_{12}+...]$.

Atom	U_{11}	U_{22}	U_{33}	U_{23}	U_{13}	U_{12}
C25B	22(6)	40(10)	41(11)	-6(7)	14(6)	11(5)
C26B	14(4)	45(6)	33(5)	7(5)	10(4)	2(4)
C27B	31(9)	29(9)	74(13)	-7(7)	13(7)	13(6)
Ni1A	20.0(2)	51.3(3)	23.1(2)	0.62(19)	6.65(18)	0.84(19)
N1A	20.1(10)	47.0(14)	24.2(10)	2.9(9)	6.2(8)	2.0(9)
N2A	23.9(11)	48.4(14)	29.4(11)	1.8(10)	12.7(9)	1.5(9)
N3A	22.1(11)	58.7(16)	23.7(11)	-2.2(10)	4.8(9)	-0.4(10)
N4A	25.4(11)	62.7(17)	29.9(12)	-5.9(11)	12.8(9)	0.9(11)
N5A	44.3(15)	82(2)	39.5(15)	-16.9(14)	21.3(12)	-10.7(15)
C1A	23.7(12)	50.4(17)	32.1(13)	5.1(12)	11.1(11)	5.0(11)
C2A	22.7(12)	53.2(18)	33.3(14)	2.3(12)	11.3(11)	4.1(11)
C3A	24.6(12)	49.2(17)	32.2(14)	5.8(12)	13.1(11)	4.7(11)
C4A	24.1(12)	52.8(17)	28.8(13)	4.9(12)	11.5(10)	4.4(12)
C5A	19.8(12)	46.4(16)	24.5(12)	5.9(11)	7.6(10)	3.9(10)
C6A	23.5(12)	45.6(16)	27.1(13)	3.1(11)	11.4(10)	4.5(11)
C7A	24.7(12)	52.4(17)	25.4(12)	6.0(12)	9.3(10)	6.6(11)
C8A	24.9(13)	49.9(17)	27.0(13)	5.1(11)	9.2(11)	4.1(11)
C9A	24.6(13)	54.0(18)	30.2(13)	1.0(12)	12.9(11)	3.6(12)
C10A	23.5(12)	50.9(17)	24.1(12)	-2.0(11)	10.3(10)	0.1(11)
C11A	24.2(12)	50.9(17)	27.2(13)	-3.4(12)	8.9(10)	-0.8(11)
C12A	35.6(15)	62(2)	36.0(15)	5.5(14)	21.1(13)	5.7(14)
C13A	40.2(17)	84(3)	46.8(18)	1.2(17)	26.5(15)	9.9(17)
C14A	56(2)	75(3)	56(2)	12.6(19)	37.6(18)	3.9(19)
C15A	41.3(17)	81(3)	34.8(15)	-4.5(16)	19.2(14)	7.2(16)
C16A	26.4(13)	64(2)	28.7(13)	8.5(13)	10.1(11)	11.6(13)

Table 3 Anisotropic Displacement Parameters ($Å^2×10^3$) for weix10. The Anisotropic displacement factor exponent takes the form: $-2π^2[h^2a^{*2}U_{11}+2hka^*b^*U_{12}+...]$.

Atom	U_{11}	U_{22}	U_{33}	U_{23}	U_{13}	U_{12}
C17A	40.8(18)	71(2)	48.0(19)	19.8(17)	15.0(15)	14.6(16)
C18A	34.4(17)	71(3)	47.7(19)	2.1(17)	0.0(14)	7.1(16)
C19A	30.4(16)	107(3)	37.2(16)	6.3(18)	10.3(13)	24.2(18)
C20A	30.5(14)	62(2)	36.5(16)	-11.6(14)	17.6(12)	-5.0(13)
C21A	23.1(19)	54(3)	27.4(19)	-7.6(16)	12.0(15)	-0.1(16)
C22A	27(2)	53(3)	33(2)	-0.9(17)	10.7(16)	5.9(17)
C23A	38(2)	64(3)	33(2)	0.6(18)	10.5(17)	7.2(19)
C24A	34(2)	77(4)	33(2)	-7(2)	-0.9(18)	13(2)
C25A	23(2)	75(3)	44(3)	-13(2)	3.2(18)	-4(2)
C26A	27.4(19)	58(3)	31(2)	-0.5(18)	11.3(16)	-3.0(17)
C27A	42(2)	67(3)	48(3)	2(2)	11(2)	-19(2)
C21C	22(4)	76(5)	41(4)	3(3)	9(3)	-12(3)
C22C	23(3)	78(5)	42(4)	3(4)	8(3)	-14(3)
C23C	26(3)	79(5)	44(4)	4(3)	7(3)	-15(3)
C24C	24(4)	78(5)	43(4)	3(3)	8(3)	-13(3)
C25C	24(3)	77(5)	42(4)	2(3)	9(3)	-12(3)
C26C	22(3)	75(5)	40(4)	2(3)	9(3)	-11(3)
C27C	26(4)	74(6)	41(5)	1(4)	9(4)	-12(4)

Table 4 Bond Lengths for weix10.

Atom	Atom	Length/Å	Atom	Atom	Length/Å
Ni1	N1	1.919(2)	Ni1A	N1A	1.919(2)
Ni1	N2	1.857(2)	Ni1A	N2A	1.863(2)
Ni1	N3	1.874(2)	Ni1A	N3A	1.874(2)

Table 4 Bond Lengths for weix10.

Atom	Atom	Length/Å	Atom	Atom	Length/Å
Ni1	C21	1.901(4)	Ni1A	C21A	1.898(4)
Ni1	C21B	1.990(8)	Ni1A	C21C	1.958(9)
N1	C1	1.347(4)	N1A	C1A	1.340(4)
N1	C5	1.382(4)	N1A	C5A	1.380(3)
N2	C6	1.338(4)	N2A	C6A	1.335(4)
N2	C10	1.342(4)	N2A	C10A	1.335(4)
N3	C11	1.328(4)	N3A	C11A	1.322(4)
N4	C11	1.332(4)	N4A	C11A	1.339(4)
N4	C20	1.314(4)	N4A	C20A	1.318(4)
N5	C20	1.163(4)	N5A	C20A	1.163(4)
C1	C2	1.387(4)	C1A	C2A	1.384(4)
C2	C3	1.392(4)	C2A	C3A	1.393(4)
C3	C4	1.401(4)	C3A	C4A	1.413(4)
C3	C12	1.518(4)	C3A	C12A	1.526(4)
C4	C5	1.374(4)	C4A	C5A	1.376(4)
C5	C6	1.483(4)	C5A	C6A	1.479(4)
C6	C7	1.386(4)	C6A	C7A	1.393(4)
C7	C8	1.414(4)	C7A	C8A	1.408(4)
C8	C9	1.406(4)	C8A	C9A	1.399(4)
C8	C16	1.531(4)	C8A	C16A	1.534(4)
C9	C10	1.376(4)	C9A	C10A	1.381(4)
C10	C11	1.487(4)	C10A	C11A	1.491(4)
C12	C13	1.535(5)	C12A	C13A	1.523(4)
C12	C14	1.543(6)	C12A	C14A	1.526(5)
C12	C15	1.539(5)	C12A	C15A	1.545(5)

Table 4 Bond Lengths for weix10.

Atom	Atom	Length/Å	Atom	Atom	Length/Å
C16	C17	1.519(6)	C16A	C17A	1.540(5)
C16	C18	1.539(5)	C16A	C18A	1.523(5)
C16	C19	1.531(4)	C16A	C19A	1.533(4)
C21	C22	1.389(9)	C21A	C22A	1.393(6)
C21	C26	1.393(6)	C21A	C26A	1.396(6)
C22	C23	1.380(8)	C22A	C23A	1.390(6)
C23	C24	1.380(6)	C23A	C24A	1.381(7)
C24	C25	1.372(7)	C24A	C25A	1.373(8)
C25	C26	1.411(6)	C25A	C26A	1.400(6)
C26	C27	1.495(8)	C26A	C27A	1.510(7)
C21B	C22B	1.389(10)	C21C	C22C	1.389(9)
C21B	C26B	1.392(7)	C21C	C26C	1.392(7)
C22B	C23B	1.379(9)	C22C	C23C	1.379(9)
C23B	C24B	1.379(7)	C23C	C24C	1.378(7)
C24B	C25B	1.375(8)	C24C	C25C	1.374(8)
C25B	C26B	1.408(7)	C25C	C26C	1.406(7)
C26B	C27B	1.494(9)	C26C	C27C	1.495(8)

Table 5 Bond Angles for weix10.

Atom	Atom	Atom	Angle/°	Atom	Atom	Atom	Angle/°
N1	Ni1	C21B	94.8(4)	N1A	Ni1A	C21C	95.8(7)
N2	Ni1	N1	82.10(10)	N2A	Ni1A	N1A	81.98(10)
N2	Ni1	N3	81.99(10)	N2A	Ni1A	N3A	82.20(10)
N2	Ni1	C21	174.63(14)	N2A	Ni1A	C21A	175.66(16)
N2	Ni1	C21B	158.5(3)	N2A	Ni1A	C21C	166.5(4)

Table 5 Bond Angles for weix10.

Atom	Atom	Atom	Angle/°	Atom	Atom	Atom	Angle/°
N3	Ni1	N1	164.09(10)	N3A	Ni1A	N1A	164.17(10)
N3	Ni1	C21	92.67(14)	N3A	Ni1A	C21A	93.52(15)
N3	Ni1	C21B	100.1(4)	N3A	Ni1A	C21C	99.8(7)
C21	Ni1	N1	103.24(14)	C21A	Ni1A	N1A	102.30(15)
C1	N1	Ni1	129.1(2)	C1A	N1A	Ni1A	129.10(19)
C1	N1	C5	116.3(2)	C1A	N1A	C5A	116.3(2)
C5	N1	Ni1	114.50(18)	C5A	N1A	Ni1A	114.48(18)
C6	N2	Ni1	119.97(19)	C6A	N2A	Ni1A	119.79(18)
C6	N2	C10	121.2(2)	C6A	N2A	C10A	121.7(2)
C10	N2	Ni1	118.53(19)	C10A	N2A	Ni1A	118.35(19)
C11	N3	Ni1	117.27(19)	C11A	N3A	Ni1A	116.78(19)
C20	N4	C11	117.5(3)	C20A	N4A	C11A	117.4(2)
N1	C1	C2	123.1(3)	N1A	C1A	C2A	123.5(3)
C1	C2	C3	120.9(3)	C1A	C2A	C3A	120.8(3)
C2	C3	C4	115.9(3)	C2A	C3A	C4A	115.9(3)
C2	C3	C12	124.3(3)	C2A	C3A	C12A	124.0(3)
C4	C3	C12	119.7(3)	C4A	C3A	C12A	120.0(2)
C5	C4	C3	121.0(3)	C5A	C4A	C3A	120.3(2)
N1	C5	C6	112.7(2)	N1A	C5A	C6A	112.7(2)
C4	C5	N1	122.5(3)	C4A	C5A	N1A	122.8(2)
C4	C5	C6	124.8(3)	C4A	C5A	C6A	124.4(2)
N2	C6	C5	110.3(2)	N2A	C6A	C5A	110.5(2)
N2	C6	C7	120.9(3)	N2A	C6A	C7A	120.4(2)
C7	C6	C5	128.7(2)	C7A	C6A	C5A	129.0(2)
C6	C7	C8	119.1(2)	C6A	C7A	C8A	119.1(2)

Table 5 Bond Angles for weix10.

Atom	Atom	Atom	Angle/°	Atom	Atom	Atom	Angle/°
C7	C8	C16	119.1(2)	C7A	C8A	C16A	119.7(2)
C9	C8	C7	118.2(3)	C9A	C8A	C7A	118.4(2)
C9	C8	C16	122.7(2)	C9A	C8A	C16A	121.9(2)
C10	C9	C8	119.3(3)	C10A	C9A	C8A	119.3(3)
N2	C10	C9	121.4(2)	N2A	C10A	C9A	121.1(2)
N2	C10	C11	110.0(2)	N2A	C10A	C11A	109.9(2)
C9	C10	C11	128.6(3)	C9A	C10A	C11A	129.1(3)
N3	C11	N4	131.1(3)	N3A	C11A	N4A	130.9(3)
N3	C11	C10	112.2(2)	N3A	C11A	C10A	112.8(2)
N4	C11	C10	116.7(2)	N4A	C11A	C10A	116.3(2)
C3	C12	C13	111.7(3)	C3A	C12A	C14A	107.4(3)
C3	C12	C14	106.9(3)	C3A	C12A	C15A	110.7(3)
C3	C12	C15	111.5(3)	C13A	C12A	C3A	111.9(3)
C13	C12	C14	109.4(3)	C13A	C12A	C14A	109.4(3)
C13	C12	C15	108.3(3)	C13A	C12A	C15A	108.7(3)
C15	C12	C14	108.9(3)	C14A	C12A	C15A	108.7(3)
C8	C16	C18	107.6(3)	C8A	C16A	C17A	108.9(3)
C17	C16	C8	109.3(3)	C18A	C16A	C8A	108.9(3)
C17	C16	C18	110.2(3)	C18A	C16A	C17A	110.2(3)
C17	C16	C19	110.2(4)	C18A	C16A	C19A	108.3(3)
C19	C16	C8	111.9(2)	C19A	C16A	C8A	111.9(2)
C19	C16	C18	107.7(3)	C19A	C16A	C17A	108.6(3)
N5	C20	N4	175.5(3)	N5A	C20A	N4A	175.6(3)
C22	C21	Ni1	120.3(4)	C22A	C21A	Ni1A	119.5(3)
C22	C21	C26	117.9(4)	C22A	C21A	C26A	117.4(4)

Table 5 Bond Angles for weix10.

Atom	Atom	Atom	Angle/°	Atom	Atom	Atom	Angle/°
C26	C21	Ni1	121.3(3)	C26A	C21A	Ni1A	122.8(3)
C23	C22	C21	122.8(5)	C23A	C22A	C21A	122.6(4)
C22	C23	C24	118.9(5)	C24A	C23A	C22A	119.6(5)
C25	C24	C23	120.1(4)	C25A	C24A	C23A	118.4(4)
C24	C25	C26	120.8(5)	C24A	C25A	C26A	122.6(5)
C21	C26	C25	119.5(4)	C21A	C26A	C25A	119.2(4)
C21	C26	C27	122.0(4)	C21A	C26A	C27A	121.7(4)
C25	C26	C27	118.4(5)	C25A	C26A	C27A	119.0(4)
C22B	C21B	Ni1	120.2(6)	C22C	C21C	Ni1A	115.6(6)
C22B	C21B	C26B	117.5(6)	C22C	C21C	C26C	117.7(7)
C26B	C21B	Ni1	121.8(6)	C26C	C21C	Ni1A	126.3(6)
C23B	C22B	C21B	122.8(8)	C23C	C22C	C21C	122.7(8)
C22B	C23B	C24B	118.9(7)	C24C	C23C	C22C	119.0(7)
C25B	C24B	C23B	120.0(6)	C25C	C24C	C23C	120.1(7)
C24B	C25B	C26B	120.7(6)	C24C	C25C	C26C	120.6(7)
C21B	C26B	C25B	119.7(6)	C21C	C26C	C25C	119.8(6)
C21B	C26B	C27B	121.0(7)	C21C	C26C	C27C	121.0(7)
C25B	C26B	C27B	119.2(7)	C25C	C26C	C27C	119.2(7)

Table 6 Torsion Angles for weix10.

A	B	C	D	Angle/°	A	B	C	D	Angle/°
Ni1	N1	C1	C2	173.6(3)	Ni1A	N1A	C5A	C6A	6.8(3)
Ni1	N1	C5	C4	-172.7(2)	Ni1A	N2A	C6A	C5A	-2.7(3)
Ni1	N1	C5	C6	5.5(3)	Ni1A	N2A	C6A	C7A	177.4(2)
Ni1	N2	C6	C5	-4.0(3)	Ni1A	N2A	C10A	C9A	-177.4(2)

Table 6 Torsion Angles for weix10.

A	B	C	D	Angle/°	A	B	C	D	Angle/°
Ni1	N2	C6	C7	175.0(2)	Ni1A	N2A	C10A	C11A	0.7(3)
Ni1	N2	C10	C9	-175.4(2)	Ni1A	N3A	C11A	N4A	-177.2(3)
Ni1	N2	C10	C11	2.1(3)	Ni1A	N3A	C11A	C10A	2.8(4)
Ni1	N3	C11	N4	-178.6(3)	Ni1A	C21A	C22A	C23A	176.4(3)
Ni1	N3	C11	C10	2.0(4)	Ni1A	C21A	C26A	C25A	-177.3(4)
Ni1	C21	C22	C23	174.6(5)	Ni1A	C21A	C26A	C27A	1.9(6)
Ni1	C21	C26	C25	-173.5(4)	Ni1A	C21C	C22C	C23C	-173.1(16)
Ni1	C21	C26	C27	3.0(8)	Ni1A	C21C	C26C	C25C	174.7(18)
Ni1	C21B	C22B	C23B	-179(2)	Ni1A	C21C	C26C	C27C	-6(3)
Ni1	C21B	C26B	C25B	176.4(11)	N1A	Ni1A	N2A	C6A	5.2(2)
Ni1	C21B	C26B	C27B	-7(2)	N1A	Ni1A	N2A	C10A	-178.8(2)
N1	Ni1	N2	C6	5.7(2)	N1A	Ni1A	N3A	C11A	0.2(6)
N1	Ni1	N2	C10	179.3(3)	N1A	Ni1A	C21A	C22A	118.2(4)
N1	Ni1	N3	C11	0.4(6)	N1A	Ni1A	C21A	C26A	-67.4(4)
N1	C1	C2	C3	-2.0(6)	N1A	C1A	C2A	C3A	-1.1(5)
N1	C5	C6	N2	-1.2(4)	N1A	C5A	C6A	N2A	-2.8(4)
N1	C5	C6	C7	179.9(3)	N1A	C5A	C6A	C7A	177.0(3)
N2	Ni1	N3	C11	-0.7(3)	N2A	Ni1A	N3A	C11A	-2.0(2)
N2	C6	C7	C8	-0.6(5)	N2A	C6A	C7A	C8A	-0.4(5)
N2	C10	C11	N3	-2.5(4)	N2A	C10A	C11A	N3A	-2.2(4)
N2	C10	C11	N4	177.9(3)	N2A	C10A	C11A	N4A	177.9(3)
N3	Ni1	N2	C6	-174.6(3)	N3A	Ni1A	N2A	C6A	-175.4(3)
N3	Ni1	N2	C10	-1.0(2)	N3A	Ni1A	N2A	C10A	0.6(2)
C1	N1	C5	C4	3.9(5)	N3A	Ni1A	C21A	C22A	-61.4(4)
C1	N1	C5	C6	-177.9(3)	N3A	Ni1A	C21A	C26A	113.0(4)

Table 6 Torsion Angles for weix10.

A	B	C	D	Angle/°	A	B	C	D	Angle/°
C1	C2	C3	C4	4.8(5)	C1A	N1A	C5A	C4A	5.4(4)
C1	C2	C3	C12	-171.7(3)	C1A	N1A	C5A	C6A	-176.4(3)
C2	C3	C4	C5	-3.3(5)	C1A	C2A	C3A	C4A	4.4(5)
C2	C3	C12	C13	-12.9(5)	C1A	C2A	C3A	C12A	-171.8(3)
C2	C3	C12	C14	106.8(4)	C2A	C3A	C4A	C5A	-2.8(5)
C2	C3	C12	C15	-134.3(4)	C2A	C3A	C12A	C13A	-12.5(5)
C3	C4	C5	N1	-1.0(5)	C2A	C3A	C12A	C14A	107.5(4)
C3	C4	C5	C6	-179.0(3)	C2A	C3A	C12A	C15A	-134.0(3)
C4	C3	C12	C13	170.8(4)	C3A	C4A	C5A	N1A	-2.1(5)
C4	C3	C12	C14	-69.5(4)	C3A	C4A	C5A	C6A	179.9(3)
C4	C3	C12	C15	49.4(4)	C4A	C3A	C12A	C13A	171.5(3)
C4	C5	C6	N2	177.0(3)	C4A	C3A	C12A	C14A	-68.5(4)
C4	C5	C6	C7	-1.9(5)	C4A	C3A	C12A	C15A	50.0(4)
C5	N1	C1	C2	-2.4(5)	C4A	C5A	C6A	N2A	175.3(3)
C5	C6	C7	C8	178.1(3)	C4A	C5A	C6A	C7A	-4.9(5)
C6	N2	C10	C9	-1.8(5)	C5A	N1A	C1A	C2A	-3.8(5)
C6	N2	C10	C11	175.7(3)	C5A	C6A	C7A	C8A	179.8(3)
C6	C7	C8	C9	0.1(5)	C6A	N2A	C10A	C9A	-1.4(5)
C6	C7	C8	C16	179.2(3)	C6A	N2A	C10A	C11A	176.6(3)
C7	C8	C9	C10	-0.4(5)	C6A	C7A	C8A	C9A	-0.8(5)
C7	C8	C16	C17	56.9(4)	C6A	C7A	C8A	C16A	178.6(3)
C7	C8	C16	C18	-62.7(4)	C7A	C8A	C9A	C10A	0.9(5)
C7	C8	C16	C19	179.2(4)	C7A	C8A	C16A	C17A	61.6(4)
C8	C9	C10	N2	1.2(5)	C7A	C8A	C16A	C18A	-58.6(4)
C8	C9	C10	C11	-175.8(3)	C7A	C8A	C16A	C19A	-178.3(3)

Table 6 Torsion Angles for weix10.

A	B	C	D	Angle/°	A	B	C	D	Angle/°
C9	C8	C16	C17	-124.0(4)	C8A	C9A	C10A	N2A	0.2(5)
C9	C8	C16	C18	116.4(4)	C8A	C9A	C10A	C11A	-177.5(3)
C9	C8	C16	C19	-1.7(5)	C9A	C8A	C16A	C17A	-119.0(3)
C9	C10	C11	N3	174.8(3)	C9A	C8A	C16A	C18A	120.8(3)
C9	C10	C11	N4	-4.8(5)	C9A	C8A	C16A	C19A	1.1(5)
C10	N2	C6	C5	-177.5(3)	C9A	C10A	C11A	N3A	175.6(3)
C10	N2	C6	C7	1.5(5)	C9A	C10A	C11A	N4A	-4.3(5)
C12	C3	C4	C5	173.2(3)	C10A	N2A	C6A	C5A	-178.6(3)
C16	C8	C9	C10	-179.5(3)	C10A	N2A	C6A	C7A	1.6(5)
C20	N4	C11	N3	0.0(6)	C12A	C3A	C4A	C5A	173.5(3)
C20	N4	C11	C10	179.5(3)	C16A	C8A	C9A	C10A	-178.5(3)
C21	Ni1	N3	C11	178.8(3)	C20A	N4A	C11A	N3A	-0.2(5)
C21	C22	C23	C24	-2.5(10)	C20A	N4A	C11A	C10A	179.7(3)
C22	C21	C26	C25	-1.2(8)	C21A	Ni1A	N3A	C11A	178.7(3)
C22	C21	C26	C27	175.3(8)	C21A	C22A	C23A	C24A	0.6(7)
C22	C23	C24	C25	1.8(9)	C22A	C21A	C26A	C25A	-2.9(7)
C23	C24	C25	C26	-0.9(10)	C22A	C21A	C26A	C27A	176.3(5)
C24	C25	C26	C21	0.6(9)	C22A	C23A	C24A	C25A	-1.7(8)
C24	C25	C26	C27	-176.0(8)	C23A	C24A	C25A	C26A	0.5(8)
C26	C21	C22	C23	2.2(10)	C24A	C25A	C26A	C21A	1.8(8)
C21B	Ni1	N2	C6	-77.3(11)	C24A	C25A	C26A	C27A	-177.4(5)
C21B	Ni1	N2	C10	96.3(10)	C26A	C21A	C22A	C23A	1.7(7)
C21B	Ni1	N3	C11	-159.0(4)	C21C	Ni1A	N2A	C6A	-76(3)
C21B	C22B	C23B	C24B	7(4)	C21C	Ni1A	N2A	C10A	100(3)
C22B	C21B	C26B	C25B	4(3)	C21C	Ni1A	N3A	C11A	-168.5(5)

Table 6 Torsion Angles for weix10.

A	B	C	D	Angle/°	A	B	C	D	Angle/°
C22B	C21B	C26B	C27B	-179(3)	C21C	C22C	C23C	C24C	-2(3)
C22B	C23B	C24B	C25B	-4(3)	C22C	C21C	C26C	C25C	2(3)
C23B	C24B	C25B	C26B	2(2)	C22C	C21C	C26C	C27C	-179(2)
C24B	C25B	C26B	C21B	-2(2)	C22C	C23C	C24C	C25C	0(3)
C24B	C25B	C26B	C27B	-178(2)	C23C	C24C	C25C	C26C	2(3)
C26B	C21B	C22B	C23B	-7(4)	C24C	C25C	C26C	C21C	-3(3)
Ni1A	N1A	C1A	C2A	172.3(2)	C24C	C25C	C26C	C27C	177.5(19)
Ni1A	N1A	C5A	C4A	-171.3(2)	C26C	C21C	C22C	C23C	1(3)

Table 7 Hydrogen Atom Coordinates (Å×10⁴) and Isotropic Displacement Parameters (Å²×10³) for weix10.

Atom	*x*	*y*	*z*	U(eq)
H3	10169.9	1851.82	3251.93	46
H1	11491.14	542.03	5729.58	51
H2	11693.85	364.47	6870.39	53
H4	10028.23	1544.21	6454.09	42
H7	9094.1	2083.59	5550.64	43
H9	8377.29	2706.77	3499.88	46
H13A	11598.82	-318.46	7881.21	107
H13B	11690.76	534.35	8491.06	107
H13C	11955.95	835.93	7947.32	107
H14A	11396.24	2675.1	7654.31	81
H14B	11168.51	2407.43	8234.54	81
H14C	10691.54	2698.33	7475.61	81
H15A	10145.49	952.15	7458.53	78

Table 7 Hydrogen Atom Coordinates (Å×10⁴) and Isotropic Displacement Parameters (Å²×10³) for weix10.

Atom	*x*	*y*	*z*	U(eq)
H15B	10626.03	561.29	8195.82	78
H15C	10464.34	-250.64	7551.19	78
H17A	8439.91	3458.24	5547.05	92
H17B	7797.92	4009.36	5095.52	92
H17C	8376.43	4367.86	4973.89	92
H18A	7730.87	1159.52	4462.66	80
H18B	7419.25	1958.02	4818.75	80
H18C	8092.62	1518.14	5244.8	80
H19A	7708.89	3858.36	3726.29	107
H19B	7192.7	3365.68	3922.38	107
H19C	7491.02	2582.94	3544.2	107
H22	10786.45	-112.75	3655.04	45
H23	11616.8	-459.33	3425.75	50
H24	12469.4	681.92	3924.06	53
H25	12503.82	2069.22	4693.12	53
H27A	11312.83	3212.29	4899.62	77
H27B	12029.44	3252.64	5162.3	77
H27C	11732.82	2479.9	5546.84	77
H22B	11420.79	3112.6	5126.98	75
H23B	12410.95	3410.27	5296.26	58
H24B	12811.07	2341.25	4674.76	55
H25B	12270.05	832.24	4024.07	41
H27D	11045.64	228.03	3300.64	72
H27E	10836.71	-112.15	3886.38	72
H27F	11454.02	-595.63	3903.94	72

Table 7 Hydrogen Atom Coordinates (Å×10⁴) and Isotropic Displacement Parameters (Å²×10³) for weix10.

Atom	*x*	*y*	*z*	U(eq)
H3A	4864.14	2810.19	-1797.89	44
H1A	3539.35	4454.85	-664.29	43
H2A	3318.59	4780.8	258.43	44
H4A	4991.23	3689.42	1500.81	42
H7A	5949.61	3197.83	1521.89	41
H9A	6675.79	2302.45	202.44	43
H13D	3380.91	5604.11	1280.12	81
H13E	3313.18	4912.54	1880.7	81
H13F	3043.95	4413.91	1122.01	81
H14D	3623.12	2644.18	1449.61	86
H14E	3835.12	3044.1	2224.14	86
H14F	4324.94	2679.01	1950.77	86
H15D	4855.73	4473.23	2339.18	77
H15E	4372.21	4898.22	2607.72	77
H15F	4514.82	5645.08	2075.81	77
H17D	6634.02	1810.39	2185.4	82
H17E	7317.35	1420.56	2411.23	82
H17F	6793.04	883.74	1748.11	82
H18D	7268.59	4183.16	1697.25	85
H18E	7612.15	3462.74	2377.71	85
H18F	6923.89	3817.48	2153.35	85
H19D	7401.89	1415.96	1116.54	89
H19E	7895.7	2059.51	1758.66	89
H19F	7555.4	2706.51	1048.93	89
H22A	4205.26	4775.46	-2089.32	46

Table 7 Hydrogen Atom Coordinates (Å×10⁴) and Isotropic Displacement Parameters (Å²×10³) for weix10.

Atom	*x*	*y*	*z*	U(eq)
H23A	3360.89	4979.79	-3117.04	56
H24A	2491.03	3926.11	-3321.39	64
H25A	2507.76	2634.66	-2509.81	61
H27G	3615.42	2246.96	-849.63	82
H27H	3485.92	1307.18	-1425.32	82
H27I	2936.73	1945.04	-1358.17	82
H22C	3546.28	2156.06	-1046.96	60
H23C	2597.74	1720.52	-1874.03	63
H24C	2232.73	2659.22	-2920.6	61
H25C	2822.2	4002.75	-3130.02	59
H27J	4306.44	4832.05	-1972.22	73
H27K	3713.73	5357.38	-2560.79	73
H27L	4058.47	4343.28	-2732.29	73

Table 8 Atomic Occupancy for weix10.

Atom	*Occupancy*	Atom	*Occupancy*	Atom	*Occupancy*
C21	0.747(6)	C22	0.747(6)	H22	0.747(6)
C23	0.747(6)	H23	0.747(6)	C24	0.747(6)
H24	0.747(6)	C25	0.747(6)	H25	0.747(6)
C26	0.747(6)	C27	0.747(6)	H27A	0.747(6)
H27B	0.747(6)	H27C	0.747(6)	C21B	0.253(6)
C22B	0.253(6)	H22B	0.253(6)	C23B	0.253(6)
H23B	0.253(6)	C24B	0.253(6)	H24B	0.253(6)
C25B	0.253(6)	H25B	0.253(6)	C26B	0.253(6)

Table 8 Atomic Occupancy for weix10.

Atom	*Occupancy*	Atom	*Occupancy*	Atom	*Occupancy*
C27B	0.253(6)	H27D	0.253(6)	H27E	0.253(6)
H27F	0.253(6)	C21A	0.766(6)	C22A	0.766(6)
H22A	0.766(6)	C23A	0.766(6)	H23A	0.766(6)
C24A	0.766(6)	H24A	0.766(6)	C25A	0.766(6)
H25A	0.766(6)	C26A	0.766(6)	C27A	0.766(6)
H27G	0.766(6)	H27H	0.766(6)	H27I	0.766(6)
C21C	0.234(6)	C22C	0.234(6)	H22C	0.234(6)
C23C	0.234(6)	H23C	0.234(6)	C24C	0.234(6)
H24C	0.234(6)	C25C	0.234(6)	H25C	0.234(6)
C26C	0.234(6)	C27C	0.234(6)	H27J	0.234(6)
H27K	0.234(6)	H27L	0.234(6)		

Table 9 Solvent masks information for weix10.

Number	X	Y	Z	Volume	Electron count	Content
1	0.000	0.000	0.000	257.1	53.3	?
2	0.000	0.500	0.500	257.1	53.3	?
3	0.500	0.000	0.000	293.9	71.6	?
4	0.500	0.500	0.500	293.9	71.6	?

3.5 References

[1] Bauer, M. R.; Di Fruscia, P.; Lucas, S. C. C.; Michaelides, I. N.; Nelson, J. E.; Storer, R. I.; Whitehurst, B. C. Put a Ring on It: Application of Small Aliphatic Rings in Medicinal Chemistry. *RSC Med. Chem.* **2021**, *12* (4), 448–471. https://doi.org/10.1039/D0MD00370K.

[2] de Meijere, A.; Kozhushkov, S. I.; Schill, H. Three-Membered-Ring-Based Molecular Architectures †. *Chem. Rev.* **2006**, *106* (12), 4926–4996. https://doi.org/10.1021/cr0505369.

[3] Lovering, F.; Bikker, J.; Humblet, C. Escape from Flatland: Increasing Saturation as an Approach to Improving Clinical Success. *Journal of Medicinal Chemistry* **2009**, *52* (21), 6752–6756. https://doi.org/10.1021/jm901241e.

[4] Lovering, F. Escape from Flatland 2: Complexity and Promiscuity. *MedChemComm* **2013**, *4* (3), 515. https://doi.org/10.1039/c2md20347b.

[5] Kuk, K.; Taylor-Cousar, J. L. Lumacaftor and Ivacaftor in the Management of Patients with Cystic Fibrosis: Current Evidence and Future Prospects. *Ther Adv Respir Dis* **2015**, *9* (6), 313–326. https://doi.org/10.1177/1753465815601934.

[6] Suzuki, E.; Kim, S.; Cheung, H.-K.; Corbley, M. J.; Zhang, X.; Sun, L.; Shan, F.; Singh, J.; Lee, W.-C.; Albelda, S. M.; Ling, L. E. A Novel Small-Molecule Inhibitor of Transforming Growth Factor β Type I Receptor Kinase (SM16) Inhibits Murine Mesothelioma Tumor Growth *In Vivo* and Prevents Tumor Recurrence after Surgical Resection. *Cancer Res* **2007**, *67* (5), 2351–2359. https://doi.org/10.1158/0008-5472.CAN-06-2389.

[7] Stepan, A. F.; Subramanyam, C.; Efremov, I. V.; Dutra, J. K.; O'Sullivan, T. J.; DiRico, K. J.; McDonald, W. S.; Won, A.; Dorff, P. H.; Nolan, C. E.; Becker, S. L.; Pustilnik, L. R.; Riddell, D. R.;

Kauffman, G. W.; Kormos, B. L.; Zhang, L.; Lu, Y.; Capetta, S. H.; Green, M. E.; Karki, K.; Sibley, E.; Atchison, K. P.; Hallgren, A. J.; Oborski, C. E.; Robshaw, A. E.; Sneed, B.; O'Donnell, C. J. Application of the Bicyclo[1.1.1]Pentane Motif as a Nonclassical Phenyl Ring Bioisostere in the Design of a Potent and Orally Active γ-Secretase Inhibitor. *J. Med. Chem.* **2012**, *55* (7), 3414–3424. https://doi.org/10.1021/jm300094u.

[8] Meijere, A. de. Bonding Properties of Cyclopropane and Their Chemical Consequences. *Angew. Chem. Int. Ed.* **1979**, *18* (11), 809–826. https://doi.org/10.1002/anie.197908093.

[9] Talele, T. T. The "Cyclopropyl Fragment" Is a Versatile Player That Frequently Appears in Preclinical/Clinical Drug Molecules. *Journal of Medicinal Chemistry* **2016**, *59* (19), 8712–8756. https://doi.org/10.1021/acs.jmedchem.6b00472.

[10] M. Marson, C. New and Unusual Scaffolds in Medicinal Chemistry. *Chemical Society Reviews* **2011**, *40* (11), 5514–5533. https://doi.org/10.1039/C1CS15119C.

[11] Toselli, F.; Fredenwall, M.; Svensson, P.; Li, X.-Q.; Johansson, A.; Weidolf, L.; Hayes, M. A. Hip To Be Square: Oxetanes as Design Elements To Alter Metabolic Pathways. *J. Med. Chem.* **2019**, *62* (16), 7383–7399. https://doi.org/10.1021/acs.jmedchem.9b00030.

[12] Messner, M.; Kozhushkov, S. I.; de Meijere, A. Nickel- and Palladium-Catalyzed Cross-Coupling Reactions at the Bridgehead of Bicyclo[1.1.1]Pentane Derivatives - A Convenient Access to Liquid Crystalline Compounds Containing Bicyclo[1.1.1]Pentane Moieties. *European Journal of Organic Chemistry* **2000**, *2000* (7), 1137–1155. https://doi.org/10.1002/1099-0690(200004)2000:7<1137::AID-EJOC1137>3.0.CO;2-2.

[13] Lopchuk, J. M.; Fjelbye, K.; Kawamata, Y.; Malins, L. R.; Pan, C.-M.; Gianatassio, R.; Wang, J.; Prieto, L.; Bradow, J.; Brandt, T. A.; Collins, M. R.; Elleraas, J.; Ewanicki, J.; Farrell, W.; Fadeyi, O. O.; Gallego, G. M.; Mousseau, J. J.; Oliver, R.; Sach, N. W.; Smith, J. K.; Spangler, J. E.; Zhu, H.; Zhu, J.; Baran, P. S. Strain-Release Heteroatom Functionalization: Development, Scope, and Stereospecificity. *J. Am. Chem. Soc.* **2017**, *139* (8), 3209–3226. https://doi.org/10.1021/jacs.6b13229.

[14] D'Auria, M. The Paternò–Büchi Reaction – a Comprehensive Review. *Photochem. Photobiol. Sci.* **2019**, *18* (10), 2297–2362. https://doi.org/10.1039/C9PP00148D.

[15] Alcaide, B.; Almendros, P.; Aragoncillo, C. Exploiting [2+2] Cycloaddition Chemistry: Achievements with Allenes. *Chem. Soc. Rev.* **2010**, *39* (2), 783–816. https://doi.org/10.1039/B913749A.

[16] De Faveri, G.; Ilyashenko, G.; Watkinson, M. Recent Advances in Catalytic Asymmetric Epoxidation Using the Environmentally Benign Oxidant Hydrogen Peroxide and Its Derivatives. *Chem. Soc. Rev.* **2011**, *40* (3), 1722–1760. https://doi.org/10.1039/C0CS00077A

[17] Padwa, A.; Murphree, S. S. Epoxides and Aziridines - A Mini Review. **2006**, 28.

[18] Subbaiah, M. A. M.; Meanwell, N. A. Bioisosteres of the Phenyl Ring: Recent Strategic Applications in Lead Optimization and Drug Design. *J. Med. Chem.* **2021**, *64* (19), 14046–14128. https://doi.org/10.1021/acs.jmedchem.1c01215.

[19] Luque, A.; Paternoga, J.; Opatz, T. Strain Release Chemistry of Photogenerated Small-Ring Intermediates. *Chem. Eur. J.* **2021**, *27* (14), 4500–4516. https://doi.org/10.1002/chem.202004178.

[20] Levterov, V. V.; Panasyuk, Y.; Pivnytska, V. O.; Mykhailiuk, P. K. Water-Soluble Non-Classical Benzene Mimetics. *Angew. Chem. Int. Ed.* **2020**, *59* (18), 7161–7167. https://doi.org/10.1002/anie.202000548.

[21] Namyslo, J. C.; Kaufmann, D. E. The Application of Cyclobutane Derivatives in Organic Synthesis. *Chem. Rev.* **2003**, *103* (4), 1485–1538. https://doi.org/10.1021/cr010010y.

[22] Ebner, C.; Carreira, E. M. Cyclopropanation Strategies in Recent Total Syntheses. *Chem. Rev.* **2017**, *117* (18), 11651–11679. https://doi.org/10.1021/acs.chemrev.6b00798.

[23] Wu, W.; Lin, Z.; Jiang, H. Recent Advances in the Synthesis of Cyclopropanes. *Org. Biomol. Chem.* **2018**, *16* (40), 7315–7329. https://doi.org/10.1039/C8OB01187G.

[24] Pellissier, H. Recent Developments in Asymmetric Cyclopropanation. *Tetrahedron* **2008**, *64* (30–31), 7041–7095. https://doi.org/10.1016/j.tet.2008.04.079.

[25] Mato, M.; Franchino, A.; García-Morales, C.; Echavarren, A. M. Gold-Catalyzed Synthesis of Small Rings. *Chem. Rev.* **2021**, *121* (14), 8613–8684. https://doi.org/10.1021/acs.chemrev.0c00697.

[26] Dombrowski, A. W.; Gesmundo, N. J.; Aguirre, A. L.; Sarris, K. A.; Young, J. M.; Bogdan, A. R.; Martin, M. C.; Gedeon, S.; Wang, Y. Expanding the Medicinal Chemist Toolbox:

Comparing Seven C(Sp ^{2})–C(Sp ^{3}) Cross-Coupling Methods by Library Synthesis. *ACS Med. Chem. Lett.* **2020**, *11* (4), 597–604. https://doi.org/10.1021/acsmedchemlett.0c00093.

[27] Turkowska, J.; Durka, J.; Gryko, D. Strain Release – an Old Tool for New Transformations. *Chem. Commun.* **2020**, *56* (43), 5718–5734. https://doi.org/10.1039/D0CC01771J.

[28] Gianatassio, R.; Lopchuk, J. M.; Wang, J.; Pan, C.-M.; Malins, L. R.; Prieto, L.; Brandt, T. A.; Collins, M. R.; Gallego, G. M.; Sach, N. W.; Spangler, J. E.; Zhu, H.; Zhu, J.; Baran, P. S. Strain-Release Amination. *Science* **2016**, *351* (6270), 241–246. https://doi.org/10.1126/science.aad6252.

[29] Delia, E. W.; Lochert, I. J. SYNTHESIS OF BRIDGEHEAD-SUBSTTTUTED BICYCLO[1.1.1]PENTANES. A REVIEW. *null* **1996**, *28* (4), 411–441. https://doi.org/10.1080/00304949609356550.

[30] Makarov, I. S.; Brocklehurst, C. E.; Karaghiosoff, K.; Koch, G.; Knochel, P. Synthesis of Bicyclo[1.1.1]Pentane Bioisosteres of Internal Alkynes and Para-Disubstituted Benzenes from [1.1.1]Propellane. *Angew. Chem. Int. Ed.* **2017**, *56* (41), 12774–12777. https://doi.org/10.1002/anie.201706799.

[31] Hoz, S.; Aurbach, D. Cyclobutane-Bicyclobutane System—I. *Tetrahedron* **1979**, *35* (7), 881–883. https://doi.org/10.1016/0040-4020(79)80110-6.

[32] Gianatassio, R.; Kadish, D. Direct Alkylation of 1-Azabicyclo[1.1.0]Butanes. *Org. Lett.* **2019**, *21* (7), 2060–2063. https://doi.org/10.1021/acs.orglett.9b00321.

[33] Nugent, J.; Arroniz, C.; Shire, B. R.; Sterling, A. J.; Pickford, H. D.; Wong, M. L. J.; Mansfield, S. J.; Caputo, D. F. J.; Owen, B.; Mousseau, J. J.; Duarte, F.; Anderson, E. A. A General Route to Bicyclo[1.1.1]Pentanes through Photoredox Catalysis. *ACS Catal.* **2019**, *9* (10), 9568–9574. https://doi.org/10.1021/acscatal.9b03190.

[34] Pickford, H. D.; Nugent, J.; Owen, B.; Mousseau, James. J.; Smith, R. C.; Anderson, E. A. Twofold Radical-Based Synthesis of *N* , *C* -Difunctionalized Bicyclo[1.1.1]Pentanes. *J. Am. Chem. Soc.* **2021**, *143* (26), 9729–9736. https://doi.org/10.1021/jacs.1c04180.

[35] Zhang, X.; Smith, R. T.; Le, C.; McCarver, S. J.; Shireman, B. T.; Carruthers, N. I.; MacMillan, D. W. C. Copper-Mediated Synthesis of Drug-like Bicyclopentanes. *Nature* **2020**, *580* (7802), 220–226. https://doi.org/10.1038/s41586-020-2060-z.

[36] Harris, M. R.; Wisniewska, H. M.; Jiao, W.; Wang, X.; Bradow, J. N. A Modular Approach to the Synthesis of *Gem* -Disubstituted Cyclopropanes. *Organic Letters* **2018**, *20* (10), 2867–2871. https://doi.org/10.1021/acs.orglett.8b00899.

[37] Molander, G. A.; Gormisky, P. E. Cross-Coupling of Cyclopropyl- and Cyclobutyltrifluoroborates with Aryl and Heteroaryl Chlorides. *J. Org. Chem.* **2008**, *73* (19), 7481–7485. https://doi.org/10.1021/jo801269m.

[38] VanHeyst, M. D.; Qi, J.; Roecker, A. J.; Hughes, J. M. E.; Cheng, L.; Zhao, Z.; Yin, J. Continuous Flow-Enabled Synthesis of Bench-Stable Bicyclo[1.1.1]Pentane Trifluoroborate Salts and Their Utilization in Metallaphotoredox Cross-Couplings. *Org. Lett.* **2020**, acs.orglett.0c00242. https://doi.org/10.1021/acs.orglett.0c00242.

[39] Nugent, J.; Shire, B. R.; Caputo, D. F. J.; Pickford, H. D.; Nightingale, F.; Houlsby, I. T. T.; Mousseau, J. J.; Anderson, E. A. Synthesis of All-Carbon Disubstituted Bicyclo[1.1.1]Pentanes by Iron-Catalyzed Kumada Cross-Coupling. *Angew. Chem. Int. Ed.* **2020**, *59* (29), 11866–11870. https://doi.org/10.1002/anie.202004090.

[40] Ociepa, M.; Wierzba, A. J.; Turkowska, J.; Gryko, D. Polarity-Reversal Strategy for the Functionalization of Electrophilic Strained Molecules via Light-Driven Cobalt Catalysis. *J. Am. Chem. Soc.* **2020**, *142* (11), 5355–5361. https://doi.org/10.1021/jacs.0c00245.

[41] Mills, L. R.; Monteith, J. J.; dos Passos Gomes, G.; Aspuru-Guzik, A.; Rousseaux, S. A. L. The Cyclopropane Ring as a Reporter of Radical Leaving-Group Reactivity for Ni-Catalyzed C(Sp^3)–O Arylation. *J. Am. Chem. Soc.* **2020**, *142* (30), 13246–13254. https://doi.org/10.1021/jacs.0c06904.

[42] Dong, Z.; MacMillan, D. W. C. Metallaphotoredox-Enabled Deoxygenative Arylation of Alcohols. *Nature* **2021**, *598* (7881), 451–456. https://doi.org/10.1038/s41586-021-03920-6.

[43] Yang, S.; Jiang, W.-T.; Xiao, B. Tertiary Cyclopropyl Carbagermatranes: Synthesis and Cross-Coupling. *Chem. Commun.* **2021**, *57* (66), 8143–8146. https://doi.org/10.1039/D1CC02930D.

[44] A pre-print of this work-in-progress was posted on Feb 21, 2022 to ChemRxiv. D. Salgueiro, B. Chi, P. Garcia-Reynaga, D. Weix, ChemRxiv 2022, DOI 10.26434/chemrxiv-2022-79l4g. This content is a preprint and has not been peer-reviewed.

[45] Daley, R. A.; Morrenzin, A. S.; Neufeldt, S. R.; Topczewski, J. J. Gold Catalyzed Decarboxylative Cross-Coupling of Iodoarenes. *J. Am. Chem. Soc.* **2020**, *142* (30), 13210–13218. https://doi.org/10.1021/jacs.0c06244.

[46] Luo, Z.; Han, X.; Fang, Y.; Liu, P.; Feng, C.; Li, Z.; Xu, X. Copper-Catalyzed Decarboxylative and Oxidative Decarbonylative Cross-Coupling between Cinnamic Acids and Aliphatic Aldehydes. *Org. Chem. Front.* **2018**, *5* (22), 3299–3305. https://doi.org/10.1039/C8QO00927A.

[47] Chen, T.-G.; Zhang, H.; Mykhailiuk, P. K.; Merchant, R. R.; Smith, C. A.; Qin, T.; Baran, P. S. Quaternary Centers by Nickel-Catalyzed Cross-Coupling of Tertiary Carboxylic Acids and (Hetero)Aryl Zinc Reagents. *Angew. Chem. Int. Ed.* **2019**, *58* (8), 2454–2458. https://doi.org/10.1002/anie.201814524.

[48] Cornella, J.; Edwards, J. T.; Qin, T.; Kawamura, S.; Wang, J.; Pan, C.-M.; Gianatassio, R.; Schmidt, M.; Eastgate, M. D.; Baran, P. S. Practical Ni-Catalyzed Aryl–Alkyl Cross-Coupling of Secondary Redox-Active Esters. *J. Am. Chem. Soc.* **2016**, *138* (7), 2174–2177. https://doi.org/10.1021/jacs.6b00250.

[49] Toriyama, F.; Cornella, J.; Wimmer, L.; Chen, T.-G.; Dixon, D. D.; Creech, G.; Baran, P. S. Redox-Active Esters in Fe-Catalyzed C–C Coupling. *J. Am. Chem. Soc.* **2016**, *138* (35), 11132–11135. https://doi.org/10.1021/jacs.6b07172.

[50] Huihui, K. M. M.; Caputo, J. A.; Melchor, Z.; Olivares, A. M.; Spiewak, A. M.; Johnson, K. A.; DiBenedetto, T. A.; Kim, S.; Ackerman, L. K. G.; Weix, D. J. Decarboxylative Cross-Electrophile

Coupling of *N* -Hydroxyphthalimide Esters with Aryl Iodides. *J. Am. Chem. Soc.* **2016**, *138* (15), 5016–5019. https://doi.org/10.1021/jacs.6b01533.

[51] Wang, J.; Hoerrner, M. E.; Watson, M. P.; Weix, D. J. Nickel-Catalyzed Synthesis of Dialkyl Ketones from the Coupling of N-Alkyl Pyridinium Salts with Activated Carboxylic Acids. *Angew. Chem. Int. Ed.* **2020**, *59* (32), 13484–13489. https://doi.org/10.1002/anie.202002271.

[52] Li, H.; Breen, C. P.; Seo, H.; Jamison, T. F.; Fang, Y.-Q.; Bio, M. M. Ni-Catalyzed Electrochemical Decarboxylative C–C Couplings in Batch and Continuous Flow. *Org. Lett.* **2018**, *20* (5), 1338–1341. https://doi.org/10.1021/acs.orglett.8b00070.

[53] Kammer, L. M.; Badir, S. O.; Hu, R.-M.; Molander, G. A. Photoactive Electron Donor–Acceptor Complex Platform for Ni-Mediated C(Sp^3)–C(Sp^2) Bond Formation. *Chem. Sci.* **2021**, *12* (15), 5450–5457. https://doi.org/10.1039/D1SC00943E.

[54] Flood, D. T.; Asai, S.; Zhang, X.; Wang, J.; Yoon, L.; Adams, Z. C.; Dillingham, B. C.; Sanchez, B. B.; Vantourout, J. C.; Flanagan, M. E.; Piotrowski, D. W.; Richardson, P.; Green, S. A.; Shenvi, R. A.; Chen, J. S.; Baran, P. S.; Dawson, P. E. Expanding Reactivity in DNA-Encoded Library Synthesis via Reversible Binding of DNA to an Inert Quaternary Ammonium Support. *J. Am. Chem. Soc.* **2019**, *141* (25), 9998–10006. https://doi.org/10.1021/jacs.9b03774.

[55] Mykura, R. C.; Songara, P.; Luc, E.; Rogers, J.; Stammers, E.; Aggarwal, V. K. Studies on the Lithiation, Borylation, and 1,2-Metalate Rearrangement of O-Cycloalkyl 2,4,6-Triisopropylbenzoates. *Angew. Chem. Int. Ed.* **2021**, *60* (20), 11436–11441. https://doi.org/10.1002/anie.202101374.

[56] Davenport, R.; Silvi, M.; Noble, A.; Hosni, Z.; Fey, N.; Aggarwal, V. K. Visible-Light-Driven Strain-Increase Ring Contraction Allows the Synthesis of Cyclobutyl Boronic Esters. *Angew. Chem. Int. Ed.* **2020**, *59* (16), 6525–6528. https://doi.org/10.1002/anie.201915409.

[57] Fawcett, A.; Murtaza, A.; Gregson, C. H. U.; Aggarwal, V. K. Strain-Release-Driven Homologation of Boronic Esters: Application to the Modular Synthesis of Azetidines. *Journal of the American Chemical Society* **2019**. https://doi.org/10.1021/jacs.9b01513.

[58] Montesinos-Magraner, M.; Costantini, M.; Ramírez-Contreras, R.; Muratore, M. E.; Johansson, M. J.; Mendoza, A. General Cyclopropane Assembly by Enantioselective Transfer of a Redox-Active Carbene to Aliphatic Olefins. *Angew. Chem. Int. Ed.***2019**, *58* (18), 5930–5935. https://doi.org/10.1002/anie.201814123.

[59] Yu, Z.; Mendoza, A. Enantioselective Assembly of Congested Cyclopropanes Using Redox-Active Aryldiazoacetates. *ACS Catal.* **2019**, *9* (9), 7870–7875. https://doi.org/10.1021/acscatal.9b02615.

[60] Planas, F.; Costantini, M.; Montesinos-Magraner, M.; Himo, F.; Mendoza, A. Combined Experimental and Computational Study of Ruthenium *N* -Hydroxyphthalimidoyl Carbenes in Alkene Cyclopropanation Reactions. *ACS Catal.* **2021**, *11* (17), 10950–10963. https://doi.org/10.1021/acscatal.1c02540.

[61] Costantini, M.; Mendoza, A. Modular Enantioselective Synthesis of *Cis* -Cyclopropanes through Self-Sensitized Stereoselective Photodecarboxylation with Benzothiazolines. *ACS Catal.* **2021**, *11* (21), 13312–13319. https://doi.org/10.1021/acscatal.1c03949.

[62] Polites, V. C.; Badir, S. O.; Keess, S.; Jolit, A.; Molander, G. A. Nickel-Catalyzed Decarboxylative Cross-Coupling of Bicyclo[1.1.1]Pentyl Radicals Enabled by Electron Donor–Acceptor Complex Photoactivation. *Org. Lett.* **2021**, *23* (12), 4828–4833. https://doi.org/10.1021/acs.orglett.1c01558.

[63] Kolahdouzan, K.; Khalaf, R.; Grandner, J. M.; Chen, Y.; Terrett, J. A.; Huestis, M. P. Dual Photoredox/Nickel-Catalyzed Conversion of Aryl Halides to Aryl Aminooxetanes: Computational Evidence for a Substrate-Dependent Switch in Mechanism. *ACS Catal.* **2020**, *10* (1), 405–411. https://doi.org/10.1021/acscatal.9b03596.

[64] Xue, W.; Jia, X.; Wang, X.; Tao, X.; Yin, Z.; Gong, H. Nickel-Catalyzed Formation of Quaternary Carbon Centers Using Tertiary Alkyl Electrophiles. *Chem. Soc. Rev.* **2021**, *50* (6), 4162–4184. https://doi.org/10.1039/D0CS01107J.

[65] Wang, X.; Wang, S.; Xue, W.; Gong, H. Nickel-Catalyzed Reductive Coupling of Aryl Bromides with Tertiary Alkyl Halides. *J. Am. Chem. Soc.* **2015**, *137* (36), 11562–11565. https://doi.org/10.1021/jacs.5b06255.

[66] Lu, X.; Wang, Y.; Zhang, B.; Pi, J.-J.; Wang, X.-X.; Gong, T.-J.; Xiao, B.; Fu, Y. Nickel-Catalyzed Defluorinative Reductive Cross-Coupling of *Gem* -Difluoroalkenes with Unactivated Secondary and Tertiary Alkyl Halides. *J. Am. Chem. Soc.* **2017**, *139* (36), 12632–12637. https://doi.org/10.1021/jacs.7b06469.

[67] Ye, Y.; Chen, H.; Sessler, J. L.; Gong, H. Zn-Mediated Fragmentation of Tertiary Alkyl Oxalates Enabling Formation of Alkylated and Arylated Quaternary Carbon Centers. *J. Am. Chem. Soc.* **2019**, *141* (2), 820–824.

[68] Makarov, I. S.; Brocklehurst, C. E.; Karaghiosoff, K.; Koch, G.; Knochel, P. Synthesis of Bicyclo[1.1.1]Pentane Bioisosteres of Internal Alkynes and Para-Disubstituted Benzenes from [1.1.1]Propellane. *Angewandte Chemie International Edition* **2017**, *56* (41), 12774–12777. https://doi.org/10.1002/anie.201706799.

[69] Peng, Y.; Luo, L.; Yan, C.-S.; Zhang, J.-J.; Wang, Y.-W. Ni-Catalyzed Reductive Homocoupling of Unactivated Alkyl Bromides at Room Temperature and Its Synthetic Application. *J. Org. Chem.* **2013**, *78* (21), 10960–10967. https://doi.org/10.1021/jo401936v.

[70] Wang, X.; Ma, G.; Peng, Y.; Pitsch, C. E.; Moll, B. J.; Ly, T. D.; Wang, X.; Gong, H. Ni-Catalyzed Reductive Coupling of Electron-Rich Aryl Iodides with Tertiary Alkyl Halides. *J. Am. Chem. Soc.* **2018**, *140* (43), 14490–14497. https://doi.org/10.1021/jacs.8b09473.

[71] Wang, Z.; Yang, Z.-P.; Fu, G. C. Quaternary Stereocentres via Catalytic Enantioconvergent Nucleophilic Substitution Reactions of Tertiary Alkyl Halides. *Nat. Chem.* **2021**, *13* (3), 236–242. https://doi.org/10.1038/s41557-020-00609-7.

[72] Börjesson, M.; Moragas, T.; Martin, R. Ni-Catalyzed Carboxylation of Unactivated Alkyl Chlorides with CO2. *J. Am. Chem. Soc.* **2016**, *138* (24), 7504–7507. https://doi.org/10.1021/jacs.6b04088.

[73] Walborsky, H. M. The Cyclopropyl Radical. *Tetrahedron* **1981**, *37* (9), 1625–1651. https://doi.org/10.1016/S0040-4020(01)98924-0.

[74] Veillard, A.; Re, G. Hybridization in Cyclopropane, Cyclobutane and Cubane. *Theoret. Chim. Acta* **1964**, *2* (1), 55–62. https://doi.org/10.1007/BF00529465.

[75] Yuan, M.; Song, Z.; Badir, S. O.; Molander, G. A.; Gutierrez, O. On the Nature of C(Sp^3)–C(Sp^2) Bond Formation in Nickel-Catalyzed Tertiary Radical Cross-Couplings: A Case Study of Ni/Photoredox Catalytic Cross-Coupling of Alkyl Radicals and Aryl Halides. *J. Am. Chem. Soc.* **2020**, *142* (15), 7225–7234. https://doi.org/10.1021/jacs.0c02355.

[76] Wang, J.; Cary, B. P.; Beyer, P. D.; Gellman, S. H.; Weix, D. J. Ketones from Nickel-Catalyzed Decarboxylative, Non-Symmetric Cross-Electrophile Coupling of Carboxylic Acid Esters. *Angew. Chem. Int. Ed.* **2019**, *58* (35), 12081–12085. https://doi.org/10.1002/anie.201906000.

[77] Ni, S.; Padial, N. M.; Kingston, C.; Vantourout, J. C.; Schmitt, D. C.; Edwards, J. T.; Kruszyk, M. M.; Merchant, R. R.; Mykhailiuk, P. K.; Sanchez, B. B.; Yang, S.; Perry, M. A.; Gallego, G. M.; Mousseau, J. J.; Collins, M. R.; Cherney, R. J.; Lebed, P. S.; Chen, J. S.; Qin, T.; Baran, P. S. A Radical Approach to Anionic Chemistry: Synthesis of Ketones, Alcohols, and Amines. *J. Am. Chem. Soc.* **2019**, *141* (16), 6726–6739. https://doi.org/10.1021/jacs.9b02238.

[78] Xi, X.; Luo, Y.; Li, W.; Xu, M.; Zhao, H.; Chen, Y.; Zheng, S.; Qi, X.; Yuan, W. From Esters to Ketones via a Photoredox-Assisted Reductive Acyl Cross-Coupling Strategy. *Angew. Chem. Int. Ed.* **2022**, *61* (3), e202114731. https://doi.org/10.1002/anie.202114731.

[79] Kim, S.; Goldfogel, M. J.; Gilbert, M. M.; Weix, D. J. Nickel-Catalyzed Cross-Electrophile Coupling of Aryl Chlorides with Primary Alkyl Chlorides. *J. Am. Chem. Soc.* **2020**, *142* (22), 9902–9907. https://doi.org/10.1021/jacs.0c02673.

[80] Everson, D. A.; B., Joseph A.;. Weix, Daniel J. Nickel-Catalyzed Cross-Electrophile Coupling of 2-Chloropyridines with Alkyl Bromides. *Synlett* **2014**, *25* (02), 233–238. https://doi.org/10.1055/s-0033-1340151.

[81] Everson, D. A.; Jones, B. A.; Weix, D. J. Replacing Conventional Carbon Nucleophiles with Electrophiles: Nickel-Catalyzed Reductive Alkylation of Aryl Bromides and Chlorides. *J. Am. Chem. Soc.* **2012**, *134* (14), 6146–6159. https://doi.org/10.1021/ja301769r.

[82] Huang, L.; Olivares, A. M.; Weix, D. J. Reductive Decarboxylative Alkynylation of N-Hydroxyphthalimide Esters with Bromoalkynes. *Angew. Chem. Int. Ed.* **2017**, *56* (39), 11901–11905. https://doi.org/10.1002/anie.201706781.

[83] Hansen, E. C.; Li, C.; Yang, S.; Pedro, D.; Weix, D. J. Coupling of Challenging Heteroaryl Halides with Alkyl Halides via Nickel-Catalyzed Cross-Electrophile Coupling. *J. Org. Chem.* **2017**, *82* (14), 7085–7092. https://doi.org/10.1021/acs.joc.7b01334.

[84] Hansen, E. C.; Pedro, D. J.; Wotal, A. C.; Gower, N. J.; Nelson, J. D.; Caron, S.; Weix, D. J. New Ligands for Nickel Catalysis from Diverse Pharmaceutical Heterocycle Libraries. *Nature Chem* **2016**, *8* (12), 1126–1130. https://doi.org/10.1038/nchem.2587.

[85] Chi, B. K.; Widness, J. K.; Gilbert, M. M.; Salgueiro, D. C.; Garcia, K. J.; Weix, D. J. In-Situ Bromination Enables Formal Cross-Electrophile Coupling of Alcohols with Aryl and Alkenyl Halides. *ACS Catal.* **2022**, *12* (1), 580–586. https://doi.org/10.1021/acscatal.1c05208.

[86] Qiao, J. X.; Cheney, D. L.; Alexander, R. S.; Smallwood, A. M.; King, S. R.; He, K.; Rendina, A. R.; Luettgen, J. M.; Knabb, R. M.; Wexler, R. R.; Lam, P. Y. S. Achieving Structural Diversity Using the Perpendicular Conformation of Alpha-Substituted Phenylcyclopropanes to Mimic the Bioactive Conformation of Ortho-Substituted Biphenyl P4 Moieties: Discovery of Novel, Highly Potent Inhibitors of Factor Xa. *Bioorganic & Medicinal Chemistry Letters* **2008**, *18* (14), 4118–4123. https://doi.org/10.1016/j.bmcl.2008.05.095.

[87] Wagner, C. E.; Jurutka, P. W.; Marshall, P. A.; Groy, T. L.; van der Vaart, A.; Ziller, J. W.; Furmick, J. K.; Graeber, M. E.; Matro, E.; Miguel, B. V.; Tran, I. T.; Kwon, J.; Tedeschi, J. N.; Moosavi, S.; Danishyar, A.; Philp, J. S.; Khamees, R. O.; Jackson, J. N.; Grupe, D. K.; Badshah, S. L.; Hart, J. W. Modeling, Synthesis and Biological Evaluation of Potential Retinoid X Receptor (RXR) Selective Agonists: Novel Analogues of 4-[1-(3,5,5,8,8-Pentamethyl-5,6,7,8-Tetrahydro-2-Naphthyl)Ethynyl]Benzoic Acid (Bexarotene). *J. Med. Chem.* **2009**, *52* (19), 5950–5966. https://doi.org/10.1021/jm900496b.

[88] Boehm, M. F.; Zhang, L.; Zhi, L.; McClurg, M. R.; Berger, E.; Wagoner, M.; Mais, D. E.; Suto, C. M.; Davies, P. J. A.; Heyman, R. A.; Nadzan, A. M. Design and Synthesis of Potent Retinoid X Receptor Selective Ligands That Induce Apoptosis in Leukemia Cells. *J. Med. Chem.* **1995**, *38* (16), 3146–3155. https://doi.org/10.1021/jm00016a018.

[89] He, Z.-T.; Hartwig, J. F. Palladium-Catalyzed α-Arylation for the Addition of Small Rings to Aromatic Compounds. *Nat Commun* **2019**, *10* (1), 4083. https://doi.org/10.1038/s41467-019-12090-z.

[90] Leal, A. S.; Zydeck, K.; Carapellucci, S.; Reich, L. A.; Zhang, D.; Moerland, J. A.; Sporn, M. B.; Liby, K. T. Retinoid X Receptor Agonist LG100268 Modulates the Immune Microenvironment in Preclinical Breast Cancer Models. *npj Breast Cancer* **2019**, *5* (1), 1–15. https://doi.org/10.1038/s41523-019-0135-5.

[91] Love, J. D.; Gooch, J. T.; Benko, S.; Li, C.; Nagy, L.; Chatterjee, V. K. K.; Evans, R. M.; Schwabe, J. W. R. The Structural Basis for the Specificity of Retinoid-X Receptor-Selective Agonists: New Insights Into the Role of Helix H12. *Journal of Biological Chemistry* **2002**, *277* (13), 11385–11391. https://doi.org/10.1074/jbc.M110869200.

[92] Boehm, M. F.; Zhang, L.; Zhi, L.; McClurg, M. R.; Berger, E.; Wagoner, M.; Mais, D. E.; Suto, C. M.; Davies, P. J. A.; Heyman, R. A.; Nadzan, A. M. Design and Synthesis of Potent Retinoid X Receptor Selective Ligands That Induce Apoptosis in Leukemia Cells. *J. Med. Chem.* **1995**, *38* (16), 3146–3155. https://doi.org/10.1021/jm00016a018.

[93] The NHP ester derived from 2-oxabicyclo[2.1.1]hexane-1-carboxylic acid could be coupled with 4-iodoanisole, but the bicyclic scaffold undergoes an as-yet undefined rearrangement. At this time, we are unsure of the exact structure of the rerarranged product.

[94] Kang, K.; Weix, D. J. Nickel-Catalyzed C(Sp3)–C(Sp3) Cross-Electrophile Coupling of In Situ Generated NHP Esters with Unactivated Alkyl Bromides. *Org. Lett.* **2022**, *24* (15), 2853–2857. https://doi.org/10.1021/acs.orglett.2c00805.

[95] Jiang, W.-T.; Yang, S.; Xu, M.-Y.; Xie, X.-Y.; Xiao, B. Zn-Mediated Decarboxylative Carbagermatranation of Aliphatic *N* -Hydroxyphthalimide Esters: Evidence for an Alkylzinc Intermediate. *Chem. Sci.* **2020**, *11* (2), 488–493. https://doi.org/10.1039/C9SC04288A.

[96] Aguirre, A. L.; Loud, N. L.; Johnson, K. A.; Weix, D. J.; Wang, Y. ChemBead Enabled High-Throughput Cross-Electrophile Coupling Reveals a New Complementary Ligand. *Chem. Eur. J.* **2021**, *27* (51), 12981–12986. https://doi.org/10.1002/chem.202102347.

[97] Kang, K.; Loud, N. L.; DiBenedetto, T. A.; Weix, D. J. A General, Multimetallic Cross-Ullmann Biheteroaryl Synthesis from Heteroaryl Halides and Heteroaryl Triflates. *J. Am. Chem. Soc.* **2021**, *143* (51), 21484–21491. https://doi.org/10.1021/jacs.1c10907.

[98] Deposition Number 2166821 contains the supplementary crystallographic data for this paper. These data are provided free of charge by the joint Cambridge Crystallographic Data Centre and Fachinformationszentrum Karlsruhe Access Structures service.

[99] Groom, C. R.; Bruno, I. J.; Lightfoot, M. P.; Ward, S. C. The Cambridge Structural Database. *Acta Cryst B* **2016**, *72* (2), 171–179. https://doi.org/10.1107/S2052520616003954.

[100] Zackasee, J. L. S.; Al Zubaydi, S.; Truesdell, B. L.; Sevov, C. S. Synergistic Catalyst–Mediator Pairings for Electroreductive Cross-Electrophile Coupling Reactions. *ACS Catal.* **2022**, *12* (2), 1161–1166. https://doi.org/10.1021/acscatal.1c05144. b).

[101] Truesdell, B. L.; Hamby, T. B.; Sevov, C. S. General C(Sp^2)–C(Sp^3) Cross-Electrophile Coupling Reactions Enabled by Overcharge Protection of Homogeneous Electrocatalysts. *J. Am. Chem. Soc.* **2020**, *142* (12), 5884–5893. https://doi.org/10.1021/jacs.0c01475.

[102] Prieto Kullmer, C. N.; Kautzky, J. A.; Krska, S. W.; Nowak, T.; Dreher, S. D.; MacMillan, D. W. C. Accelerating Reaction Generality and Mechanistic Insight through Additive Mapping. *Science* **2022**, *376* (6592), 532–539. https://doi.org/10.1126/science.abn1885.

[103] Yamada, C.; Pahk, M. J.; Liu, R. S. H. Photosensitized Cyclization Reaction of 2-Phenylhexa-1,5-Diene. *J. Chem. Soc. D* **1970**, No. 14, 882. https://doi.org/10.1039/c29700000882.

[104] Sauers, R. R.; Hagedorn, A. A.; Van Arnum, S. D.; Gomez, R. P.; Moquin, R. V. Synthesis and Photochemistry of Heterocyclic Norbornenyl Ketones. *J. Org. Chem.* **1987**, *52* (25), 5501–5505. https://doi.org/10.1021/jo00234a001.

[105]Palkowitz, M. D.; Laudadio, G.; Kolb, S.; Choi, J.; Oderinde, M. S.; Ewing, T. E.-H.; Bolduc, P. N.; Chen, T.; Zhang, H.; Cheng, P. T. W.; Zhang, B.; Mandler, M. D.; Blasczak, V. D.; Richter, J. M.; Collins, M. R.; Schioldager, R. L.; Bravo, M.; Dhar, T. G. M.; Vokits, B.; Zhu, Y.; Echeverria, P.-G.; Poss, M. A.; Shaw, S. A.; Clementson, S.; Petersen, N. N.; Mykhailiuk, P. K.; Baran, P. S. Overcoming Limitations in Decarboxylative Arylation via Ag–Ni Electrocatalysis. *J. Am. Chem. Soc.* **2022**, *144* (38), 17709–17720. https://doi.org/10.1021/jacs.2c08006.

[106] Sim, B. A.; Griller, D.; Wayner, D. D. M. Reduction Potentials for Substituted Benzyl Radicals: PKa Values for the Corresponding Toluenes. *J. Am. Chem. Soc.* **1989**, *111* (2), 754–755. https://doi.org/10.1021/ja00184a066.

[107] He, Z.-T.; Hartwig, J. F. Palladium-Catalyzed α-Arylation for the Addition of Small Rings to Aromatic Compounds. *Nat Commun* **2019**, *10* (1), 4083. https://doi.org/10.1038/s41467-019-12090-z.

[108] Barzanò, G.; Mao, R.; Garreau, M.; Waser, J.; Hu, X. Tandem Photoredox and Copper-Catalyzed Decarboxylative C(Sp^3)–N Coupling of Anilines and Imines Using an Organic Photocatalyst. *Org. Lett.* **2020**, *22* (14), 5412–5416. https://doi.org/10.1021/acs.orglett.0c01769.

[109] Wang, J.; Cary, B. P.; Beyer, P. D.; Gellman, S. H.; Weix, D. J. Ketones from Nickel-Catalyzed Decarboxylative, Non-Symmetric Cross-Electrophile Coupling of Carboxylic Acid Esters. *Angew. Chem. Int. Ed.* **2019**, *58* (35), 12081–12085. https://doi.org/10.1002/anie.201906000.

[110] Gao, L.; Wang, G.; Cao, J.; Chen, H.; Gu, Y.; Liu, X.; Cheng, X.; Ma, J.; Li, S. Lewis Acid-Catalyzed Selective Reductive Decarboxylative Pyridylation of *N* -Hydroxyphthalimide Esters: Synthesis of Congested Pyridine-Substituted Quaternary Carbons. *ACS Catal.* **2019**, *9* (11), 10142–10151. https://doi.org/10.1021/acscatal.9b03798.

[111] Qin, T.; Malins, L. R.; Edwards, J. T.; Merchant, R. R.; Novak, A. J. E.; Zhong, J. Z.; Mills, R. B.; Yan, M.; Yuan, C.; Eastgate, M. D.; Baran, P. S. Nickel-Catalyzed Barton Decarboxylation and Giese Reactions: A Practical Take on Classic Transforms. *Angew. Chem. Int. Ed.* **2017**, *56* (1), 260–265. https://doi.org/10.1002/anie.201609662.

[112] Polites, V. C.; Badir, S. O.; Keess, S.; Jolit, A.; Molander, G. A. Nickel-Catalyzed Decarboxylative Cross-Coupling of Bicyclo[1.1.1]Pentyl Radicals Enabled by Electron Donor–Acceptor Complex Photoactivation. *Org. Lett.* **2021**, *23* (12), 4828–4833. https://doi.org/10.1021/acs.orglett.1c01558.

[113] Ni, S.; Padial, N. M.; Kingston, C.; Vantourout, J. C.; Schmitt, D. C.; Edwards, J. T.; Kruszyk, M. M.; Merchant, R. R.; Mykhailiuk, P. K.; Sanchez, B. B.; Yang, S.; Perry, M. A.; Gallego, G. M.; Mousseau, J. J.; Collins, M. R.; Cherney, R. J.; Lebed, P. S.; Chen, J. S.; Qin, T.; Baran, P. S. A Radical Approach to Anionic Chemistry: Synthesis of Ketones, Alcohols, and Amines. *J. Am. Chem. Soc.* **2019**, *141* (16), 6726–6739. https://doi.org/10.1021/jacs.9b02238.

[114] Toriyama, F.; Cornella, J.; Wimmer, L.; Chen, T.-G.; Dixon, D. D.; Creech, G.; Baran, P. S. Redox-Active Esters in Fe-Catalyzed C–C Coupling. *J. Am. Chem. Soc.* **2016**, *138* (35), 11132–11135. https://doi.org/10.1021/jacs.6b07172.

[115] Fawcett, A.; Pradeilles, J.; Wang, Y.; Mutsuga, T.; Myers, E. L.; Aggarwal, V. K. Photoinduced Decarboxylative Borylation of Carboxylic Acids. *Science* **2017**, *357* (6348), 283–286. https://doi.org/10.1126/science.aan3679.

[116] Watanabe, E.; Chen, Y.; May, O.; Ley, S. V. A Practical Method for Continuous Production of Sp3-Rich Compounds from (Hetero)Aryl Halides and Redox-Active Esters. *Chem. Eur. J.* **2020**, *26* (1), 186–191. https://doi.org/10.1002/chem.201905048.

[117] Maiwald, M. M.; Wagner, A. T.; Kratsch, J.; Skerencak-Frech, A.; Trumm, M.; Geist, A.; Roesky, P. W.; Panak, P. J. 4,4′-Di-Tert-Butyl-6-(1H-Tetrazol-5-Yl)-2,2′-Bipyridine: Modification of a Highly Selective N-Donor Ligand for the Separation of Trivalent Actinides from Lanthanides. *Dalton Trans.* **2017**, *46* (30), 9981–9994. https://doi.org/10.1039/C7DT01864A.

[118] Chi, B. K.; Widness, J. K.; Gilbert, M. M.; Salgueiro, D. C.; Garcia, K. J.; Weix, D. J. In-Situ Bromination Enables Formal Cross-Electrophile Coupling of Alcohols with Aryl and Alkenyl Halides. *ACS Catal.* **2022**, *12* (1), 580–586. https://doi.org/10.1021/acscatal.1c05208.

[119] Huffman, K. R.; Schaefer, F. C. Preparation and Reactions of N-Cyanoamidines. *J. Org. Chem.* **1963**, *28* (7), 1812–1816. https://doi.org/10.1021/jo01042a017.

[120] Huang, A.; Moretto, A.; Janz, K.; Lowe, M.; Bedard, P. W.; Tam, S.; Di, L.; Clerin, V.; Sushkova, N.; Tchernychev, B.; Tsao, D. H. H.; Keith, J. C.; Shaw, G. D.; Schaub, R. G.; Wang, Q.; Kaila, N. Discovery of 2-[1-(4-Chlorophenyl)Cyclopropyl]-3-Hydroxy-8-(Trifluoromethyl)Quinoline-4-Carboxylic Acid (PSI-421), a P-Selectin Inhibitor with Improved Pharmacokinetic Properties and Oral Efficacy in Models of Vascular Injury. *J. Med. Chem.* **2010**, *53* (16), 6003–6017. https://doi.org/10.1021/jm9013696.

[121] Brandstätter, M.; Huwyler, N.; Carreira, E. M. Gold(I)-Catalyzed Stereoselective Cyclization of 1,3-Enyne Aldehydes by a 1,3-Acyloxy Migration/Nazarov Cyclization/Aldol

Addition Cascade. *Chem. Sci.* **2019**, *10* (35), 8219–8223. https://doi.org/10.1039/C9SC02828E.

[122] Chen, T.-G.; Zhang, H.; Mykhailiuk, P. K.; Merchant, R. R.; Smith, C. A.; Qin, T.; Baran, P. S. Quaternary Centers by Nickel-Catalyzed Cross-Coupling of Tertiary Carboxylic Acids and (Hetero)Aryl Zinc Reagents. *Angew. Chem. Int. Ed.* **2019**, *58* (8), 2454–2458. https://doi.org/10.1002/anie.201814524.

[123] Wrackmeyer, B. Carbon-13 NMR Spectroscopy of Boron Compounds. *Progress in Nuclear Magnetic Resonance Spectroscopy* **1979**, *12* (4), 227–259. https://doi.org/10.1016/0079-6565(79)80003-5.

[124] Lévesque, É.; Goudreau, S. R.; Charette, A. B. Improved Zinc-Catalyzed Simmons–Smith Reaction: Access to Various 1,2,3-Trisubstituted Cyclopropanes. *Org. Lett.* **2014**, *16* (5), 1490–1493. https://doi.org/10.1021/ol500267w.

[125] Wiberg, K. B.; McMurdie, N. Formation and Reactions of Bicyclo[1.1.1]Pentyl-1 Cations. *J. Am. Chem. Soc.* **1994**, *116* (26), 11990–11998. https://doi.org/10.1021/ja00105a046.

[126] Bruker-AXS (2019). APEX3. Version 2019.11-0. Madison, Wisconsin, USA.

[127] Krause, L.; Herbst-Irmer, R.; Sheldrick, G. M.; Stalke, D. Comparison of Silver and Molybdenum Microfocus X-Ray Sources for Single-Crystal Structure Determination. *J Appl Crystallogr* **2015**, *48* (Pt 1), 3–10. https://doi.org/10.1107/S1600576714022985.

[128] a) Sheldrick, G. M. (2013b). XPREP. Version 2013/1. Georg-August-Universität Göttingen, Göttingen, Germany.

[129] Sheldrick, G. M. (2013a). The SHELX homepage, http://shelx.uni-ac.gwdg.de/SHELX/.

[130] Sheldrick, G. M. It SHELXT – Integrated Space-Group and Crystal-Structure Determination. *Acta Crystallographica Section A* **2015**, *71* (1), 3–8. https://doi.org/10.1107/S2053273314026370.

[131] Sheldrick, G. M. Crystal Structure Refinement with It SHELXL. *Acta Crystallographica Section C* **2015**, *71* (1), 3–8. https://doi.org/10.1107/S2053229614024218.

[132] Dolomanov, O. V.; Bourhis, L. J.; Gildea, R. J.; Howard, J. A. K.; Puschmann, H. It OLEX2: A Complete Structure Solution, Refinement and Analysis Program. *Journal of Applied Crystallography* **2009**, *42* (2), 339–341. https://doi.org/10.1107/S0021889808042726.

[133] Guzei, I. A. (2007-2013). Programs Gn. University of Wisconsin-Madison, Madison, Wisconsin, USA.

Chapter 4: Efforts Towards Nickel-Catalyzed XEC of Redox-Active Esters with Heteroaryl Chlorides

4.1 Introduction

In the year since publication of the work presented in Chapter 3,[1] the scope of chemical space accessible via decarboxylative arylation of alkanoic acids (and their redox-active derivatives) has expanded. First, Macmillan reported a metallaphotoredox approach for the coupling of alkanoic acids with aryl bromides.[2] The authors were able to achieve such breadth in the scope with respect to both carboxylic acids and aryl bromides with the use of phthalimide as a key additive to stabilize the requisite Ni^{II}-aryl intermediate, however phthalimide may not be effective in all cases.[3] Baran reported an electrochemical system for the coupling of NHP esters with aryl halides, which relied upon passivation of the electrode surface with silver nanoparticles.[4] The scope of this reaction is, by far, the largest of any reported net-reductive arylation of RAEs, showing examples of couplings with aryl iodides, bromides, and even 3 examples of couplings with heteroaryl chlorides. However, the need for specialized photochemical and electrochemical setups can hinder the adoption of these methods for synthesis at large scales, and parallel synthesis at smaller scales.

Cross-electrophile coupling of RAEs of aryl halides promoted by a chemical reductant avoids the need for a specialized reactor, but the scope is currently limited to couplings with aryl iodides and electron-deficient aryl bromides. We envisioned 3 strategies would be most useful in expanding decarboxylative XEC to work with aryl substrates more challenging than electron-deficient aryl bromides: 1) In our previous publication we found that electron-rich NHP ester derivatives generated radicals more slowly than their electron-deficient counterparts, therefore we envisioned that even more electron-rich redox-active esters could be prepared and tested. 2) Slow oxidative addition into the aryl halide relative to radical

generation from a RAE was a significant hurdle in our previous publication and would only become more problematic as we shift to more and more difficult oxidative additions. To find better oxidative addition reactivity we, with the help of our collaborators at Janssen decided to look more broadly at different classes of ligands to promote this reaction. 3) Lewis acidic zinc halide salts have been reported to facilitate reduction of NHP esters by the zinc. As ZnX_2 salts are necessarily generated when zinc is employed as reductant, consumption of NHP esters could be autocatalytic in this regme. If we explore organic reductants which can reduce the nickel catalyst through an inner-sphere mechanism rather than an outer-sphere electron transfer, then we can ensure that reduction of the NHP ester is only mediated by the nickel catalyst. This potential change in mechanism could circumvent the autocatalysis proposed under conditions utilizing zinc as reductant and would turn off deleterious background reactivity.

4.2 Attempted Syntheses of Electron-Rich Redox–Active Esters

We found that increased electron-density on the phthalimide backbone of NHP esters led to a decreased rate of radical formation, enabling more selective cross-couplings with aryl bromides of varying electronics. We hypothesized that *N*-hydroxyphthalimide derivatives with stronger electron-donating groups would be useful for expanding the scope of arylation reactions of RAEs to include (hetero)aryl chlorides. Thus far, the strongest electron-donating group we had appended to *N*-hydroxyphthalimide had been a methoxy group (σ_p = -0.27). I proposed that a dialkyl amine should be a sufficiently strong electron donating group (NMe_2 σ_p = -0.83) to impart slower radical generation than a methoxy group. We envisioned that NMe_2NHP could be synthesized in three steps (see below):

Figure 4.1 Approach for the synthesis of 4.4

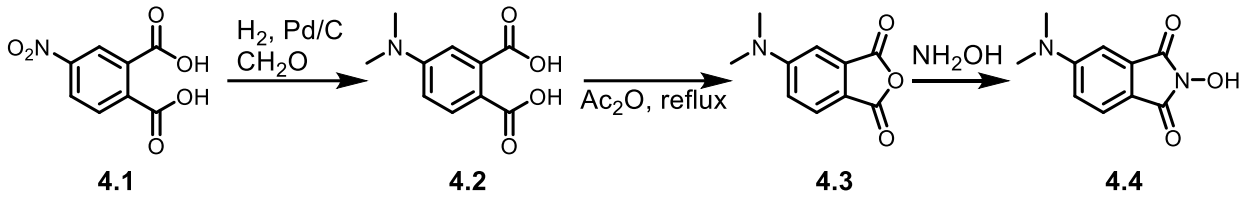

While this route was promising due to the availability of 4-nitrophthalic acid, initial attempts at the one-pot reduction/reductive amination proved to be too low-yielding to provide quantities of NMe_2 NHP sufficient for systematic testing. Perhaps alternative conditions for the reductive amination step would provide more synthetically tractable yields for further studies, though these were not investigated. I was able to synthesize BCP derived RAE X to perform an HTE scale optimization of couplings of redox-active esters with aryl bromides from the Merck Informer library, see experimental section for more detail.

Borrowing from approaches for the syntheses of PROTACs,[5] I envisioned an alternative strategy for the introduction of electron-donating groups onto the backbone of N-hydroxyphthalimide would be to first synthesize a fluorinated N-hydroxyphthalimide and then perform a nucleophilic aromatic substitution reaction with a suitable nucleophile. Morpholine was the first choice as nucleophile as it is an easily accessible, nucleophilic secondary amine. Subjection of 4-fluoro N-hydroxy phthalimide to previously reported nucleophilic aromatic substitution conditions led to recovery of both starting materials, suggesting more forcing conditions would be necessary. Attempts at promoting the reaction at elevated temperature did lead to nucleophilic aromatic substitution reactivity, however the isolated product was the homologated N-hydroxyphthalimide shown in **Figure 4.2**. We presume this product arises from morpholine reacting with the cyclic imide and undergoing a ring-ring opening reaction, potentially promoted by the hydrofluoric acid formed following nucleophilic aromatic

substitution. Systematic screening of reaction temperature, solvent, and exogenous bases should lead to conditions that form the desired N-hydroxyphthalimide derivative in high yields.

Figure 4.2 Synthesis of **4.6**

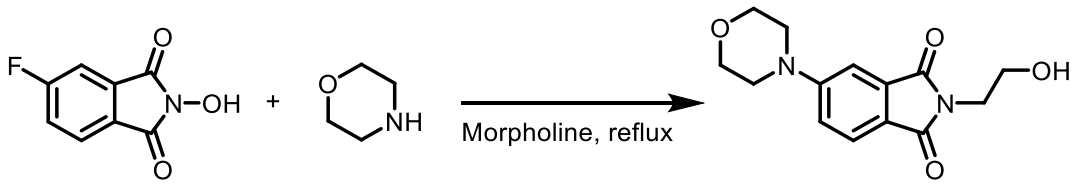

4.5 **4.6**

In addition to electron-rich N-hydroxyphthalimide derivates, I sought to investigate the reactivity of heteroaryl N-hydroxyimides. Thiophenepyrrolediones have been extensively studied in the field of organic electronics[6] so we envisioned that their synthesis could be adapted to tolerate *N*-hydroxy analogues. Initial attempts mirrored the syntheses of *N*-hydroxyphthalimide derivatives, treating 3,4-thiophenedicarboxylic acid with acetic anhydride to form the corresponding cyclic anhydride followed by imide formation with hydroxylamine. Anhydride formation proceeded smoothly, however, treatment of this anhydride with hydroxylamine led to the formation of *N*-hydroxy amide **4.9**, a common intermediate in the synthesis of thiophenepyrrolediones. Attempts at ring closure using common carboxylic acid activating reagents such as $SOCl_2$,CDI, DIC, and DCC have so far been unsuccessful. A potential alternative could be to synthesize thiophenepyrolledione then oxygenate the nitrogen atom.[7]

Figure 4.3 Synthesis of **4.9**.

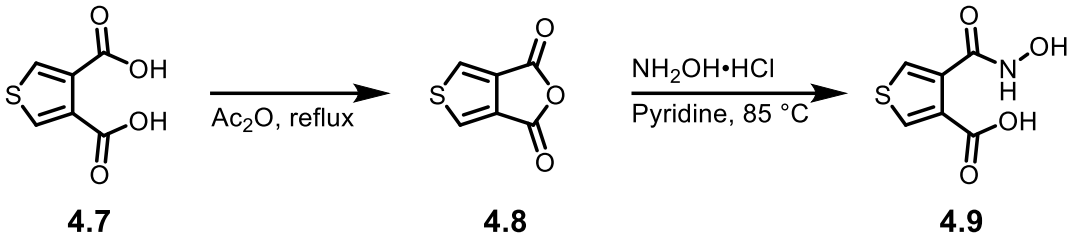

4.7 **4.8** **4.9**

4.3 Catalyst Exploration with Zinc as Reductant

In order to maximize our chances of finding a catalyst that could promote challenging oxidative additions without accelerating the rate of RAE consumption we, with the help of our collaborators at Janssen, developed an XEC catalyst screening plate. The kit was designed to include 24 N-donor ligands that are common, rare, or not used for XEC reactions that have sites which allow for tuning of ligand sterics and electronics. We sought to include representative examples of bipyridine, terpyridine, pyridyl carboxamidine, and oxazoline based ligands. From each ligand was generated the corresponding ligated $Ni^{II}Br_2$ complex, which were then dispensed in shell vials, packed in groups of 24 (see below), and shipped to Madison.

Figure 4.4 Catalyst Screening Plate Map

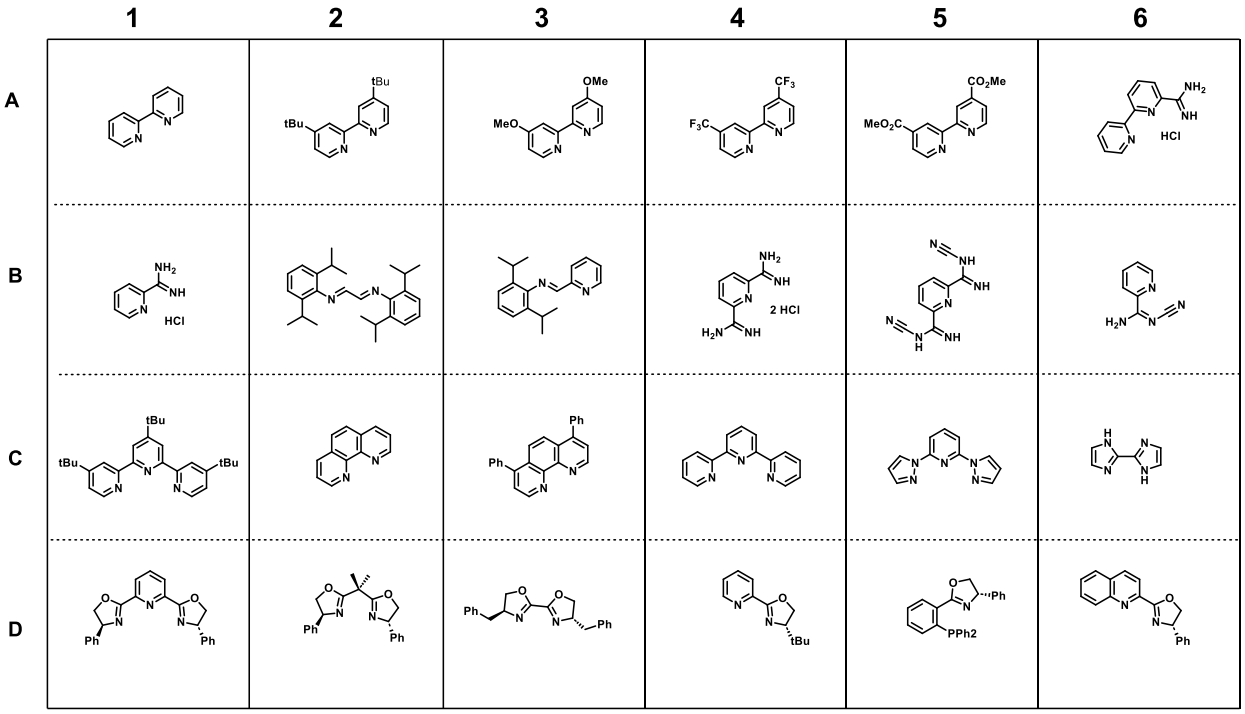

Our intention was to use these catalyst plates to quickly screen reactions between a secondary NHP ester and a variety of aryl bromides and chlorides with the hopes of finding a general ligand class that could broadly promote the reductive arylation of NHP esters. We opted for an NHP ester that generated a non-stabilized secondary radical which contained a functional group handle that can be effectively visualized via SFC-MS. Aryl halides were chosen both for their ease of visualization on our analytical instruments, a range of oxidative addition reactivity from activated aryl bromide to unactivated aryl chloride.

Figure 4.5 Strategy for Reaction Optimization

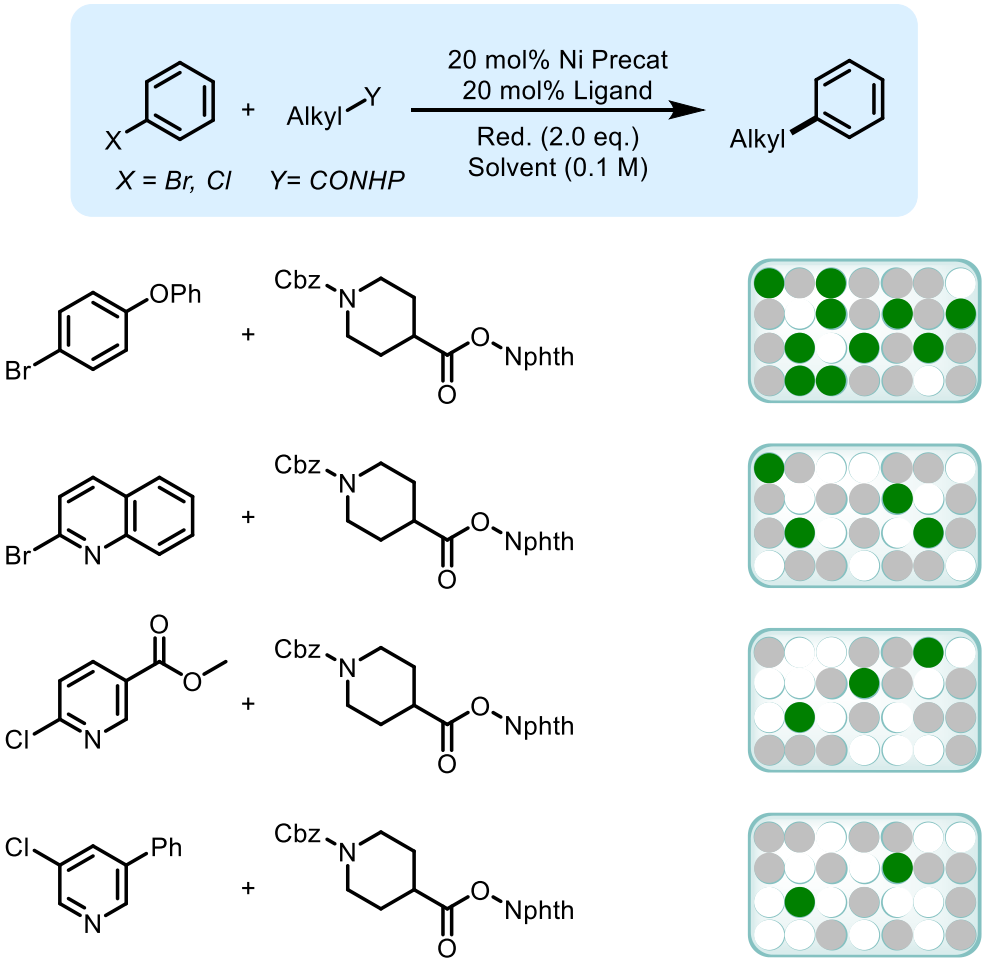

Preliminary results from catalyst screens against aryl chlorides are shown below:

Figure 4.6 Catalyst Screen with 3-chloro 5-phenylpyridine[a]

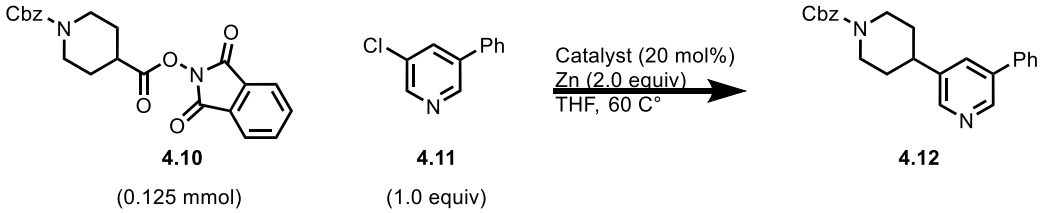

	1	2	3	4	5	6
A	 0.02	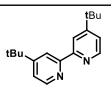 0.22	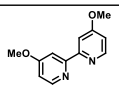 0.07	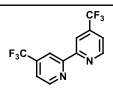 0.03	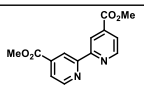 0.03	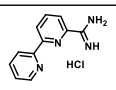 **0.45**
B	 0.10	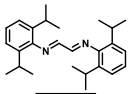 **0.31**	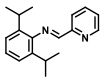 0.12	 0.08	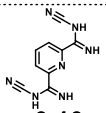 0.10	 **0.25**
C	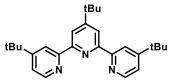 0.09	 0.00	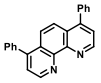 0.01	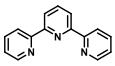 0.01	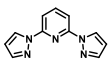 0.01	 0.02
D	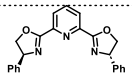 0.02	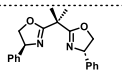 0.02	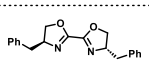 0.02	 0.02	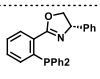 0.02	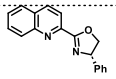 0.02

[a]Reactions run at 10 μmol scale. Assay yields are raw product/internal standards (UV) ratios vs. 5 μmol 2,4,6 trimethyl pyridine determined via SFC-MS. See experimental section for more detail.

Figure 4.7 Catalyst Screen with methyl 6-chloronicotinate[a]

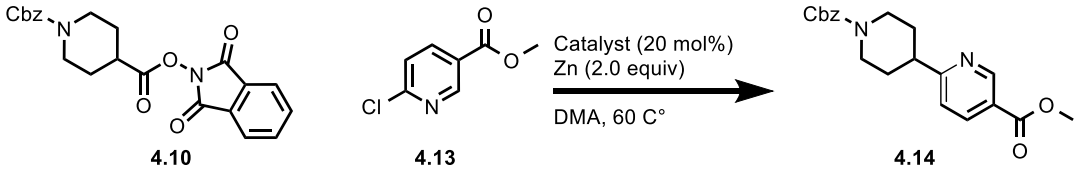

	1	2	3	4	5	6
A	6.2%	4.9%	4.3%	5.3%	5.1%	4.5%
B	6.6%	0.3%	3.4%	0.8%	0.6%	1.9%
C	4.9%	1.8%	2.4%	3.8%	4.9%	1.9%
D	4.2%	3.5%	3.5%	3.8%	2.1%	1.9%

[a]Reactions run at 10 μmol scale. Assay yields are corrected product/internal standards (UV) ratios vs. 5 μmol 2,4,6 trimethyl pyridine determined via SFC-MS. See experimental section for more detail.

Thus far, I have only performed the catalyst screen on two of the four proposed aryl halide coupling partners. For both aryl chlorides screened, bipyridine, bpyridfine carboxamidine, pyridyl carboxamidine, and imine-based ligands provide the highest product to internal standard ratio. Performing the same screen on the proposed aryl bromides will hopefully point us in the direction of a generalist ligand class and aid in the optimization of a broadly selective arylation of RAEs. Future goals include scaling up the highest yielding reactions, isolation of the cross-coupled product as well as side products, and determination of correction factors to ensure accurate reporting of reaction yields. With an optimal catalyst,

other variables such as solvent, additives, temperature, and RAE identity will be studied to determine their effect on reaction outcome.

4.4 Reaction optimization with organic reductants

Concurrent with our efforts to find a general catalyst for zinc-promoted reductive arylation of NHP esters, we sought to assess whether soluble organic reductants could be used to promote this transformation. An organic reductant could provide three distinct advantages: 1) organic reductants which reduce the nickel catalyst via an inner-sphere mechanism would avoid background reduction of the NHP ester, ensuring coupled activation of both coupling partners. 2) Organic reductants which do not form Lewis acidic salts upon oxidation would avoid autocatalytic consumption of the NHP ester and would hopefully promote a more selective reaction. 3) The use of an organic reductant would allow the reaction to become completely homogeneous, which would allow the reaction to be more easily scaled down or up. Inspired by a recent review published by Hazari and Zultanski,[8] I began investigating the utility of organic reductants for decarboxylative XEC.

Initial investigations began following a protocol developed by Reisman for the coupling of NHP esters with alkenyl bromides wherein 1,1,2,2-tetrakis(dimethylamino)ethylene (TDAE) was used as the reductant, and TMSBr and NaI were used to promote fast reactivity.[9] Reisman noted that the more benign TMSCl was not effective in this reaction as this additive would promote formation of unreactive alkenyl chlorides from the corresponding alkenyl bromide. The temperature of the reaction had little effect on the reaction outcome, likely due to reaction completion occurring prior to the reaction mixture reaching the desired elevated temperature. The reaction mixtures immediately began bubbling vigorously following the addition of TDAE and bubbling was complete by the time the reaction vials were placed in the appropriate

reaction carousels, further corroborating the rapid nature of this reaction. Exchanging the solvent for THF, which, in our previous publication was shown to slow NHP ester reactivity, did prevent the vigorous bubbling seen in reactions with DMA. We found under these conditions that both NaI and TMSBr were necessary to promote cross-coupling. Due to the instability of TDAE and the use of TMSBr we chose to forgo further optimization of these conditions and investigated alternative organic reductants.

Table 4.1 Decarboxylative XEC promoted by TDAE[a]

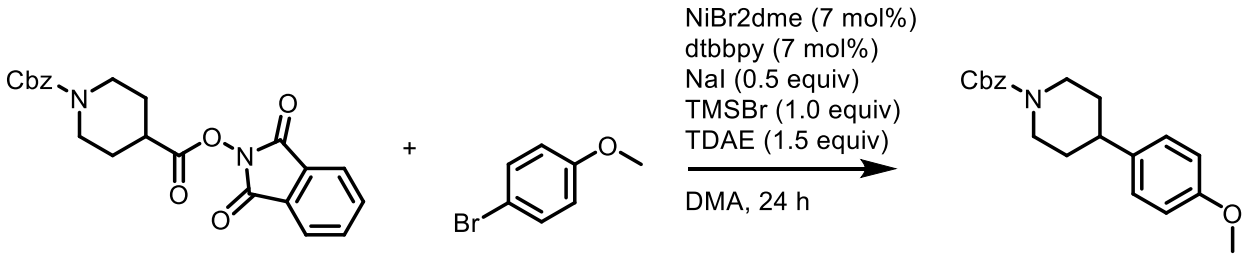

4.10 **4.15** **4.16**

Deviation	Solvent	ArBr:IS	Ar-Ar:IS	P:IS
T= 20 °C	DMA	8.8	0	7.0
T= 40 °C	DMA	8.8	0	6.3
T= 60 °C	DMA	8.5	0	6.6
T= 80 °C	DMA	8.4	0	7.1
T= 100 °C	DMA	8.2	0	7.3
No Additives	THF	12.6	0	0
NaI Only	THF	8.3	0	0
TMSBr Only	THF	3.2	4.6	6.2
None	THF	3.4	0	7.2

[a]Reactions run at 0.125 mmol scale. Assay yields are raw product/internal standards (FID) ratios vs. 10 mol% 1,3,5-trimethoxybenzene determined via GC-FID.

Work from Gong[10] and Fu[11] has shown that bis(pinacoloto)diboron (B_2pin_2) in the presence of a nucleophilic base is capable of turning over nickel catalysts in XEC reactions. This is proposed to proceed through formation of a boronate complex, which can undergo transmetallation onto the nickel catalyst followed by reductive elimination to form X-BPin and a reduced nickel species. The mechanism proposed by Gong is shown below:

Figure 4.8 Proposed mechanism for XEC with B_2Pin_2 as reductant.

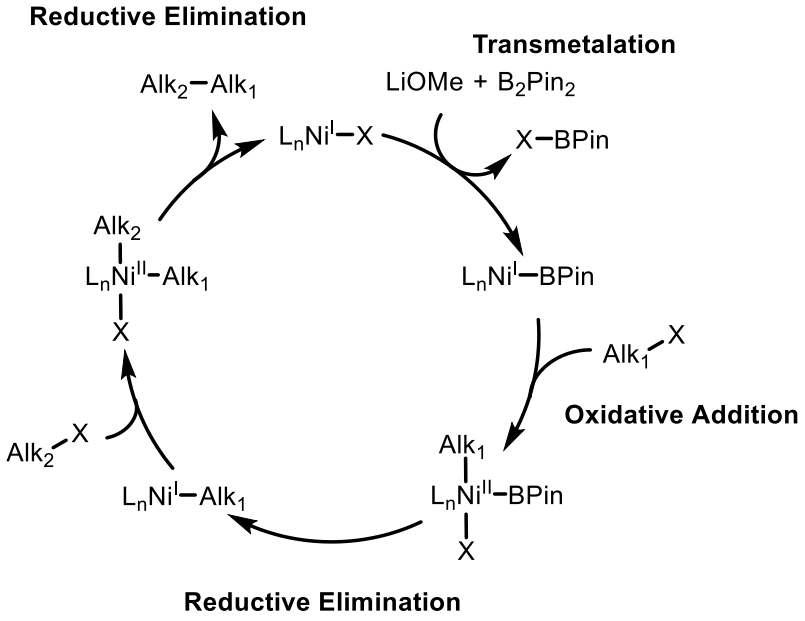

Typically, alkoxide bases are used promote reduction of nickel species by B_2Pin_2, however such unhindered nucleophilic bases could prove problematic for reactions with NHP esters as the combination would lead to transesterification to form the methyl ester. Because of this apparent base/reactant incompatibility, I set out to find a base that could promote reduction of the nickel catalyst without degradation of the NHP ester. Most of the bases screened proved to be ineffective except for potassium carbonate, and inorganic fluoride sources like potassium fluoride and cesium fluoride. I decided to perform further studies with

potassium carbonate as its relatively low cost would make it a desirable base to use for future, larger scale reactions.

Table 4.2 Base Screen.[a]

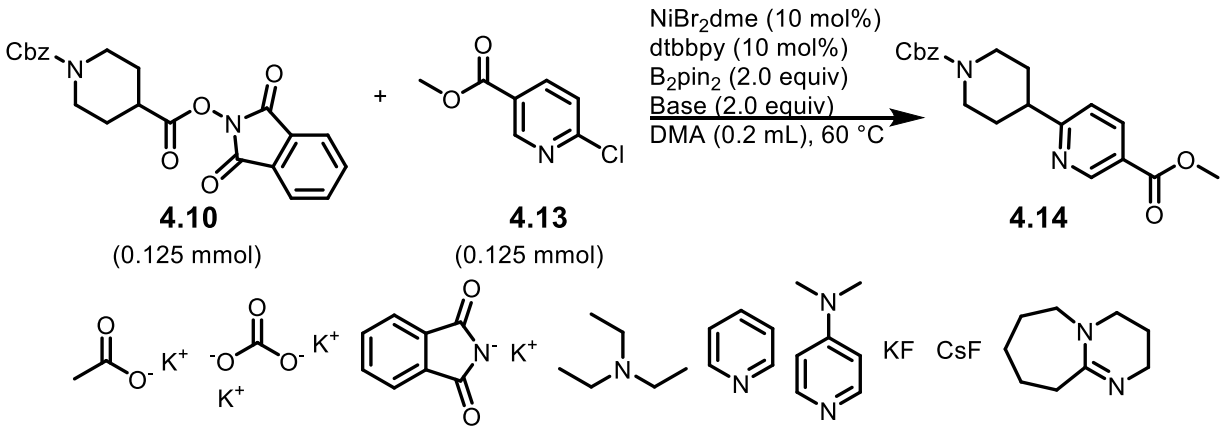

Base	Product	Ar-Ar	Ar-H	Alk-H	Alk-Alk	NHP ester	Ar-Cl
KOAc	0.00	0.00	0.00	0.00	0.00	0.40	2.90
K_2CO_3	0.02	0.09	0.03	0.00	0.00	0.16	2.15
KNphth	0.00	0.00	0.00	0.00	0.00	0.76	2.13
Et_3N	0.00	0.00	0.00	0.00	0.00	0.54	2.22
Pyridine	0.00	0.00	0.00	0.00	0.00	0.55	2.46
DMAP	0.00	0.00	0.00	0.00	0.00	0.44	2.08
KF	0.01	0.10	0.00	0.00	0.00	0.00	2.71
CsF	0.02	0.01	0.00	0.00	0.00	0.00	1.65
DBU	0.00	0.00	0.00	0.00	0.00	0.00	1.98

[a]Reactions run at 0.125 mmol scale. Assay yields are raw product/internal standards (UV) ratios vs. 50 mol% 2,4,6 trimethyl pyridine determined via SFC-MS. See experimental section for more detail.

With a base/reductant system compatible with the reactants, I then performed a ligand screen with these conditions. Because the mechanism for reduction of nickel is different under these conditions than in reactions promoted by zinc, I envisioned two outcomes of this screen: 1) the best ligands would remain the same as in **Figure 4.7** regardless of reductant, suggesting that the nickel species is predominantly reducing the NHP ester or 2) there would be little to

no overlap between the best ligands in this screen and the best ligands seen in **Figure 4.7**, suggesting that zinc is predominantly reducing the NHP ester under the conditions shown in **Figure 4.7** while a nickel species is reducing the NHP ester in **Figure 4.9**.

Figure 4.9 Catalyst Screen with K_2CO_3/B_2Pin_2 as Reductant.[a]

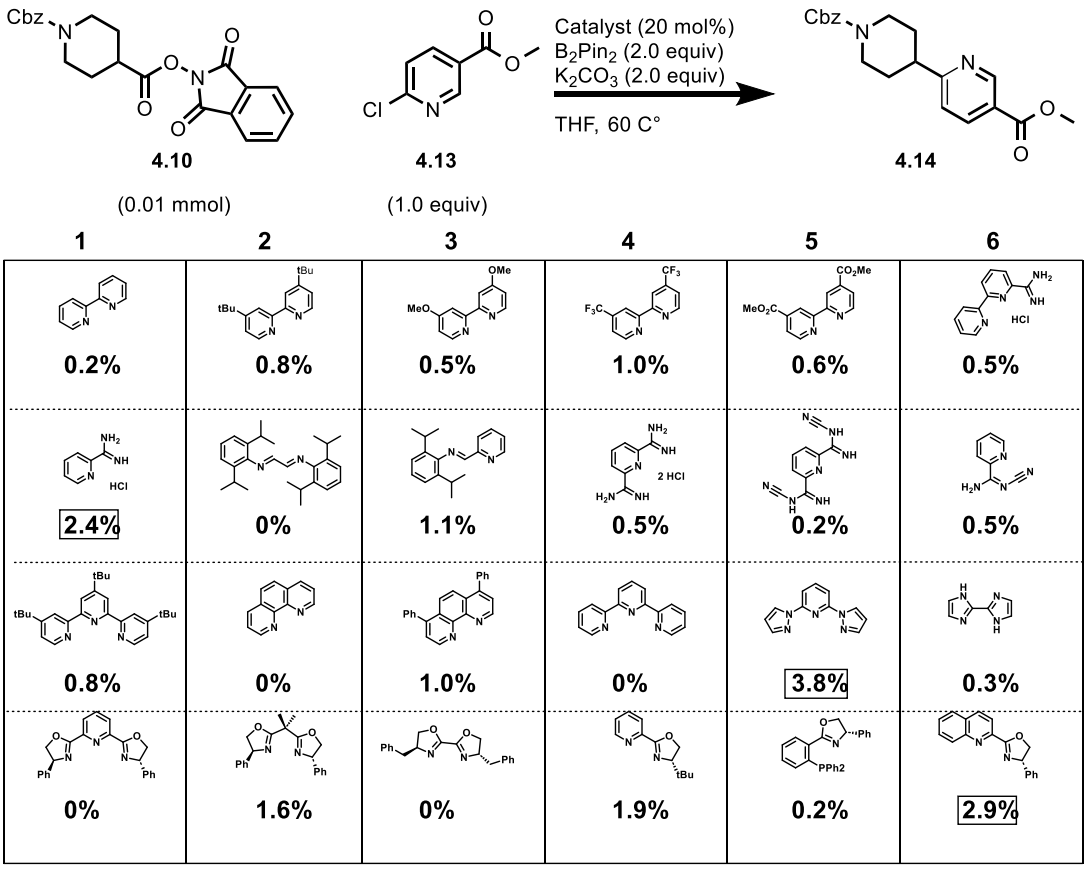

[a]Reactions run at 10 μmol scale. Assay yields are corrected product/internal standards (UV) ratios vs. 5 μmol 2,4,6 trimethyl pyridine determined via SFC-MS. See experimental section for more detail.

Interestingly, there was some overlap in catalysts that were effective with both Zn and B_2Pin_2 as reductants with bispyrazolopyridine and pyridyl carboxamidine being effective under both conditions. Though these results were promising, our goal of achieving a fully homogeneous reaction amenable to smaller and larger scale reactions has not been achieved as K_2CO_3 is insoluble under the reaction conditions. To achieve this goal, I reevaluated the base

used in this reaction, this time screening the bases against some of the top ligands found in **Figure 4.9** in the event that I found some base/ligand complementarity. In this screen I investigated DABCO, more soluble fluoride sources such as tetraalkylammonium fluoride salts, a sterically hindered phenolate to hopefully disfavor transesterification, as well as a phosphazene base and ammonium carbonate.

Figure 4.10 Ligand and Soluble Base Screen.[a]

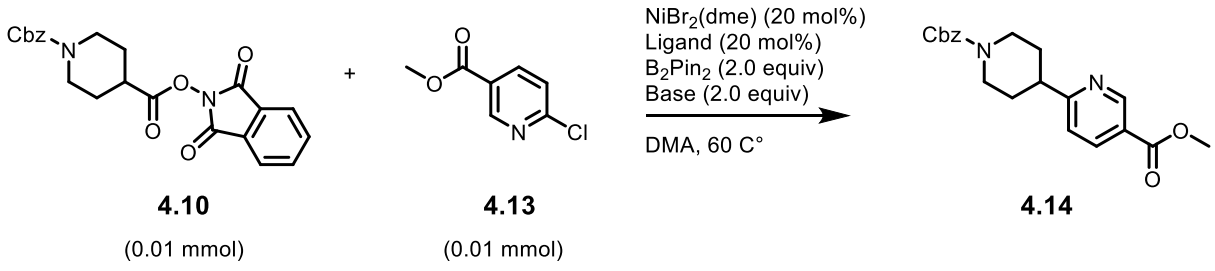

	0%	0.8%	2.1%	0	0	0
HCl	0.6%	1.1%	0.6%	0	0	0
	2.4%	1.0%	5.6%	0	0	0
Ph	0%	0.6%	1.9%	0	0	0

[a] Reactions run at 10 μmol scale. Assay yields are corrected product/internal standards (UV) ratios vs. 5 μmol 2,4,6 trimethyl pyridine determined via SFC-MS. See experimental section for more detail.

Tetraalkylammonium fluorides promoted the reaction regardless of which ligand was employed, DABCO was only successful with 2/4 ligands chosen, and the other bases were not effective at promoting the reaction. The sterically hindered phenolate still promoted transesterification, suggesting that further tuning of alkoxide/phenoxide bases would be needed in order for them to be compatible with this reaction. Future work on this front will entail validating these reactions on larger scale and, with the help of our collaborators at Janssen, adapting these conditions to higher density plate formats to facilitate in rapid optimization and exploration of the scope of this reaction.

Our ultimate goal is to be able to couple redox-active esters with any aryl halide, but even a system that can provide reliable, high yields in cross-couplings with electron rich aryl bromides without the need for electrochemical or photochemical setups would be an advance. A fully homogeneous reaction system would allow us to both optimize the reaction and explore the scope using 1536 well plates. Knowledge gained from this effort could help enable future work towards coupling redox-active esters with phenol derivatives, further expanding the chemical space accessible by decarboxylative cross-couplings.

4.5 Experimental

4.5.1 Reagents

Metals

All metal catalysts and metal reductants, unless otherwise noted, were stored and handled in a nitrogen-filled glovebox. Nickel(II) bromide ethylene glycol dimethyl ether complex ($NiBr_2$(dme)) was purchased from Millipore Sigma and used as received. The reductant used was zinc flake, -325 mesh, 97% (Alfa Aesar). We observed no difference in reactivity between zinc flake and zinc dust.

Ligands

Pyridyl carboxamidine ligands were synthesized according to literature procedures. All other ligands were purchased from commercial suppliers and used without purification.

Substrates

All carboxylic acids were purchased from commercial suppliers and used without purification.

Solvents

Tetrahydrofuran (THF) and dichloromethane (DCM) were purified by passage though activated alumina and molecular sieves in a solvent purification system (Inert Corporation) and stored in a nitrogen-filled glovebox. Anhydrous dimethylacetamide (DMA) was purchased from Millipore Sigma, stored in a glovebox, and used as received.

Other Reagents

All starting materials were purchased from commercial suppliers and used without purification unless otherwise indicated.

4.5.2 Methods

NMR Spectroscopy

^{1}H and ^{13}C-NMR spectra were acquired on a 500 MHz Avance spectrometer equipped with a DCH cryoprobe (Bruker), at a sample temperature of 25 °C. NMR spectra were recorded with TopSpin 3.5.6 (Bruker).

Referencing and absolute referencing to TMS, apodization, Fourier transform, phase and baseline corrections, and spectral analyses were carried out with MestReNova 12.0.4 (Mestrelab Research). NMR chemical shifts are reported in ppm and are referenced to TMS (δ = 0.00 ppm). Coupling constants (J) are reported in Hz.

Gas Chromatography (GC)

GC analyses were performed on an Agilent 7890A GC equipped with dual DB-5 columns (20 m × 180 µm × 0.18 µm), dual FID detectors, and hydrogen as the carrier gas. A sample volume of 1 µL was injected at a temperature of 300 °C and a 100:1 split ratio. The initial inlet pressure was 20.3 psi but varied as the column flow was held constant at 1.8 mL/min for the duration of the run. The initial oven temperature of 50 °C was held for 0.46 min followed by a temperature ramp of 65 °C/min up to 300 °C. The total run time was 5.0 min and the FID temperature was 325 °C.

GC/MS Analysis

GC/MS analyses were performed on a Shimadzu GCMS-QP2010 equipped with an RTX-5MS column (30 m × 0.25 mm × 0.25 μm) with a quadrupole mass analyzer using helium as the carrier gas or with an Agilent 5977A GC/MSD using MassWorkds 4.0 from CERNO bioscience. The analysis method used in all cases was 1 μL injection of sample, an injection temp of 250 °C, and a 20:1 split ratio. The initial inlet pressure was 8.1 psi, but varied as the column flow was held constant at 1.0 mL/min for the duration of the run. The interface temperature was held at 275 °C, and the ion source (EI^+, 30 eV) was held at 200 °C. The initial oven temperature was held at 60 °C for 1 min with the detector off, followed by a temperature ramp, with the detector on, to 300 °C at 20 °C/min. Total run time was 13.00 min.

Supercritical Fluid Chromatography Mass Spectrometry (SFC/MS)

SFC/MS analyses were performed on a Waters ACQUITY UPC^2 equipped with ACQUITY UPC^2 PDA and ACQUITY QDa Detector. A Daicel Dcpack SFC-A column (3 mm ID × 150 mm L, 3 μm PS) was used for separations. The eluent was a mixture (97:3 CO_2/MeOH) with a flow rate of 2 mL/min at 40 °C with a ABPR at 1500 psi. We are grateful to Joe Barendt and Chiral Technologies for the donation of the SFC-A column used in this work.

Chromatography

Chromatography was performed on silica gel (EMD, silica gel 60, particle size 0.040-0.063 mm) using standard flash techniques, on a Teledyne Isco CombiFlash instrument using pre-packaged cartidges, on a Teledyne Isco Rf-200 (detection at 210 nm and 280 nm), or on a Biotage Isolera One (detection at 210 nm and 400 nm, on Sfar Duo columns). Products were visualized by UV, PMA stain, or fractions were analyzed by GC. Purifications using an HPLC were performed using a Teledyne ACCQ Prep HPLC system using an XBridge C18 column (5

μm, 100×50 mm), mobile phase of 5-100% ACN in 20 mM NH4OH over 17 min and then hold at 100% ACN for 3 min, at a flow rate of 80 mL/min.

Elemental Analysis

Elemental analyses were performed by CENTC Elemental Analysis Facility at University of Rochester, funded by NSF CHE-0650456.

High Resolution Mass Spectrometry

UW-Madison: High resolution mass spectra (HRMS) Mass spectrometry data was collected on a Thermo Q Exactive™ Plus (thermofisher.com) via flow injection with electrosprayionization or via ASAPMS™ (asap -ms.com) by the chemistry mass spectrometry facility at the University of Wisconsin – Madison. The purchase of the Thermo Q Exactive Plus in 2015 was funded by NIH Award 1S10 OD020022 to the Department of Chemistry

4.5.3 General Procedures

4.5.3.1 General Procedure A: Synthesis of NHP Esters Using DIC.

To a round-bottom flask charged with a magnetic stir bar was added carboxylic acid (1.0 equiv), *N*-hydroxyphthalimide (1.0 equiv), *N,N*-dimethylaminopyridine (DMAP) (0.1 equiv), and dichloromethane (resulting in a solution 0.1 M in carboxylic acid). To this solution was added *N,N*-diisopropylcarbodiimide (DIC) (1.1 equiv) and the flask was capped with a rubber septum affixed with a vent needle. The resulting mixture was allowed to stir for at rt (20-22 °C)18 h. After this time, the reaction mixture was then filtered through a short pad of silica gel into a round bottom flask. The silica gel was rinsed with additional dichloromethane (~50 mL) into the flask. The solvent was removed under reduced pressure on a rotary evaporator. The crude material was recrystallized from hot methanol to afford the pure NHP ester.

4.5.3.2 General Procedure B: Decarboxylative Cross-Electrophile Coupling

Reactions were set up in a N_2 filled glove box. A catalyst solution was prepared by sequentially charging an oven dried scintillation vial with a PTFE-coated stirbar, $NiBr_2$(dme) (7.2 mg, 0.025 mmol, 20 mol%) and ligand (0.025 mmol, 20 mol%). The solids were dissolved in DMA (0.2 mL) and the contents were stirred for 30 min, resulting in a homogeneous solution. A separate oven-dried 1-dram vial with a PTFE-coated stirbar was charged with NHP ester (0.125 mmol, 1.0 equiv), aryl halide (0.125 mmol, 1.0 equiv), reductant (0.25 mmol, 2.0 equiv) internal standard. To the vial containing NHP ester, aryl halide, and reductant was added 0.2 mL of the prepared catalyst solution. The reactions were sealed with a screw cap fitted with a PTFE-faced silicone septum before being removed from the glovebox. The contents of the reaction vessel were stirred (1200 RPM) at r.t. (20-22 °C) for 24 h.

GC Analysis (modified below)

The reactions were monitored by GC analysis. Samples were prepared by the removal of a 25 μL aliquot of the crude reaction mixture with a gas-tight syringe. The aliquot was diluted with EtOAc (1.00 mL), then the resulting solution was filtered through a 2-cm celite plug in a Pasteur pipette into a 2 mL GC vial. The resulting solution was analyzed by GC and yields were determined based on the peak area of the analyte compared to 1,3,5-trimethoxybenzene as an internal standard.

SFC-MS Analysis

The reactions were monitored by GC analysis. Samples were prepared by the removal of a 25 μL aliquot of the crude reaction mixture with a gas-tight syringe. The aliquot was diluted with EtOAc (1.00 mL), then the resulting solution was filtered through a 2-cm celite plug in a Pasteur pipette into a 2 mL GC vial. The resulting solution was analyzed by GC and yields were

determined based on the peak area of the analyte compared to 2,4,6-trimethylpyridine as an internal standard.

4.5.4 High Throughput Experimentation (HTE) Screening

4.5.4.1 HTE screening of Strained-ring NHP esters with the Merck Informer Library

Catalyst Stock Solutions

Stock solutions of catalyst for HTE screening were prepared in a N_2-filled glovebox in separate dram vials. An oven dried dram vial equipped with a PTFE-coated stir bar was sequentially charged with $NiBr_2$(dme, ligand, and THF (0.75 mL). The vial was capped with a PTFE-coated screw cap and the contents stirred at rt for 30 min to afford a (0.067 M) catalyst stock solution.

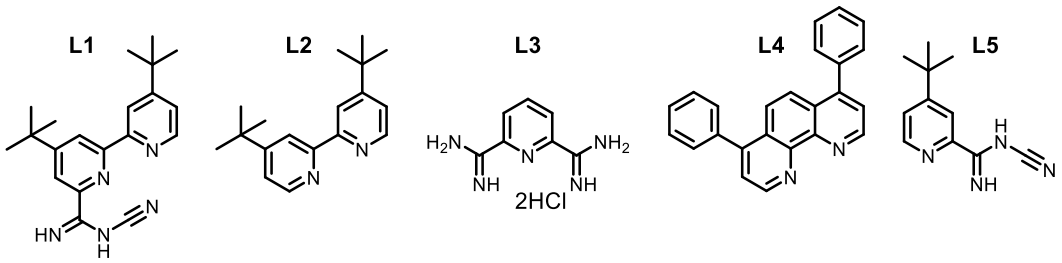

Solution 1: $NiBr_2$dme (14.6 mg, 0.05 mmol, 0.2 equiv), ^{tbu}bpyCAM^{CN} (**L1** 16.8 mg, 0.05 mmol, 0.2 equiv)

Solution 2: $NiBr_2$dme (14.6 mg, 0.05 mmol, 0.2 equiv) and dtbbpy (**L2** 13.4 mg, 0.05 mmol, 0.2 equiv).

Solution 3: $NiBr_2$dme (14.6 mg, 0.05 mmol, 0.2 equiv) and bathophenanthroline (**L3** 16.6 mg, 0.05 mmol, 0.2 equiv).

Solution 4: $NiBr_2$dme (14.6 mg, 0.05 mmol, 0.2 equiv) and Pyridine-2,6-bis(carboximidamide) dihydrochloride (**L4** 11.8 mg, 0.05 mmol, 0.2 equiv).

Solution 5: $NiBr_2$dme (14.6 mg, 0.05 mmol, 0.2 equiv) and 4-(tert-butyl)-N-cyanopicolinimidamide (**L5** 10.1 mg, 0.05 mmol, 0.2 equiv).

Stock Solutions of NHP Esters

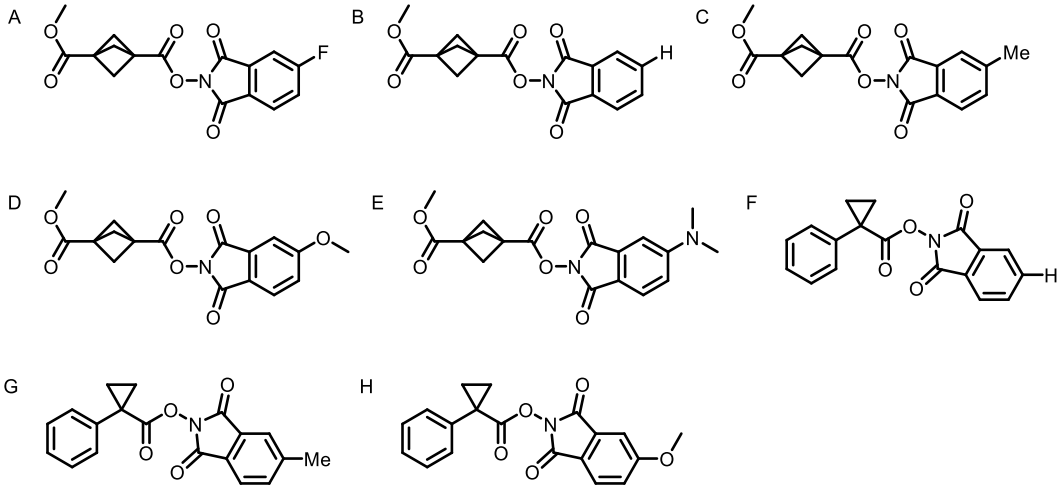

Note: Due to the poor solubility of these NHP esters in THF, the prepared stock solutions were made more dilute than the standard reaction conditions to afford homogeneous solutions. Eight NHP esters were chosen for high-throughput screening. Stock solutions of NHP esters **A-E**, sufficient for 10 reactions at a 0.01 mmol scale, were prepared in a N_2-filled glovebox by weighing each NHP ester (0.1 mmol) into a dram vial followed by addition of anhydrous THF (0.9 mL), before sealing the vial with a PTFE-lined cap and briefly shaking the mixture by hand for 30 seconds. Stock solutions of

NHP esters **F-H**, sufficient for 25 reactions at a 0.01 mmol scale, were prepared in a N_2-filled glovebox by weighing each NHP ester (0.25 mmol) into a dram vial followed by addition of anhydrous THF (2.25 mL), before sealing the vial with a PTFE-lined cap and briefly shaking the mixture by hand for 30 seconds. Stock solutions were prepared immediately prior to use in HTE screening studies.

Stock Solutions of Aryl Bromides

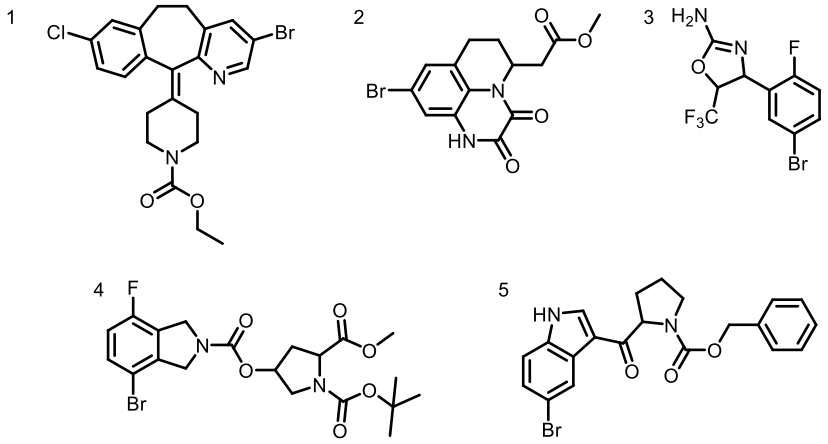

Note: Due to the poor solubility of these aryl bromides esters in THF, the prepared stock solutions were made more dilute than the standard reaction conditions to afford homogeneous solutions Five aryl bromide cores were chosen for high-throughput screening. In a N_2-filled glovebox, a stock solution of aryl bromide **1**, sufficient for 30 reactions at a 0.01 mmol scale, was prepared by weighing aryl bromide **1** (0.3 mmol) into a dram vial followed by the addition of anhydrous THF (3.6 mL). Stock solutions of aryl bromides **2-**5, sufficient for 20 reactions at a 0.01 mmol scale were prepared by weighing each aryl bromide (0.2 mmol) into a dram vial before addition of anhydrous

THF (2.4 mL) and briefly shaking the mixture by hand for 30 seconds until completely homogenous.

Preparation of Zinc-Coated ChemBeads

Zinc-coated ChemBeads (5% w/w) were prepared following a literature procedure. In a N_2-filled glovebox, to a 20-mL scintillation vial was charged 22.8 g of glass ChemBeads and 1.2 g (9.1 mmol) Zn. The vial was sealed, then removed from the glovebox. The vial was placed on a conical vortex mixer and agitated for 30 minutes to ensure even coating of the beads.

Preparation of Internal Standard Stock Solution

In a N_2-filled glovebox, an oven dried dram vial was sequentially charged with1,3,5-trimethoxybenzene (201.8 mg, 1.2 mmol) and THF (1.8 mL). The vial was capped with a PTFE-coated screw cap and the vial was shaken by hand for 30 seconds, resulting in a homogeneous solution

General Procedure for HTE Screening

All operations were performed in a N_2-filled glovebox. To each well of a 96-well (8 rows by 12 columns) aluminium block assembly equipped with 8 × 30 mm vials was dosed 30 mg of Zn-coated ChemBeads (5% loading wt/wt) using a calibrated scoop and a non-static funnel (Image 2). NHP Ester and aryl bromide substrates were dosed into each well by first transferring stock solutions of each NHP ester and aryl bromide into separate channels of eight-channel polypropylene deep-well reservoirs followed by transferring 90 µL of each NHP ester stock solution to their respective wells (Image 3) and 60 µL of each aryl bromide stock solutions to

their respective wells (Image 3) using a multi-channel pipette. To each well was added 15 µL of a stock solution of trimethoxybenzene internal standard (1.68 mg, 0.01 mmol, 1 equiv) in acetonitrile and 30 uL of a stock solution of catalyst (Image 3). The well-plate vials were sealed with an electric screwdriver at torque setting 6 in a diagonal pattern (Image 4), using an aluminum lid, and the block was placed onto a heater/shaker (Torrey Pines Echotherm) set at 60 °C (actual temperature was found to be ~20 °C lower) and orbital speed at 8 to heat/shake overnight for 36 h (Image 5).

	Col 1	Col 2	Col 3	Col 4	Col 5	Col 6	Col 7	Col 8	Col 9	Col 10	Col 11	Col 12
Row 1	A,1	A,1	A,1	A,1	A,1	F,4	F,4	F,4	F,4	F,4	H,2	x
Row 2	B,1	B,1	B,1	B,1	B,1	G,4	G,4	G,4	G,4	G,4	H,2	x
Row 3	C,1	C,1	C,1	C,1	C,1	H,4	H,4	H,4	H,4	H,4	H,2	x
Row 4	D,1	D,1	D,1	D,1	D,1	F,2	F,2	F,2	F,2	F,2	H,2	x
Row 5	E,1	E,1	E,1	E,1	E,1	G,2	G,2	G,2	G,2	G,2	H,2	x
Row 6	F,5	F,5	F,5	F,5	F,5	F,3	F,3	F,3	F,3	F,3	x	x
Row 7	G,5	G,5	G,5	G,5	G,5	G,3	G,3	G,3	G,3	G,3	x	x
Row 8	G,5	G,5	G,5	G,5	G,5	H,3	H,3	H,3	H,3	H,3	x	x

L1
L2
L3
L4
L5

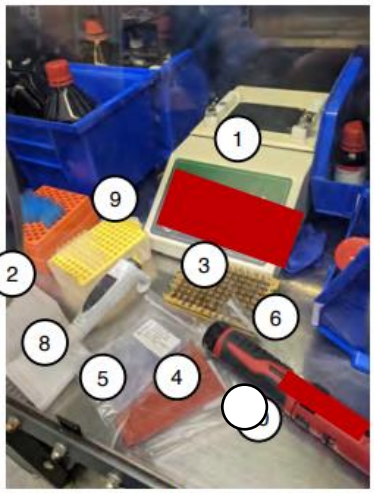

Image 1. HTE Equipment with prepared NHP ester and aryl bromide stock

Setup Parts (SKU#)

1. Torrey Pines Ectotherm Shaker/Heater
2. 8-Channel Deep Well Reservoir (32008)
3. Paradox 96-Well Photoredox Block Assembly (96973) loaded with 8×30mm shell vials (884001)
4. Rubber mat (96965)
5. Plastic film linings (96967)
6. Abbvie calibrated ChemBead scoops
7. Non-static funnel
8. Sartorius Picus electronic 8-channel pipette, 5 – 120 µL
9. Sartorius 0.5 – 200 µL pre-sterilized Optifit Tips (790200)
10. Milwaukee cordless screwdriver (2101-21)

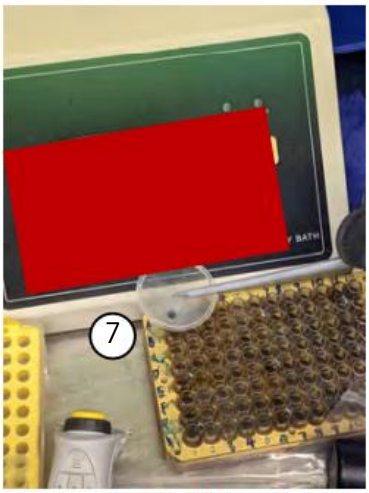

Image 2. Addition of zinc-coated ChemBeads

Image 3. Addition of stock solutions

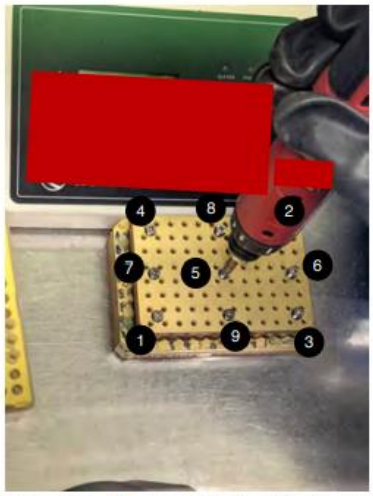

Image 4. Sealing plate in the pattern shown at torque setting of 6.

Image 5. Heating/shaking the block assembly in a glovebox for 36 hours.

Workup and Analysis

The reaction block was removed from the shaker apparatus and allowed to cool to rt. The aluminum lid was removed, then each well was treated with an ammonia solution in MeOH (100 uL) via multi-channel autopipette. The vials were re-sealed and the reaction block was placed back on the shaker for 30 minutes. The aluminum block was then removed from the glovebox, the lid was removed, and 100 µL of MeOH was added to each well to dilute the reaction mixtures. 300 µL aliquots were taken from each well and were then filtered through a 0.2 µm filter plate into a 340 µL 96-well collection plate (Images 6 and 7). The plate was then analyzed by SFC-MS.

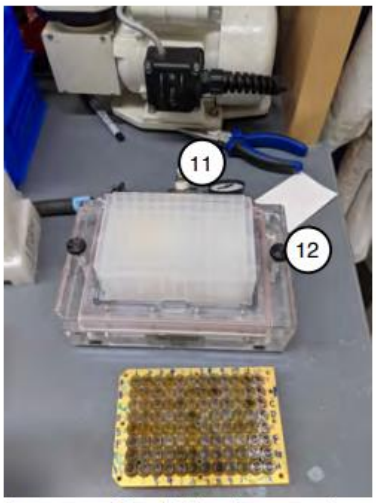

Image 6. Filtration setup into a 96-well collection plate.

Image 7. Finished Plate sealed with a round well cap mat for SFC-MS analysis

Workup Parts (SKU#)

11. 2mL Hydrophilic filter plate, 0.2µm polypropylene membrane (96222-10)
12. Vacuum manifold filtration system (96844)
13. 340µL 96-well collection plate with V-shaped well bottoms and SiliGuard low binding coating (96340GC) with clear adhesive sealing film (Analytical Sales 961802)

d

Figure 4.11 HTE optimization for the coupling of BCP RAEs with Loratidine.

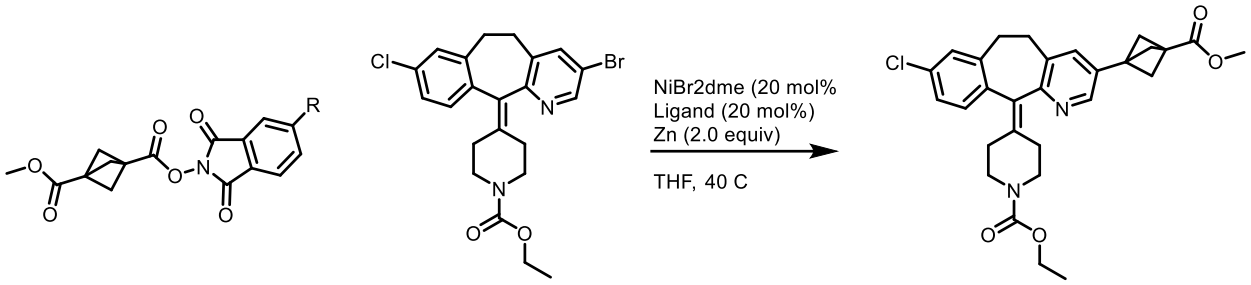

	^{TBU}BPYCAM^{CN}	DTBBPY	PYBCAM	BPHEN	PYCAM
R=F	**0.84**	**0.76**	**1.16**	**0.19**	**1.30**
R=H	**3.18**	**1.06**	**1.93**	**0.65**	**1.96**
R=ME	**0.69**	**0.42**	**1.16**	**2.27**	**5.01**
R=OME	**0.25**	**1.71**	**1.51**	**0.98**	**1.58**
R=NME_2	**1.16**	**1.61**	**0.52**	**0.55**	**1.17**

Product/Internal standard ratios (UV) vs 100 mol% 1,3,5-trimethoxybenzene. Ratios determined by SFC-MS

Figure 4.12 HTE optimization for the coupling of Merck Informer X5

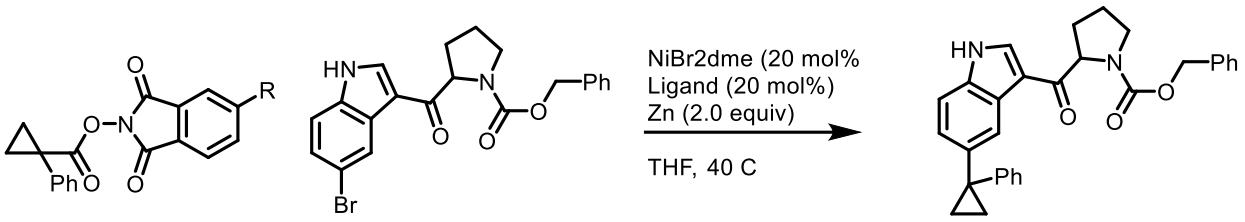

	^{tBu}BPYCAM^{CN}	DTBBPY	PYBCAM	BPHEN	PYCAM
R=H	7.96	0.82	2.06	0.30	0.46
R=ME	10.27	0.14	2.05	0.61	0.85
R=OME	0.63	0.36	0.42	0.39	0.40

Product/Internal standard ratios (UV) vs 100 mol% 1,3,5-trimethoxybenzene. Ratios determined by SFC-MS

Figure 4.13 HTE optimization for the coupling of Merck Informer X4

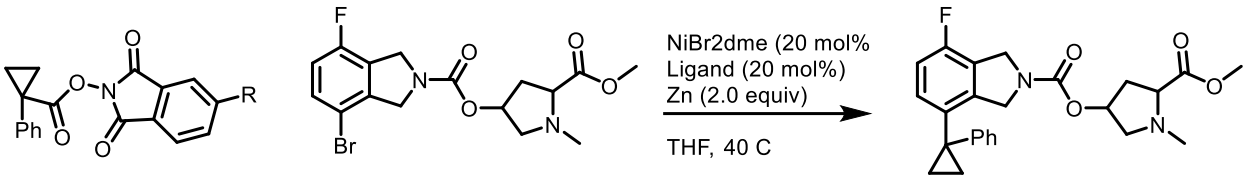

	^{tBu}BPYCAM^{CN}	DTBBPY	PYBCAM	BPHEN	PYCAM
R=H	0.02	0.01	0.01	0.12	0.03
R=ME	0	0.06	0.02	0.06	0.04
R=OME	0.15	0.31	0.02	0.02	0

Product/Internal standard ratios (UV) vs 100 mol% 1,3,5-trimethoxybenzene. Ratios determined by SFC-MS

Figure 4.14 HTE optimization for the coupling of Merck Informer X1

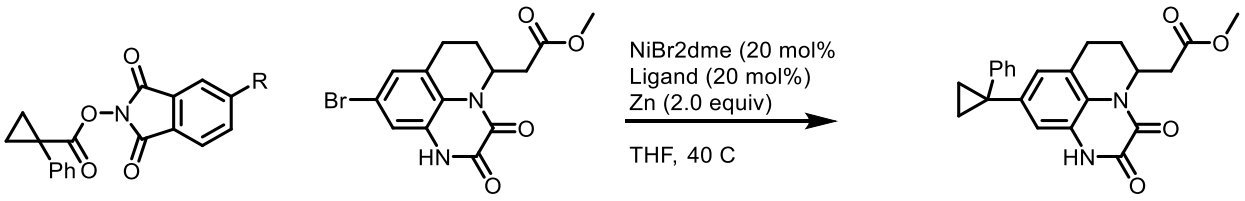

	^{TBU}BPYCAM^{CN}	DTBBPY	PYBCAM	BPHEN	PYCAM
R=H	0	2.25	3.79	0.68	2.40
R=ME	0	0	4.64	6.43	4.60
R=OME	0	0	0.94	0	2.45

Product/Internal standard ratios (UV) vs 100 mol% 1,3,5-trimethoxybenzene. Ratios determined by SFC-MS

Figure 4.15 HTE optimization.

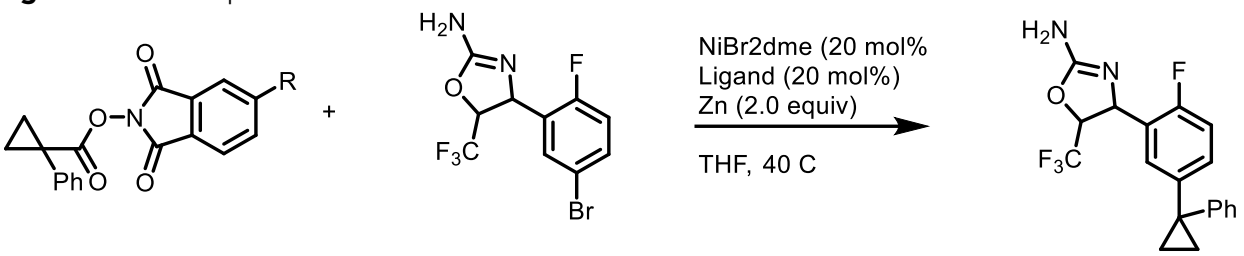

	^{TBU}BPYCAM^{CN}	DTBBPY	PYBCAM	BPHEN	PYCAM
R=H	0.42	0.08	0.17	0.53	0.08
R=ME	0	0.91	0.84	1.18	0.26
R=OME	3.35	0	2.68	0.48	0.93

Product/Internal standard ratios (UV) vs 100 mol% 1,3,5-trimethoxybenzene. Ratios determined by SFC-MS

4.5.4.2 HTE screening using Janssen Catalyst Plates

Preparation of Stock Solutions

Stock solutions of NHP ester, aryl halide, and B_2Pin_2 (when relevant), were prepared as 0.3 M solutions in the reaction solvent, either DMA or THF.

Preparation of Zinc-Coated ChemBeads

Zinc-coated ChemBeads (5% w/w) were prepared following a literature procedure. In a N_2-filled glovebox, to a 20-mL scintillation vial was charged 22.8 g of glass ChemBeads and 1.2 g (9.1 mmol) Zn. The vial was sealed, then removed from the glovebox. The vial was placed on a conical vortex mixer and agitated for 30 minutes to ensure even coating of the beads.

Preparation of K_2CO_3-Coated ChemBeads

K_2CO_3-coated ChemBeads (5% w/w) were prepared following a literature procedure. In a N_2-filled glovebox, to a 20-mL scintillation vial was charged 10 g of glass ChemBeads and 0.5 g (3.6 mmol) K_2CO_3. The vial was sealed, then removed from the glovebox. The vial was placed on a conical vortex mixer and agitated for 30 minutes to ensure even coating of the beads.

General Procedure for HTE Screening using catalyst plates (Zn)

All operations were performed in a N_2-filled glovebox. To each well of a 24-well (4 rows by 6 columns) aluminium block assembly equipped with 8 × 30 mm vials was dosed 30 mg of Zn-coated ChemBeads (5% loading wt/wt) using a calibrated scoop and a non-static funnel (Image 2). The NHP esters and aryl bromide were dosed into each well by first transferring stock solutions of each NHP ester and aryl bromide into separate channels of eight-channel polypropylene deep-well reservoirs followed by transferring 30 µL of each NHP ester stock solution to their respective wells and 30 µL of the aryl bromide stock solutions to each well using a multi-channel pipette. The well-plate vials were sealed with an electric screwdriver at torque setting 6 in a diagonal pattern (Image 4), using an aluminum lid, and the block was placed onto a heater/shaker (Torrey Pines Echotherm) set at 80 °C (actual temperature was found to be ~20 °C lower) and orbital speed at 8 to heat/shake overnight for 24 h.

Workup and Analysis

The reaction block was removed from the shaker apparatus and allowed to cool to rt. The aluminum block was then removed from the glovebox, the lid was removed, and 250 µL of MeOH was added to each well to dilute the reaction mixtures. 300 µL aliquots were taken from

each well and were then filtered through a 0.2 μm filter plate into a 340 μL 96-well collection plate. The plate was then analyzed by SFC-MS.

Figure 4.16 Reaction data from Figure 4.3

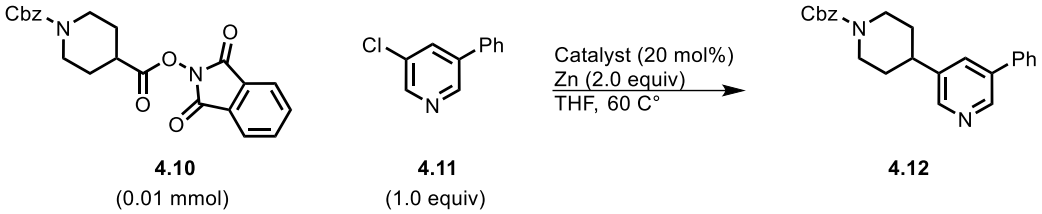

4.10 (0.01 mmol) **4.11** (1.0 equiv) **4.12**

POSITION	PRODUCT	AR-CL	AR-H	AR-AR	ALK-ALK	ALK-H	NHP ESTER
A1	0.02	10.60	0.12	0.00	0.00	0.00	0.56
A2	0.22	6.87	5.56	0.00	0.00	0.00	0.50
A3	0.07	5.08	0.08	0.00	0.00	0.00	0.71
A4	0.03	7.39	0.04	0.00	0.04	0.00	0.14
A5	0.06	11.23	0.39	0.00	0.08	0.00	0.19
A6	0.45	9.33	0.12	0.00	0.00	0.00	0.66
B1	0.10	7.13	0.48	0.00	0.00	0.00	1.17
B2	0.31	8.11	1.68	0.00	0.00	0.00	0.69
B3	0.12	8.93	0.17	0.00	0.00	0.00	0.51
B4	0.08	8.58	0.00	0.00	0.00	0.00	0.50
B5	0.10	9.44	0.37	0.00	0.00	0.00	1.27
B6	0.25	12.45	0.49	0.00	0.00	0.00	1.74
C1	0.09	11.24	0.70	0.00	0.06	0.00	0.93
C2	0.00	7.93	0.09	0.00	0.00	0.02	0.32
C3	0.01	8.14	0.19	0.00	0.00	0.00	0.57
C4	0.01	8.20	0.09	0.00	0.00	0.02	0.24
C5	0.01	4.32	0.00	0.00	0.00	0.00	0.31
C6	0.02	9.06	0.25	0.00	0.00	0.01	0.65
D1	0.01	8.32	0.10	0.00	0.00	0.00	0.21
D2	0.00	5.34	0.12	0.00	0.01	0.00	0.15
D3	0.03	5.14	0.15	0.00	0.00	0.00	0.65
D4	0.03	8.31	0.00	0.00	0.00	0.01	0.35
D5	0.02	8.16	1.34	0.00	0.00	0.00	0.15
D6	0.04	5.11	0.38	0.00	0.00	0.02	0.00

Figure 4.17 Reaction data from Figure 4.4

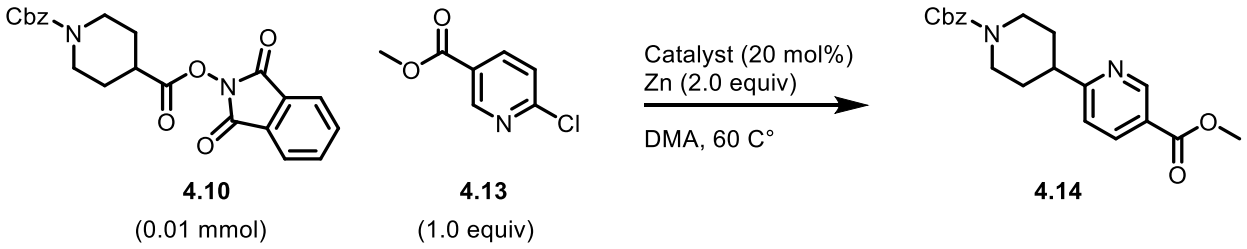

POSITION	PRODUCT	AR-AR	AR-H	ALK-H	ALK-ALK	BETA HYDRID	P/AR-AR
A1	0.39	0.98	0.12	0.01	0.07	0.01	0.39
A2	0.31	0.26	0.20	0.02	0.02	0.01	1.19
A3	0.27	0.35	0.20	0.01	0.06	0.03	0.77
A4	0.33	0.23	0.16	0.01	0.04	0.01	1.44
A5	0.32	4.56	0.18	0.02	0.09	0.00	0.07
A6	0.28	0.54	2.53	0.02	0.05	0.00	0.51
B1	0.41	0.29	0.25	0.01	0.10	0.01	1.39
B2	0.02	0.06	0.32	0.06	0.00	0.00	0.37
B3	0.21	0.42	0.22	0.00	0.03	0.00	0.49
B4	0.05	0.14	0.11	0.00	0.00	0.00	0.35
B5	0.04	0.04	0.05	0.89	0.00	0.00	0.91
B6	0.12	0.08	0.32	0.04	0.02	0.01	1.60
C1	0.31	0.59	0.21	0.03	0.04	0.00	0.52
C2	0.11	0.56	0.43	0.01	0.01	0.00	0.19
C3	0.15	0.31	0.18	0.01	0.01	0.01	0.49
C4	0.24	0.50	0.19	0.02	0.04	0.01	0.47
C5	0.31	0.42	0.16	0.12	0.11	0.00	0.73
C6	0.12	0.09	0.22	0.04	0.02	0.00	1.33
D1	0.26	0.70	0.21	0.01	0.07	0.01	0.37
D2	0.22	0.22	0.22	0.01	0.02	0.01	0.98
D3	0.22	0.22	0.20	0.02	0.09	0.01	0.99
D4	0.24	0.14	0.22	0.01	0.04	0.01	1.72
D5	0.13	0.07	0.50	0.02	0.03	0.03	1.90
D6	0.12	0.08	0.18	0.01	0.05	0.00	1.47

General Procedure for HTE Screening Using Catalyst Plates (B_2Pin_2)

All operations were performed in a N_2-filled glovebox. To each well of a 24-well (4 rows by 6 columns) aluminium block assembly equipped with 8 × 30 mm vials was dosed 75 mg of K_2CO_3-coated ChemBeads (5% loading wt/wt) using a calibrated scoop and a non-static funnel (Image 2). The NHP esters and aryl bromide were dosed into each well by first transferring stock solutions of each NHP ester and aryl bromide into separate channels of eight-channel polypropylene deep-well reservoirs followed by transferring 20 μL of each NHP ester stock solution 20 μL of the aryl halide stock solution, and 20 μL of B_2Pin_2 to each well using a multi-channel pipette. The well-plate vials were sealed with an electric screwdriver at torque setting 6 in a diagonal pattern (Image 4), using an aluminum lid, and the block was placed onto a heater/shaker (Torrey Pines Echotherm) set at 80 °C (actual temperature was found to be ~20 °C lower) and orbital speed at 8 to heat/shake overnight for 24 h.

Workup and Analysis

The reaction block was removed from the shaker apparatus and allowed to cool to rt. The aluminum block was then removed from the glovebox, the lid was removed, and 250 μL of MeOH was added to each well to dilute the reaction mixtures. 300 μL aliquots were taken from each well and were then filtered through a 0.2 μm filter plate into a 340 μL 96-well collection plate (Images 6 and 7). The plate was then analyzed by SFC-MS.

Figure 4.18 Reaction data from Figure 4.6

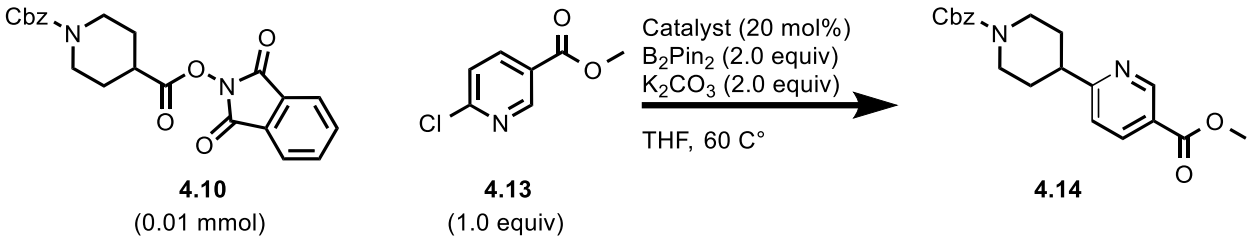

4.10
(0.01 mmol)

4.13
(1.0 equiv)

4.14

POSITION	PRODUCT	AR-AR	AR-H	ALK-H	ALK-ALK	BETA HYDRID	P/AR-AR
A1	0.39	0.98	0.12	0.01	0.07	0.01	0.39
A2	0.31	0.26	0.20	0.02	0.02	0.01	1.19
A3	0.27	0.35	0.20	0.01	0.06	0.03	0.77
A4	0.33	0.23	0.16	0.01	0.04	0.01	1.44
A5	0.32	4.56	0.18	0.02	0.09	0.00	0.07
A6	0.28	0.54	2.53	0.02	0.05	0.00	0.51
B1	0.41	0.29	0.25	0.01	0.10	0.01	1.39
B2	0.02	0.06	0.32	0.06	0.00	0.00	0.37
B3	0.21	0.42	0.22	0.00	0.03	0.00	0.49
B4	0.05	0.14	0.11	0.00	0.00	0.00	0.35
B5	0.04	0.04	0.05	0.89	0.00	0.00	0.91
B6	0.12	0.08	0.32	0.04	0.02	0.01	1.60
C1	0.31	0.59	0.21	0.03	0.04	0.00	0.52
C2	0.11	0.56	0.43	0.01	0.01	0.00	0.19
C3	0.15	0.31	0.18	0.01	0.01	0.01	0.49
C4	0.24	0.50	0.19	0.02	0.04	0.01	0.47
C5	0.31	0.42	0.16	0.12	0.11	0.00	0.73
C6	0.12	0.09	0.22	0.04	0.02	0.00	1.33
D1	0.26	0.70	0.21	0.01	0.07	0.01	0.37
D2	0.22	0.22	0.22	0.01	0.02	0.01	0.98
D3	0.22	0.22	0.20	0.02	0.09	0.01	0.99
D4	0.24	0.14	0.22	0.01	0.04	0.01	1.72
D5	0.13	0.07	0.50	0.02	0.03	0.03	1.90
D6	0.12	0.08	0.18	0.01	0.05	0.00	1.47

4.5.5

4.5.6 Specific Procedures and Product Characterization

1-(5-fluoro-1,3-dioxoisoindolin-2-yl) 3-methyl bicyclo[1.1.1]pentane-1,3-dicarboxylate (4.17)

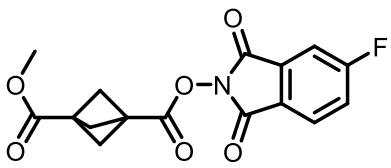

The title product was prepared according to General Procedure A using 3-(methoxycarbonyl)bicyclo[1.1.1]pentane-1-carboxylic acid (0.17 g, 1.0 mmol, 1.0 equiv), 5-fluoro-2-hydroxyisoindoline-1,3-dione (0.18g, 1.0 mmol, 1.0 equiv) *N,N*-dimethylaminopyridine (12 mg, 0.1 mmol, 0.1 equiv), and *N,N*-diisopropylcarbodiimide (0.14 g, 1.1 mmol. 1.1 equiv). Purification of the crude material by FCC (0-100% EtOAc/Hex) using 12 g silica afforded the title product (233 m 0g, 0.70 mmol, 70%) as a white solid.

^{1}H NMR (500 MHz, $CDCl_3$) δ 7.91 (dd, *J* = 8.3, 4.5 Hz, 1H), 7.58 (dd, *J* = 6.9, 2.3 Hz, 1H), 7.46 (td, *J* = 8.5, 2.3 Hz, 1H), 3.73 (s, 3H), 2.55 (s, 6H).

^{13}C{^{1}H} NMR (126 MHz, $CDCl_3$) δ 168.82, 166.70 (d, *J* = 259.1 Hz), 164.60, 160.71, 160.46 (d, *J* = 2.8 Hz), 131.69 (d, *J* = 9.5 Hz), 126.71 (d, *J* = 9.5 Hz), 124.72 (d, *J* = 3.3 Hz), 121.89 (d, *J* = 23.4 Hz), 112.09 (d, *J* = 25.2 Hz), 53.63, 52.03, 38.62, 35.36.

HRMS (ESI) m/z calculated for $C_{16}H_{13}FNO_6$ [M+H]+ 334.0721, found 334.0715.

MP =178 -180 °C.

1-(5-(dimethylamino)-1,3-dioxoisoindolin-2-yl) 3-methyl bicyclo[1.1.1]pentane-1,3-dicarboxylate (4.18)

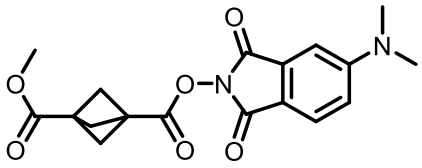

The title product was prepared according to General Procedure A using 3-(methoxycarbonyl)bicyclo[1.1.1]pentane-1-carboxylic acid (0.17 g, 1.0 mmol, 1.0 equiv 5-(dimethylamino)-2-hydroxyisoindoline-1,3-dione (0.21 g, 1.0 mmol, 1.0 equiv) *N,N*-dimethylaminopyridine (12 mg, 0.1 mmol, 0.1 equiv), and *N,N*-diisopropylcarbodiimide (0.14 g, 1.1 mmol. 1.1 equiv). Purification of the crude material by FCC (0-100% EtOAc/Hex) using 12 g silica afforded the title product (243 mg, 0.71 mmol, 71%) as a bright yellow solid.

^{1}H NMR (500 MHz, $CDCl_3$) δ 7.67 (d, *J* = 8.6 Hz, 1H), 7.08 (d, *J* = 2.5 Hz, 1H), 6.83 (dd, *J* = 8.6, 2.5 Hz, 1H), 3.72 (s, 3H), 3.13 (s, 6H), 2.54 (s, 6H).

^{13}C{^{1}H} NMR (126 MHz, $CDCl_3$) δ 169.0, 165.1, 163.1, 162.4, 157.1, 154.7, 131.5, 125.8, 115.1, 113.8, 106.3, 53.6, 52.0, 42.3, 40.5, 23.5.

HRMS (ESI) m/z calculated for $C_{18}H_{19}N_2O_6$ [M+H]+ 359.12376, found 359.1234.

MP = 160-163 °C.

3,4-Thiophenedicarboxylic Anhydride (4.8)

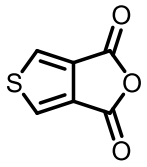

The title product was prepared according to a literature procedure. 3,4-thiophenedicarboxylic acid (10 g, 0.058 mol) was dissolved in acetic anhydride (25 mL). The reaction mixture was heated to 140 °C and left to stir overnight. After this time, the reaction mixture was allowed to cool to r.t. and the acetic anhydride was removed in vacuo to afford the product as a pale brown solid which was recrystallized from toluene to afford the title product (7.6 g, 0.049 mol, 85%) as a pale yellow solid. Characterization data match those reported in the literature. [12]

^{1}H NMR (500 MHz, $CDCl_3$) δ 8.02 (s, 2H).

^{13}C{^{1}H} NMR (126 MHz, $CDCl_3$) δ 156.2, 135.1, 129.1.

4-(hydroxycarbamoyl)thiophene-3-carboxylic acid (4.9)

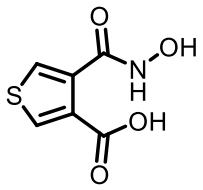

A 100 mL round-bottom flask equipped with a stir bar was charged with hydroxylamine hydrochloride (3.2 g, 1.01 equiv, 45.5 mmol) and pyridine (50 mL), then stirred at 25 °C for 30 min until the solid reagent was fully dissolved. 3,4-Thiophenedicarboxylic Anhydride (7 g, 1.0 equiv, 45 mmol) was added and the reaction mixture was heated to 85 °C for 12 h. It was then allowed to cool to 25 °C, then poured into water (25 mL). The resulting solution was acidified with hydrochloric acid to pH = 2, at which point a brown solid crashed out. The resulting solid was collected by filtration and subsequently washed with H_2O (5 × 200 mL) and pentane (5 × 200 mLto afford the title product (7.4 g, 40 mmol, 90%).

^{1}H NMR (500 MHz, D_6-DMSO) δ 13.48 (s, 1H), 11.25 (s, 1H), 9.24 (s, 1H), 8.28 (d, *J* = 3.3 Hz, 1H), 7.91 (d, *J* = 3.3 Hz, 1H).

^{13}C{^{1}H} NMR (126 MHz, D_6-DMSO) δ 163.7, 162.0, 135.8, 134.8, 133.4, 130.4.

4-fluoro-2-hydroxy-1(H)-isoindole-1,3-dione (4.5)

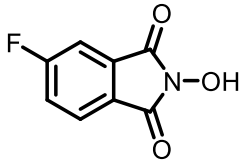

A 100 mL round-bottom flask equipped with a stir bar was charged with hydroxylamine hydrochloride (1.4 g, 1.01 equiv, 20.2 mmol), pyridine (25 mL) then stirred at 25 °C for 30 min until the solid reagent was fully dissolved. 4-Fluorophthalic anhydride (3.3 g, 1.0 equiv, 20 mmol) was added and the reaction mixture was heated to 85 °C and left to overnight. The resulting solution was acidified with hydrochloric acid to pH = 2, at which point a white solid crashed out. The resulting solid was collected by filtration and subsequently washed with H_2O (5 × 200 mL) and pentane (5 × 200 mL) to afford the title product (1 g, 5.5 mmol, 28%). Characterization data matched those reported in the literature.[13]

^{1}H NMR (500 MHz, D_6-DMSO) δ 10.93 (s, 1H), 7.91 (dd, J = 8.1, 4.6 Hz, 1H), 7.79−7.73 (m, 1H), 7.70−7.61 (m, 1H)

^{13}C{^{1}H} NMR (126 MHz, D_6-DMSO) δ 163.3 (d, J =3.2 Hz), 161.2 (s), 156.4 (d, J= 261.3 Hz), 137.5 (d, J= 8.0 Hz), 131.4 (s), 122.9 (d, J= 19.9 Hz), 119.6 (d, J= 3.2 Hz), 114.7 (d, J=12.5 Hz).

2-(2-hydroxyethyl)-5-morpholinoisoindoline-1,3-dione (4.6)

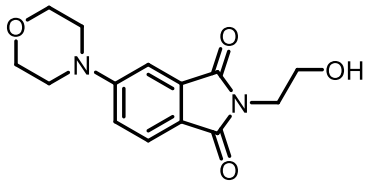

A 25 mL round-bottom flask equipped with a stir bar was charged with 4-fluoro-2-hydroxy-1(H)-isoindole-1,3-dione (0.27 g, 1.5 mmol) and morpholine (15 mL). The reaction flask was equipped with a Liebig condenser, and the reaction mixture was heated to 130 °C and allowed to stir overnight. After this time the reaction mixture was cooled to room temperature and concentrated in vacuo. The reaction mixture was then diluted with H2O, acidified to pH ~5 and extracted with DCM (3 ×100 mL). The combined organic layers were dried with Na_2SO_4, the solvent was removed in vacuo, and the resulting oil was purified by flash chromatography to afford the title product (53 mg, 0.19mmol, 13 %) as a bright yellow solid.

^{1}H NMR (500 MHz, $CDCl_3$) δ 7.68 (d, *J* = 8.4 Hz, 1H), 7.27 (d, *J* = 2.4 Hz, 1H), 7.03 (dd, *J* = 8.5, 2.4 Hz, 1H), 3.89 – 3.86 (m, 4H), 3.85 (s, 3H), 3.40 – 3.33 (m, 4H).

^{13}C{^{1}H} NMR (126 MHz, $CDCl_3$) δ 169.3, 168.9, 155.5, 134.4, 124.9, 120.7, 117.6, 108.4, 66.4, 61.3, 47.7, 40.8.

4.6 References

[1] Salgueiro, D. C.; Chi, B. K.; Guzei, I. A.; García-Reynaga, P.; Weix, D. J. Control of Redox-Active Ester Reactivity Enables a General Cross-Electrophile Approach to Access Arylated Strained Rings**. *Angewandte Chemie International Edition* **2022**, *61* (33), e202205673. https://doi.org/10.1002/anie.202205673.

[2]Prieto Kullmer, C. N.; Kautzky, J. A.; Krska, S. W.; Nowak, T.; Dreher, S. D.; MacMillan, D. W. C. Accelerating Reaction Generality and Mechanistic Insight through Additive Mapping. *Science* **2022**, *376* (6592), 532–539. https://doi.org/10.1126/science.abn1885.

[3] Pitchai, M.; Ramirez, A.; Mayder, D. M.; Ulaganathan, S.; Kumar, H.; Aulakh, D.; Gupta, A.; Mathur, A.; Kempson, J.; Meanwell, N.; Hudson, Z. M.; Oderinde, M. S. Metallaphotoredox Decarboxylative Arylation of Natural Amino Acids via an Elusive Mechanistic Pathway. *ACS Catal.* **2023**, *13* (1), 647–658. https://doi.org/10.1021/acscatal.2c05554.

[4]Palkowitz, M. D.; Laudadio, G.; Kolb, S.; Choi, J.; Oderinde, M. S.; Ewing, T. E.-H.; Bolduc, P. N.; Chen, T.; Zhang, H.; Cheng, P. T. W.; Zhang, B.; Mandler, M. D.; Blasczak, V. D.; Richter, J. M.; Collins, M. R.; Schioldager, R. L.; Bravo, M.; Dhar, T. G. M.; Vokits, B.; Zhu, Y.; Echeverria, P.-G.; Poss, M. A.; Shaw, S. A.; Clementson, S.; Petersen, N. N.; Mykhailiuk, P. K.; Baran, P. S. Overcoming Limitations in Decarboxylative Arylation via Ag–Ni Electrocatalysis. *J. Am. Chem. Soc.* **2022**, *144* (38), 17709–17720. https://doi.org/10.1021/jacs.2c08006.

[5]Sosič, I.; Bricelj, A.; Steinebach, C. E3 Ligase Ligand Chemistries: From Building Blocks to Protein Degraders. *Chem. Soc. Rev.* **2022**, *51* (9), 3487–3534. https://doi.org/10.1039/D2CS00148A.

[6] Guo, X.; Ortiz, R. P.; Zheng, Y.; Kim, M.-G.; Zhang, S.; Hu, Y.; Lu, G.; Facchetti, A.; Marks, T. J. Thieno[3,4- *c*]Pyrrole-4,6-Dione-Based Polymer Semiconductors: Toward High-Performance, Air-Stable Organic Thin-Film Transistors. *J. Am. Chem. Soc.* **2011**, *133* (34), 13685–13697. https://doi.org/10.1021/ja205398u.

[7]Lee, H.-J.; Kong, Y.-S.; Kim, S.-S. Novel N-Hydroxymethylation of Phthalimide by Titanium Dioxide Photocatalyst in Methanol. *Bulletin of the Korean Chemical Society* **2009**, *30* (2), 295–296. https://doi.org/10.5012/bkcs.2009.30.2.295.

[8]Charboneau, D. J.; Hazari, N.; Huang, H.; Uehling, M. R.; Zultanski, S. L. Homogeneous Organic Electron Donors in Nickel-Catalyzed Reductive Transformations. *J. Org. Chem.* **2022**, *87* (12), 7589–7609. https://doi.org/10.1021/acs.joc.2c00462.

[9]Suzuki, N.; Hofstra, J. L.; Poremba, K. E.; Reisman, S. E. Nickel-Catalyzed Enantioselective Cross-Coupling of *N* -Hydroxyphthalimide Esters with Vinyl Bromides. *Org. Lett.* **2017**, *19* (8), 2150–2153. https://doi.org/10.1021/acs.orglett.7b00793.

[10] Xu, H.; Zhao, C.; Qian, Q.; Deng, W.; Gong, H. Nickel-Catalyzed Cross-Coupling of Unactivated Alkyl Halides Using Bis(Pinacolato)Diboron as Reductant. *Chem. Sci.* **2013**, *4* (10), 4022. https://doi.org/10.1039/c3sc51098k.

[11] Lu, X.; Wang, Y.; Zhang, B.; Pi, J.-J.; Wang, X.-X.; Gong, T.-J.; Xiao, B.; Fu, Y. Nickel-Catalyzed Defluorinative Reductive Cross-Coupling of *Gem* -Difluoroalkenes with Unactivated Secondary and Tertiary Alkyl Halides. *J. Am. Chem. Soc.* **2017**, *139* (36), 12632–12637. https://doi.org/10.1021/jacs.7b06469.

[12] Reinecke, M. G.; Newsom, J. G.; Chen, L.-J. Thermolysis of Thiophenedicarboxylic Acid Anhydrides as a Route to Five-Membered Hetarynes. *J. Am. Chem. Soc.* **1981**, *103* (10), 2760–2769. https://doi.org/10.1021/ja00400a046.

[13] Wentzel, B. B.; Donners, M. P. J.; Alsters, P. L.; Feiters, M. C.; Nolte, R. J. M. N - Hydroxyphthalimide/Cobalt(II) Catalyzed Low Temperature Benzylic Oxidation Using Molecular Oxygen. *Tetrahedron* **2000**, *56* (39), 7797–7803. https://doi.org/10.1016/S0040-4020(00)00679-7.

4.7 NMR Spectra

^{1}H NMR spectrum of 4.17 (500 MHz, $CDCl_3$)

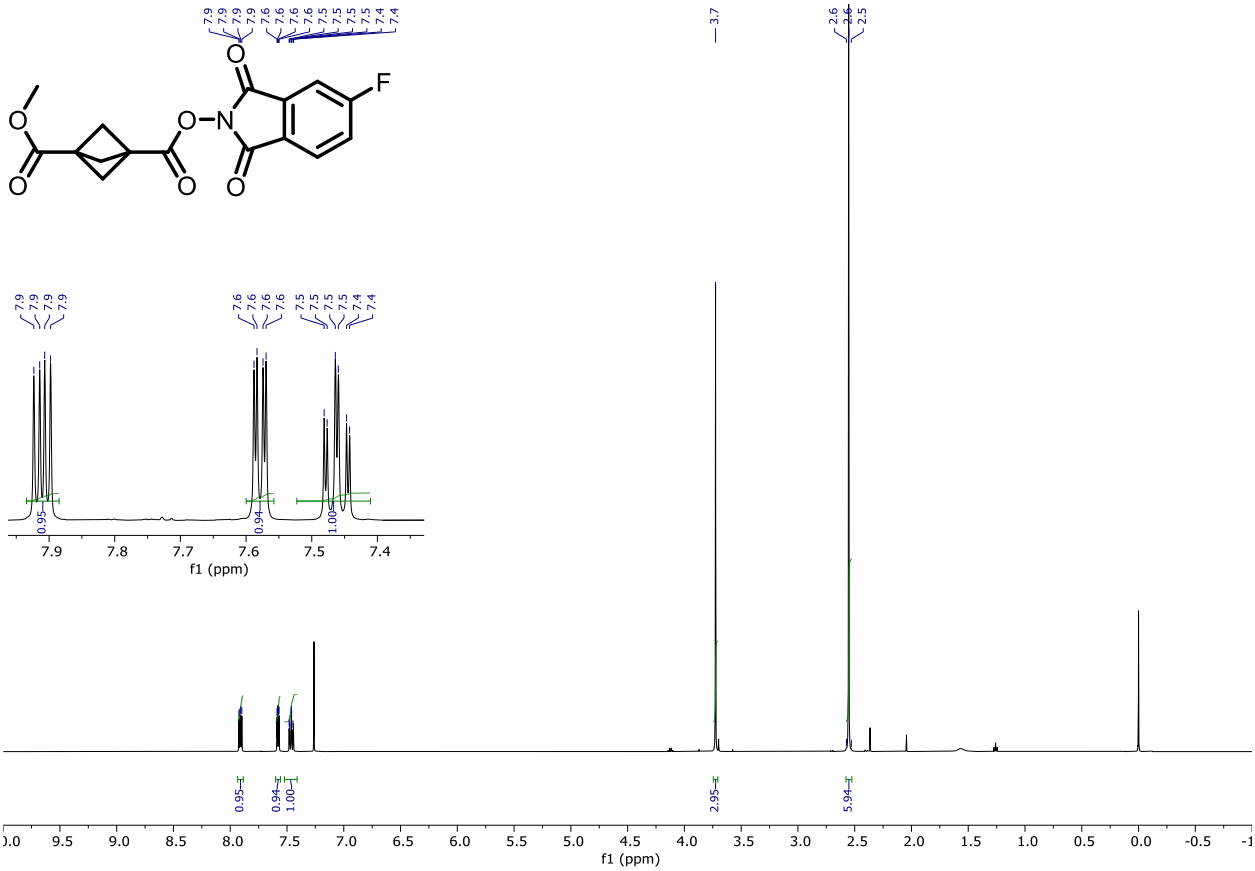

^{13}C NMR spectrum of 4.17 (126 MHz, $CDCl_3$)

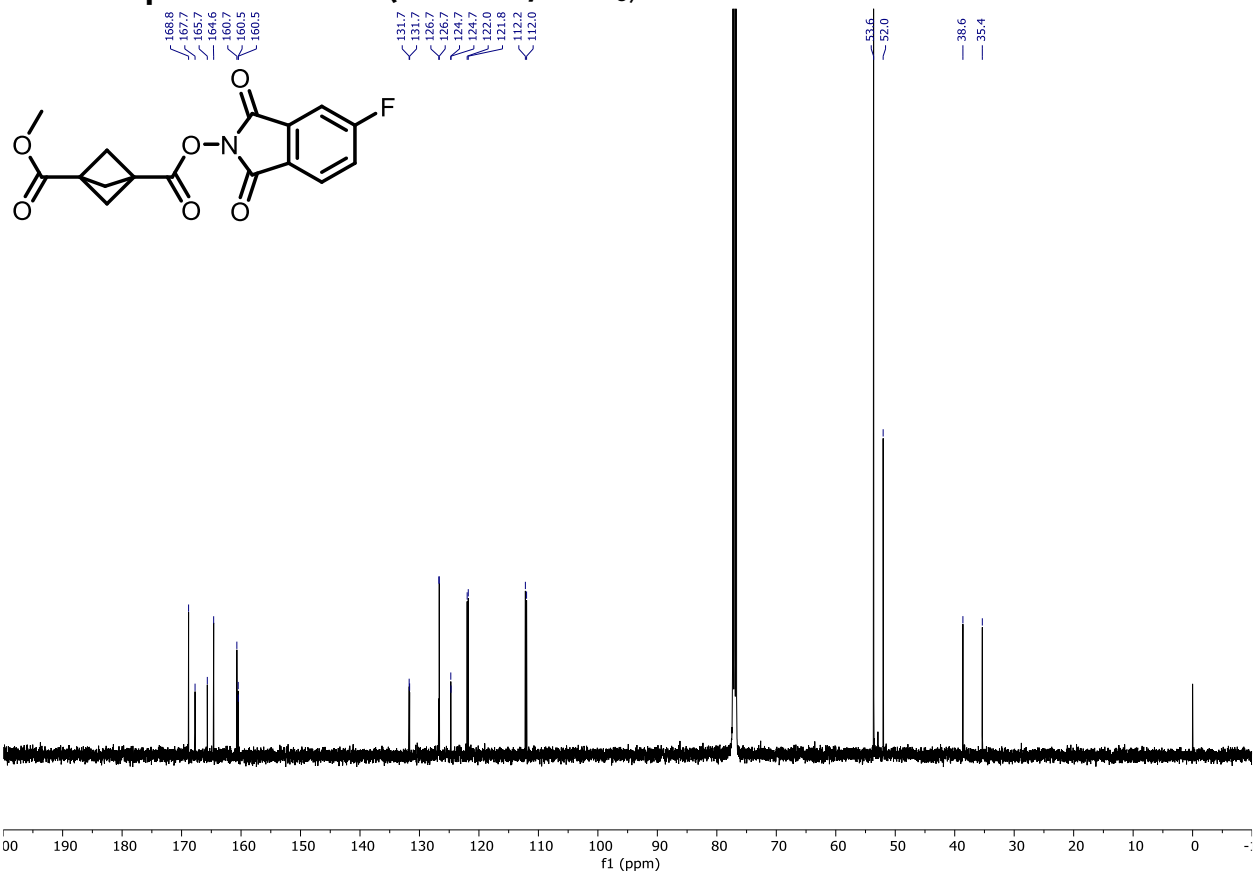

^{1}H NMR spectrum of 4.18 (500 MHz, $CDCl_3$)

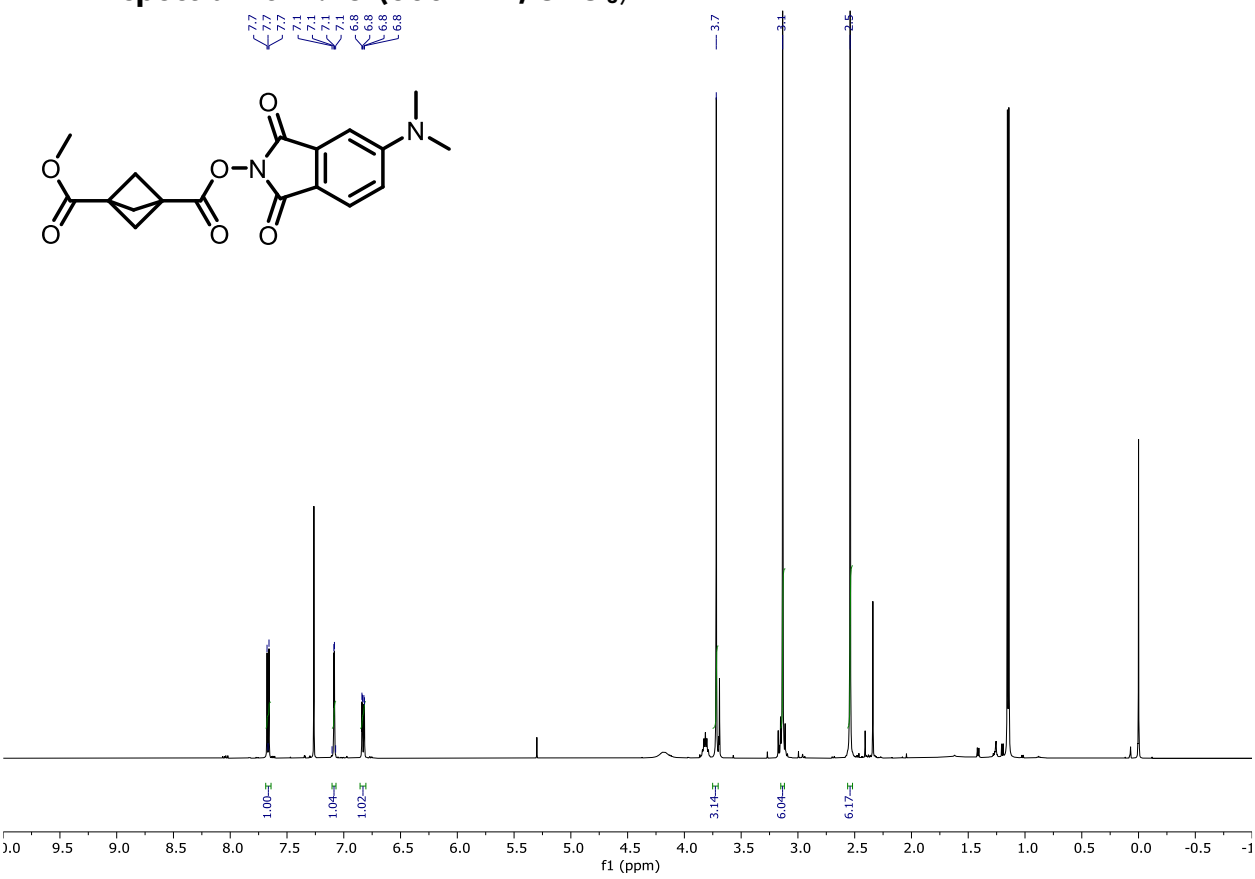

^{13}C NMR spectrum of 4.18 (126 MHz, $CDCl_3$)

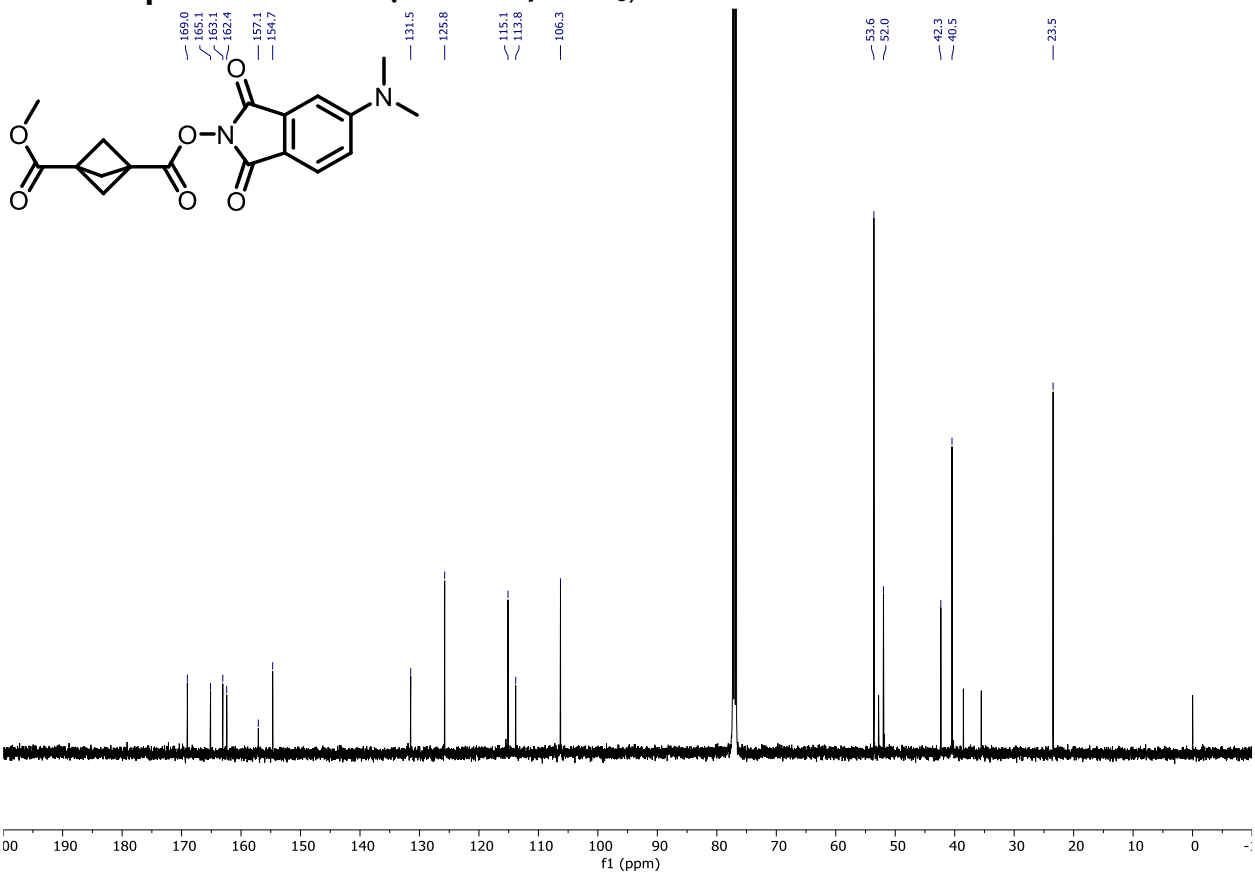

^{1}H NMR spectrum of 4.9 (500 MHz, DMSO)

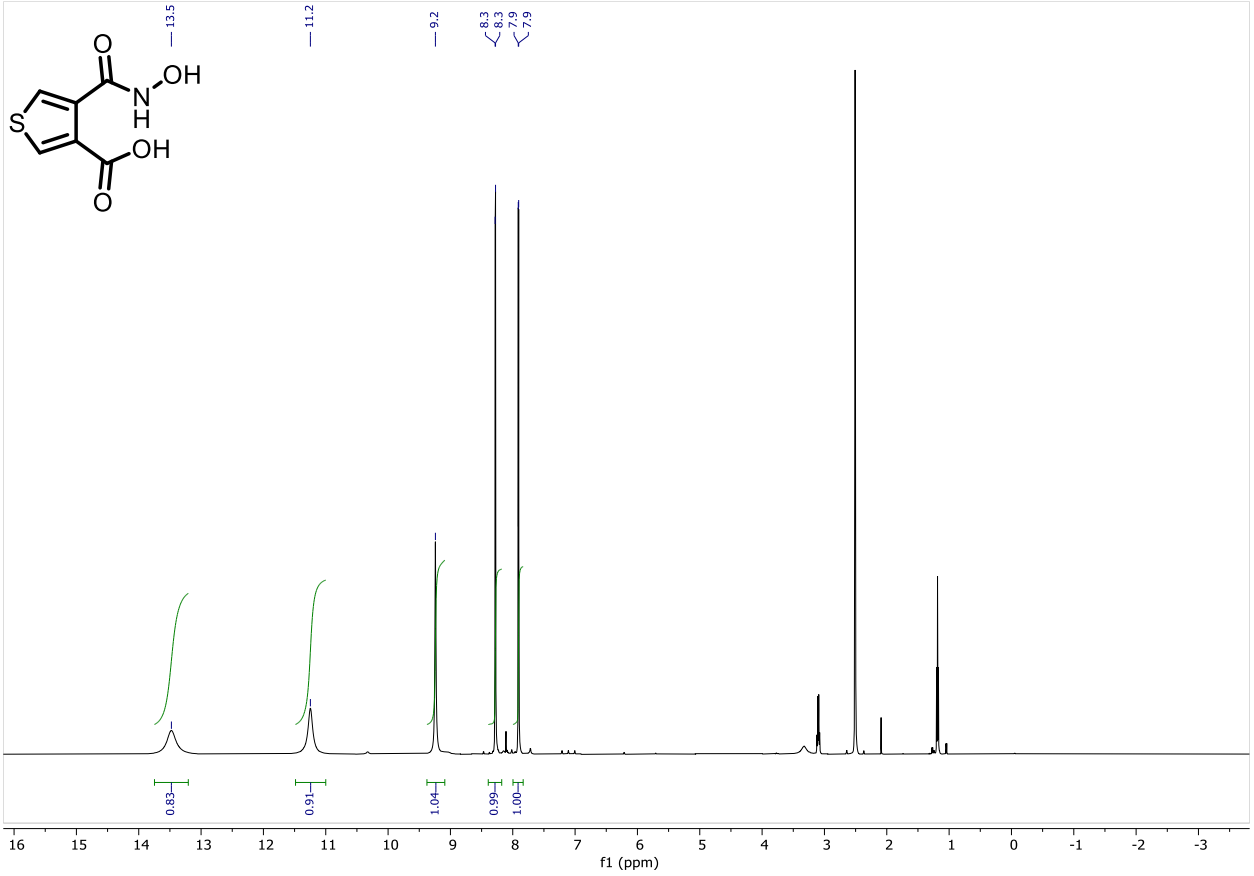

^{13}C NMR spectrum of 4.9 (126 MHz, DMSO)

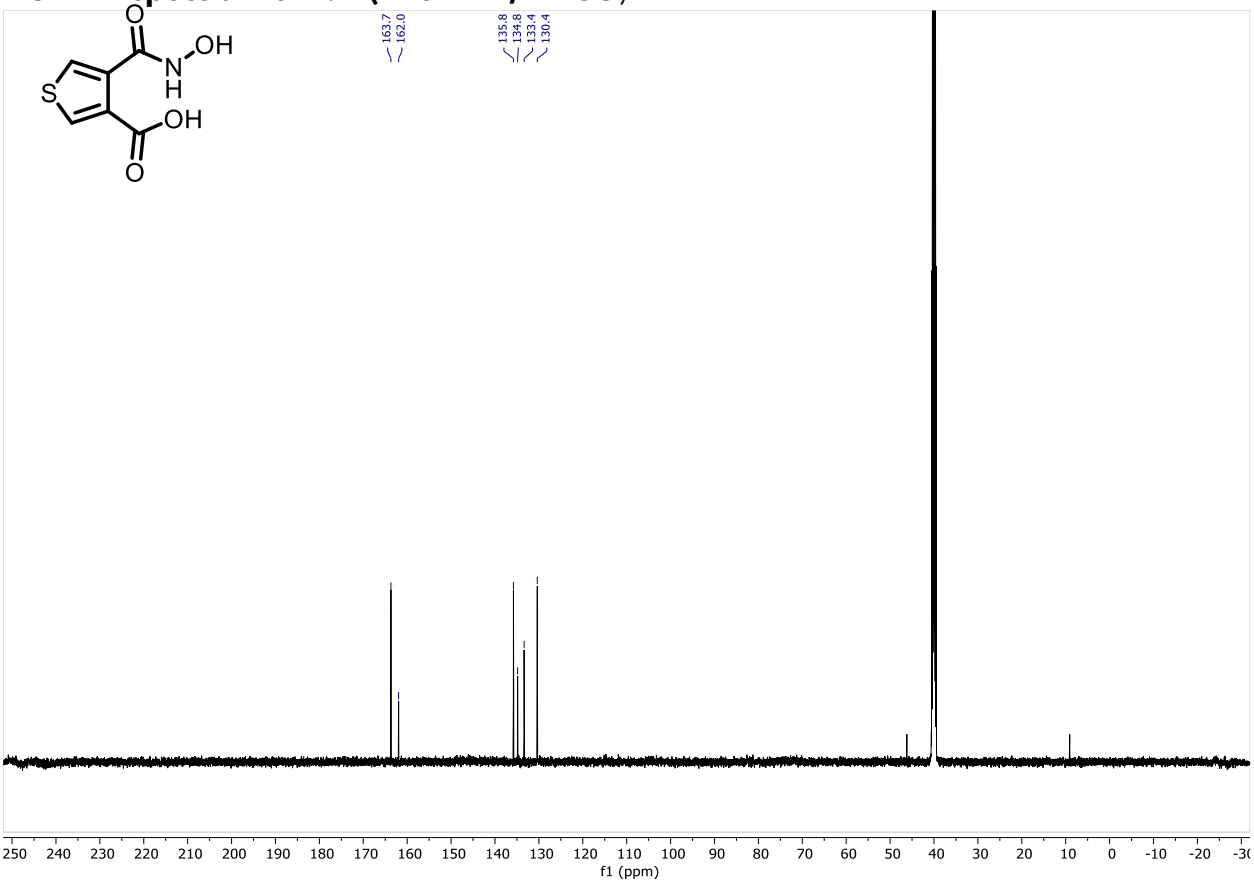

^{1}H NMR spectrum of 4.6 (500 MHz, $CDCl_3$)

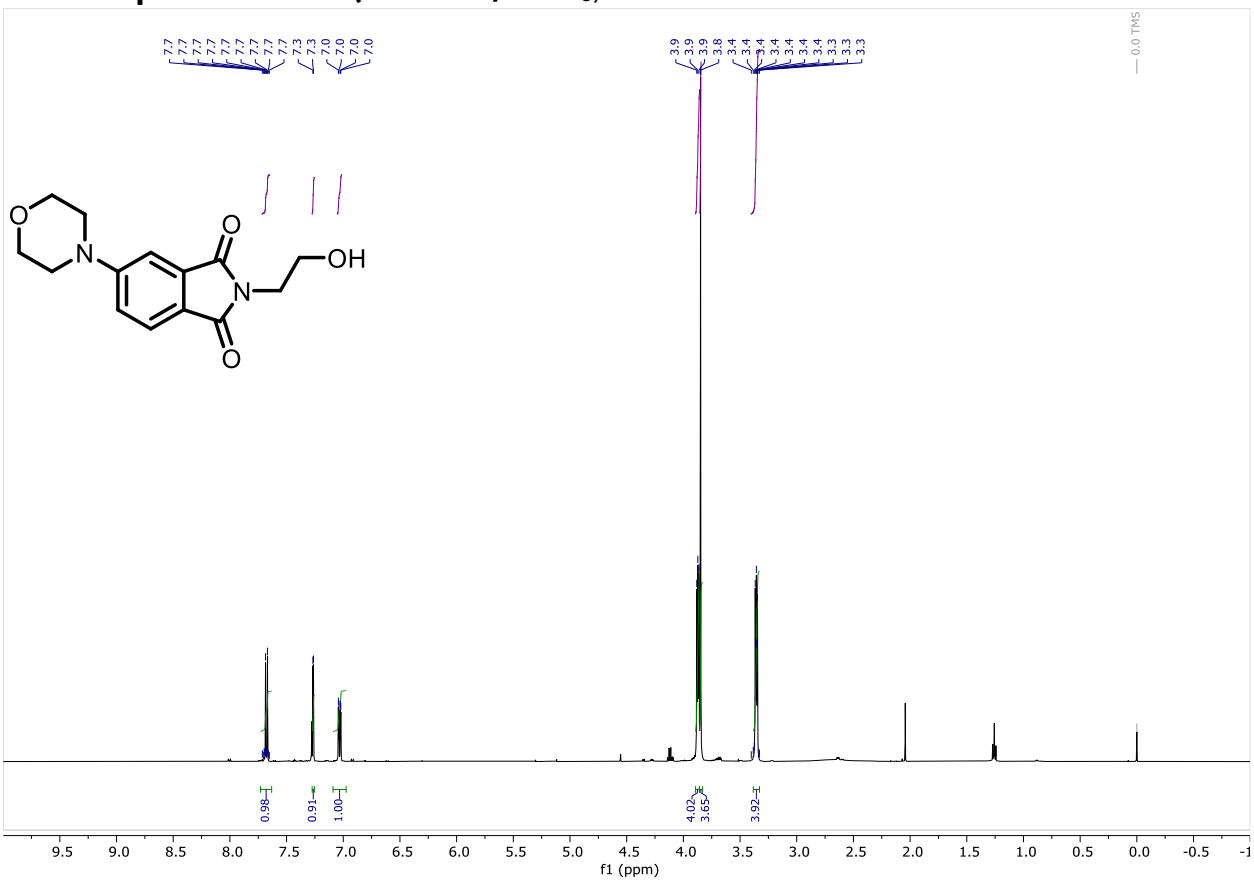

^{13}C NMR spectrum of 4.6 (126 MHz, $CDCl_3$)